Experimental and Theoretical Study of Severe Core Damage Scenario in PHWR

By

DEB MUKHOPADHYAY

ENGG01200704016

CI Name; Bhabha Atomic Research Centre, Mumbai

A thesis submitted to the

Board of Studies in Engineering

In partial fulfillment of requirements

for the Degree of

DOCTOR OF PHILOSOPHY
of
HOMI BHABHA NATIONAL INSTITUTE

August, 2014

Homi Bhabha National Institute

Homi Bhabha National Institute

Recommendations of the Viva Voce Committee

As members of the Viva Voce Committee, we certify that we have read the dissertation prepared by Deb Mukhopadhyay entitled "Experimental and Theoretical Study of Severe Core Damage Scenario in PHWR" and recommend that it may be accepted as fulfilling the thesis requirement for the award of Degree of Doctor of Philosophy.

Chairman-	**Prof. R. K. Singh**	**Date** oct 05 2015
Guide/Convener-	**Prof A.K. Ghosh**	**Date** 05.10.2015
Member 1-	**Prof. A. P. Tiwari**	**Date** 09.10.2015
Member 2-	**Prof. S. S. Taliyan**	**Date** 16/11/2015
Examiner-1	**Prof. P. K. Das** **IIT Kharagpur**	**Date** 5.10.2015

Final approval and acceptance of this dissertation is contingent upon the candidate's submission of the final copies of the dissertation of HBNI.

I hereby certify that I have read this dissertation prepared under my direction and recommended that it may be accept as fulfilling the dissertation requirement.

Date 20.11.2015

Place: MUMBAI

Dr. A. K. Ghosh
Guide

STATEMENT BY AUTHOR

This dissertation has been submitted in partial fulfillment of requirements for an advanced degree at Homi Bhabha National Institute (HBNI) and is deposited in the Library to be made available to borrowers under rules of the HBNI.

Brief quotations from this dissertation are allowable without special permission, provided that accurate acknowledgement of source is made. Requests for permission for extended quotation from or reproduction of this manuscript in whole or in part may be granted by the Competent Authority of HBNI when in his or her judgment the proposed use of the material is in the interests of scholarship. In all other instances, however, permission must be obtained from the author.

D Mukhopadhyay

Deb Mukhopadhyay

DECLARATION

I, hereby declare that the investigation presented in the thesis has been carried out by me. The work is original and has not been submitted earlier as a whole or in part for a degree / diploma at this or any other Institution / University.

Dmukhopadhyay

Deb Mukhopadhyay

List of Publications arising from the thesis

Journal

1. **Deb Mukhopadhyay**, P. K. Sahoo and A. K. Ghosh "Heat Transfer Study of a Submerged Reactor Channel under a boil-off condition", Kerntechnik, Volume 77, No. 6, Dec. 2012, pp. 425-430. ISSN: 0932-3902

2. **Deb Mukhopadhyay,** P. K. Vijayan "Experimental and Analytical Study of a Simulated Collapsed PHWR Reactor Channel Under Accident Condition", International Journal of Nuclear Energy Science and Engineering (IJNESE), Volume 3 Issue 4, Dec. 2013, pp 109-117, ISSN: 2226-3225

3. **Deb Mukhopadhyay**, P. K. Vijayan, A. K. Ghosh and P. K. Sahoo, "Experimental study of PHWRs Debris Bed Under Boil-off Condition", Kerntechnik, Volume 79, No. 1, Jan. 2014, pp. 1-10, ISSN: 0932-3902.

Conference

1. O. Gokhale, **Deb Mukhopadhyay**, A. K. Ghosh, "Severe Accident Analysis to evolve insight for severe accident management guide lines for large pressurized heavy water reactor", Proceedings, 2nd International Conference on Reliability, Safety & Hazard (ICRESH 2010), December 2010, Mumbai, IEEE catalog No.: CFP1082L-ART, ISBN: 978-1-4244-8342-6/10 ©IEEE

2. **Deb Mukhopadhyay**, P. K. Vijayan, A. K. Ghosh, Investigation of Calandria Vessel as an ultimate barrier to Corium relocation for PHWRs, paper no. HMTC1300581, Proceedings of the 22th National and 11th International ISHMT-ASME Heat and Mass Transfer Conference Dec. 28-31, 2013, IIT Kharagpur, India

DMukhopadhyay

Deb Mukhopadhyay

DEDICATIONS

I would like to dedicate my work to my parents Dr. Ajit Kumar Mukherjee and Smt. Dipa Mukherjee who have inspired me from my childhood for carrying out scientific research for societal benefits.

I also dedicate my work to Dr. Partha Roy, Chemical Engineering Department, University College of Science and Technology, University of Calcutta who had inculcated research aptitude deeply during my student days.

I also dedicate my work to Shri H. S. Kushwaha, Former Director, Health Safety and Environment Group, Bhabha Atomic Research Centre who had inspired me tremendously for last two decades and encouraged me continuously to bring out new findings, establishing new physical models and resolving several issues in the field of Nuclear Reactor Safety.

ACKNOWLEDGEMENTS

I take this opportunity to express my heartfelt gratitude to Dr. A. K. Ghosh, Former Director, Health Safety and Environment Group, BARC and my guide who inspired me most in last one decade for carrying out this work and enriched my work with his continuous guidance. I am extremely thankful to Shri K. K. Vaze, Director, Reactor Design and Development Group, BARC and Dr. R. K. Singh, Head Reactor Safety Division to provide me research support for continuing my long experimental investigation. I am also thankful to my colleague in Core Safety Studies Section of Reactor Safety Division, especially Shri Onkar Gokhale who had used the proposed mathematical model in the original form and suggested several improvements towards development for a better model. I am grateful to Prof. Pradeep Kumar Sahoo of IIT Roorkee who was enthralled with the new experimental findings and discussions at a length have helped to improve the interpretation of the experimental results. Internal reviews by the Doctoral committee chaired by Prof. L. M. Gantayet were extremely helpful by directing this research to a successful and logical end. I thank eminent members of the doctoral committee Prof. B. K. Dutta, Prof. P. Satyamurthy and Prof. A. P. Tiwari for their kind advice and suggestions to improve the quality of this work. My colleague and friend Shri Mithilesh Kumar of Reactor Safety Division, BARC had always given me support to keep the work going when they became sluggish or unstable. I acknowledge my wife Smt. Sutapa Mukhopadhyay and my daughter Swarnali who have supported me through out the long period and I could not achieve the completion of my thesis without their love and support.

CONTENTS

SYNOPSIS

Installed Indian Pressurized Heavy Water Reactors (PHWRs) are of 220 and 540 MWe capacity. The reactor core configuration in a typical PHWR is horizontal with several parallel reactor channels. Nuclear heat is removed from fuel bundles by the coolant and transferred to the steam generator's secondary side leading to steam production. All the reactor channels are submerged in a pool of heavy water called moderator housed in Calandria. Under postulated severe accident condition with unavailability of all modes of heat sink, reactor channels will undergo heat-up. The exposed channels due to moderator boil-off will undergo thermo-mechanical deformation leading to their failures. Limited experiments carried out by AECL, Canada, indicated that failures will generate long segments of the reactor channels. The generated long segments will form a dry debris bed which will be supported by still submerged channels. Further cascading failure of still submerged channels is envisaged once the load bearing capacity of the submerged channel exceeds due to accumulated weight from dry debris bed. All the segmented reactor channels will form a submerged debris bed at the bottom of Calandria. This scenario is internationally accepted. PWR specific debris bed as observed post TMI-2 accident and from several experiments are found to be very much different than PHWR specific debris bed. Post TMI-2 investigation shows that debris bed particles are small in size and majority are in the range of 5-6 mm. Extensive experimental and analytical programs were launched post TMI-2 accident to understand the heat-up and quenching aspects of PWR specific debris bed. The generated insights were being used to formulate the Severe Accident Management Guidelines (SAMG) for PWR community. On a similar line for PHWRs, sufficient research support is needed to establish the "Technical Basis Document" for SAMGs formulation. The early phase of severe accident of PHWRs is well understood through several experimental and analytical model supports. However all the late phase phenomena of the accident are not very well understood. The thermal-hydraulic characterization of PHWR-specific debris bed is found to be one of the major component that provide support to evolving “Technical Basis Document” for PHWR for actions like addition to water into Calandria and Calandria Vault for In-Calandria debris retention. The thermal-hydraulic characterization of PHWR specific debris bed study has not being reported so far in open literature. The present work is intended to study and characterize the heat-up pattern of PHWR-specific debris bed so that flow behaviour in such debris could be identified and possibility of dry out/CHF for the fully/partially submerged debris bed as well as the behaviour of the exposed dry debris bed could be established. The local hot spot formation and it’s propagation at the central region during boil-off period is of interest for PHWR as observed during PWR specific debris bed experiments. The local hot spot of the submerged debris bed becomes unmanageable to quench under some conditions. The scope of the study includes experimental study for the PHWR specific bed characterization and mathematical model development taking insights from the experiments. This study may be a first step to formulate the Technical Basis Document for Severe Accident Management (SAM) strategy of water addition into Calandria to remove decay heat from debris bed in a PHWR. Under this study, it is also attempted to employ the debris bed model to examine the integrity of the Calandria for a large PHWR. The roadmap for the present work is illustrated in Fig. 1,

The experimental plan involves study of boil-off heat transfer pattern for a segmented single reactor channel at different submergence levels. As the individual disassembled reactor channel in the submerged condition will have a typical configuration where the original concentric configuration of fuel bundle, Pressure Tube (PT) and Calandria Tube (CT) will be lost and an eccentric configuration among these three components will be established with a line contact between PT to CT. To study the debris bed heat transfer behavior, a constituent of the debris bed i.e. a submerged single reactor channel segment has been studied.

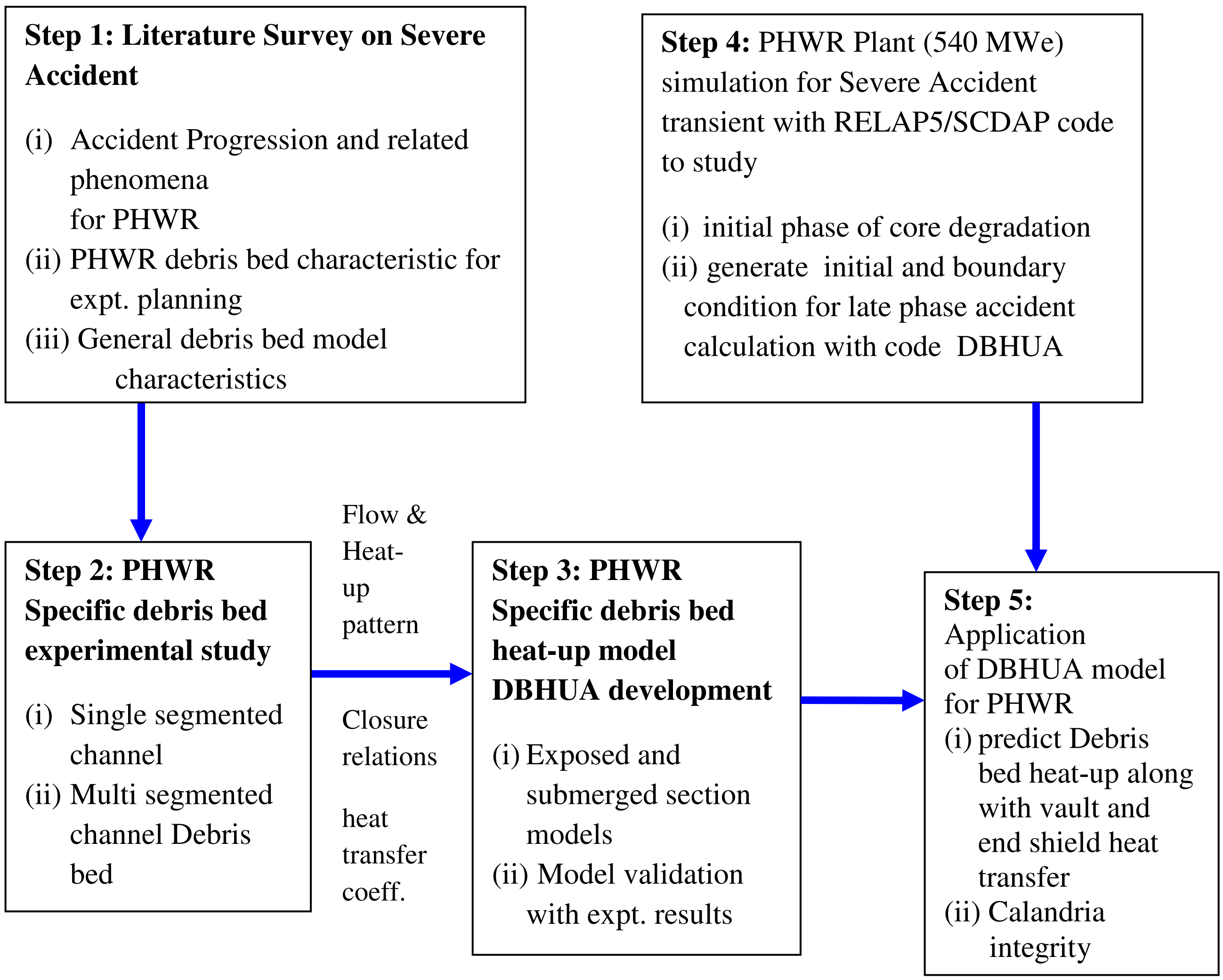

Fig. 1: Road map for PHWR Debris bed heat-up study

The investigation primarily looks for dryout in the top section of the fuel bundle arising from large steam voids at different submergence level. The situation is similar to an open pool boiling condition. The test section of the segmented channel consists of an assembly of electrical heater rod, simulating fuel bundle and channel components like Pressure Tube and Calandria Tube.

Two kinds of experiments are conducted under this program. The first kind of experiment has been carried out with a single segmented channel to study effect of different submergence levels and different power levels on fuel bundle heat-up. The single channel experiment is carried out at power 6-8 kW which gives equivalent to 1.5 - 1.9 times more than the expected 1% core decay power at the late phase of accident. A higher power is chosen to simulate peak power location of the maximum rated channel which is higher than the average channel power. The experiment shows that the bundle gets heated up under nearly exposed condition only. The generated steam flow is found to be sufficient to remove the heat from the bundle and keep it at lower temperature. Heat transfer coefficient correlations are proposed for the submerged and exposed part of the bundle from the single channel experimental data. Subsequently, a scaled down multiple channel debris bed heat-up experiments have been carried out with ten segmented channels. The scaling includes conservation of decay power to moderator volume ratio, debris bed hydraulic and heated equivalent diameters and moderator thermal-hydraulic conditions. Each of the segmented channels is similar to that of the single segmented channel experimentation. Heat-up of this debris bed is observed with respect to different water levels and at power levels of 10, 20 and 30 kW, typical to decay power levels of 0.25%, 0.5% and 0.75% of reactor full power respectively. Due to power supply limitations a decay power of 1% could not be achieved in the test section. It has been observed from the set of experiments carried out for multiple channel debris bed that fully submerged debris bed does not get heated up and fuel rod temperature remains at saturation temperature. Heat-up is observed for exposed channels only, however the heat-up rate is limited with steam and radiative cooling. For exposed debris bed, channels surrounded by neighboring channels get heated up more as compared to channels at the periphery of the debris bed. The existing heat transfer relations for equivalent conductivity and natural convection of heat generating debris bed are being modified to suit the PHWR specific debris bed.

A mathematical model **D**ebris **B**ed **Heat-up** **A**nalysis (DBHUA) for PHWR specific debris bed has been developed to predict the heat-up pattern for PHWR debris bed housed in the Calandria. The insights generated from the experiments like the boiling pattern and associated flow pattern and developed closure relations are used to formulate the model. It solves the 2-D (r, z) energy equation involving porosity and average properties of material and fluid. The debris bed is discretized in several nodes which represent heat source from reactor channels. The model is treated separately in two parts. One part deals with exposed debris bed and the other deals with submerged debris bed. Separate closure relations are applied for these two parts which gets dynamically changed from moderator boil-off. The energy equation accounts for reactor's decay power and chemical energy released from Zircaloy-steam reaction and radiative and convective heat transfer from the heated body. Regarding the closure relations, heat transfer coefficient correlation developed from experiments for fully/partially submerged channels has been used for convective heat transfer predictions. For exposed section of debris bed with fully exposed channels, a PWR specific equivalent conductivity (radiative and conductive) approach along with natural convection and radiation heat transfer to fluid are used for predicting debris bed heat-up. However for the natural convection heat transfer, the correlation is modified by replacing the debris particle diameter as characteristic length with hydraulic and heated equivalent diameter of the debris bed for computing Grasshoff and Nusselt numbers respectively. Radiative heat exchange between topmost layer of channels of the exposed debris bed with the Calandria wall has been accounted as well as heat exchange between peripheral channels of the exposed debris bed in contact with Calandria wall is accounted with thermal contact conductance. Heat transfer from Calandria external surface is modeled with different options like constant wall temperature or boiling heat transfer. The CHF and heat transfer coefficient correlations as used for hemispherical sphere are being used for boiling situation. The DBHUA model prediction for temperature has been compared with experimental results from the multiple segmented channels debris bed heat-up experiment carried out at 10 and 20 kW power levels. The model predictions compare well with the experimental data for the submerged debris bed however for exposed debris bed the model under predicts the fuel rod temperatures by 8-10%. A sensitivity analyses has been carried out with debris bed experimental model to understand the influence of different heat transfer models like equivalent conductivity (based on local conduction and radiation) and natural convection on the exposed debris bed heat-up pattern. It is observed from the analyses that natural convection plays the most significant role for debris bed internal heatup as compared to equivalent conductivity model. As the PHWR specific debris bed is highly porous, heat removal through convection is found to be better and the contribution from effective conductivity for debris bed heat-up is found to be less significant.

DBHUA model has been applied for analyzing the late phase of the severe accident scenario when the channels are disassembled and collapsed in the Calandria bottom. For the extended analysis, components like Calandria Vault concrete and End Shield of reactor block are modeled with 1-D energy equation and lumped parameter approach respectively. This will give a complete model for reactor block.

As DBHUA model requires the initial and boundary conditions for calculation, a full plant simulation has been carried out for 540 MWe PHWR under Station Black Out (SBO) condition without operator intervention like flooding the secondary side of SG etc. The initial and boundary conditions required for DBHUA simulation are number of collapsed channels which form the debris bed, decay power level and thermal hydraulic conditions of moderator, End Shield components (water and steel balls) and Calandria Vault (water and concrete). The boundary conditions are obtained from a full plant (Primary Heat Transport System, Steam generator secondary side, moderator, End Shield and Calandria Vault) analysis which has been carried out with code RELAP5/Mod3.4/ SCDAP, till the total core collapse to calandria bottom. DBHUA prediction shows that debris bed does not show any heat-up till the bed is submerged into water. After the total exposure the bed heat-up is found to begin and attains a pseudo steady state due to availability of several heat sinks. The heat-up of the topmost and bottom most section is much lower as compared to the central location. This is due to Calandria structure which acts as a heat sink associated with boil off of Calandria Vault as indicated with fall in level. Debris bottom and Calandria bottom temperature starts rising once the Calandria Vault water falls below the Calandria. Calandria wall integrity is found to be lost as the vessel wall attains its melting temperature once the vault water falls below the Calandria bottom level.

In summary, thermal-hydraulic characterization has been carried out for PHWR specific debris bed with single and multiple channel debris experimentation. Closure models are proposed for debris bed related energy equation. The closure models and insights generated on heat transfer and flow boiling behaviour from the experiment enabled to formulate the numerical model DBHUA for predicting debris bed heat-up. The model has been applied for predicting the 540 MWe PHWR late phase severe accident behaviour and the assessment of Calandria integrity.

List of Figures:

List of Tables:

Chapter 1

Introduction

Evolution of the Indian PHWR design has come a long way right from 220 MWe units of Rajasthan Atomic Power Station (RAPS) to current 700 MWe units which are at licensing stage. Enormous amount of construction, operation & maintenance experience and adoption of state of the art technology for engineering and analysis has contributed in development of a proven, robust, safe and reliable model of the Indian PHWR, which will fulfill the energy requirements of the country to a large extent. Indian PHWR is a combination of inherent and engineered safety features, incorporating Defense-In-Depth (DID) through active and/or passive means to cope with Design Basis Accident. The three fundamental safety functions namely (1) control of the reactivity; (2) removal of residual heat from the fuel; (3) confinement of radioactive material and control of operational discharges, as well as limitation of accidental releases are implemented in the design.

The DID approach implemented for PHWRs provide a graded protection against a large variety of transients, incidents and accidents, including equipment failures and human error within the plant and events initiated outside the plant. The levels are intended to be independent to the extent practicable. The general objective of DID is to ensure that a single failure, whether an equipment failure or a human failure, at one level of defense, and even a combination of failures at more than one level of defense, does not propagate to jeopardize DID at subsequent levels. The independence of different levels of defense is crucial to meeting this objective. There are five levels defined for DID. Following are the level description and their engineering implementation for PHWR.

Level-1: Prevention of abnormal operation and failures -

Conservative design and high quality in construction and operation are introduced for level-1. The objective of the first level of defense is the prevention of abnormal operation and system failures. At this level of DID, regulatory guides are used for the detailed design of PHWR. Various national and international codes and guides are also referred for the design. The emphasis throughout is to produce a robust design having sufficient safety margins so as to ensure safety under all normal operating conditions throughout the design life. Strict control is exercised during the manufacturing and commissioning processes to assure the reproduction of intended design.

Level 2: Control of abnormal operation and detection of failures -

Control, limiting and protection systems and other surveillance features are provided for level -2. The second level of defense will detect these failures, to avoid or to control the abnormal operation. At this level of DID, systems and procedures are in place for PHWR to detect abnormal conditions and controlling them so as to minimize deviation from normal operation.

Level 3: Control of accidents within the design basis -

Engineered Safety Features (ESFs) and accident procedures are provided for level - 3. Should the second level fail, the third level ensures that the Engineered Safety Features will be performed by activation of specific safety systems and other safety. For PHWR there are dual system for reactor protection namely Shutdown System- 1 &-2 and Emergency Core Cooling System and Containment cleanup systems.

Level 4: Control of severe plant conditions, including prevention of accident progression and mitigation of the consequences of severe accidents. Should the second and third level fails, the fourth level actions ensure the all three safety functions are maintained with external means. For PHWR provision of Fire Fighting Water (FFW) injection into Steam Generator, Primary Heat Transport System, Calandria and Calandria Vault takes care of control of severe plant condition.

Level 5: Mitigation of radiological consequences of significant releases of radioactive materials, Off-site emergency response procedures to implement counter measures in public domain in case of offsite release of radioactivity are available for all Indian PHWR units

As a part of Level-1 activity of DID, Postulated Initiating Events (PIEs) are analyzed to ascertain adequacy of various safety systems those are designed to mitigate consequences arising from Design Basis Accidents (DBAs). The PHWR PIEs for DBAs include Control rod withdrawal, Loss of Coolant Accident (LOCA), Main Steam Line Break, Station Blackout for limited period, LOCA with failure of Emergency Core Cooling System etc. There are postulations of Beyond Design Basis Accident (BDBAs) which considers failure of multiple safety functions like LOCA with failure of shutdown system, LOCA with failure of ECCs and SBO, unmitigated SBOs etc. Some of the BDBAs can lead to sever accident where core melt down is expected.

As mentioned in DID, consideration of severe accidents for a nuclear power plant (NPP) is an essential component of the defense-in-depth approach used in nuclear safety and its importance has been realized during the major severe accidents namely TMI-2, Chernobyl and Fukushima. Severe accidents have a very low probability, but may have significant consequences resulting from nuclear fuel degradation. As severe accidents involve very complex physical phenomena that take place during various stages of accident progression, a systematic severe accident study is essential to understand the phenomena. The study includes related experimentation to understand the physics of the phenomena, formulation of a mathematical model, development of computer code for accident analysis and prediction of accident behaviour with the analysis code. Based on the acquired knowledge from the experiments, physical models for each such phenomenon are developed which are incorporated in Severe Accident Analysis computer programs. The codes are used as a tool to support engineering judgment, based on which specific measures are taken to mitigate the effects of severe accidents. They are also used to determine accident management strategies and “source term” estimation.

Some of the Beyond Design Basis Events (BDBE) for Pressurized Heavy Water Reactors (PHWRs) may lead to core damage where core geometry is expected to be damaged. This comes under the category of Severe Core Damage Accident (SCDA) [1]. To mention some of the events which may lead to SCDA, like Station Black Out (SBO) without heat sink, Loss of Coolant Accident (LOCA) along with Loss of Emergency Core Cooling System (ECCS) and unavailability of moderator heat sink etc. Although a substantial progress has been achieved in the understanding of severe accident scenario in Pressurized Water Reactors (PWRs), a lot remains to be done in this respect for PHWRs. PHWRs have several distinct design/inherent features of which limit the scale of fuel heat-up and slow down the accident progression to a large extent. However without operator's mitigation support on a longer time frame the mentioned scenarios will lead to a severe accident situation [1]. Of particular relevance to this work is the Severe Core Damage Accident scenario in PHWR, where reactor channels are postulated to slump into the Calandria bottom and form a heat generating terminal debris bed which continues to get heated from its decay power.

The specific motivation to this work originates from efforts to characterize the thermal-hydraulic behaviour of PHWR specific debris bed which is expected to be much different from the debris bed considered for severe accident analyses for Pressurized Water Reactor. The experiments carried out for PWR heat-up study post TMI-2 accident and physical models developed later are not envisaged to be suitable for analyzing the heat-up behavior for PHWR debris bed. The PHWR channel heat-up experiments indicate that the PHWR debris may consists of predominantly long segmented reactor channels with intact fuel bundle inside the channels which will provide the decay heat for boiling the moderator housed in Calandria. In comparison to the PHWR debris bed, the PWR debris bed comprises of 5-6 mm heat generating spherical and non-spherical particles which gets formed from Molten Fuel Coolant Interaction (MFCI) phenomena between the molten corium jets/drop coming in contact with lower plenum water. This kind of debris was evident during post TMI-2 investigation and subsequently in various MFCI experiments carried out for PWR. The PWR debris bed configuration is considered to be predominantly constituted with spherical particles as compared to long tubular debris bed for PHWR.

Information generated from the PWR experimental/analytical studies on debris bed heat up and quenching is largely used for planning Severe Accident Management Guidelines (SAMGs) [2, 3]. The guidelines are usually built after studying the heat-up and quenching behaviour for taking decision on (a) state of reactor suitable for injecting water and associated time frame to mobilize the hook ups (b) success of water injection for debris quenching (c) hydrogen generation and deciding numbers and positioning of hydrogen recombiners. The heat-up and quenching behaviour are also being used on deciding the accident "Source term" as the fission product settlement and revaoprisation are decided by both the factors. On a similar line PHWR experimental/analytical study is formulated to generate insight for formulating the Technical Basis document for SAMGs on the above mentioned line.

The objective of the doctoral work is to investigate the heat-up pattern of debris bed specific to PHWR and develop related physical model for the same. It is aimed that the study can bring out an understanding of two phase flow pattern of the heat generating debris bed and channel heat-up pattern for the submerged and exposed channels. These generated insights help to formulate a physical model which can model PHWR specific debris bed in a better way for formulating a PHWR SAMGs.

The scope of the work is distributed in two parts. Under the first part, experimental investigations are planned. This includes setting up of (i) a small experimental setup to investigate the heat-up behavior of a submerged single reactor channel in isolation, which is a constituent of the debris bed and (ii) a scaled down experimental setup which is constituted of several segmented reactor channels to investigate PHWR-specific debris bed. Analytical studies are planned in the second part. This includes (i) development of physical models with the generated information from the above mentioned two experiments (ii) development of a computational model from the physical model and it's validation with the multiple channel debris bed experiment and (iii) application of the model for a PHWR based plant.

The thesis is organized as follows,

Chapter 1 introduces the topic and gives a brief overview of the work. This chapter also describes the key design characteristic of PHWR, brief description of PHWR and description of severe accident phenomena for PHWRs. As the study revolves around of PHWR design and its associated severe accident, hence brief descriptions of both design and accident progression as envisaged are provided.

Chapter 2 gives an overview of the existing study so far carried out to characterize the distinction between PWRs and PHWRs debris bed and connects the proposed study to bring out the relevance towards the proposed investigation for PHWRs. The chapter also discusses the models used for conductive, convective and radiative heat transfer for debris bed.

Chapter 3 describes the experimental program for a segmented single channel and multiple segmented channel debris bed experimentation and its observation on boil-off pattern and inferences. The experimentation also looks into local dry out phenomenon from counter current flow limitation as evidenced for PWR debris bed. The experimental data enables to develop heat transfer coefficient correlation for partially/fully submerged channel. The behaviour of effective conductivity and convective heat transfer coefficients with debris interior temperature has been studied.

Chapter 4 presents physical models development for predicting the PHWR specific debris bed heat-up which is based on the information generated from the experimental work. Estimation of temperature transients of submerged and exposed reactor channels are predicted with 2-D (r,z) transient conduction model of the debris bed with closure relations like effective conductivity, convective and radiative heat transfer. For the application of the model to reactor problem the model has been extended with more numbers of structures simulating End Shield and Calandria Vault. Heat transfer to the structures is accounted with 1-D transient conduction model. Available closure relations like convective and radiative heat transfer for these structures are used for predictions of their heat-up. The continuity of heat transfer between debris bed-Calandria-End shield/Calandria Vault-containment has been ensured. Boil-off of End-shield and Calandria Vault water are modeled with control volume approach where energy equations are solved to estimate the steam generation rate and drop in level. The chapter also describes the validation of the debris bed model with multiple channel debris bed experimental data. The influence of sensitive parameters effective conductivity and convective heat transfer coefficient which govern the debris bed heat transfer are identified.

Chapter 5 describes the application of the developed computer code **D**ebris **B**ed **H**eat **U**p **A**nalysis (DBHUA) for large IPHWR (540 MWe PHWR). A Station Black Out scenario has been selected for the analysis. The analysis has been carried out in two parts. In the first part, the early phase of degradation has been analyzed with code RELAP5/mod 3.4 and taking the input from the early phase analysis the late phase analysis for debris bed heat-up has been carried out with code DBHUA. The calculation predicts the Calandria integrity during this accident. The early and late phase simulation provides the analysis for entire severe core damage scenario under SBO in PHWR.

Chapter 6 summarizes major achievements of the present work. Suggestions for future work are also included.

1.1 Design Characteristic of IPHWRS

IPHWRs have several inherent safety related characteristics of PHWRs which are helpful in a severe accident scenario. The first is concerning prompt criticality. A low excess reactivity maintained due to on power refueling and the presence of two independent fast acting shutdown systems of diverse nature helps to prevent the reactor to become prompt critical during reactivity insertion accident.

Secondly, due to the separation of the high pressure, high temperature coolant circuit and the low pressure, low temperature moderator system, the reactivity and shutdown mechanisms in the moderator are unaffected by the disturbance in the coolant loop. This is contrary to severe accident scenario of PWRs where the fuel heat-up melts down the shutdown system at very early stage of accident progression. Further, a large inventory of sub cooled moderator surrounding the reactor channels provides an effective heat sink under some accident scenarios, so accident progression to severe core damage depends on the availability of the moderator and heat removal by the moderator cooling system. It has been envisaged that water surrounding the Calandria in Calandria Vault system can further hold the reactor channels in debris within the Calandria in a severe accident scenario. This prevents the corium debris falling on the concrete floor which can lead to core-concrete interaction under severe accident.

1.2 Brief Description of PHWRs [4]

There are two kinds of PHWRs exists in India. The small 220 MWe PHWR based power plants are more in number as of today as compared large 540MWe PHWR. In addition, design of 700 MWe PHWR is under licensing stage. The following sections describe some of the important features of these reactors related to this work.

1.2.1 Reactor and auxiliary

Reactor Channels

The 220 MWe and 540 MWe PHWR reactor core has several reactor channels in parallel. Fig. 1.1 shows the schematic of a reactor channel. These reactor channels span the Calandria horizontally between the two End-shields and are located within two equal figure-of-eight loops. For 540 MWe the tow loops can be isolated from each other under certain accident conditions. Each reactor channel consists of a zirconium/niobium alloy pressure tube surrounded by a zircaloy-2 Calandria Tube with CO_2 gap (annulus gap) in between. Each reactor channel contains twelve fuel bundles for both 220 MWe and 540 MWe. The fuel bundles are made up of 19 and 37 fuel pin elements for 220 MWe and 540 MWe respectively. Each fuel element consists of zircaloy-4 tubes containing natural UO_2 pellets. The reactor channels exhibit a large variability in total channel powers and in axial bundle powers.

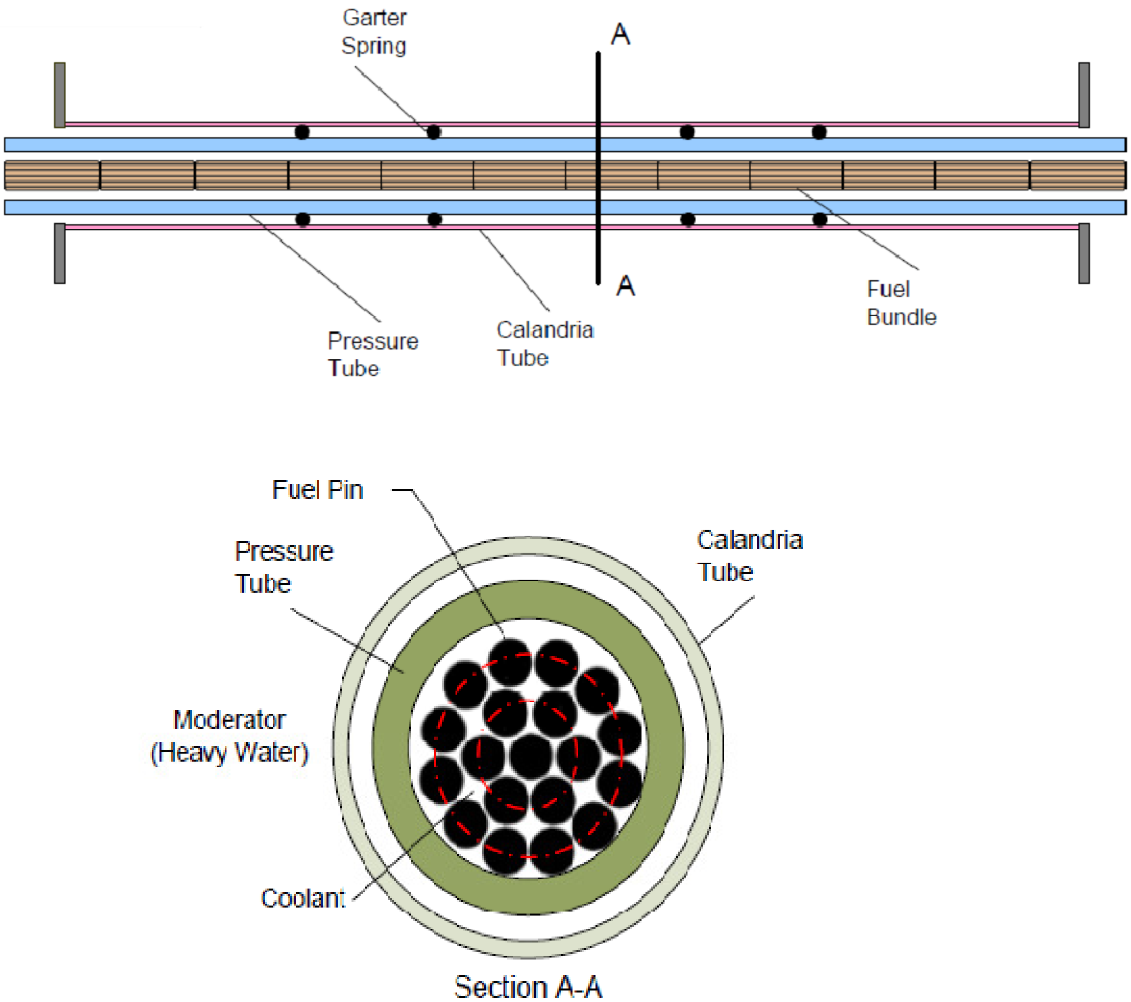

Fig. 1.1 : Schematic of a PHWR Reactor Channel

Calandria

The Calandria houses the reactor channels that span it horizontally and reactivity mechanisms that span it vertically (Fig. 1.2). The moderator system is fully independent of the heat transport system. The moderator system includes two pumps and two shell and tube heat exchangers. The moderator system head tank maintains the moderator level in the Calandria within the required range by accommodating moderator swell and shrink resulting from temperature fluctuations. The heavy water in the Calandria functions as a heat sink in the unlikely event of a loss of coolant accident coincident with failure of ECCS. The capability of this heat sink is assured by controlling the heavy water temperature in the Calandria within specified limits.

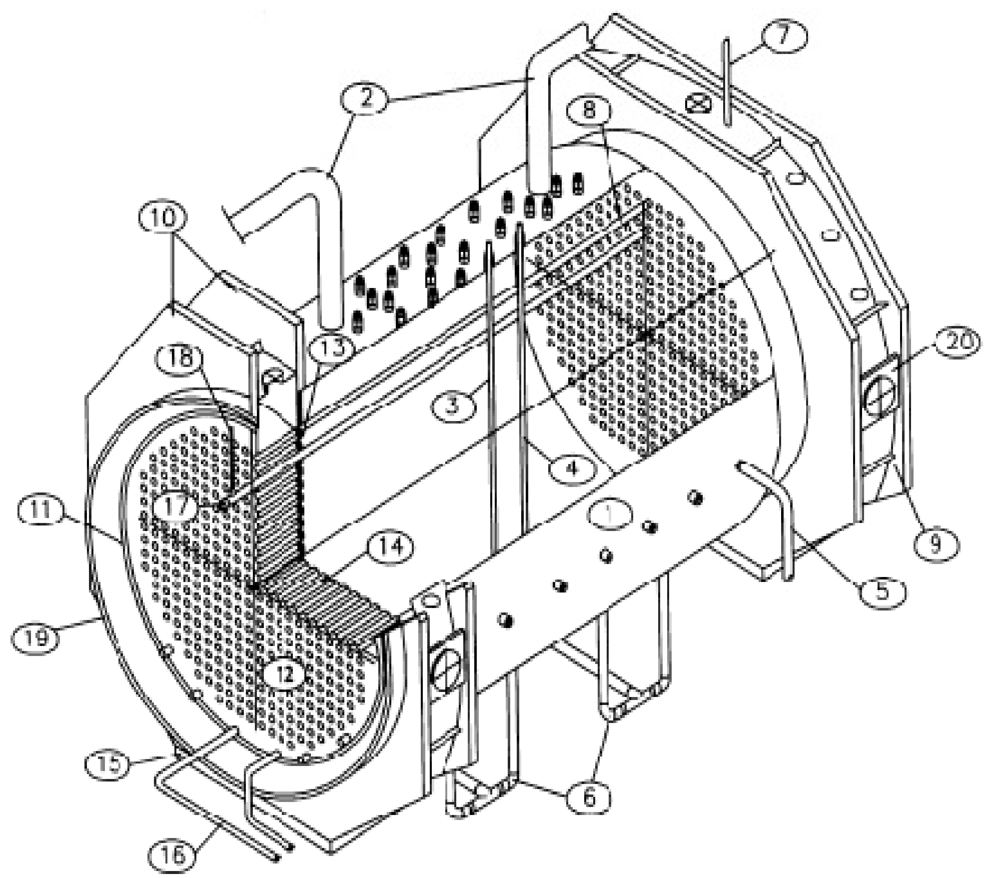

1. Calandria shell	2. Over Pressure Relief Device	3. Shutdown
4. Shutdown System #1	5. Moderator Inlet	6. Moderator Outlet
7. Vent Pipe	8. Reactor Channel Assembly	9. End Shield (ES)
10. ES Support Structure	11.Main Shell Assembly	12. Tube Sheet Fuelling Machine (F/M) Side
13. Tube Sheet Cal. side	14. Lattice Tube	15. ES support plate
16. ES Cooling Inlet	17. End Fitting Assembly	18. Feeder Pipes
19. Outer Shell	20. Support	

Fig. 1.2: Schematic of Calandria with all components

End shields

The two End-shields are integral parts of the reactor assembly. Each End shield is a cylindrical shell bounded by the Calandria tube sheet (Calandria side) and the fuelling tube sheet (Fuelling Machine side) and spanned by reactor channels. To provide biological shielding and cooling, the End shields are filled with carbon steel balls and demineralized light water cooled by the End-shield cooling system. The end-shields are not part of the moderator pressure boundary, but may provide a thermal barrier to severe accident progression by resisting thermal attack by any debris contained within the Calandria shell under severe accident conditions. The End-shields share a common cooling system with the Calandria Vault. When the corium pool level is high, the molten corium may overflow from the main shell of the Calandria into the sub-shell and contacts the Calandria Tube sheet which is in contact with the end shield. Then the tube sheet will be easily heated up and may fail, allowing a molten corium to flow into the end shield which is filled with steel balls. It is not expected, however, that the corium will be released into the fuelling machine room after melting all of the steel balls in the end shield.

Calandria Vault

The Calandria Vault is built of ordinary concrete and is filled with light water which functions as a biological shield under normal operating conditions and may act as a passive heat sink under certain severe accident scenarios. For example, if hot dry debris is collected in the bottom of Calandria after core disassembly and heats up, the Calandria Vault water may remove the decay heat from the Calandria through the Calandria wall. External vessel cooling considered to be an important accident management programme in PWRs, whereas in PHWR external cooling by Calandria Vault water is in its inherent design.

The Calandria Vault floor has a significant spreading area for any potential core debris. The schematic of the vault is shown in Fig. 1.3. The corium pool formed in the Vault will not touch the Calandria. There are two layers of concrete below the Calandria Vault floor. The thick concrete floor provides a significant time (many days) for ablation by the hot molten debris. Reactor building ventilation system provides venting of Calandria Vault, End shields, and delay tanks. In addition to this venting, rupture discs are provided on the combined vent lines to relieve over pressure caused by boiling of the Calandria Vault water.

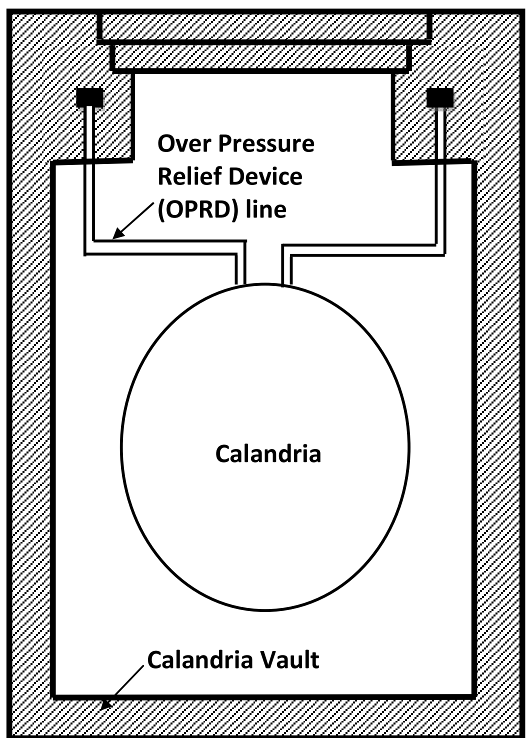

Fig. 1.3 : Schematic of Calandria housed in Calandria Vault

End Shield cooling

The end-shield cooling system is common to the two-end-shields and the Calandria Vault. The coolant flow is modulated through its heat exchangers to maintain specified temperature distributions in the end-shields and the Calandria Vault. At normal full power operation, the re circulated cooling water removes the anticipated cooling load of about 7.3 MW for 540 MWe. While lower than the decay heat under normal conditions, the heat removal capacity is enhanced under higher coolant temperatures. For example, if a loss of moderator cooling contributes to a severe core damage and dry hot debris in the Calandria, the heat removal by the shield water cooling system becomes the dominant heat sink and is expected to successfully do so at elevated water temperatures.

1.2.2. Primary heat transport system

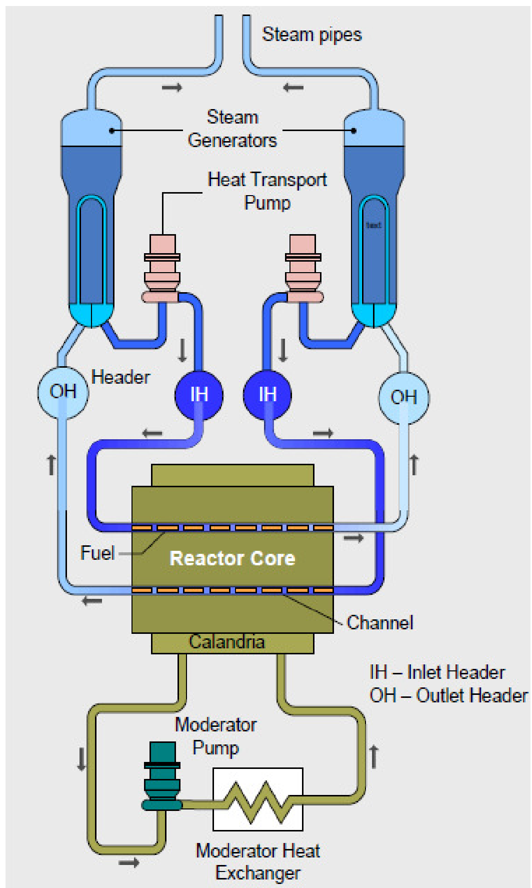

Fig. 1.4: Schematic of Primary Heat Transport and Moderator Circulation System

A standardized 220 MWe Indian PHWR has 306 horizontal reactor channels in a figure-of eight loop configuration, with one pair of steam generators and pumps in each bank of Primary Heat Transport System (PHTS) loop. The schematic of Primary Heat Transport and Moderator Circulation System is shown in Fig. 1.4. A 540 MWe PHWR has two PHTS loops with 392 reactor channels. Each loop has one pair of steam generators and pumps. These two loops are connected by a Pressurizer which controls the pressure of both the loops.

1.2.3 Emergency Core Cooling System (ECCS)

The ECCS assures fuel cooling following a loss of coolant accident by refilling the core and re circulating coolant through the core for long term heat removal from the fuel. The heat picked up by ECCS water is rejected to the process water in the ECCS heat exchangers. In the Indian 220 MWe PHWRs, the ECCS incorporates (a) High pressure heavy water injection (b) Intermediate pressure light water injection and (c) Low pressure long term recirculation. The high pressure heavy water injection is provided by a system of accumulators containing D_2O pressurized by nitrogen. Intermediate pressure light water injection is provided by a system of two accumulators and a pressurized nitrogen gas tank. When the PHTS pressure falls further, low pressure light water injection occurs, followed by recirculation provided by pumps. Injection of ECCS water takes place through two of the four headers, which are selected on the basis of the size and location of the break [4].

1.2.4 Shutdown systems

Indian PHWRs have two diverse, passive shutdown systems which are independent of each other. In a typical 540 MW(e) unit (a) Primary Shutdown System (PSS) -1 consists of 28 cadmium sandwiched stainless steel rods of worth 72 mk (Fig. 1.5), which move into the low pressure moderator system, and (b) Shutdown system -2 injects liquid poison into the moderator.

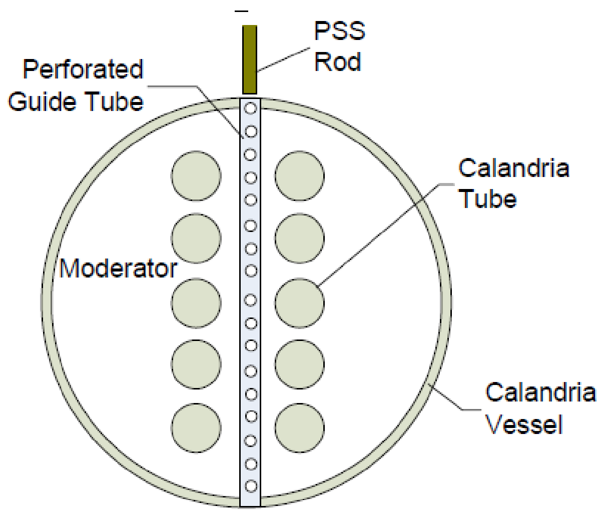

Fig. 1.5: Schematic of shutdown system-1

1.2.5 Containment system

Double containment is employed in Indian PHWRs and the containment structures are of concrete. A typical double containment structure of 540 MWe [4] is shown in Fig. 1.6. The primary containment is a pre-stressed concrete structure, consisting of a perimeter wall topped by a pre-stressed concrete dome. The outer or secondary containment envelope is a reinforced, cylindrical concrete wall topped by a reinforced concrete dome. The primary containment uses an epoxy coating to form a liner for added leak tightness and ease of decontamination. Primary containment houses reactor and its various associated systems. In case of postulated loss of coolant accident, the containment holds the fission products released from the reactor and/or its coolant in such a way that the release of fission products to the environment is within the acceptable and prescribed limits. The secondary containment does not house any plant system. The high enthalpy steam lines passing through the secondary containment space are designed to pass through pipe sleeves to eliminate the need for designing the secondary containment for postulated pipe break of steam line resulting in internal pressure and temperature loading.

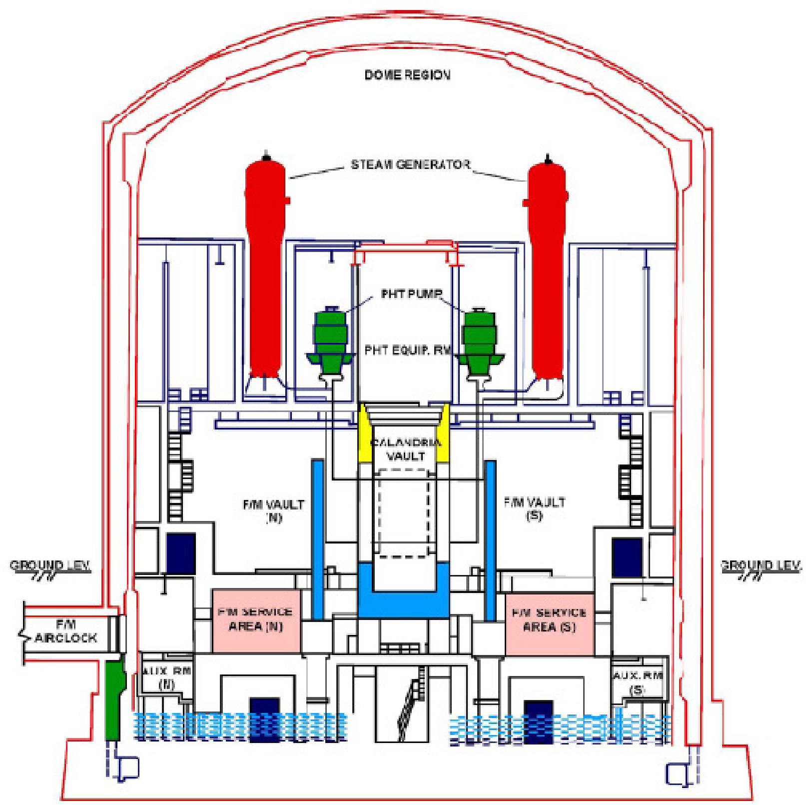

Fig. 1.6: Schematic of Double containment for 540 MWe PHWR

The nuclear containment structures provide biological shielding to limit the radiation dose to the public and plant personnel in the case of design basis accidents. The annulus between the two containment walls is maintained under vacuum with a provision of continuous monitoring for any accidental release of fission products to the annulus space from the inner primary containment. This double containment design ensures almost zero ground release to the environment. Another notable feature of the containment structure is that the double barrier also serves to effectively resist external and internal missile impact loads.

1.3 Description of Severe Accident Phenomena for PHWRs [1]

For a PHWR, accidents that could result in damage to the reactor core fall into two classes — those for which the core geometry is preserved, Limited Core Damage Accidents (LCDAs), and those for which the core geometry is lost, Severe Core Damage Accidents (SCDAs) [1]. The LCDAs can involve single reactor channels or the entire core. For example a feeder break can result in overheating of the fuel in the affected channel or a LOCA with loss of ECCS could lead to widespread fuel damage. In both cases, however, the presence of the moderator as a secondary heat sink prevents failure of the reactor channels and core degradation. In this sense, the LCDAs are distinct from accident sequences for a LWR as they can involve fuel damage without core relocation. For an accident to proceed to severe core damage there must be multiple reactor channel failures leading to significant core degradation. Such a situation in a PHWR is possible only if the heat sink of the moderator is lost. Typically, SCDA initiates as a LCDA, but unavailability of moderator cooling and makeup to remove heat leads to moderator boil off, allowing uncovered reactor channels to heat up and fail. Thus the early stages of a SCDA for a PHWR are different from those of a LWR where the presence of the heavy water moderator slows down the progression of core disassembly. Once the core has become fully disassembled and has collected at the bottom of the Calandria, subsequent behaviour is likely to be different as the debris bed consists of long channels to that in a LWR with the core relocated into the lower vessel head.

1.3.1 LCDA –full core events

Extreme scenarios for this family of accidents is LOCAs with loss of ECCS that typically involve core voiding, fuel overheating, fuel and reactor channel deformations at moderate and low PHTS pressures, hydrogen generation and release of fission products from the fuel. Deformation of the reactor channel creates heat transfer paths from the fuel to the moderator, thereby limiting the consequences.

1.3.1.1 Thermal-hydraulic behaviour

The early stages of a full core LCDA are dominated by the blowdown behavior (refer Fig. 1.7). The transient will start with a pulse in reactor power as the voiding coolant has a positive feedback on reactivity. This pulse is quickly terminated by shutdown of the reactor and adds to the stored energy in the fuel at the start of the transient. A characteristic of PHWRs is the figure of eight configuration for the PHTS. For a LOCA, the pass with the break will start depressurizing first, followed by the unbroken pass.

Once the PHTS has depressurized, the remaining liquid coolant boils off, and the resulting steam flows out the break. The flows in the primary system can be complex with buoyancy forces and steam-induced pressure gradients producing inter-channel flows through the connections provided by the headers. When steaming ceases, the remaining vapor in the PHTS, consisting of steam and hydrogen, continues to flow driven by buoyancy forces. Not much hydrogen is produced, because there is no fresh steam available to maintain the Zircaloy oxidation. Fission products released from the fuel are distributed through, and largely retained in, the PHTS during this stage. It follows from the preceding explanation that appreciable amounts of fission products and hydrogen are released from a break in the PHTS only during the period when liquid water is available below the reactor headers. The duration of this period is accident-scenario specific.

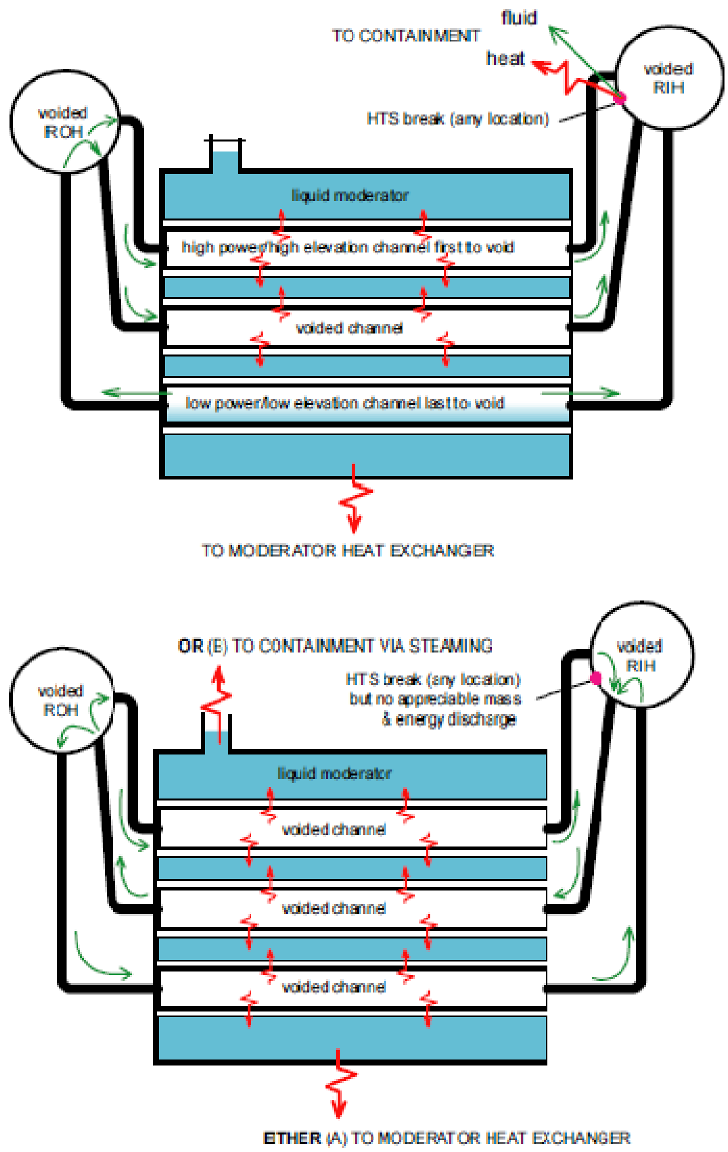

Fig. 1.7: Thermal Hydraulic Behaviour in a Full Core LOCA

Large LOCAs with their flashing-induced, early voiding of the PHTS will have a short period. Small LOCAs with a boil-off induced voiding of the PHTS will have a longer period, but at low decay power levels and correspondingly modest peak fuel temperatures. If the fuelling machines are connected to the reactor during a LCDA, they form part of the primary heat transport system, and are therefore subject to the depressurization transient. In the longer term, any fuel in the fuelling machine will heat up, and in the absence of the secondary heat sink provided by the moderator, the hot fuel can breach the fuelling machine boundary and provide a release path to containment for the fission products and any hydrogen generated in the fuelling machine. A special consideration for assessing the consequences of a LCDA is the presence of pre-existing leaks in steam generator tubes. These leaks provide a path beyond containment for any portions of the transient where the secondary system is not isolated.

1.3.1.2. Fuel behaviour

In a LOCA with loss of ECCS, the fuel is at decay power and the PHTS pressure is reduced. As the residual liquid in the reactor channels boils off the fuel bundles become uncovered. While there may be an initial spike in fuel temperatures due to the pulse in reactor power, the fuel does not reach very high temperature until most of the water has been removed. Certain large breaks can cause rapid voiding of channels in a portion of the core. Under these conditions there could be rapid heat-up of the voided channels, but most accidents in whole core LCDA category start with the boil-off of stratified coolant.

During the early stages of a LOCA with loss of ECCS, changing thermal-hydraulic conditions can result in flow reversals that forcibly translate the fuel bundles within the reactor channel. Since the fuel is still relatively cool, break-up of the fuel bundles is not expected. As the accident proceeds, the fuel will heat up and axially expand. If there is not enough free axial gap, the expansion will be constrained, leading to deformation and possible break up of fuel bundles. As a channel voids, the uncovered fuel heats up in steam. When the fuel reaches sufficiently high temperatures, the chemical heat released by the exothermic reaction of steam with zirconium-alloy fuel sheath supplements the decay heat. Convective heat removal from the channel by a mixture of superheated steam and hydrogen is small, and the fuel is cooled mainly by thermal radiation to the surrounding pressure tube. Therefore, for severe temperature excursions, the hottest fuel rods are in the interior of the fuel bundle because these rods radiate to hot, surrounding rods instead of to a relatively cool Pressure Tube wall. Fuel and Pressure Tube temperatures continue to increase until a heat balance is reached where the heat generated in the fuel is removed by the steam flow (a smaller fraction) and radiation/conduction to the externally cooled Calandria Tube (a larger fraction). The transient is complicated by deformation of the fuel and the Pressure Tube, which alter the heat conduction paths as well as the hydraulic characteristics of inner sub channels in the fuel bundle. Peak fuel rod temperatures are reached around the time the fuel bundle starts slumping. The values of peak temperature are accident-scenario specific. The interior of high-power fuel bundles could reach the Zircaloy melting point if the channel were to void rapidly and remain voided thereafter. The additional energy deposition into the fuel caused by the positive void reactivity feedback before the reactor is tripped contributes to high fuel rod temperatures. In the long term, the temperatures decrease slowly with decreasing decay power. A redistribution of stored energy in the fuel after the reactor is shutdown, and the fuel temperature rise later on, lead to fission gas release from the fuel grains and grain boundaries to the fuel-to-cladding gap. This increases the internal pressure in the fuel rod.

Hot fuel cladding will balloon due to the difference between the internal gas pressure and the coolant pressure. The free volume in a PHWR fuel rod is relatively small, and therefore ballooning in a localized region with the highest cladding temperature will balance the internal and external pressures. The fuel cladding may fail during ballooning by various mechanisms, including over-strain, oxide cracking, oxygen embrittlement and beryllium-braze crack penetration. The ballooning of fuel cladding causes some flow area obstruction. Following ballooning, the fuel pellets relocate to the bottom of ballooned fuel cladding and cracking during the temperature excursion may lead to further relocation of fuel fragments. Prolonged exposure to high temperatures causes sagging of the fuel rods and deformation of the softened end plates. While end plates may maintain some spacing between the ends of fuel rods, within a short distance, the fuel rods sag into contact and fuse with each other [5–7]. For very high temperature excursions, the bundle becomes a coarse debris pile at the bottom of the Pressure Tube. The fuel pellets are retained in perforated and oxidized cladding shells. All distorted bundle geometries impede access of steam to the interior subchannels, which reduces the energy contribution from Zircaloy oxidation. Gross fuel bundle deformation is accompanied by thermal-chemical interactions of UO_2 and Zircaloy, particularly if the peak temperature approaches the melting point of Zircaloy. Limited amounts of molten material may be formed due to interaction between UO_2 and Zircaloy below their melting points, depending on the interface temperature and contact pressure. UO_2/Zircaloy interaction also leads to reduction of the fuel as uranium oxide fuel dissolves in molten Zircaloy. Experiments show that surface tension forces retain the small amounts of liquefied materials in the inter-element voids. Some molten material (largely from the end caps and end plates) may relocate onto the Pressure Tube, causing intense localized hot spots on the Pressure Tube.

1.3.1.3 Reactor channel behaviour

Small and medium LOCA transients can lead to Pressure Tube heat-up while the internal pressures remain relatively high. The dominant mode of Pressure Tube deformation is ballooning

[8, 9]. If the channels void more gradually, the Pressure Tubes will not heat up until the residual pressure is low. Under these conditions, the Pressure Tube will sag into contact with the Calandria Tube. Upon contact between the Pressure and Calandria Tubes, the stored energy in the hot Pressure Tube augments the heat transfer from radiation and conduction. If there is insufficient subcooling margin during ballooning contact, there can be extensive film boiling on the outside of the Calandria Tube. Under these conditions the temperatures of the combined Calandria and Pressure Tubes can escalate to the point of failure. Such failures are not a concern for sagging contact because any film boiling is localized and does not lead to temperature escalation. Extreme temperature excursions to the Zircaloy melting point result in the relocation of molten metal onto the composite wall of the submerged tube. An unstable dryout patch arises at the point of molten material contact that does not produce any noticeable deformation of the composite tube. If in the longer term, the Pressure Tube is exposed to a hydrogen/steam mixture with very little steam, the protective nature of the oxide layer may be diminished allowing hydrogen to be picked up by the zirconium alloy pressure tube. This hydrogen may embrittle the Pressure Tube, impairing its ability to withstand loads induced at low temperatures, such as those imposed by quenching due to late introduction of emergency cooling.

1.3.1.4 Reactor core behaviour

During normal operation, the local temperature distribution of the moderator is quite complex because of the interplay of the forced and natural circulation fields in a large liquid volume that has significant internal heat generation. After the reactor shuts down, the moderator temperature generally decreases due to the combined effect of temperature homogenization (mixing) and continued heat removal from the moderator with a reduced heat load. The temperature homogenization is rapid and therefore the available subcooling margin is uniform throughout the core. Continued heat removal from the moderator lowers the alternate heat sink temperature in the longer term (tens of minutes).

1.3.1.5. Containment behaviour

The initial discharge of a high-enthalpy coolant from the PHTS is considered as part of the design basis and containment can withstand it with margin to spare. Some designs employ dousing to condense steam and wash out fission products. In the longer term, core decay heat is transferred to the moderator and dissipated through the moderator heat exchangers with no appreciable energy released into the containment. If the moderator heat exchangers are unavailable, and there is make-up to the calandria vessel, decay heat can be removed by boiling of the moderator. Under these conditions, local air coolers in containment prevent any long term pressurization. Hydrogen produced by oxidation of the hot core components will be discharged into containment during the blowdown and steaming phases of the accident. Additional hydrogen will be generated when emergency coolant is eventually injected into the core to restore the internal heat sink. On a long term time scale (days), radiolysis of water pools in containment releases hydrogen at a slow, but sustained rate. Hydrogen released from the PHTS and liquid pools in the containment is dispersed into the containment atmosphere by buoyancy-induced flow patterns, aided by the effects of local air coolers. Depending on the reactor design, the potential for highly energetic hydrogen burns [10, 11] can be diminished through dilution, the use of igniters and passive autocatalytic recombiners.

Current Indian PHWRs use a double concrete containment. The inner containment is a cylinder and dome of pre-stressed concrete, with an epoxy lining for leak tightness. The outer containment is a cylinder and dome of reinforced concrete. The intervening space is maintained at a negative pressure with a purging arrangement. A suppression pool between drywell and wet well volumes in containment is used to limit peak pressures. The suppression pool also provides a source of long term low pressure emergency core cooling. Local air coolers provide pressure control and heat removal, and there is a filtered system for controlled gas discharge in the longer term.

1.3.1.6 Fission product behaviour

Fission products are present in fuel grains, fuel grain boundaries and fuel-to-cladding gap. The proportions of the total inventory in these locations depend on the fuel operating history. The on-power refueling of PHWRs means that there is a broad spectrum of rod fission product inventories in any given channel. Upon failure of the fuel cladding, gap inventories are available for immediate release — the nature of the released fission products depends on their chemical form and associated volatility as a function of temperature [12]. Grain-boundary and fuel-grain inventories releases are driven by temperature-dependent diffusion, or mechanical breakup of the fuel. Once released from the fuel, fission products are carried by thermal-hydraulic flows to the break in the PHTS. A unique aspect of PHWRs is the large surface area of relatively cool metal components immediately adjacent to the reactor channels (i.e. end fittings, feeder pipes and headers) through which the fission products must travel. These assemblies can retain significant quantities of fission products through deposition, or through pool scrubbing if they remain water filled.

The actual transport, deposition and re-suspension phenomena for fission products are not unique to PHWRs [13]. Much of the fuel will remain well below the Zircaloy melting point in LCDAs at decay power. As a result, noble gases and a subset of fission products that could be volatilized at intermediate fuel temperatures (i.e. iodine, cesium, tellurium, ruthenium and strontium) will be the dominant species entering containment. There are no structural materials in the PHTS that could be volatilized in this accident family and complicate the fission product chemistry (e.g. control rod materials are in the liquid moderator, not the reactor channels). The behaviour of fission products in containment is determined by the interactions of aerosol and gaseous species. The radioisotope of primary concern is iodine for its relatively high abundance and biological interactions. A good understanding of the chemical behaviour of iodine in PHWR containments has been developed.

The kinetic processes governing iodine behaviour following an accident are complex. Based on experiments and modeling studies, it has been determined that iodine will be released to containment primarily as non-volatile cesium iodide (CsI), with a small fraction of gaseous species (assumed to be molecular iodine, I_2, for conservatism). While cesium iodide dissolves readily in water forming non-volatile I^-, radiation fields cause radiolytic processes that can form volatile I_2, which will partition from solution to the gas phase. In the gas phase, I_2 can be oxidized to non-volatile iodine oxides (e.g. HOI, IO_3^-) or be reduced back to dissolved I^- by various thermally and radiolytically driven reactions.

Dissolved iodine can also react with organic species to form organic iodides that can also partition to the gas phase. Finally, iodine species can be deposited on surfaces, or participate in surface-catalyzed reactions. The presence of radiation fields in containment (after a postulated accident) prevents chemical equilibrium from being achieved. Instead time-dependent chemical, mass transfer and surface sorption reactions determine iodine behaviour. The rates of these reactions are functions of concentration, radiation dose and dose rate, pH, temperature and impurities.

1.3.2 SCDA Event

The phenomenology of severe core damage accidents is unique to PHWRs until a corium bed is formed at the bottom of the Calandria. The subsequent behaviour of corium is similar to that of LWRs, but there are differences in corium composition (i.e. proportions of UO_2, Zr and other materials) and corium geometry (i.e. debris bed with large number of channels and a surface to volume ratio, which is given by the shape of the Calandria or the containment compartment). A SCDA can result from a LCDA with loss of the moderator heat sink, or from events where loss of primary coolant flow is associated with loss of multiple safety systems. The initial stages of the LCDA are described in Section 1.3.1.

In the latter sequence, the PHTS is initially at full pressure, with heat from the fuel causing pressure rises that are relieved by the instrumented relief valves. Eventually the volumes above the reactor headers are voided, and the upper, high power, reactor channels start to void and overheat. Under the influence of the full system pressure and temperature gradients, one of the voided channels will rupture, depressurize the PHTS, and initiate the automatic injection of emergency coolant from the ECCS accumulator tanks. Once accumulator tanks of ECCS has been depleted the reactor core will continue to heat up in a configuration similar to the late stages of a whole core LCDA.

1.3.2.1. In-vessel phenomena

1.3.2.1.1 PHWR core disassembly

As described in earlier section, as long as the reactor channels remain surrounded by moderator, the core geometry will be maintained. If moderator cooling and makeup are unavailable, the water level in the Calandria will start to drop and uncover the upper reactor channels as shown in Fig 1.8 (a). The moderator level may also drop suddenly for an in-core break (channel break) that leads to discharge of the moderator. Uncovered reactor channels heat up and deform by sagging as illustrated in Fig. 1.8 (b). Eventually, channel segments break off and form a coarse debris bed, which rests on still-intact lower channels [14–16] as shown in Fig. 1.8 (c). This suspended debris bed imposes a load on the channels below and alters the steam flow patterns in the Calandria. In time, the suspended debris also includes materials from uncovered in-core devices. When the weight of the suspended debris exceeds the load-bearing capacity of the reactor channel plane just below the water level, it is envisaged that most of the core collapses into the water pool at the bottom of the Calandria. Only some channel stubs at high core elevations remain in the voided portion of the Calandria. These stubs may join the debris bed later in time. Materials at the bottom of the Calandria are called terminal debris, because they are at their final (terminal) location in the context of the core disassembly.

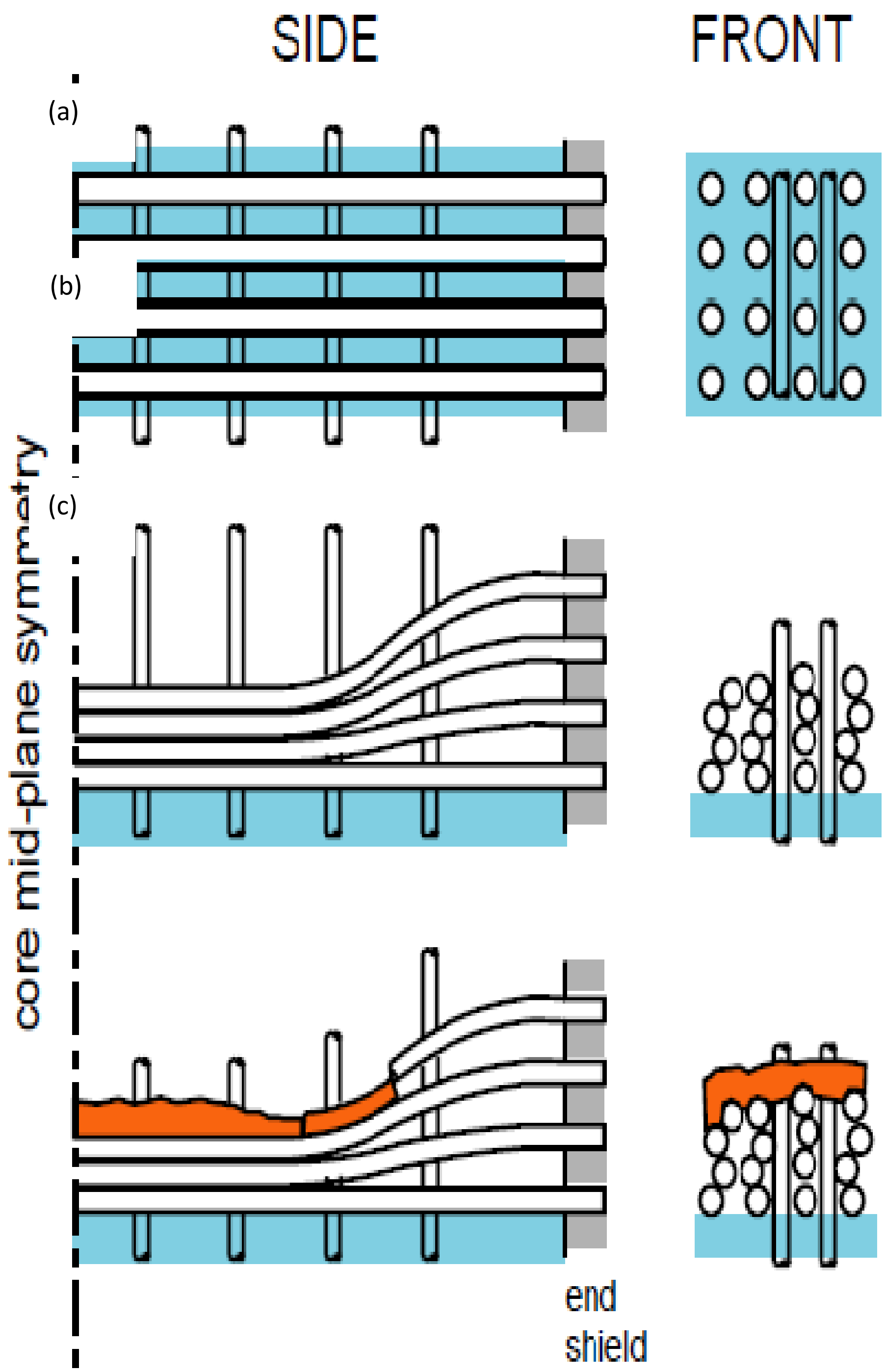

Fig. 1.8 : Conceptual Schematic of reactor channel sagging and disassembly

Perforations of Calandria and Pressure Tube walls allow steam access into the annulus gap, which contains zirconium-alloy surfaces that are not protected by appreciable ZrO_2 layers. Steam also gains access to fuel surfaces within the Pressure Tube, which may have been steam-starved before the channel has broken apart. There is ample supply of fresh steam in the Calandria and the metal channel components are hot at this point in time. Such conditions are favorable to the Zr-steam reaction. The main impediment to a ‘runaway’ reaction is the absence of pressure gradients across the length of channel debris segments to drive the steam into the interior of channels.

Steam supply into the interior of debris is a source of uncertainty for subsequent chemical heat and hydrogen generation rates. Sensitivity analyses show a range of possible thermal responses of the debris bed. At one end of the spectrum, oxidation rates are modest and the debris remains solid until the core collapses. At the other end of the spectrum, chemical heat released within the debris causes the zirconium alloys to melt while the debris is still suspended. Molten cladding is largely retained in the slumped fuel bundle by surface tension forces. Any liquid metal formed in the annulus gap is mobile and can relocate into the water pool at the bottom of the Calandria.

Local zirconium-alloy melt relocation processes (before the liquid metal is spilled from the debris) feedback on hydraulic characteristics in the interior of channels and alter the surface area available for metal oxidation. Further feedback arises due to debris compaction. Hot channels are weight-loaded as well as ‘shaken’ when channels at lower elevations become uncovered and deform, causing the suspended debris bed to shift downwards. All these feedback processes tend to reduce the rate of exothermic oxidation within the debris pile.

A special case of suspended debris is a channel stub at the reactor end shield face, left behind after the channel breaks up. Depending on the accident sequence, these stubs can expose the interior of broken pressure tubes to fresh steam, but little steam enters the annulus gap, which is open on one side only. These stubs invariably contain low-power fuel and can conduct heat laterally to the end shields. Therefore, they can remain solid and suspended for a long time.

There are two modes of suspended debris relocation to the bottom of the Calandria:

(a) Intermittent, small pours of liquid zirconium alloy and/or a dropping of a small mass of fragmented solid debris

(b) A sudden drop of a large mass of hot, solid material

The pours of liquid zirconium alloy are relatively small amounts (kilograms to tens of kilograms) of melt. Upon contact with liquid water, the melt reacts with it and partially oxidizes. The chemical reactivity of the melt makes it highly improbable for the molten material droplets to form a stable suspension in liquid water, which is a precondition of steam explosion. Some hydrogen may generated during the pour. If fragmented, a molten stream solidifies while travelling through water. Otherwise, the stream can reach the Calandria wall where the liquid metal spreads and freezes. There are no particular safety concerns with these small, intermittent pours of reactive, molten metal into water at saturation temperature. A large mass of solid materials relocates rapidly (tens of seconds) when enough suspended debris accumulates above the water level to exceed the load-bearing capacity of the first plane of submerged channels. The load is carried mainly by the Calandria Tubes, which are relatively cool. The thicker Pressure Tubes within the Calandria Tubes are hot and thus weaker. The failure mechanism is Calandria Tube pullout from the rolled joint at the tube-sheet of the Wnd shield. Once the first submerged plane of channels cannot support the weight of the suspended debris, the planes at lower elevations invariably cannot support the load. A ‘cascading’ process occurs in which the load is transmitted to channels below while being increased by the mass of channels just pulled out. The whole core, except the channel stubs left behind during the formation of the suspended debris bed, collapses on a rather short time scale (minutes) into the residual liquid pool. This conceptual event is illustrated in Fig. 1.9. Once the core has collapsed all core materials are under water. The terminal debris predominantly consists of the pulled off channels at temperatures well below the melting point of Zircaloy and the solid channel debris below the melting point of UO_2. The embrittled debris is likely to fragment during the core collapse. The channels that were submerged and failed by pull out, maintain their tubular geometry.

Strong steam surges may arise as the stored heat is transferred to water depending on the channel heat-up condition. The Calandria has four large relief ducts, but even with the large relief flow area, the transient pressurization could pose an integrity challenge. The quenching of long channel segments is complex, because their exterior is not hot and their interior can only be accessed via a limited flow area at the ends of the segments. Eventually, the stored heat in the terminal debris bed is removed by vaporization of water.

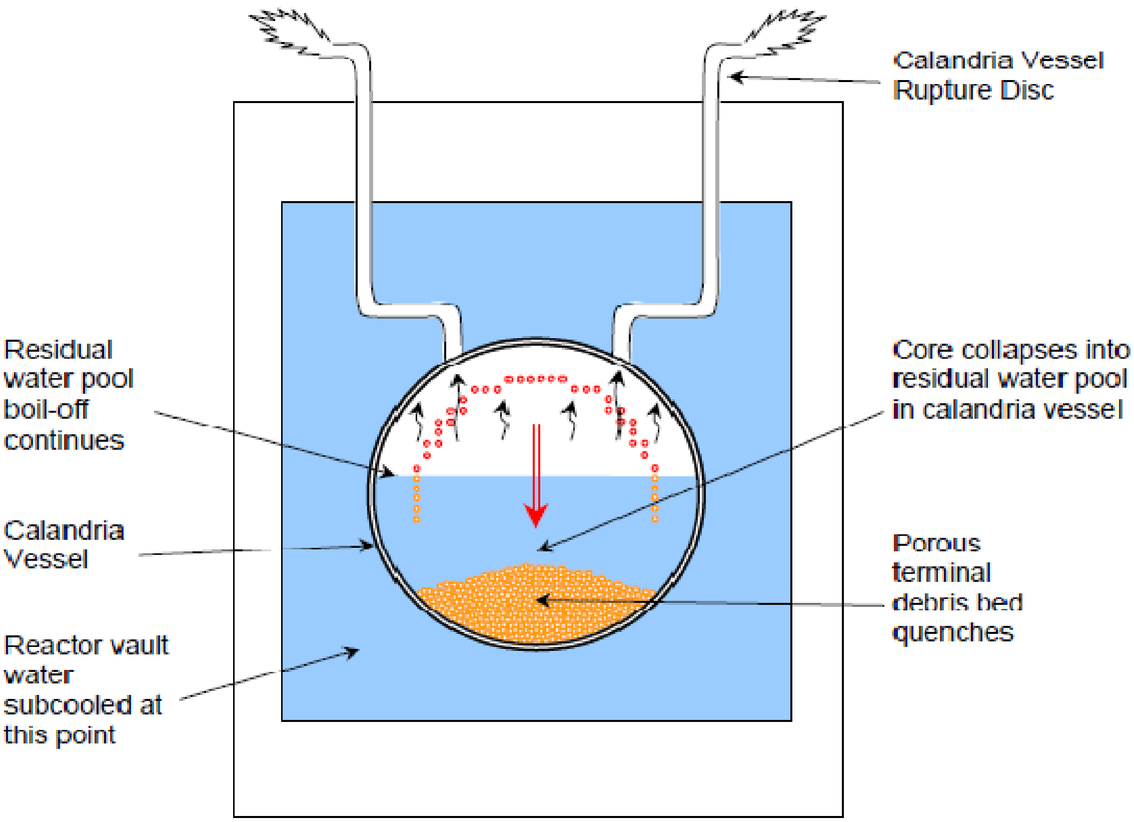

Fig. 1.9 : A schematic showing the collapse of the core into the residual water below

The quenched PHWR specific debris bed is a coarse mixture of ceramic and metallic materials at low temperatures. As water evaporates, this mixture is gradually uncovered. The processes are similar to water boil-off from a reactor channel. Steam flow rates through the debris decrease with decreasing water level, but the uncovered materials do not reach very high temperatures until essentially all water is evaporated. Exothermic oxidation of Zircaloy could come into play during the process of drying out the debris. Eventually, the dry terminal debris reheats in a non-oxidizing environment and compacts. A ‘crucible’ is formed where materials adjacent to the externally cooled Calandria wall and materials at the top of the debris pile are solid. The interior of the crucible may contain molten or liquefied materials (Fig.1.10).

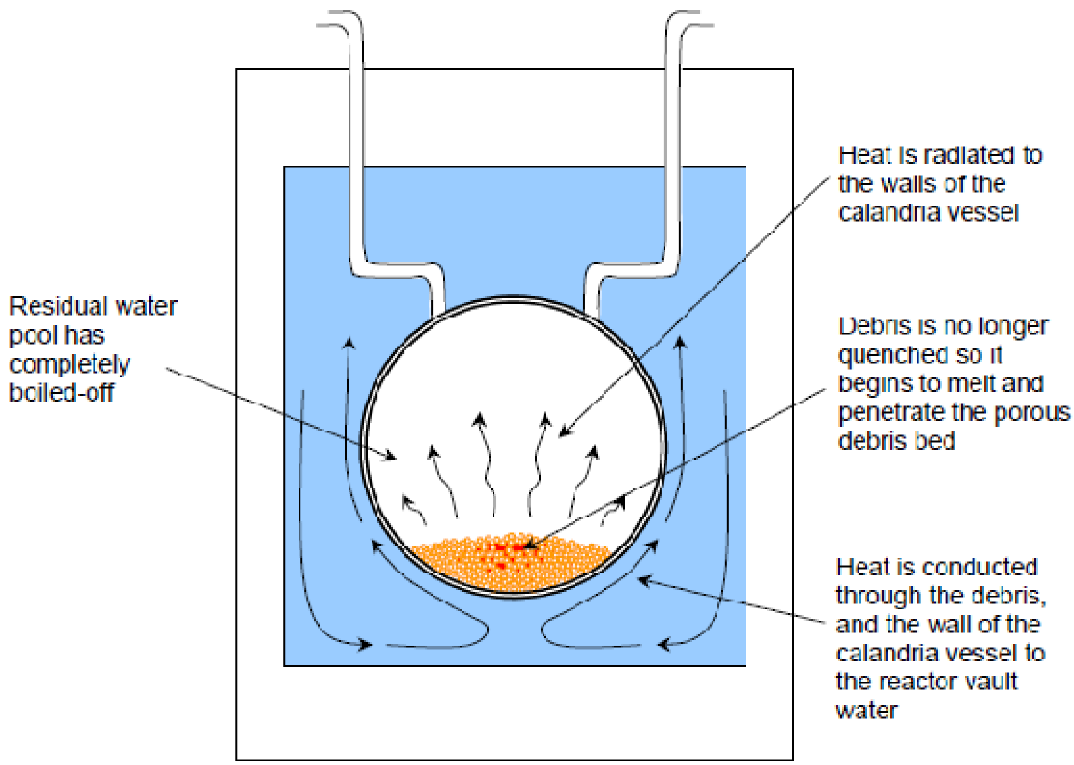

Fig. 1.10: Conceptual Schematic of the debris bed, with beginning of molten corium formation and the evolution of natural circulation in the reactor Calandria Vault water

With the formation of the terminal debris bed, the question of possible re-criticality arises. While the volume of the reactor is smaller, the probability of re-criticality is low because the moderator is boiling off, control rod materials are mixed with the fuel debris and there is a large upper surface area for neutron leakage.

1.3.2.1.2 In-vessel corium retention

Corium can be retained in the Calandria or the Calandria Vault as illustrated in Fig. 1.11.

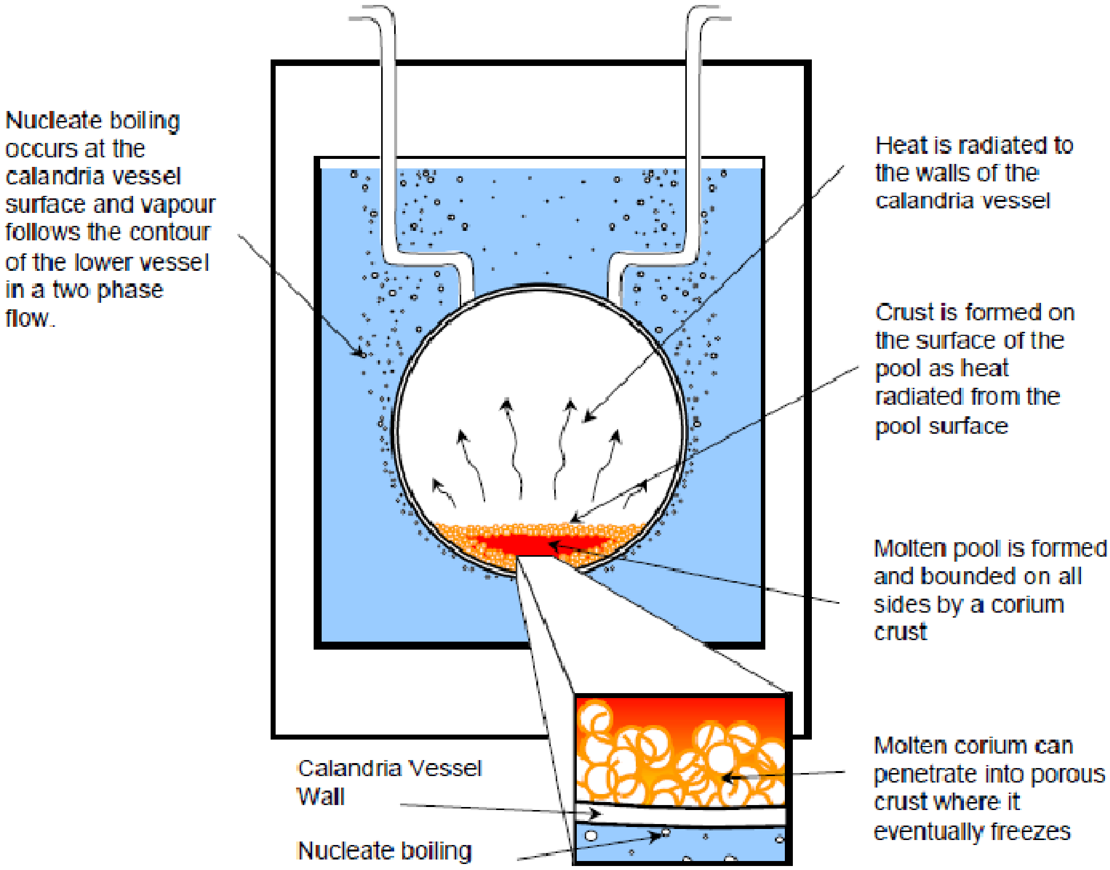

Fig. 1.11 : Conceptual schematic shows the formation of solid crust, which will surround the molten corium on the cooler surfaces of the Calandria

The surface-to volume ratio of the debris bed is large, resulting in low heat fluxes as well as short heat conduction distances within the corium bed. Low heat fluxes avoid possible problems with convective heat removal on the waterside. Water-cooled walls completely surround the top debris surface to ensure effective heat transfer by thermal radiation.

(a)

(b)

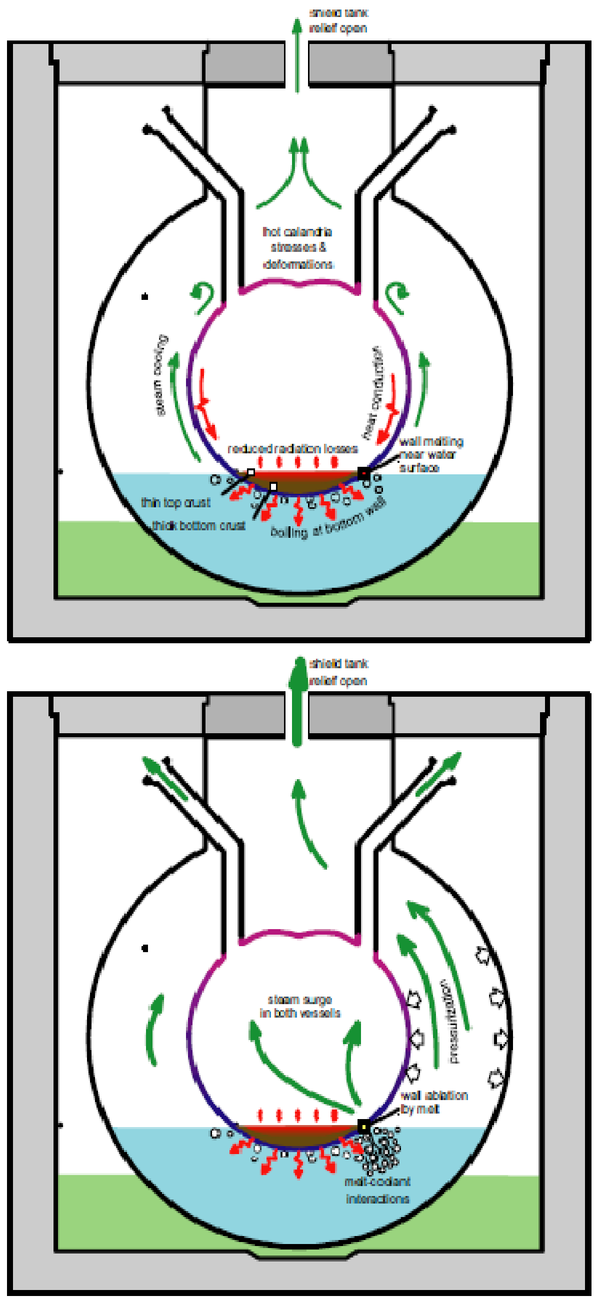

Fig. 1.12: Conceptual schematic for vessel to vessel relocation phenomena

The corium configuration within the Calandria is expected to be stable as two alternate heat sinks are available (i.e. active heat removal by heat exchangers and passive heat removal by boiling and make up). For the corium bed to relocate to the Calandria Vault, the water level around the Calandria must decrease to approximately the elevation of the corium bed surface as illustrated in Fig. 1.12 (a). The relocation of molten corium from the Calandria to the Vault will proceed relatively slowly. The melt pool near the corium surface is not particularly deep (so there is no significant head to drive the melt flow) and the pressure acts in opposition to the melt flow. These conditions can be expected to produce slow transfer rates and moderate steam surges that can be accommodated by combined relief paths of the Calandria and the Calandria Vault. On the other hand, the potential for steam explosions arises as fragmented corium droplets can form quasi-stable slurries in water. If the Calandria Vault survives the integrity challenges brought about by the corium interactions with water, a stable configuration is again reached.

1.3.2.3. Fission product and hydrogen releases

Fission products and hydrogen are released gradually before the reactor core starts to disassemble and in intermittent bursts after the accident progresses into a severe core damage sequence. Steam flow into the debris, which also sets the transport of products from the debris, predominantly affects the releases of fission products as well as hydrogen in these later stages. The boundary conditions in the suspended debris bed are amenable to additional fission product releases from fuel as well as additional hydrogen production. Relatively hot channel materials are reconfigured during the channel disassembly such that heat loss from the debris is limited to that provided by steam/hydrogen flow through the interior. Meanwhile, the availability of fresh steam in the interior produces chemical heat and hydrogen. Temperature excursions of the debris are controlled by how much steam gets into the interior of the debris (i.e. by chemical heat generation). If the steam flow is optimal there could be a temperature excursion to the melting point of zirconium. The coarse debris geometry (i.e. long channel segments) provides mitigating effects to prevent runaway oxidation. The duration of releases from the suspended debris is capped by the collapse of the core under the suspended debris load. Hydrogen will be produced during any relocation of the molten zirconium alloys into the water pool prior to the collapse. Fission product and hydrogen releases are small during the debris quenching and re-heating stages. Volatile fission products have largely been released at this stage of a SCDA. Hence, fragmentation of the fuel during quenching is not an important fission product release mechanism. As noted earlier, temperatures during debris dry-out and reheating are modest such that no appreciable hydrogen is produced. As temperatures rise in the dry corium bed (up to a liquefaction point), the less volatile fission products become mobile, but there are no driving forces (other than concentration gradients at the top surface) to drive vapours from the debris bed. No hydrogen is produced in a dry corium bed that is contained in a metal vessel.

1.3.2.4. Fission product transport

There could be multiple release pathways from a corium-retaining vessel. The principal pathway is through the pressure relief ducts of the Calandria or the relief paths of the two interconnected vessels. The secondary pathway is through an ex-core break in the PHTS, which might lead into containment or outside containment if a containment bypass is the postulated initiating event. Fission products will deposit on metal surfaces of release pathways. A resuspension of the deposited fission products upon any subsequent heat up of the metal walls is then possible. Nevertheless, in the absence of purging gas source in the vessel, the only release mechanism is diffusion through the relief paths, which is negligible on the scale of severe core damage accidents. Hence, any appreciable transport of fission products from the corium containing vessel is during steam surges, which accompany corium motions. Any fission products present in the vessel atmosphere are purged by the steam surge. With the exception of coolant jet and pool interactions, containment transport phenomena are the same as those identified in earlier section for LCDAs. Small amounts of non-fuel materials with low melting points (from in-core devices) might supplement fission product aerosols. However, the aerosol concentrations are still ‘lean’, because there are no mechanisms to produce airborne particles of materials with high melting points that can enter containment. If forced circulation of the containment atmosphere remains available, transport of the aerosols would be dominated by turbulent deposition in the local air coolers and their associated ducts. If forced circulation were unavailable, the distribution of aerosols in containment would be governed by natural circulation of the containment atmosphere.

1.3.2.5. Containment behaviour

Additional hydrogen will be released intermittently during periods of core debris motion in the Calandria, always in conjunction with significant steaming. Hydrogen surges may temporarily produce elevated concentrations in the containment atmosphere. Otherwise containment behaviour is as described for LCDAs.

1.3.3. Ex-vessel phenomena

Accidents involving ex-vessel phenomena must progress through the stages of the in-vessel SCDAs before corium can enter containment. This accident category is typically associated with severe challenges to the integrity of the containment (i.e. generation of non-condensable and flammable gases to pressurize the containment, and degradation of containment structures through interaction with corium) in conjunction with significant airborne fission products burden brought about by the same processes that cause pressurization. Decay of the radionuclide inventory in containment provides an additional heat load. A pressure-induced failure of the containment boundary under these conditions would release large amounts of radioactive materials into the environment. The water inventories of the Calandria and Calandria Vault systems must be evaporated for the corium-concrete interactions to come into play. This vaporization would over pressurize the containment well before the core/concrete interactions could commence, unless the steam pressure is relieved by other means. Any subsequent core-concrete interactions occur at reduced pressures and failed or otherwise vented containment maintains some fission products retention capabilities.

1.3.3.1 Melt release

By the time an accident has reached the point that molten material is released into containment, the primary system will have been depressurized for a long period of time, so there is no mechanism for pressurized melt ejection. Thus the mechanism for melt release will be a ‘pour’ through the failure point(s) of the Calandria Vault. The amount of melt released will depend on the location of the failure point(s).

1.3.3.2 Fuel coolant interactions

Depending on the specific design of the reactor, there can be water present underneath the stream of molten corium exiting the Calandria Vault. The interaction between the molten material and water can result in energetic reactions causing pressure loadings, further oxidation of molten metals, and release of additional fission products. There is the potential for steam explosion, triggered for example by molten material impacting on the submerged containment floor.

1.3.3.3 Molten corium concrete interaction

If there is insufficient cooling of the melt released from the CalandriaVault (melt is too deep for cooling by conduction and not enough water to provide additional cooling), the molten corium will react with the concrete floor. This interaction leads to release of steam, non condensable gases such as carbon dioxide and combustible gases such as hydrogen and carbon monoxide. If containment is still intact, the erosion of the containment structures and the resulting pressure rise and potential for energetic burns can pose a late-phase threat to containment integrity.

As described above the anticipated accident progression for LCDA and SCDA, the phenomena associated with LCDA is well understood through various experiments, metallurgical investigations followed by theoretical model developments. However the SCDA event and associated phenomena are conceptualized so far and are not well investigated. The above described accident progression of SCDA is largely evolved on lumped model calculations and extension of basic information generated during LCDA investigations and SCDA specific experiment on channel disassembly. No scaled down experiments are carried out so far to investigate in-vessel debris bed behaviour. This may be due to technical difficulties and cost involvement for simulating PHWR specific debris bed which consists of long reactor channels.

The specific objective of this study is to characterize the PHWR specific debris bed heat-up pattern which is not carried out yet so far. The characterization involves debris bed boil-off behaviour and associated thermal behaviour. Attempt has been made to utilize the characterization study to develop models which predicts the debris bed heat up behaviour in a realistic manner. The generated heat-up information in turn is helpful to (i) assess the hydrogen generation during late phase of the accident which is expected to be large due presence of large zirconium and (ii) planning the severe accident management in an efficient manner.

The scope of the study is to carry out experiments and model development to assess large scale PHWR debris bed heat-up pattern for power plant.

Chapter 2

Literature Survey

The porous media can be naturally formed (e.g., rocks, sand beds, sponges, woods) or fabricated (e.g., catalytic pellets, wicks, insulations). A review of engineered porous materials is given in Schaefer [17] and the physics and chemistry of porous media is reviewed by Banavar et al. [18]. The applications are in the areas of chemical, environmental, mechanical, and petroleum engineering and in geology. As expected, the range of pore sizes or particle sizes (when considering the solid matrix to be made of consolidated or nonconsolidated particles) is vast and can be of the order of molecular size (ultra micropores with $3 < d < 7$ A°, where d is the average pore size), the order of centimeters (e.g., pebbles, food stuff, debris), or larger. Fig. 2.1 gives a classification of the particle size based on measurement technique, application, and statistics. A review of the particle characteristics for particles with diameters smaller than 1 cm is given by Porter et al. [19].

Also shown in Fig. 2.1 is the capillary pressure in a water-air system with the mean radius of curvature equal to the particle radius. It is clear that as the particle size spans over many orders of magnitude, the handling of the radiative heat transfer and the significance of forces such as capillarity and gravity also vary greatly.

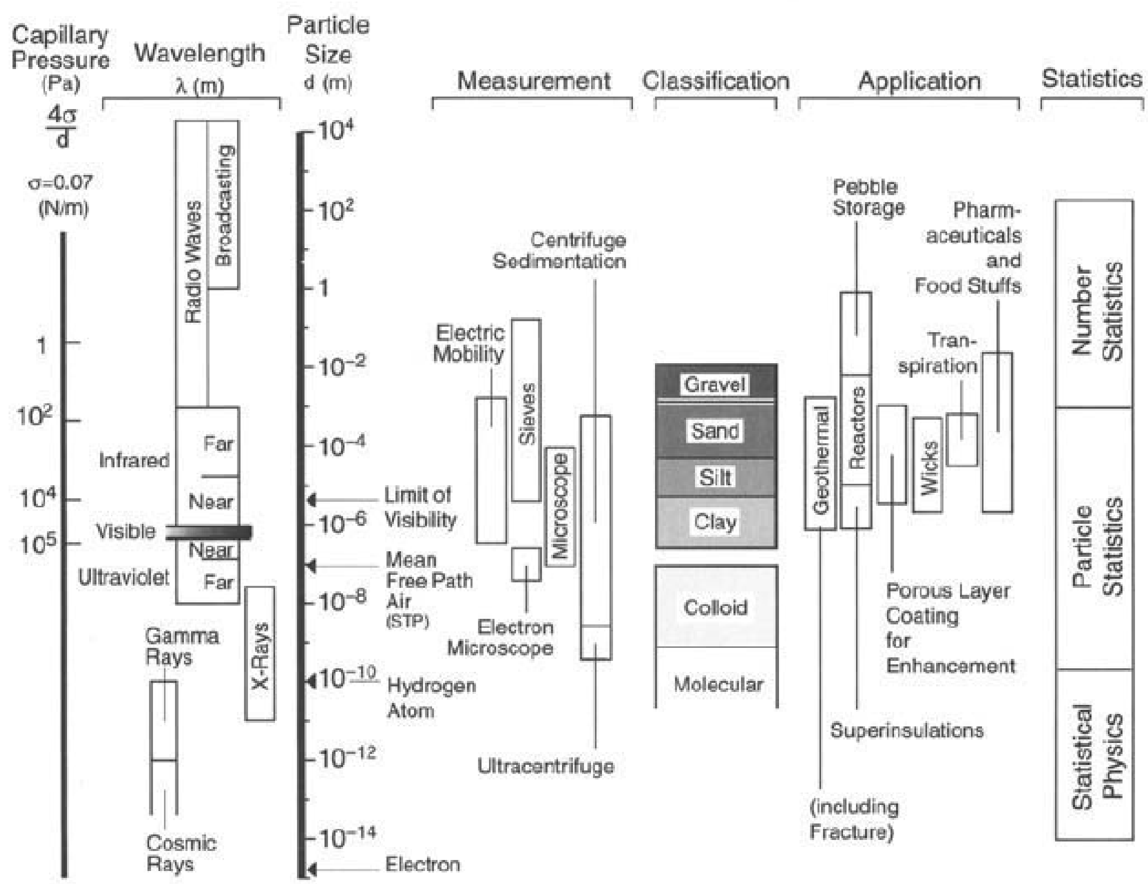

Fig. 2.1 : Particle sizes and their classifications, measurements, and applications [20]

Fig. 2.2 gives a classification of the transport phenomena in porous media based on the single- or two-phase flow through the pores as discussed by Kaviany [20]. Fig. 2.3 renders these phenomena at the pore level. Description of transport of species, momentum and energy, chemical reaction (endothermic or exothermic), and phase change (solid/liquid, solid/gas, and liquid/gas) at the differential, local phase-volume level and the application of the volume-averaging theories lead to a relatively accurate and yet solvable local description.

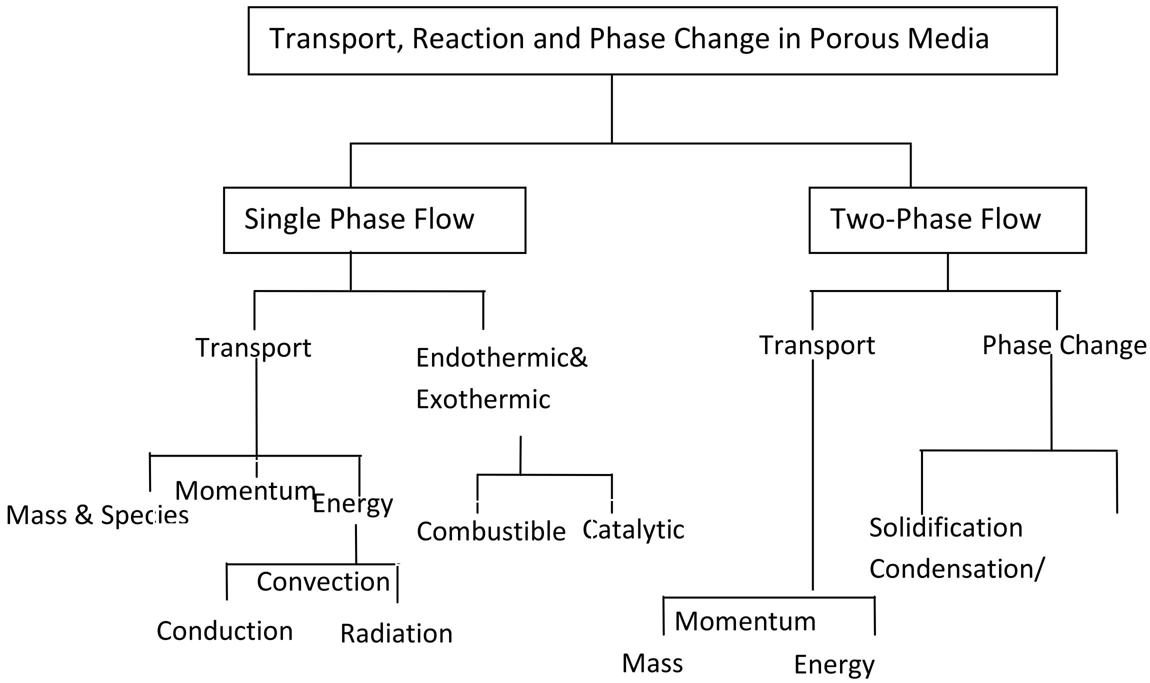

Fig. 2.2 : Treatment of transport, reaction and phase change in porous media [20]

As illustrated in Fig. 2.2 and 2.3 the heat transfer aspect in debris bed is rather complex due to the presence of rigid and stationary permeable solid bodies. In general, the process is described at a small length scale which is larger than the linear dimension of the pore or the linear dimension of a solid particle. This requires the use of the local volume-averaging theories. Depending on the validity, local mechanical and thermal equilibrium or non-equilibrium may be imposed between the fluid (liquid and/or gas) and solid phases.

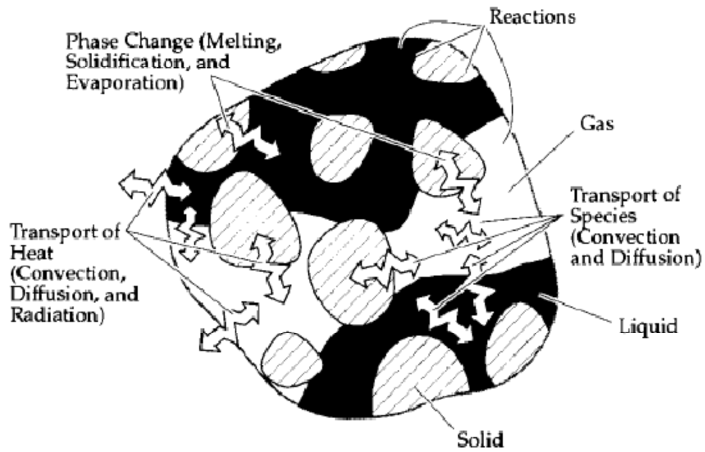

Fig. 2.3 : A schematic for the pore level transport, reaction and phase change [20]

2.1 Debris bed Description under PWR Severe Accident Scenario:

In context to debris bed formation during severe accident in a nuclear reactor like PWR, it is found to be scenario specific. The configuration of debris bed size distribution, shapes and packing are found to be highly uncertain as observed during post TMI-2 accident investigation. The major information for debris bed configuration was obtained during a post TMI-2 accident investigation carried out by Akers et al. [21] and OECD [22]. TMI-2 has provided an unique information that may not be readily obtainable from smaller scale experiments. However, a comparison between TMI-2 and severe damage found in Loss of Flow Test (LOFT) and Power Burst Facility (PBF) show similarity in distribution and behavior of core material, suggesting similar core melt progression pattern.

The major information on late phase core melt progression has come from post-accident examinations of the end state configuration of the TMI-2 reactor core and metallographic analysis of the core debris. Apart from that considerable information on some boundary conditions and parameters during the different accident sequences was also obtained by indirect analyses using the system measurements available during the accident. The post accident end state configuration of the core is illustrated in Fig. 2.4 which shows different kinds of debris in the lower plenum. Broughton [23] carried out investigation through closed-circuit television and mechanical probing operations and arrived at this core state.

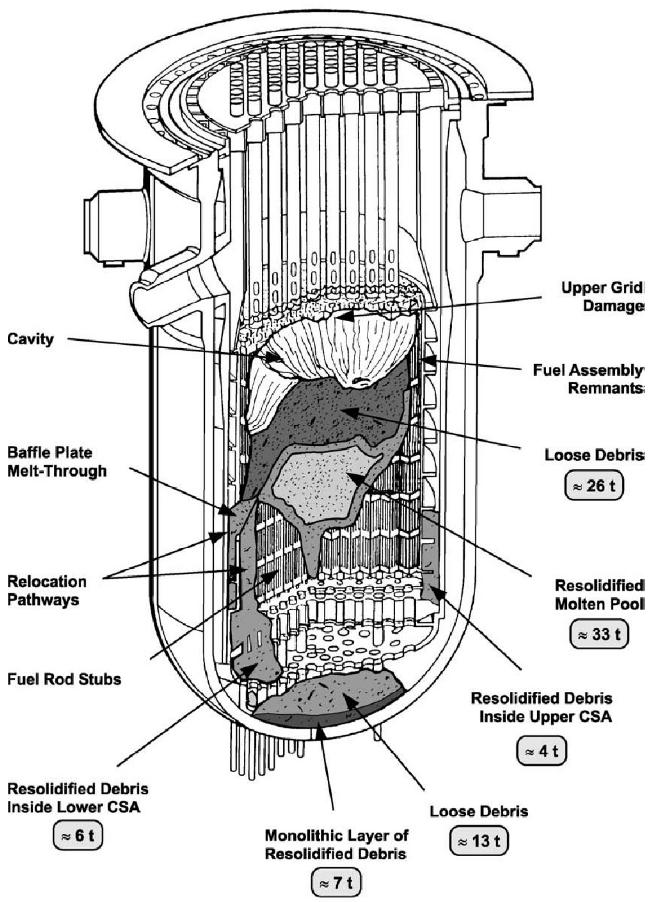

Fig. 2.4 : TMI-2 core end state showing core debris, molten pool, crust and cavity

A large cavity was found at the top of the core extending nearly across the full core diameter. The cavity was surrounded by standing fuel rods of varying damage all around the core periphery. Highly localized melt ablation damage was observed at the upper grid on top of the cavity, that did not progress significantly higher and was probably caused by hot gas flow from the core and in-vessel natural circulation. The other upper plenum structures and hot leg nozzles were found to be essentially intact. A loose core debris bed rested on top of previously molten core materials beneath the cavity. This particulate debris, 3–10% of which was less than 1 mm in diameter as reported by Petit and Olsen et al. [24, 25] included a mixture of fuel pieces, cladding shards, foamy/porous previously molten fuel and structural, or control materials [25]. It is believed that this loose debris was formed during an effort to cool the core at 174 min into the accident. Nearly 30 m^3 of water were injected into the core in less than 15 s probably leading to thermal shock- induced shattering of the oxidized and highly embrittled fuel rod remnants in the upper core regions. Metallographic examinations of debris particles indicated that most of the core debris bed mass remained at temperatures below 1727^0 C or was exposed to higher temperatures only for short times. Part of the debris was found to contain some particles of previously once-molten U–Zr–O mixture indicating peak temperatures greater than around 1927^0 C. A few particles were once-molten $(U, Zr)O_2$ and UO_2 with peak temperatures between about 1800^0 C and 2730^0 C as reported by Eidam [26]. The respective mass of each of these fractions is not available in the considered literature. The loose core debris bed was surrounded by both, fuel rod remnants at the upper level and a horseshoe-shaped ring of consolidated core material at the lower level. It extended into the upper core support assembly through the horseshoe ring opening at the east side of the core and a melted hole in the vertical baffle plates.

The consolidated region of previously molten core materials beneath the upper loose core debris bed was found to be about 3 m in diameter with a depth of approximately 1.5 m near the centre and 0.25 m at the outer edges. The central part of this consolidated region was composed of re-solidified $(U, Zr)O_2$ ceramics, that was laced with previously molten metallics in a large variety of chemical interaction stages. Akers and McCardell [27] observed that the central region was additionally surrounded by a crust of previously molten ceramics and metals that had obviously not been oxidized. It is believed that the central part of the consolidated region had previously been in a molten state due to surface heat transfer from such kind of large-volume core materials agglomeration being too inefficient to compensate for the internal fission product decay heat production. It is likely that densification of this region, as the molten pool grew, contributed to the formation of the cavity observed at the top of the core (Fig. 2.4). The lower crust rested on fuel rod stubs, which varied in length from 0.2 to 1.5 m and extended upward from the lower grid to the bottom of the re-solidified mass. On the east side of the core four adjacent fuel assemblies were found to be completely replaced by re-solidified core material (Fig. 2.4) indicating that molten core material had drained into this region [28]. Post-accident inspections during the defueling revealed that the primary relocation pathway of molten corium had obviously been through a large melted hole of about 1.5 m height and 0.6 m width in the baffle plates adjacent to these fuel assemblies. It was estimated that 12,400 kg of loose and 6,700 kg of agglomerated core debris rested on the lower head. Video examinations of the lower plenum prior to the core bore operations indicated that resolidified core debris had accumulated to a depth of about 0.75–1 m above the lower head wall. The debris extended radially to the downcomer except in the north quadrant of the lower head, where a high steep face of rock was detected at about 1m from the core centerline.

Visual observations of the lower loose core debris bed indicated the particle size to vary widely ranging from granular debris less than a few millimeters in diameter near the centre to larger rock-like formations 10–30 cm across near the lower head wall. Two types of core debris were identified by Broughton et al. [23] as shown in Fig. 2.5.

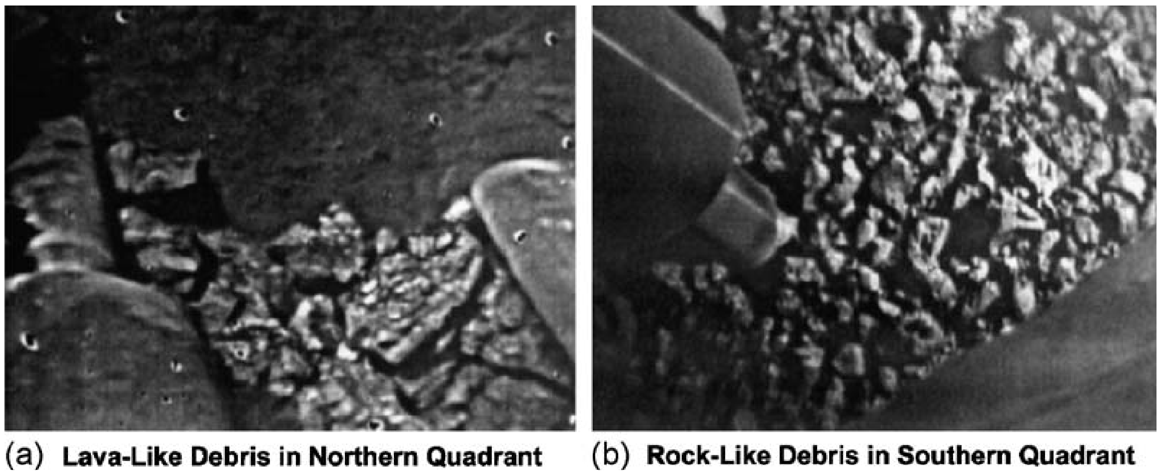

Fig. 2.5. Images of resolidified core material from lower debris bed

Lava-like formations reproduced from video images in Fig. 2.5(a) were observed in the northern quadrant of the RPV, while rock-like particulate core debris covered the lower head in the southern quadrant (Fig. 2.5(b)). The loose core debris resting upon the RPV lower head was completely removed as part of the defueling efforts revealing a variable surface topography of an extremely hard and monolithic core debris layer as reported by Wolf et al. [28].

Virtually no adherence of this layer to the lower head wall could be detected during the defueling. Numerous samples taken from this layer were examined and found to be quite homogeneous with relatively small variations in composition and density. Because of the similarity between the composition of the ceramic debris in the lower plenum and the material in the central molten core region, i.e. primarily previously molten $(U, Zr)O_2$, it was suggested that the material in the lower plenum came from the central core region. In most of the samples interconnected porosity was observed – probably caused by bubbling of steam or structural material vapours as suggested by Wolf et al. [28] implying that at least part of the debris layer must have remained molten on the lower head for a sufficient time in order to allow bubble formation and coalescence to occur. Moreover, the presence of urania and zirconia rich (U, Zr)O_2 phases in most samples indicated a gradual cool-down of the debris layer rather than a rapid quenching.

Several PWR-Specific experiments have been carried out post TMI-2 accident to understand the formation of corium debris as a result of fuel-coolant interaction (energetic or not). Magallon [29] carried out investigations in two large scale experimental facilities namely, FARO and KROTOS at JRC-Ispra between 1991 and 1999. The FARO quenching experiments series was planned to generate data on the debris bed initial conditions and morphology after the core melt has slumped and quenched into water in a range of conditions typical of in- and ex-vessel situations where as KROTOS experiment was planned to carry out tests which generate information on the finest debris resulting from an explosion. Experiments were performed with 3–177 kg of UO_2–ZrO_2 and UO_2–ZrO_2–Zr melts, quenched in water at depth between 1 and 2 m, and pressure between 0.1 and 5.0 MPa. The effect of various parameters such as melt composition, system pressure, water depth and subcooling on the quenching processes, debris characteristics and thermal load on bottom head were investigated, thus, giving a large spectrum of data for realistic reactor situations. The available data related to debris coolability aspects in particular are (i) geometrical configuration of the collected debris (ii) partition between loose and agglomerated ("cake") debris and (iii) particle size distribution with and without energetic interaction.

As discussed by Magallon [29], out of these two large scale experiments in general, the debris bed was formed of a conglomerate ("cake" or "hard layer" in the TMI-2 terminology) in contact with the bottom plate and overlaying fragmented debris. Two typical configurations of debris beds with cake involving a large mass of corium, namely L-24 and L-28 from FARO test series are shown in Figs. 2.6 (a) and (b) respectively.

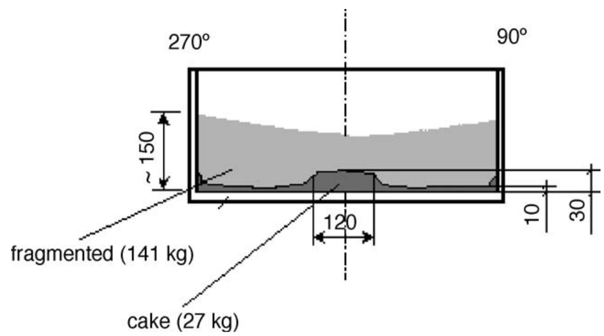

Fig. 2.6 (a) : FARO L-24 expt. Debris bed configuration

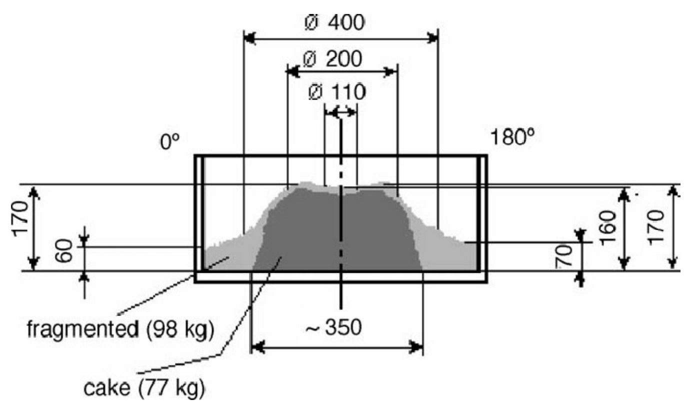

Fig. 2.6 (b) : FARO L-28 expt. debris bed configuration

The schemes in the figures are virtual sections of the debris beds in a plane perpendicular to the bottom plate along the centerline. FAROL-24 debris bed was uniformly distributed over the surface of the debris catcher with a slight depression toward the centre (Fig. 2.6 (a)). The cake was entirely covered by the loose debris. A thin hard layer was covering the entire catcher surface, as if part of the melt had spread on it. The centre of the cake looked like a piled-up debris. Fig. 2.7 shows a photograph of L-24 and L-28 debris bed surface as found. FARO L-28 debris bed configuration was noticeably different than L-24. For L-28 the piled-up hard part in the centre arrived almost up to the top of the debris bed. It was covered only by a thin layer of loose debris (~2 cm) having size of order 1 cm as shown Fig. 2.6(b)).

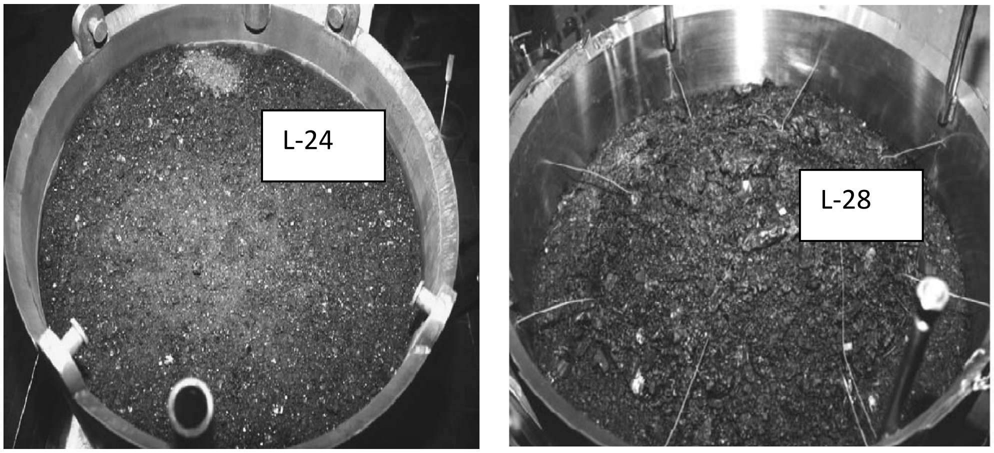

Fig.2.7 : Photograph of FARO L-24 and L-28 expt. debris [29]

A small depression about 1 cm depth was present at the top of the cake, which looked like if a jet had impinged in the centre. Contrarily to L-24, the cake was not extending all over the cross-section of the catcher. It had a diameter of only 35 cm at the base (Fig. 2.8), debris catcher had diameter 66 cm). The major part of the loose debris having dimension less than 10 mm occupied the rest of the space to the catcher wall.

Fig. 2.8 : FARO L-28 expt.: Cake found after removing the loose debris

A study made on particle size distributions of the loose debris for FARO experiments shows that mass averaged particle size is between 2.6 and 4.8 mm whatever the test conditions and outcome (Fig. 2.9)

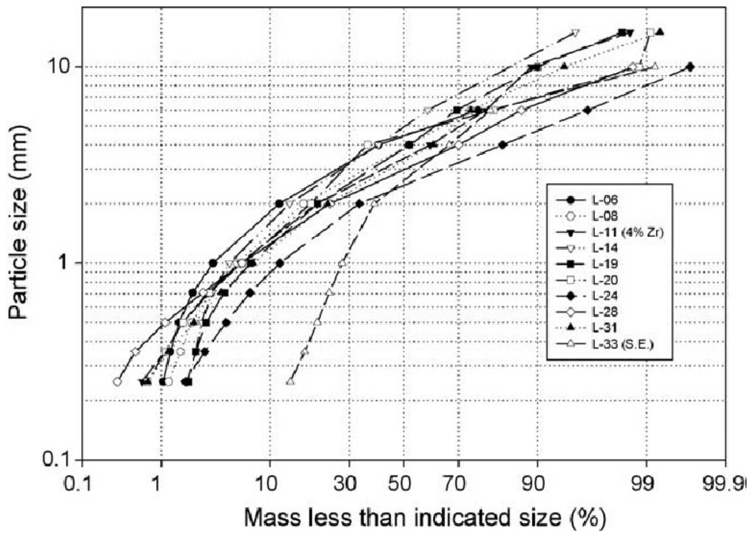

Fig. 2.9 : Particle size distribution in FARO Test

However this range changes to 3.5–4.8 mm when considering only test performed in saturation conditions and with a diameter of the release orifice of 100 mm. The KROTOS corium test series included tests both under subcooled and near saturated conditions at ambient pressure and subcooled tests at an elevated pressure from 0.2 to 0.37 MPa. Corium melt masses in these tests varied from 2.4 to 5.1 kg (~2800^0 C). None of these tests with corium produced an energetic steam explosion. However, propagating low energy events, with a maximum energy conversion ratio of 0.16%, were observed in some cases when an external trigger was applied. Present experimental evidence suggests that the water depletion in the mixing zone suppresses energetic steam explosions with corium melts at ambient pressure and in the present pour geometry. On the other hand, elevated pressure reduces significantly the integral void fraction also with corium allowing better melt/water contact at triggering than at low pressure and generation of mild interactions.

A comparison of particle size distributions in selected KROTOS and FARO tests in which no explosion was recorded as illustrated in Fig. 2.10. Similar profiles are observed for both the tests debris, but slightly smaller particles are generated in KROTOS. The differences may be due to differences in injection velocity (larger in KROTOS than in FARO at the very beginning of the injection) and in jet diameter (30 mm in KROTOS against 100 mm in FARO).

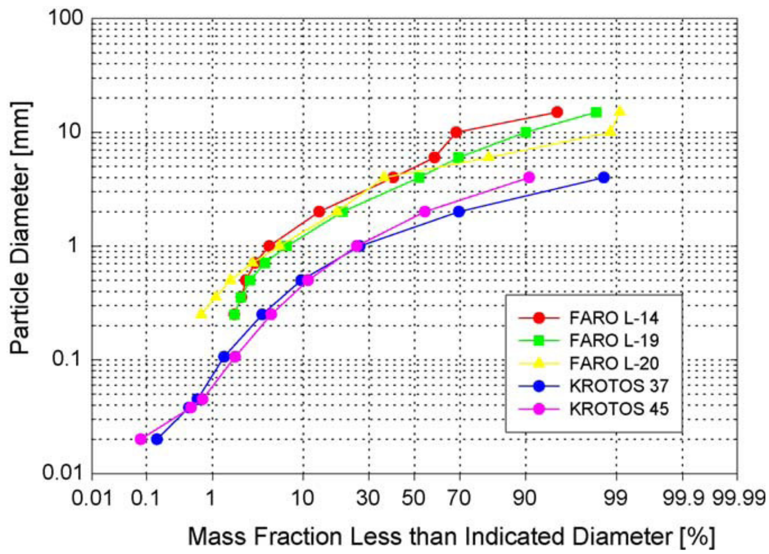

Fig. 2.10: Particle size in corium KROTOS tests as compared to FARO

The experiments concluded that tests performed at high pressure showed that, except for the test with Zr metal in the melt, the debris was made of a cake in contact with the bottom and overlaying fragments, as in TMI (hard layer and loose debris, respectively). A channeling structure of the cake at contact with the bottom plate is the rule and seems to confirm the hypothesis of a “gap” as one of the main contributors to cooling the bottom head during the TMI-2 accident. No attack of the bottom plate was noticed in any of the FARO tests, but the temperature of the plate upper surface remained at values well above saturation for durations in relation with the cake mass. Quenching data and post-test analysis of the debris beds suggest that in all cases the cake was largely formed from melt that did not experienced break-up during melt fall through water, i.e., that the jet break-up length was larger than the water pool depth. As being out of the scope of the experimental programme, porosity and permeability of the cake were not evaluated.

Visual observations of the cake internals show a rather compact structure with vertical cracks. In the only long pour test performed in saturated conditions, the cake consisted of two clearly separated superposed layers, even though the pour was continuous. The reason for existence of two layers in the debris is due to insufficient molten jet surface stripping. As a result of Kelvin Helmoltz and Raleigh Taylor instability, the surface material is stripped off to form smaller particles. As the distance between the jet release and test vessel bottom is not sufficient, all the jet material is not get stripped off or fragmented. Thus the core of the jet gets solidified as a cake where as the stripped of material remained as loose debris. Loose debris mean particle size were in the range 3.0–4.8 mm in all tests where no special event occurred. As the number of parameters varied was large with respect to the number of tests performed, it is not possible to establish a more precise classification of the particle size as a function of the test conditions. In tests at low pressure and saturated water, part of the finest debris produced during quenching (<1 mm) was entrained out of the test section. This was also the case at high pressure when metallic zirconium was present in the corium, which enhanced significantly quenching and steam production with respect to pure oxidic corium. In case of steam explosion, FARO and KROTOS experiments showed that very fine debris may remain longer in suspension in the water before settling and forming a sort of mud on the top of the quenched part, which may influence cooling.

Alternatively, the explosion can disperse part of this fine debris in other locations inside the vessel or the containment. Furthermore, similarities observed in FARO and KROTOS explosion debris (and efficiency) makes the use small scale steam explosion propagation data valuable for extrapolation to larger scale. The FARO and KROTOS data are helpful especially for assigning realistic initial conditions for long-term debris cooling calculations. The melt quantities used in FARO were about one order of magnitude higher than in previous work. Thus, the data represent a noticeable step for the assessment of code extrapolation capabilities to calculate quenching and cooling of core material in reactor severe accident conditions.

2.2 Debris Bed description under PHWR Severe Accident (SA) Scenario:

In context to PHWR severe accident, the in-vessel degradation phenomena as discussed in section 1.3.2.1.1 of Chapter 1, describes the formation of suspended debris followed by formation of terminal debris. Small-scale CANDU core disassembly tests was conducted by Mathew et al. [30] with single, double and multiple channels to understand the behaviour of CANDU channels during moderator boil-off, when the channels are expected to sag and to break up to form debris. Experimental investigation has been carried out with 1:5 scaled down multiple channels with 12 bundle simulators. The stress level and the channel stiffness are being conserved by the investigators. The channels were stacked one on top of the other so that midpoint sag, channel temperature, channel axial movement, channel end load and channel disassembly could be monitored. The schematic of the multiple channel setup is illustrated in Fig. 2.11.

In a typical test, the channel has been held in the range of reactor operating temperature at ~300°C until thermal equilibrium was reached. The power was then increased so that the channel reaches a maximum temperature in the range 1300°C to 1400°C. The heat-up rate up to the maximum test temperature was varied in the range 0.1 to 1.2°C/s [30] in different tests to cover the expected heat-up rate of fuel channels when uncovered by the moderator. The channels were held at the maximum temperature for holding times in the range 600 - 5500 s in the single channel tests. In the two-row test, after the top channel temperature increases from its equilibrium temperature of ~300°C, the channel below is powered from its equilibrium temperature of ~300°C after a time lag of ~2000 s.

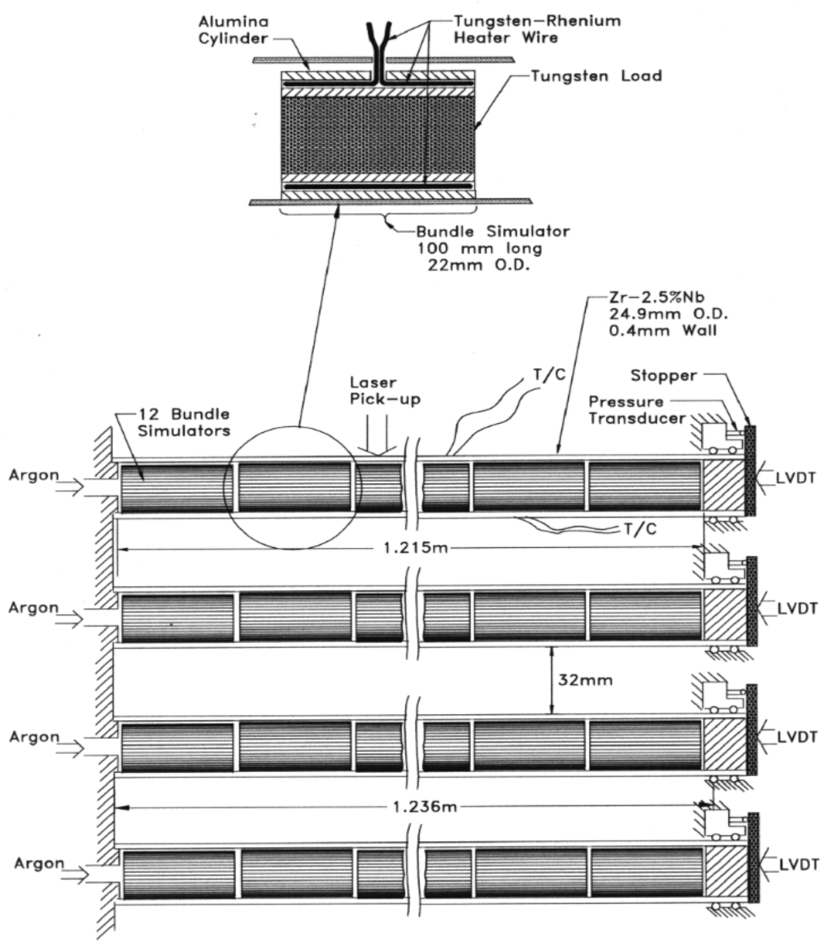

Fig. 2.11 Schematic of Channel layout for disassembly experiment [30]

The time lag corresponds to the approximate time required to uncover the next channel below in a CANDU core undergoing a severe core damage accident. In addition to monitoring the various test data and videotaping the test, post-test examination of the channel is conducted in which the axial sag profile, any changes to the original diameter and wall thickness along the top and bottom at various locations were measured. The channel is also radiographed to determine the post-test location of the heaters. The view at the end of disassembly experiments for three channel configuration is shown in Fig. 2.12

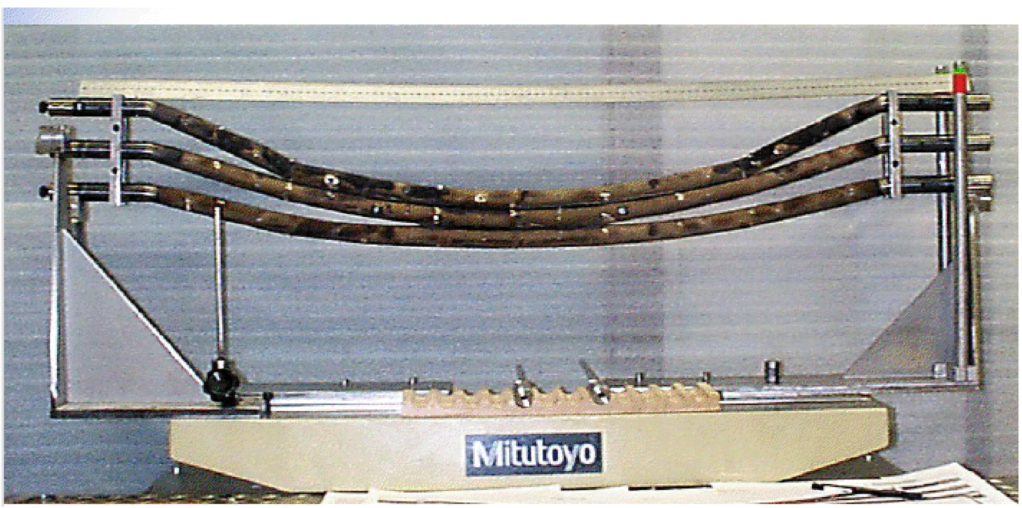

Fig. 2.12 Photograph of the channel disassembly experiment [30]

The tests with single, double and multiple channels show that a significant sag only of reactor channel has occurred at a temperature above 800 °C, leading to significant wall-thinning and break-up of the bundle-to-bundle gap regions near the channel ends for the top row as support is being provided by lower channels. It is concluded from the study that coarse debris, as long as ~10 bundles equivalent reactor channel is expected through channel disassembly process which will be the major constituents of the terminal debris.

2.3 Heat Transfer and Fluid Flow Models for Debris Bed:

As the earlier sections describes the nature of debris bed those are expected from PWR and PHWR undergoing a severe accident, it is of interest and essential to study heat transfer treatment given to regular debris bed used for different industrial purposes. The insights generated from the study can be extended to build model specific to PHWR debris bed. Over several years researchers have investigated the heat transfer aspects of the debris bed with varying sizes, porosity and material ranging from metallic to non-metallic. Following sections describes the heat transfer treatment considering modes of heat transfers like conduction, convection and radiations,

conduction heat transfer model for debris bed: The conduction heat transfer through fully-saturated matrices (i.e., a single-phase fluid occupying the pores), through any heterogeneous media, depends on the structure of the matrix and the thermal conductivity of each phase. One of the most difficult aspects of the analysis of heat conduction through a porous medium is the structural modeling. This is because the representative elementary volumes are three-dimensional and have complicated structures that vary greatly among different porous media. Since the thermal conductivity of the solid phase is generally different than that of the fluid, the manner in which the solid is interconnected influences the conduction significantly. Even when dealing with the non consolidated particles, the contact between the particles plays a significant role.

For the analysis of the macroscopic heat flow through heterogeneous media, the local volume-averaged (or effective) properties such as the effective thermal conductivity k_e is used. The effective thermal conductivity is considered to be summation of k_{ec} and k_r, as given in Eqn. (2.1)

$$k_e = k_{ec} + k_r \tag{2.1}$$

Where,

k_e: effective conductivity

k_{ec}: effective conductivity (conduction only for solid and fuid)

k_r: radiative conductivity

These local effective properties such as the heat capacity (ρC_p), thermal conductivity (k), and radiation absorption and scattering coefficients (σ_a) and (σ_s) need to be arrived at from the application of the first principles to the volume over which these local properties are averaged, that is, the representative elementary volume. The effective thermal conductivity is expected to depend on the following,

(a) The thermal conductivity of each phase and the relative magnitude of k_s/k_f
(b) The structure of the solid matrix and the extent of the continuity of the solid phase
(c) The contact resistance between the nonconsolidated particles and the solid surface oxidation/surface coatings
(d) For gases, ratio of the mean free path and the average linear pore dimension (i.e., the Knudsen number). For large Knudsen number the bulk gas conductivity cannot be used for the fluid phase.

Determination of the thermal conductivity of saturated porous media involves application of the point conduction (energy) equation to a point in the representative elementary volume of the matrix and the integration over this volume. It is realized that at the pore level there will be a difference ΔT_d between the temperature at a point in the solid and in the fluid. Similarly, across the representative elementary volume, the maximum temperature difference ΔT_e. However, it is assumed that these temperature differences are much smaller than those occurring over the system dimension ΔT_L. Thus, assumption of local thermal equilibrium is given by,

$$\Delta T_d < \Delta T_e << \Delta T_L \tag{2.2}$$

With this assumed negligible local temperature difference between the phases, it is assumed that within the local representative elementary volume $V = V_f + V_s$, the solid and fluid phases are in local thermal equilibrium.

For packed beds of particles and for the entire range of values of k_s/k_f (larger and smaller than unity) some empirical correlations are available for the isotropic effective thermal conductivity k_e. Three of these are constructed by Krupiczka [20], Kunii and Smith [20], and Zehnder and Schltinder [20]. An extensive review of the literature on the effective thermal conductivity prior to 1960 is given by Krupiczka [20]. The prediction of Krupiczka given for $0.2 < \varepsilon < 0.6$ is illustrated in Eqn. 2.3.

$$\frac{k_e}{k_f} = \left(\frac{k_s}{k_f}\right)^{+0.280-0.757\log\varepsilon-0.057\log\left(k_s/k_f\right)} \tag{2.3}$$

The prediction of Kunii and Smith [29] for $0.260 < \varepsilon < 0.476$ is given in Eqn. 2.4.

$$\frac{k_e}{k_f} = \varepsilon + \frac{(1-\varepsilon)}{\phi_2 + 4.63(\varepsilon - 0.26)(\phi_1 - \phi_2) + 2/3\left(k_f/k_s\right)} \tag{2.4}$$

where $\varphi_1 = \varphi_1 (k_f /k_s)$ and $\varphi_2 = \varphi_2 (k_f /k_s)$ and they are monotonically decreasing functions of k_s/k_f.

The prediction of Zehnder and Schltinder [20] is as follows (Eqn. 2.5),

$$\frac{k_e}{k_f} = 1-(1-\varepsilon)^{1/2} + \frac{2(1-\varepsilon)^{1/2}}{1-(k_f/k_s)B}\left\{\frac{[1-(k_f/k_s)]B}{[1+(k_f/k_s)B]^2}\ln\frac{1}{(k_f/k_s)B} - \frac{B+1}{2} - \frac{B-1}{1-(k_f/k_s)B}\right\} \tag{2.5}$$

where, $B = 1.25\left(\frac{1-\varepsilon}{\varepsilon}\right)^{10/9}$

Prasad et al. [31] performed experiments for k_s/k_f larger and smaller than unity (but for only one order magnitude to either side of unity) and examined the accuracy of the preceding three predictions. In Fig.2.13, the experimental results of Prasad et al. [31], Nozad [32], and other experimental results reported are plotted against these correlations. While for moderate values of k_s/k_f the four predictions are in agreement, for high values, predictions with Krupiczka found to be lower only the Hadley [33] correlation is found to predict the effective thermal conductivity correctly.

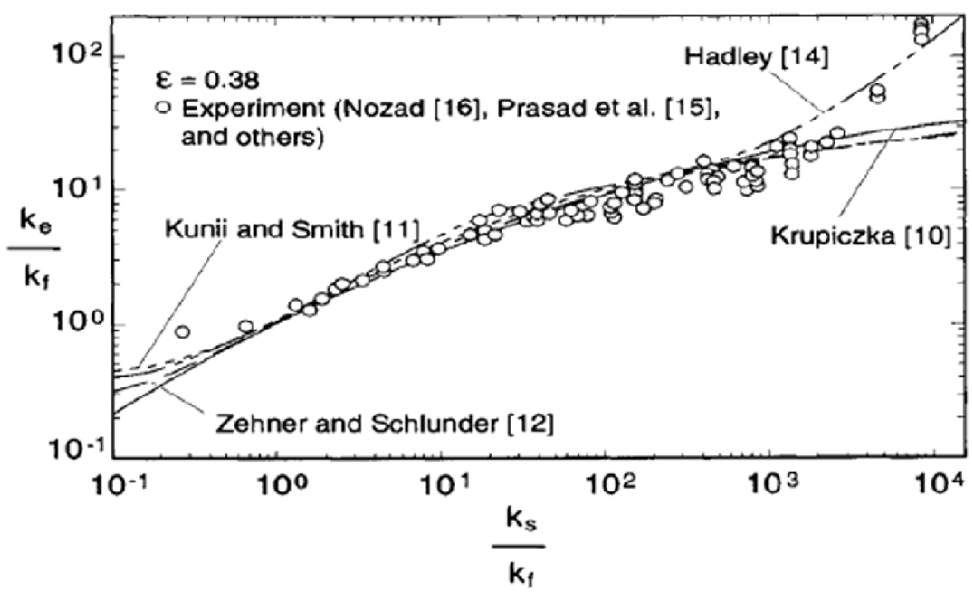

Fig. 2.13: Comparison of several correlations for the effective thermal conductivity with experimental results from several sources [20]

The pore-level structure of the solid and fluid phases significantly influences the effective conductivity, and in general the specifications of and k_s/k_f do not suffice. When gases are involved, rarefaction (for small pore size, for low pressure, or near constrictions) should be attended. The thermal conduction of each phase is temperature-dependent (and for gases, also pressure-dependent), and that should also be considered.

The Imura-Takegoshi [34] also proposed for equivalent conductivity model (k_e) l for debris bed with a porosity ranging from 0.4-0.5. The expression for k_{ec} is given by Eqn. 2.6 - Eqn. 2.9.

$$k_{ec} = \left[\Psi + \frac{1 - \Psi}{\phi + \frac{1 - \phi}{\nu}}\right] k_g \tag{2.6}$$

$$\Phi = 0.3P\varepsilon^{1.6}\upsilon^{-0.044} \tag{2.7}$$

$$\upsilon = \frac{k_s}{k_g} \tag{2.8}$$

$$\Psi = \frac{\varepsilon - \phi}{1 - \phi} \tag{2.9}$$

Where,

k_g : thermal conductivity of fluid or vapour in pores

k_s : thermal conductivity of solid material

ε : porosity of debris

The correlation is found to be adopted for severe accident damage progression modeling by Siefken et al [35] as the porosity and debris sizes for the correlation falls in line with size and porosity for PWR debris bed as discussed in earlier sections. The correlation is adopted in the COUPLE model of the severe accident analysis code RELAP/SCDAP.

Flow and convective heat transfer model for single phase debris bed: As we consider simultaneous fluid flow and heat transfer in porous media, the role of the macroscopic (Darcean) and microscopic (pore-level) velocity fields on the temperature field needs to be examined. Experiments have shown that the mere inclusion of $u_d \bullet \nabla T$ in the energy equation does not accurately account for all the hydrodynamic effects. The pore-level hydrodynamics also influence the temperature field. Inclusion of the effect of the pore-level velocity non uniformity on the temperature distribution (called the dispersion effect and generally included as a diffusion transport) is the main focus in this section.

The bulk resistance to flow of an incompressible fluid through a solid matrix, as compared to the resistance at and near the surfaces confining this solid matrix, was first measured by Darcy [20]. Since in his experiment the internal surface area (interstitial area) was many orders of magnitude larger than the area of the confining surfaces, the bulk shear stress resistance was dominant. His experiment used nearly uniform size particles that were randomly and loosely packed, that is, a nonconsolidated, uniform, rigid, and isotropic solid matrix. The macroscopic flow was steady, one-dimensional, and driven by gravity. A schematic of the flow is given in Fig. 2.15. The mass flow rate of the liquid was measured and the filtration or filter velocity u_D was determined by dividing mass flow rate by the product of the fluid density (assumed incompressible) and the cross-sectional area "A" of the channel (which was filled with the particles and then the liquid was flown through it).

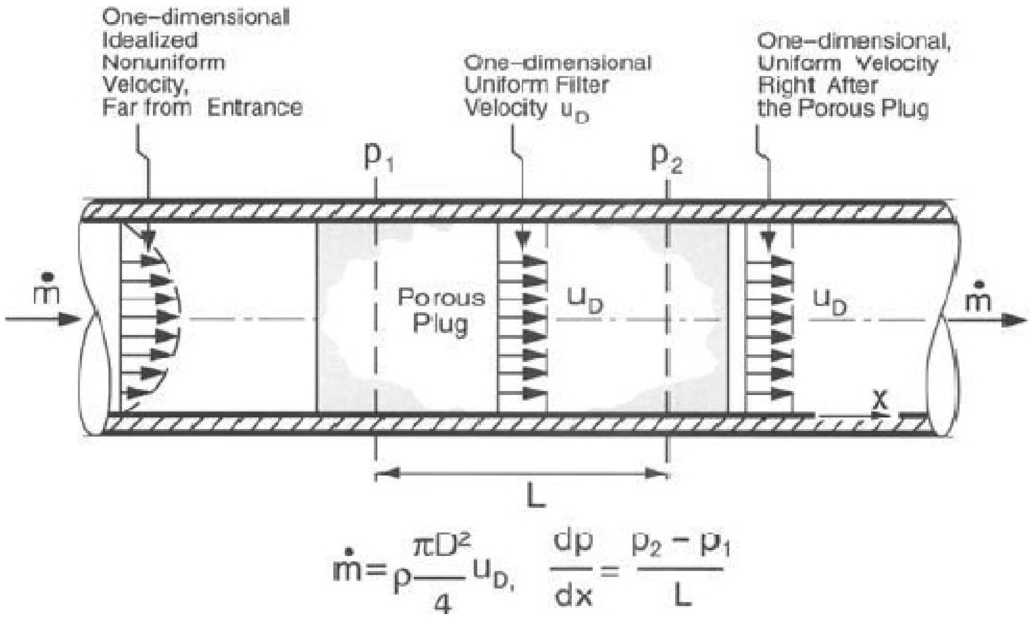

Fig. 2.14: Determination of filter (or Darcy) velocity.

In applying a volumetric force balance to this flow, he discovered that the bulk resistance can be characterized by the viscosity of the Newtonian fluid (fluid parameter) μ and the permeability of the solid matrix (solid matrix parameter) K, such that,

$$-\frac{dp}{dx} = \frac{\mu}{K} u_D \tag{2.10}$$

where the dimension of K is in square of length, such as m^2. Interpretation of Eqn. 2.10 has evolved and one unit still used is "darcy". One darcy is the permeability of a matrix when a cubic sample with each side having a width of 1 cm is used and a fluid with viscosity of 1 centipoise is flown (one-dimensional) through it, resulting in a pressure drop of 1 atmosphere (1.013×10^5 Pa). One unit of darcy equals 9.87×10^{-13} m^2. The permeability accounts for the interstitial surface area, the fluid particle path as it flows through the matrix, and other related hydrodynamic characteristics of the matrix. The Darcy model has been examined rather extensively and is not closely followed for liquid flows at high velocities and for gas flows at very low pressures and very high velocities.

At low gas pressures and for small pore size, the mean free path of the gas molecules may be on the order of the pore size and therefore velocity slip occurs (Knudsen effect), resulting in higher permeabilities. However, an increase in the permeability due to an increase in gas pressure has been found in some experiments. Scheidegger [36] discusses the effect of the Knudsen slip, the internal surface roughness, surface absorption, capillary condensation, and molecular diffusion on the measured permeability. By examining these effects at the pore level, it becomes clear that the measured gas and liquid permeability can be noticeably different.

For isotropic media where the pressure gradient ∇p and the velocity vector u_D are parallel, Eqn. 2.11 is generalized to,

$$-\nabla p = \frac{\mu}{K} u_D \tag{2.11}$$

In an effort to extend the Darcy law, the following momentum equation has been suggested by Brinkman [37] and extended to the high-velocity regime for isotropic media and is as follows (Eqn. 2.12),

$$\frac{\rho_o}{\varepsilon}\left(\frac{\partial u_D}{\partial t} + u_D.\nabla u_D\right) = -\frac{\delta\langle p\rangle^f}{\partial x_i} + \frac{\mu'}{\varepsilon}\nabla^2 u_D - \frac{\mu}{K}u_D - \frac{F\varepsilon}{K^{1/2}}\rho|u_D|u_D \tag{2.12}$$

Viscous shear stress term (other than the bulk viscous shear stress) was included to account the shear stresses initiated at the surfaces bounding the porous media (macroscopic shear). This was attempted to arrive at an equivalent of the Navier-Stokes equation for the description of flow through porous media.

Note that the viscosity used in both the microscopic and macroscopic viscous terms is the fluid viscosity. Lundgren [38], in giving justification to the Brinkman equation, shows that for spherical particles μ'= μg(ε), where 0 < g(ε) and g(1) = 1 but others have used μ' > μ.

For the matrices obeying the modified Ergun relation we have, Eqn. 2.13

$$\frac{F\varepsilon}{K^{1/2}} = \frac{1.8(1-\varepsilon)}{\varepsilon^3}\frac{1}{d} \quad \text{where } K = \frac{1}{180}\frac{\varepsilon^3}{(1-\varepsilon)^2}d^2 \tag{2.13}$$

Some other semi-heuristic momentum equations have been recommended, among these is the following Eqn. 2.14 where Ergun constant C_E is placed instead of Fε.

$$\frac{\rho_o}{\varepsilon}\left(\frac{\partial u_D}{\partial t} + u_D.\nabla u_D\right) = -\nabla p + \rho f + \frac{\mu}{\varepsilon}\nabla^2 u_D - \frac{\mu}{K}u_D - \frac{C_E}{K^{1/2}}\rho|u_D|u_D \tag{2.14}$$

Following are the significance of each term of L. H. S and R. H. S

L.H. S term = macroscopic inertial force

R. H. S 1st term = pore pressure gradient

R. H. S 2nd term = body force

R. H. S 3rd term = force due to macroscopic or bulk viscous shear stress

R. H. S. 4th term = force due to microscopic viscous shear stress, Darcy term

R. H. S 5th term = microscopic inertial force (Ergun inertial term)

This is a semi heuristic volume-averaged treatment of the flow field. The experiments of Dybbs and Edwards [39] show that the macroscopic viscous shear stress diffusion and the flow development (convection) are significant only over a length scale of from the vorticity generating boundary and the entrance boundary, respectively. However, Eqn. 2.14 predicts these effects to be confined to distances of the order of $K^{1/2}$ and Ku_D/μ, respectively. It is noted that $K^{1/2}$ is smaller than d. Then Eqn. 2.14 predicts a macroscopic boundary-layer thickness, which is not only smaller than the representative elementary volume "l" when l>> d, but even smaller than the particle size. However, Eqn. 2.14 allows estimation of these macroscopic length scales and shows that for most practical cases, the Darcy law (or the Ergun extension) is sufficient.

The convective heat transfer of the debris bed is governed either by forced or natural convection. Eqn. 2.15 to Eq. 2.18 as proposed by Tung [40] and Eqn. 2.19 to Eqn. 2.20 as proposed by Edwards [41] illustrates correlation for forced and natural convection respectively for debris bed.

For forced convection,

$$\mathrm{Nu_{conv}} = 0.27\mathrm{Re}^{0.8}\mathrm{Pr}^{0.4} \tag{2.15}$$

Where,

$\mathrm{Nu_{conv}}$: Nusselt number for convection

Re : Reynold's number

Pr : Prandtl number

$$Nu_{conv} = (hD_p)/\mathrm{k_g} \tag{2.16}$$

Where,

h : convective heat transfer coefficient

$\mathrm{D_p}$: effective diameter of debris particle

$\mathrm{k_g}$: thermal conductivity of vapour

The Reynold's number is given by the equation

$$Re = \rho_g v_g D_p/\mu_g \tag{2.17}$$

Where,

ρ_g : density of vapour

v_g : velocity of vapour

D_p : effective diameter of debris particle

μ_g : viscosity of vapour

The Prandtl number is given by the equation

$$Pr = \mu_g c_g/k_g \tag{2.18}$$

Where ,

μ_g : viscosity of vapour

c_g : heat capacity of vapour

k_g : thermal conductivity of vapour

The ranges of parameter for which this correlation is based are,

$$0.7 \le Pr \le 5$$

$$18 \le Re \le 2400$$

$$0.4 \le \varepsilon \le 0.5$$

For natural convection,

$$Nu_{nat} = KRa^{0.25} \tag{2.19}$$

Where,

Nu_{nat} : Nusselt number for natural convection , K = 0.3 $\quad 0 \leq Ra \leq 50$

0.4 $\quad 50 \leq Ra \leq 200$

0.5 $\quad 200 \leq Ra \leq 10^6$

0.6 $\quad 10^6 \leq Ra \leq 10^8$

Ra : Rayleigh number

The Rayleigh number is calculated by the equation

$$Ra = Gr \, . \, Pr = \frac{\rho_g^2 \, g \, D_p^3 \beta \Delta T}{\mu_g^2} \mathrm{Pr} \qquad (2.20)$$

Where,

g : acceleration of gravity

β : volume coefficient of expansion of vapour

ΔT : local temperature difference between debris and vapour $(T_D - T_g)$

The above mentioned correlation are found to be adopted for severe accident damage progression modeling by Siefken et al [35] as the porosity and debris sizes for the correlation are similar to PWR debris bed. The correlations are adopted in the COUPLE model of code RELAP/SCDAP.

Radiation heat transfer model for debris bed: The fundamentals of radiation heat transfer in absorbing/emitting/scattering media have been given by Chandrasekhar [42], Ozisik [43] and Siegel and Howell [44], Some of the principles are briefly given herein. Their approach treats the solid-fluid phases as a single continuum. Therefore, the following applies to heterogeneous (solid and fluid phases are present simultaneously) differential elements. A schematic showing the coordinate system for a plane-parallel geometry (which is the geometry used through most of this chapter) is given in Fig. 2.15. The unit vector in the beam direction is given by “s” and the length of the position vector is given by “S”. The incident beam is shown with subscript i and the incident solid angle is shown by dω. Following are the assumptions:

(a) It is assumed that the particle size is much smaller than the linear size of the system. Then, the radiative properties are averaged over a representative elementary volume with a linear dimension ‘l’, such that d << l<< L.

(b) The matrix-fluid system is treated as a continuum by assuming that the local thermal equilibrium exists in accord with the treatment of conduction and convection.

(c) Azimuthal symmetry is assumed so that $I_\lambda(\theta, \varphi) = I_\lambda(\theta)$

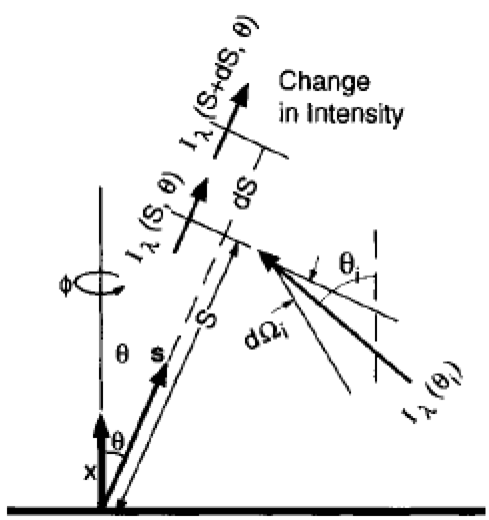

Fig. 2.15: A schematic of the coordinate system

The equation of radiative transfer for radiation in a direction θ becomes (Eqn. 2.21),

$$\frac{\partial I_\lambda(S)}{\partial S} = -\langle\sigma_{\lambda a}\rangle I_\lambda(S) + \langle\sigma_{\lambda a}\rangle I_{\lambda b}[T(S)] - \langle\sigma_{\lambda s}\rangle I_\lambda(S) + \frac{\langle\sigma_{\lambda s}\rangle}{2}\int_{-1}^{1} I_\lambda(S,\theta_i)\langle\phi_\lambda\rangle(\theta_i \to \theta)d\cos\theta_i \tag{2.21}$$

The arrow indicates from the incident to the scattered direction and θ_o is the angle between the incident (θ_i) and scattered (θ) beam.

The divergence of the total radiative heat flux (Eqn. 2.22), which is used in the energy equation, is found from the radiative transfer equation by its integration over $\int_{4\pi} d\omega$ and $\int_0^{\infty} d\lambda$.

$$\nabla.q_r = 4\pi\int_0^{\infty}\langle\sigma_{\lambda a}\rangle I_{\lambda b}(S)d\lambda - 2\pi\int_0^{\infty}\langle\sigma_{\lambda a}\rangle\int_{-1}^{1} I_{\lambda}(S,\theta)d\mu d\lambda \tag{2.22}$$

When no other mode of heat transfer is present and the emitted and absorbed energy are equal, then $\nabla.\ q_r=0$, and the state of radiative equilibrium exists.

The approximate radiant conductivity model for a one dimensional, plane geometry with emitting particles under the steady-state condition is given by Vortmeyer [45] (Eqn. 2.23),

$$q_r = \frac{F\sigma}{[(1+\rho_w)/(1-\rho_w)] + L/d}\left(T_1^4 - T_2^4\right) \tag{2.23}$$

where F is called the radiative exchange factor and the properties are assumed to be wavelength independent. If $\rho_w = 0$ and the bed is several particles deep (L), then the first term of the denominator can be neglected. Then, for $T_1 - T_2 < 200$ K, a radiant conductivity is defined [45] (Eqn. 2.24),

$$q_r = -k_r \nabla T, \tag{2.24}$$

Where,

$$k_r = 4Fd\sigma T_m^3$$

The approach has many limitations, but the single most important limitation is that the value of 'F' cannot be easily calculated. Of all the methods, the Monte Carlo method can be used for calculating 'F' for semi-transparent particles. The value of 'F' also depends upon the value of the conductivity of the solid phase. In the Kasparek experiment [45] infinite conductivity is assumed, which is justified for metals. Similarly, the case of zero conductivity can be easily treated by considering the rays to be emitted from the same point at which they were absorbed. However, the intermediate case, that is, when the conductivity is comparable to the radiant conductivity, shows a strong dependence of radiant conductivity on the solid conductivity. The extent of this dependence may be seen by comparing the difference in the values of 'F' in Table 2.1 corresponding to low and high emissivity. If the conductivity was small, all the 'F' values would be close to those obtained for the $\varepsilon_r = 0$ case. Thus, a simple tabulation of F as in Table 2.1 is of limited use. On the other hand, this approach is simple.

Table 2.1: Radiation exchange factor "F" ($\varepsilon = 0.4$)

Model	Emissivity				
	0.2	0.35	0.6	0.85	1.0
Two-flux (diffuse)	0.88	0.91	1.02	1.06	1.11
Two-flux (specular)	1.11	1.11	1.11	1.11	1.11
Discrete ordinate (diffuse)	1.09	1.15	1.25	1.38	1.48
Discrete ordinate (specular)	1.48	1.48	1.48	1.48	1.48
Argo and Smith	0.11	0.21	0.43	0.74	1.00
Vortmeyer	0.25	0.33	0.54	0.85	1.12
Kasparek (experiment)	-	0.54	-	1.02	-
Monte Carlo (diffuse)	0.32	0.45	0.68	0.94	1.10
Monte Carlo (specular)	0.34	0.47	0.69	0.95	1.10

Determination of F : Many different models are available for the prediction of F, and these are reviewed by Vortmeyer [45]. Here, the main emphasis is on examining the validity of the radiant conductivity approach by comparing the results of some of these models with the Monte Carlo simulations and with the available experimental results.

A solution to this problem based on the two-flux model is given by Tien and Drolen [46] (Eqn. 2.25).

$$F = \frac{2}{d\left(\bar{\sigma}_{\lambda a} + 2\bar{\sigma}_{\lambda s}\right)} \tag{2.25}$$

which can be written as,

$$F = \frac{2}{3(1-\varepsilon)\left(\eta_{\lambda a} + 2B\eta_{\lambda s}\right)} \tag{2.26}$$

For isotropic scattering, B = 0.5 and Eqn. 2.26 becomes independent of the particle emissivity (for large particles). The low and high conductivity limits of this problem have been explored experimentally [46] and by the Monte Carlo method [47]. In the low-conductivity asymptote, the rays are considered to be emitted from the same point on the sphere at which they were absorbed. In the high-conductivity asymptote, an individual sphere is assumed to be isothermal and a ray absorbed by the sphere is given an equal probability of being emitted from anywhere on the sphere surface. This results in an increase in the radiant conductivity, because the rays absorbed on one side can be emitted from the other side thus bypassing the radiative resistance. In the general problem, the solid and the radiant conductivities can have arbitrary magnitudes. Then, the radiative heat flux q_r for this one-dimensional, plane geometry is given by Eqn. 2.27. The radiant conductivity k_r is given by Eqn. 2.28, where,

$$F = F\left(k_s^*, \varepsilon_r, \varepsilon\ \right) \tag{2.27}$$

and T_m is the mean temperature. The dimensionless solid conductivity k* is defined as

$$k_s^* = \frac{k_s}{4d\sigma T_m^3} \tag{2.28}$$

Within the bed, the radiation is treated by combining the ray tracing with the Monte Carlo method. The conduction through the spheres is allowed by solving for the temperature distribution in a representative sphere for each particle layer in the bed. The results for ε= 0.476 and various values of ε and k* have been obtained for both diffusive and specular surfaces. The results are shown in Fig. 2.16 (a) and (b).

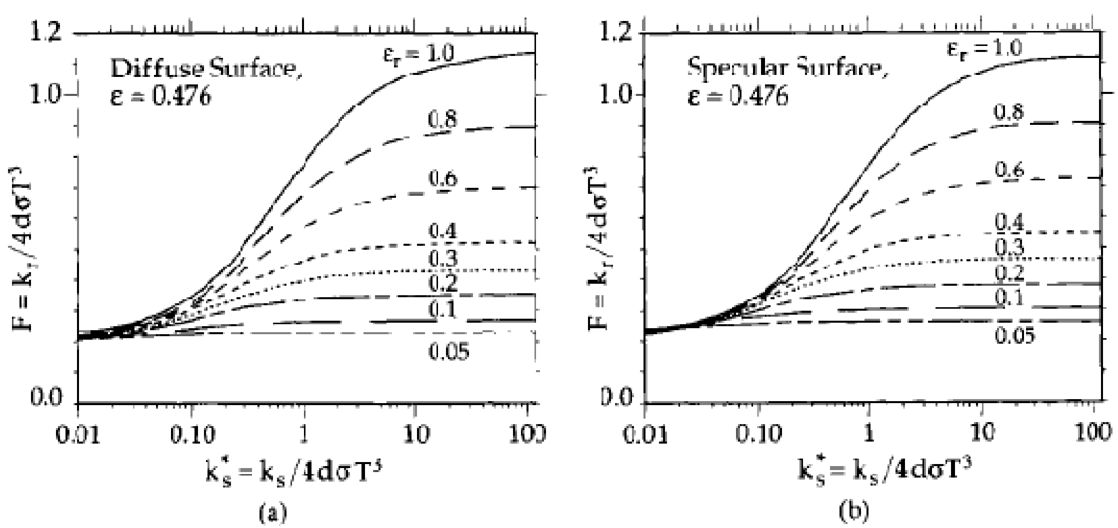

Figure: 2.16 Effect of dimensionless solid conductivity on the dimensionless radiant conductivity for (a) diffuse particle surface and (b) specular particle surface

The results for both surfaces are nearly the same. Both low and high k* asymptotes are present. The low k* asymptotes are reached for k* < 0.10 and the high k* asymptote is approached for k* > 10. There is a monotonic increase with ε_r, that is, as absorption increases, the radiant conductivity increases for high k*.

The results of Fig. 2.16 (a) and (b) have been correlated using Eqn. (2.29),

$$F = a_1 \varepsilon_r \tan^{-1}\left(a_2 \frac{k_s^{*a_3}}{\varepsilon_r} \right) + a_4 \tag{2.29}$$

for given ε, the best-fit values of the constants are given in Table 2.2.

Table 2.2 Constants in the exchange factor correlation ($\varepsilon = 0.476$)

	Specular	Diffuse
a_1	0.5711	0.5756
a_2	1.4704	1.5353
a_3	0.8237	0.8011
a_4	0.2079	0.1843

The computer-intensive nature of the problem prevented a thorough sweep of the porosity range as an independent variable. However, the effect of the porosity in the high conductivity limit has been discussed by Singh and Kaviany [47]. For example, by decreasing the porosity from 0.6 to 0.5, the magnitude of *F* changes from 0.47 to 0.51 for $\varepsilon_r = 0.35$ (specular surfaces) and from 0.94 to 0.97 for $\varepsilon_r = 0.85$ (diffuse surfaces). In practical packed beds, the porosity ranges between 0.3 to 0.6 with a value of 0.4 for randomly arranged, loosely packed monosized spheres. Therefore, the sensitivity of the radiant conductivity with respect to the porosity (as compared to other parameters) is not expected to be very significant.

Heat transfer model for debris bed heat-up: The heat transfer in a dry debris bed is found to be treated with an equivalent conductivity and porosity approach by Kaviany [20]. Eqn. 2.30 represents the energy equation proposed by Kaviany [8] and later on adapted by Siefken et al. [35] for PWR debris bed model for accident analysis code RELAP5/SCDAP. Eqn. 2.30 has been used for a steam void fraction higher than 0.8 for the prediction of heat-up of PWR specific debris bed.

$$(1-\varepsilon)\rho_D c_D \frac{\partial}{\partial t}(T) = \frac{\partial}{\partial x}\left(k_e \frac{\partial T}{\partial x}\right) + \frac{\partial}{\partial y}\left(k_e \frac{\partial T}{\partial y}\right) + Q - hA(T_d - T_b) \quad (2.30)$$

Where,

ρ_D : density of particles

c_D : heat capacity of debris particles

k_e : effective thermal conductivity

Q : volumetric heat generation

T : temperature of mixture of debris and intestinal fluid

T_d and T_b : temperature of debris and steam temperature

It is to be noted that parameters like volumetric heat generation, effective conductivity and porosity of the energy Eqn. 2.30 are responsible for deciding the heat up of the debris bed where as heat removal is governed heat transfer coefficient.

2.4 Conclusion:

The above mentioned literature survey indicates that a substantial information is available to characterize debris bed that may arise from PWR severe accident. Post TMI-2 accident and subsequent several experiments with corium material have helped to establish the characterization of debris bed. The debris bed is found to consists of loose and rock type debris. Limited experiment for PHWR has established to characterize the size and nature of debris bed. The limitation of experimentation for PHWR to understand the nature of debris bed has come from simulation of long channels heat up with large power requirements and with conservation of structural characteristics like channel stiffness. It became difficult for the experimenter to maintain the channel stiffness and other metallurgical properties.

The information on heat treatment of debris bed with porosity range of 0.4-0.5 and particle size from micrometer to 10 mm is found to be exhaustive. The models for closure relations are also found to be well studied. The study has undergone extensive research as debris bed heat transfer is having an industrial applications. Chemical industries where the particle beds are used as a catalyst in chemical reactors for accelerating chemical reactions is one of the major field of applications. Similar heat transfer treatment for heat generation debris bed model is also observed for PWR severe accident analysis model. However no such heat transfer treatment has been noticed in literature for PHWR debris bed which is having more open structures as it may be constituted with long reactor channels with fairly big diameters of 110-120 mm as compared with 5-6 mm particle size of a PWR debris bed. As severe accident is considered very recently for PHWRs, hence heat transfer studies related to such debris bed is a nascent field. As information on heat up characterization of PHWR specific debris bed (experimental investigation and mathematical model) is not available in open literature, this aspect stands to be the research gap area for PHWR community. The objective of this investigation is to close this research gap area to the extent possible and rest will be covered in the future work.

Chapter 3

Experimentation and analysis

Under severe accident condition following a postulated initiating event (PIE), disassembly of reactor channels is anticipated in PHWRs as described in Chapter 2. The accumulation of segmented long reactor channels at the bottom of Calandria form a debris bed (see Fig. 3.1a.) as concluded by Mathew et al. [30] from their channel disassembly experiments. During the process of disassembly the eccentricity of fuel bundle to PT and PT to CT of the reactor channel is expected to be lost from the original configuration and a new configuration where the components will become off-centre with each other as shown in Fig. 3.1b. A new configuration of the reactor channel appears with fuel bundle, PT and CT, where a line contact gets established among them.

An experimental plan has been conceived with an objective to characterize heat transfer and fluid flow behaviour of PHWR specific bed. Literature study carried out and described in Chapter 2 shows that an extensive heat transfer and fluid flow characterization has been done over decades for PWR specific debris bed and subsequently used for debris bed specific to different industries. An understanding of heat and fluid flow behaviour has been felt necessary for PHWR specific debris bed to understand the flow boiling pattern of submerged, partially submerged and exposed debris bed and any heat transfer crisis that may come in the debris bed. Apart from insight generation as mentioned in the experimental plan, it will be prudent to look into the applicability of existing PWR debris bed heat transfer treatment for PHWR specific debris bed as well as generation of heat transfer closure relations from the experimental results which can be a support for theoretical model formulation.

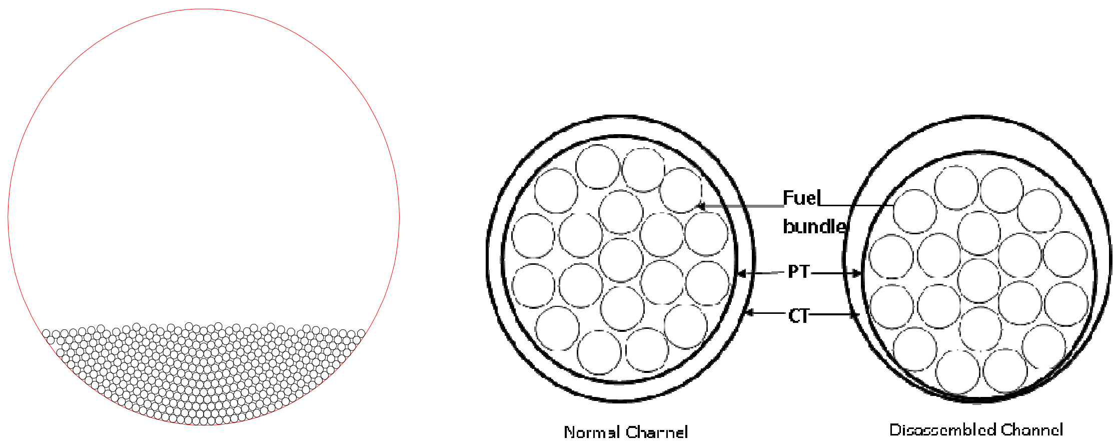

(a) Debris bed with maximum packed disassembled reactor channels

(b) Fuel bundle, PT and CT arrangement of a Normal and disassembled channel

Fig. 3.1: Schematic of collapsed reactor channels forming the debris bed

During the investigation special attention has been given on two aspects. The first aspect is related to boiling crisis of the submerged and partial submerged channels and the other one is heat transfer for exposed debris bed. It is of interest to note that each submerged disassembled channels will undergo atmospheric pool boiling at a low decay power (≈ 1%), in a restricted environment as the nuclear fuel bundles resides inside the PT of the reactor channel. The study of effect of restricted boiling on heat transfer is of importance as the large steam void present within the channel which may degrade heat transfer from fuel bundles leading to a heat-up. Related to exposed debris bed heat transfer, convective heat transfer in between channels inter space is expected to be different as the debris constituent channels are long and having larger diameter as compared to debris bed with small particles.

As the disassembled long reactor channels form the debris bed, it has been a challenge for experimental simulation of such large debris bed configuration. However experiments have been conducted with (i) a single segmented channel and (ii) multiple segmented channels debris bed to understand the thermal-hydraulic behaviour of the debris bed under heat-up condition.

Scaling of the experiments aims to conserve decay power/unit channel length, decay power to moderator volume ratio, debris bed hydraulic and heated equivalent diameters and moderator thermal-hydraulic conditions. These conserved parameters and simulation of heat generating segmented channels are expected to yield similar heat up pattern for the fuel bundles and fluid flow pattern for the submerged and exposed debris bed as expected in the reactor scale. Investigations are done for an average core power ranging from 1-0.25% decay power, different debris bed submergence levels for a fuel heat-up ranges from 100-650°C. A range of decay power is considered for the experiment as the expected time of channel disassembly may vary based on the accident scenario.

The outcome from the experiment will help to establish PHWR specific debris bed thermal and fluid flow characterization which will enable to establish a theoretical model. Following sections describes these experiments and their findings.

3.1 Single segmented channel debris bed experimentation:

The disassembled channel as shown in Fig. 3.1(b) is simulated through experiments to study the heat-up pattern of the fuel bundles for fully submerged to nearly exposed condition. The experiments also aim to establish the boil-off pattern and obtain closure relations like heat transfer coefficients for exposed and submerged section of the fuel bundle.

A test matrix shown in Table 3.1 has been used for the study which shows power and submergence levels of the reactor channel as test variables.

Table 3.1 : Test Matrix for single channel experiment

Power (kW)	Water level (mm)	Power (kW)	Water level (mm)
6	110^{+}	8	110^{+}
	50		50
	30		30
	20		20
	10		10

A schematic representation of the test matrix is illustrated in Fig. 3.2 where three components Fuel bundle, PT and CT are shown at different submergence levels. The fuel bundle is simulated with heater rod; termed as Fuel Rod (FR) to represent equivalence of 19 pin fuel bundle. The single channel experiment has been scaled at decay power level only. The experiments simulated a 1% decay power per unit length of the maximum rated channel of 3.2 MWe of 220 MWe

PHWR and corresponding maximum rated bundles location with a peaking factor of 1.3. This corresponds to 6 and 8 kW power levels for 1% of 3.2 MWe power and 1.3 times peak power (due to cosine flux) of the same channel respectively. As the selected powers are 1.5-1.9 times higher than the average channel power of the 220 MWe PHWR core, the experiment aimed to investigate the situation which can lead to a worst heat transfer environment within the channel.

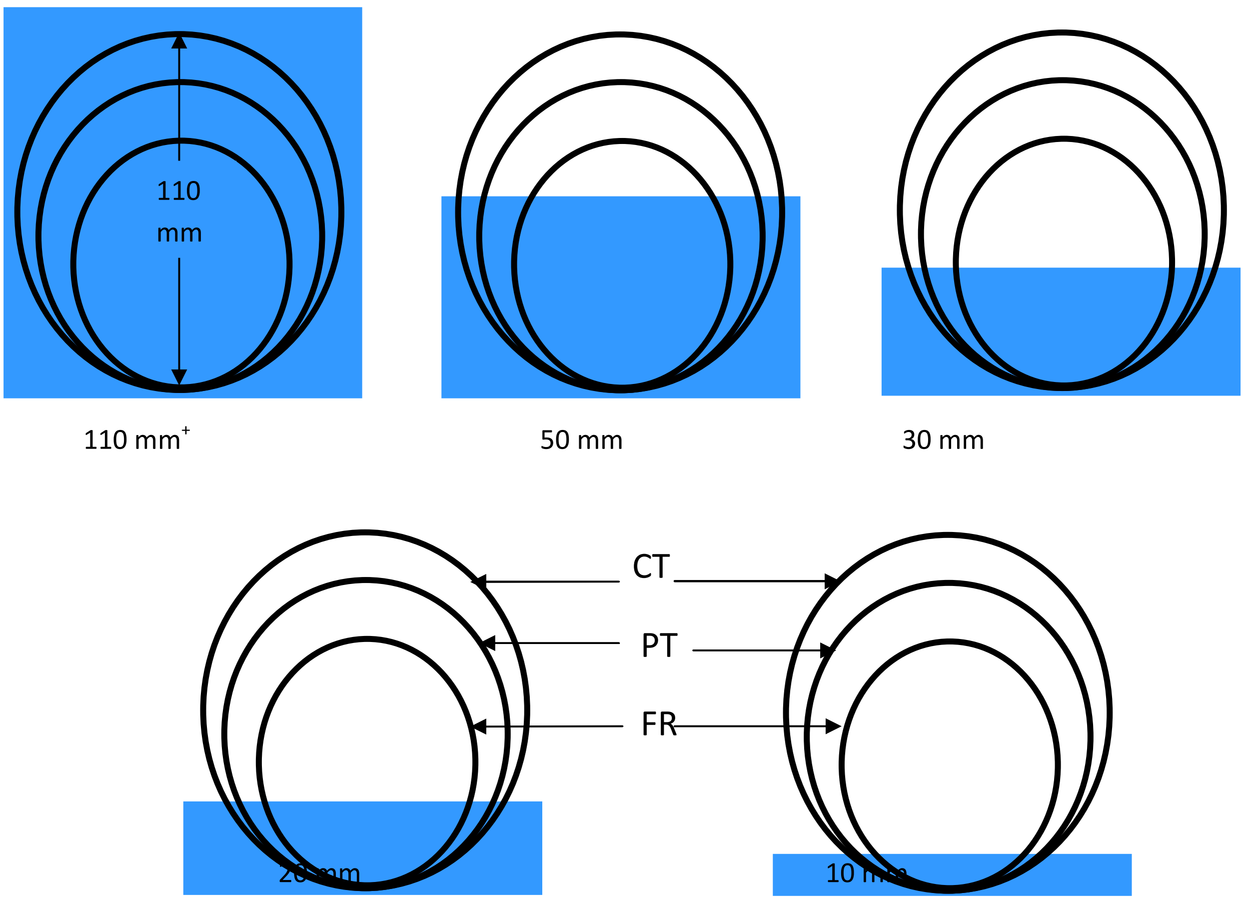

Fig 3.2 : Schematic representation of various water levels of the test matrix

As the fuel bundles are simulated with a single Fuel Rod (FR), the surface heat flux is higher (30-40 kW/m^2) as compared to the maximum rated channel average and maximum rated fuel bundle heat fluxes (6.6-8.58 kW/m^2). Higher heat flux of the FR also covers the heat flux of 10.5

kW/ m^2 for the maximum rated pin (50.2 kW/m) of the reactor core at 1% decay power level. In fact the heat flux of FR covers a high decay power level (4.6%). The excess surface heat flux will lead to a higher chance of dry out situation of the FR. The diameter of the FR is selected to conserve the hydraulic diameter (6.5 mm) of the channel. This helps to conserve the hydraulic resistance characteristics. As moderator available during the boil-off phase is large hence sufficient inventory is considered for all the submergence level for this single channel experiment. This also helps to maintain the levels for each experiment which is not being maintained through any external means. To save electrical power and time, the initial water levels for each experiment are obtained by successively removing water from tank.

3.1.1 Experimental setup:

The test setup is illustrated in Fig. 3.3. The test section, simulating the segmented reactor channel is housed in a cylindrical tank (1050 mm long and 445 mm diameter). The tank is kept in a horizontal position and kept open to atmosphere. The tank water simulates moderator water available for submerged reactor channel heat removal situation. The test section of 970 mm length consists of an assembly of a SS heater rod, PT and CT. The heater rod is made of a SS tube of 3 mm thickness having 63.5 mm outer diameter. The provided length is closely equivalent to twice the reactor fuel bundle length. The typical thin PT (Zr, 2.5 wt% Nb) and CT (Zircaloy-2) with above mentioned dimensions are used. In the test section, all three components are placed in such a manner that their axial centers are collinear with that of the cylindrical tank and their contacts lie at the bottom as shown in Fig. 3.2. The surface of the tank is being insulated with thermal wool to make the system adiabatic as much as possible.

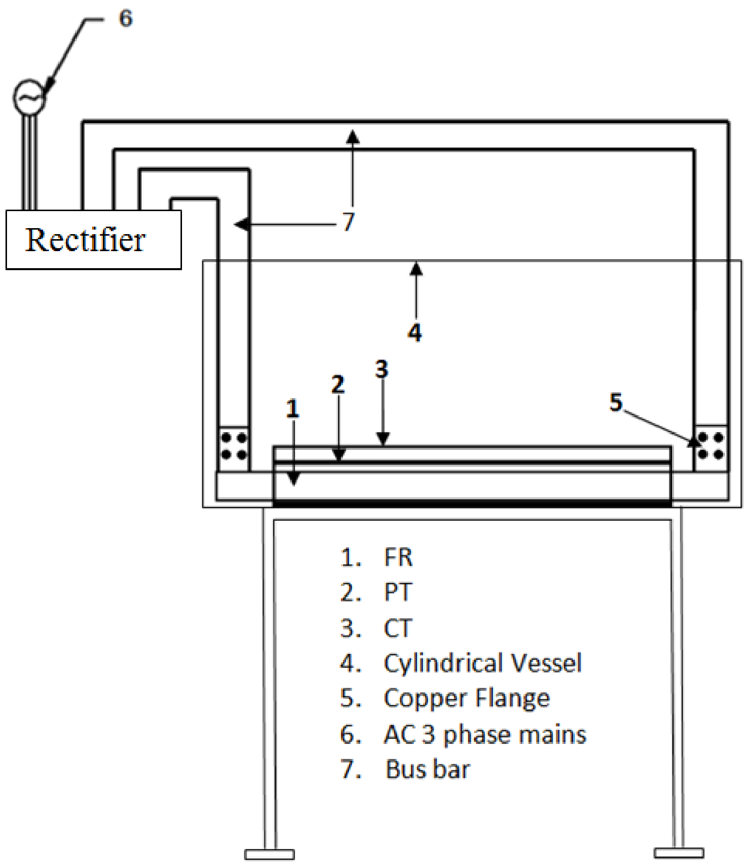

Fig. 3.3: Schematic of the test setup of single channel debris bed experiment

Heat generation is simulated in segmented reactor channel. A DC rectifier power supply of capacity 42 kW (12V/3500A) is being used. The FR is connected to bus bars of rectifier at both the ends by copper flanges. A copper foil inserted in between flange and FR has helped to reduce electrical contact resistance. The clamps are bent into L-shaped to accommodate the horizontal gap between the bus bars. The flange is connected to the rectifier by four 99% electrolytic grade copper bus bars having cross-sectional area of 10 mm x 6 mm.

The temperatures of FR are measured with minerally insulated ungrounded K-type thermocouples of 0.5mm outer diameter. The calibrated (five point calibration method) thermocouples were spot welded on FR, PT and CT. Routing of thermocouples were done with thin SS/Zr foils, spot welded to the respective metallic surface. This is done to avoid differential expansion. The temperature on PT, CT and FR are measured at center of the test section. Four and nine numbers of thermocouples are used to record the temperature of the FR, PT and CT respectively as shown in Fig. 3.4.

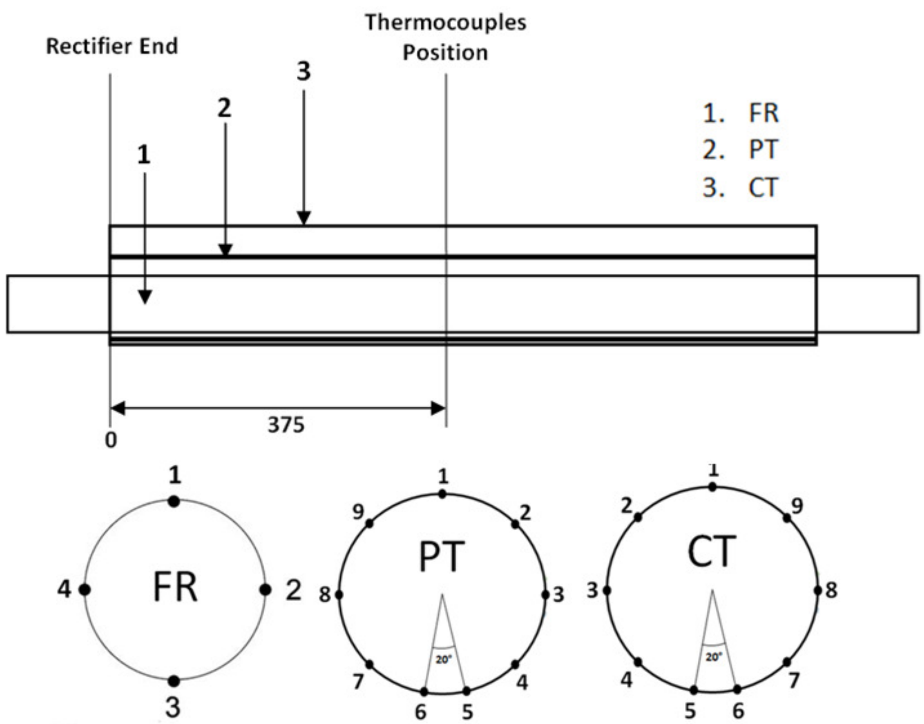

Fig. 3.4: Axial location and circumferential configuration of thermocouples

For PT and CT thermocouples are placed at an angular position of 0°, 45°, 90°, 135°, 170°, 190°, 225°, 270°, 315° with respect to vertical plane starting from top of the tubes. Accurate temperature measurement at bottom surface of PT and CT are carried out by placing two thermocouples at 10° apart. Fixing thermocouples in this manner ensured proper line contact between FR, CT and PT. The initial levels of each experiment are measured from a manual level indicator. The temperatures were recorded at an interval of 1s using a Data Acquisition System (DAS).

Power calibration is carried out during the water preheating (60°C) period by calori-metric method. Power to coolant is estimated from rise in fluid temperature. A uniform fluid heat-up is ensured by stirring the water at a regular interval. The measured electrical power from current and voltage input across the FR is found to be in well agreement with thermal power calculated from fluid heat-up and the system heat loss. The system heat loss is found to be 3% of the electrical power input.

3.2.1 Results and discussions

Two experiments at different power levels and with different water levels are carried out to investigate the heat-up pattern of the single channel. The results are discussed in the following subsections.

(i) Thermal response for 6 kW power

Tank water was heated to 60°C as a prerequisite to the test. In the preliminary heating period, readings of all the thermocouple are checked. A power of 6 kW was applied to heat up the test section. The experiment is continued till constant temperature of FR was established. The circumferential temperature variation at the middle section of FR, PT and CT for is shown in Fig. 3.5. It is observed that rate of temperature rise of FR is linear in the initial period, after which it decreases and attains a constant temperature. The maximum temperature reached in the

FR is about 98°C at the top of the tube. While in case of PT and CT the rate of temperature rise is linear throughout the experiment. The maximum temperature of PT and CT is obtained at the bottom i.e. 92°C and 82°C respectively. The reason for this is that the bottom part is in direct contact with the FR and gets more heat transfer from FR due to conduction. Eventually constant temperature is achieved at all the locations as water absorbs the total amount of heat dissipated by FR and gets boiled off.

(a)

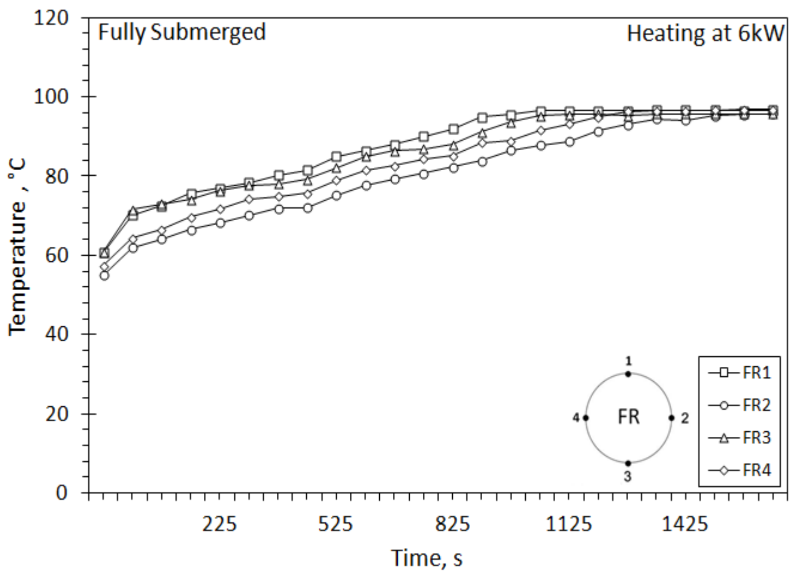

(b)

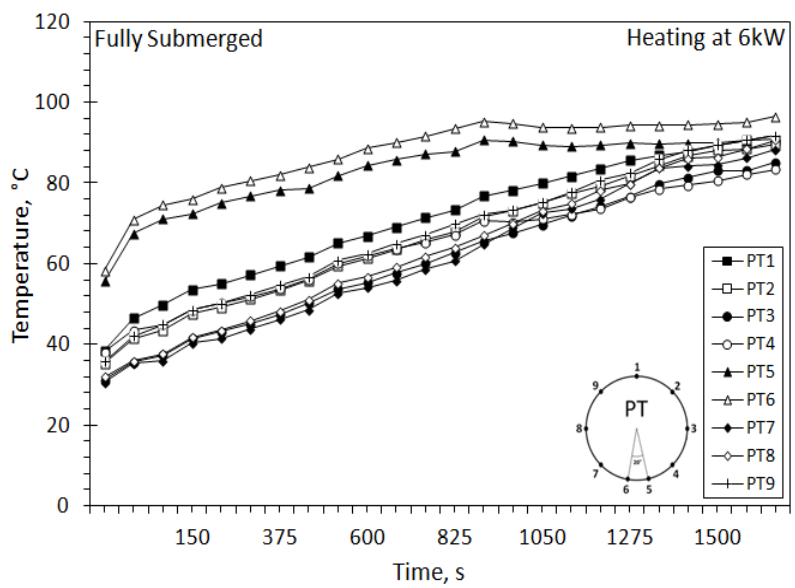

(c)

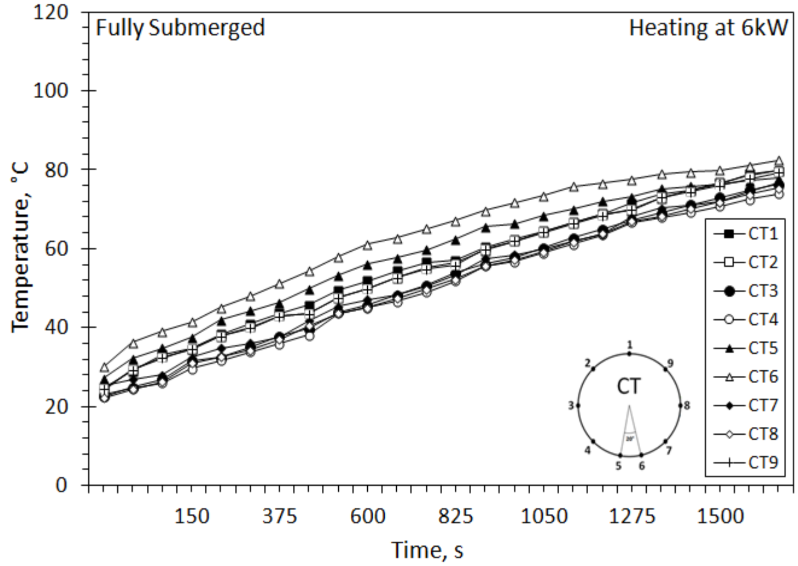

Fig. 3.5: Circumferential temperature history of (a) FR (b) PT and (c) CT for fully submerged case for 6 kW heating

The circumferential temperature variation of FR, PT and CT for 30 mm water level is shown in Fig. 3.6. It is observed that temperature of the at the top of FR rises sharply at the beginning, reaches a maximum (124°C), and then comes back to the temperature of recorded for other thermocouples locations.

(a)

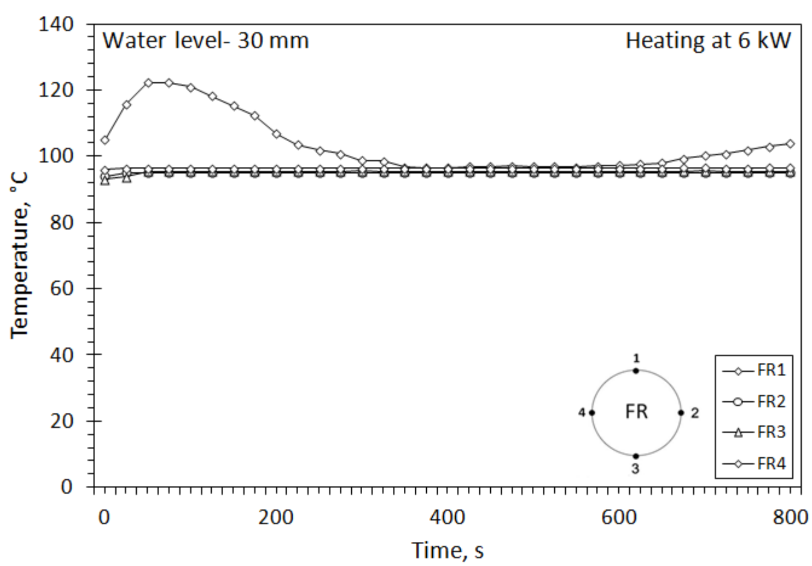

(b)

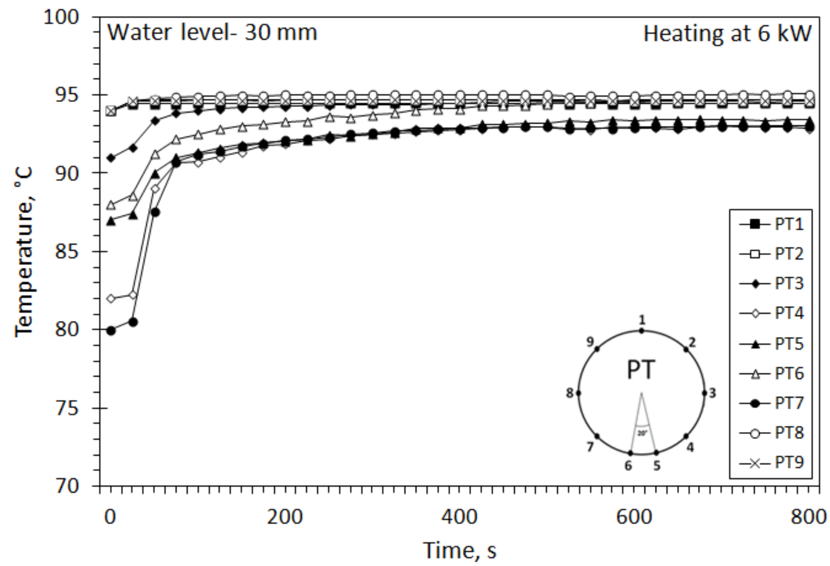

(c)

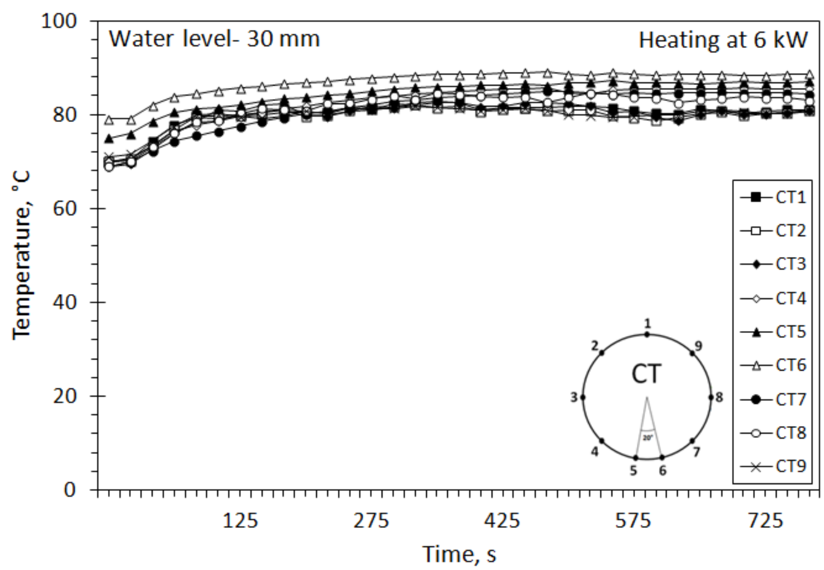

Fig. 3.6. Circumferential temperature history of (a) FR (b) PT and (c) CT for partially submerged (30 mm) case for 6 kW heating

As expected, the thermocouple at the top of the fuel rod will attain a higher temperature as it has been exposed to air from beginning of the experiment. The drop in temperature of the top of the FR is attributed to the cooling effect of the vapor generated in the annulus of the FR and PT. At the beginning of heating, heat transfer from the FR to PT is by radiation and conduction. During this period, the temperature of the exposed FR rises rapidly. With the time, the temperature of the water in the annulus between FR and PT reaches the boiling point and starts boiling. The vapor formed moves in the upward direction and sets up a convective current. The temperature of the vapor is same as that of the water and is much lower than the exposed FR. This causes the cooling of the FR, hence the temperature drops. The drop in temperature depends on water level and heating rate of the FR. The temperature of the PT and CT as shown in Fig 3.6 illustrates that the temperature of the exposed section remains at higher than that of the submerged section.

The thermal behavior of all the components (FR, PT, CT) are in expected line as heat transfer in the submersed section is higher than that of the exposed section due to vigorous nucleate boiling. The temperature of exposed PT increased quickly within 50 s and stabilizes near 96°C, while submersed PT takes a longer time and stabilizes at around 92°C. Similar temperature variation is also observed for CT. The maximum temperature of CT is found around 90°C. It is to be noted that at pseudo steady state maximum circumferential temperature variation in FR, PT and CT is found to be 4-5°C only.

(ii) Thermal response for 8 kW power

The circumferential temperature variation of FR, PT and CT for fully submerged condition is similar to case of 6 kW heating rate as shown in Fig. 3.7. However, the maximum temperature at FR1 was 99°C, at PT 96°C and at CT 88°C respectively. The maximum temperatures are higher because of higher heating load.

The temperature profiles follow a similar trend to that of the 6 kW heating with same water level (30 mm). However the maximum temperature of the exposed FR is 178°C as shown in Fig. 3.8, which is much higher than the temperature attained in 6 kW heating rate case.

(a)

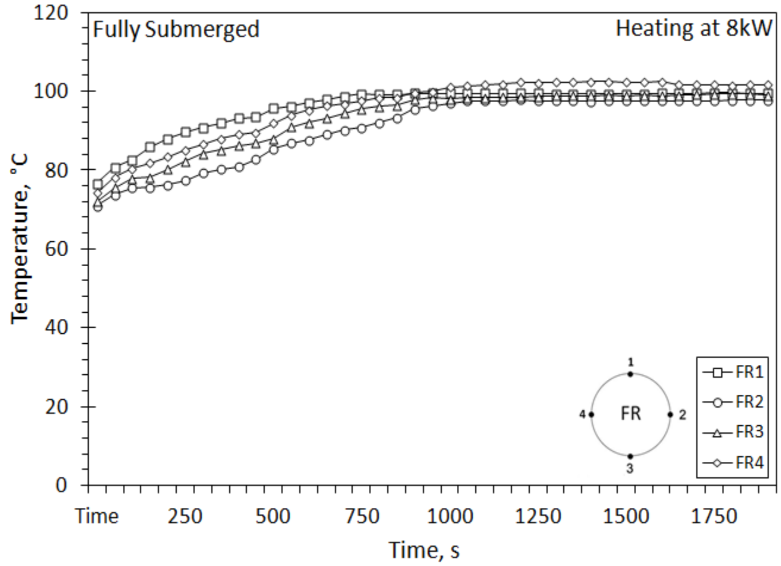

(b)

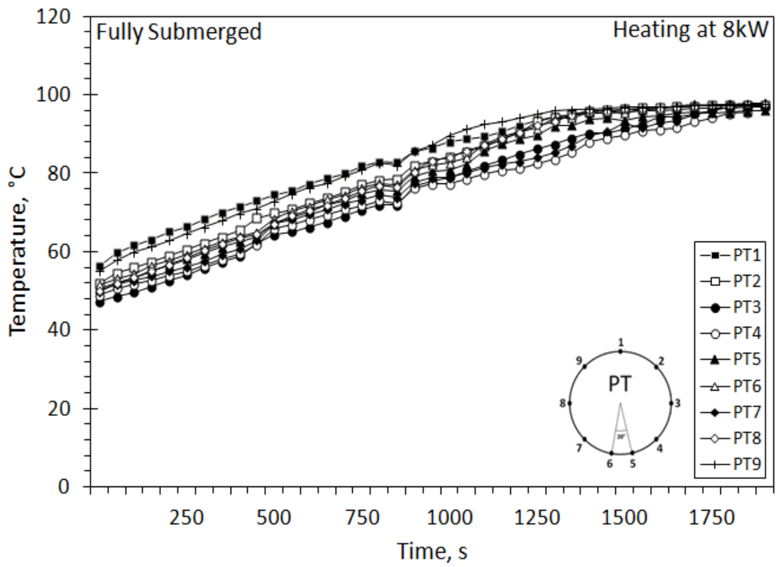

(c)

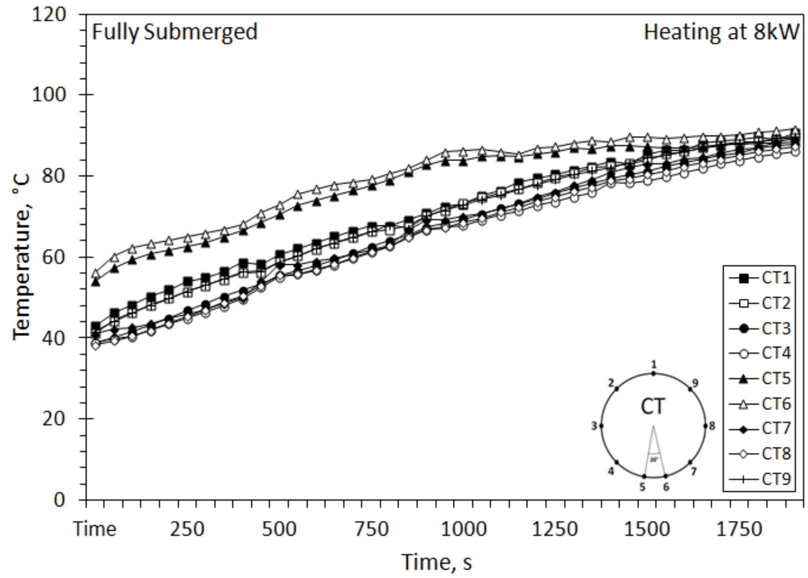

Fig. 3.7: Circumferential temperature variation of (a) FR, (b) PT and (c) CT with time in fully submerged case for 8 kW heating

(a)

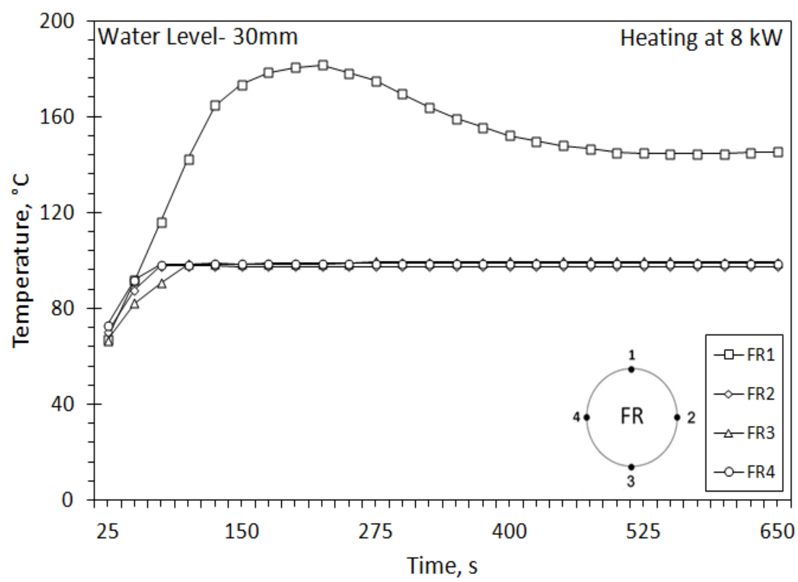

(b)

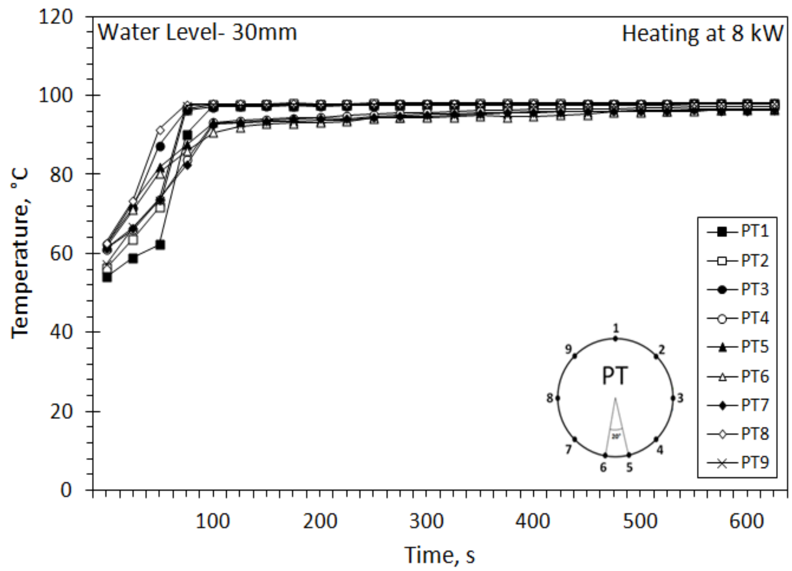

(c)

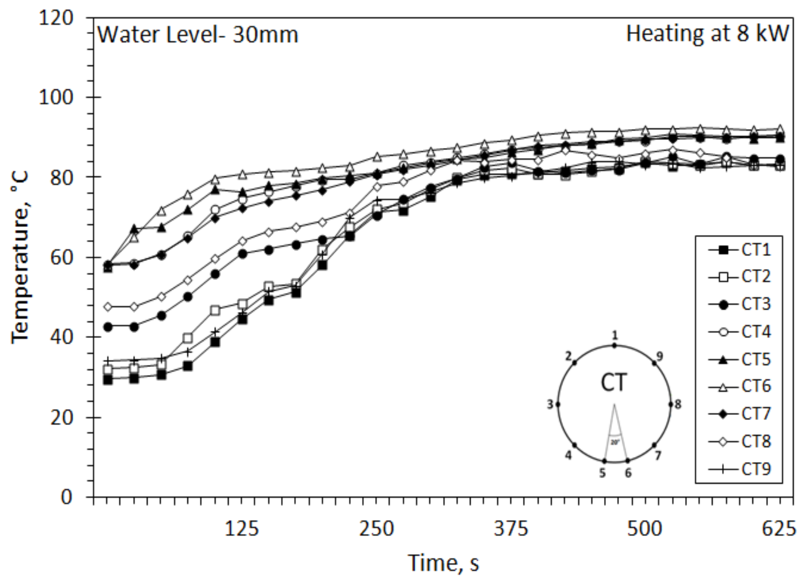

Fig. 3.8: Circumferential temperature variation of (a) FR, (b) PT and (c) CT for partially submerged (30 mm) case for 8 kW heating

It is to be noted that at 30 mm water level three thermocouples (FR1, 2 and 4) mounted on the FR surface are exposed during the experimentation (Refer Fig. 3.2 and Fig. 3.3). Out of these three T/Cs, FR1 has resulted maximum temperature and other two temperatures remained low. As the FR2 and FR4 locations are nearby the water-steam interface, the locations are cooled immediately with generated steam from the submerged section, where as FR1 is at steam starved condition due it's top position which has resulted to maximum temperature. The equilibrium temperature of the exposed section of PT remains marginally higher than the other locations. The PT temperature exposed to air, was at lower temperature initially and later on attains a higher temperature than the bottom section during attainment of pseudo steady state. As PT receives heat to a greater extent from exposed FR via convection and radiation as compared to heat received at PT bottom through FR-PT line contact hence in equilibrium the upper section of PT attains a higher temperature as compared to bottom section. In the case of the CT, the bottom section is found to be at higher temperature as compared to upper section through out the experimentation period. As the FR and PT are having line contact with CT at bottom hence there is a better heat transfer from FR-PT-CT via contact conductance as compared to less amount of heat received from PT via convection. This appears to be the prime reason for having higher temperature at bottom for CT as compared to top section.

3.1.2: Effect of Submergence on Peak FR Temperature

As already mentioned, experiments are conducted at different water levels of 110^{+}-10 mm range, temperature of the submerged section in all cases are found to be near the water saturation temperature, but the exposed section attains different temperature. The temperature variation of the topmost part of FR with time at different water levels is shown in Fig. 3.9 for (a) 6 kW and (b) 8 kW heating. The Fig. 3.9 illustrates that till submergence to 20 mm the steam cooling is sufficient to limit the temperature rise of FR. At very low level of submergence (10 mm) the steam generation is not sufficient to remove heat from exposed section, thus a continued heatup is evident.

(a)

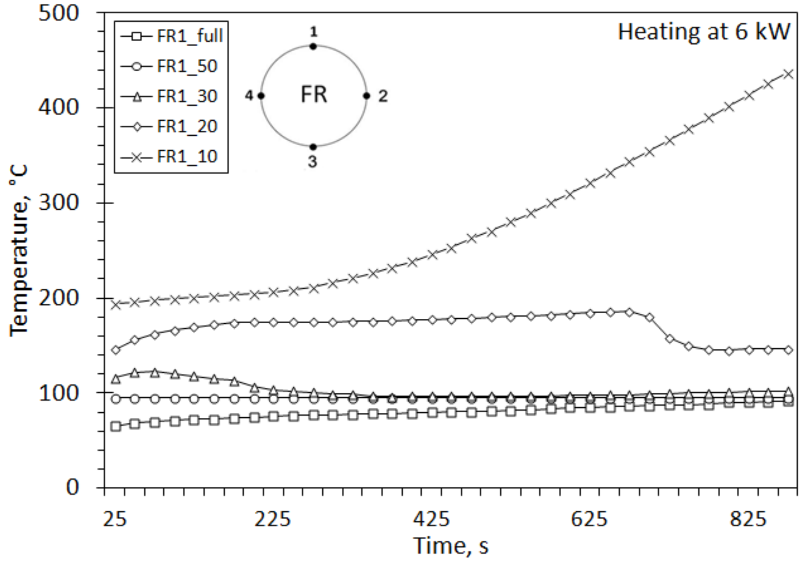

(b)

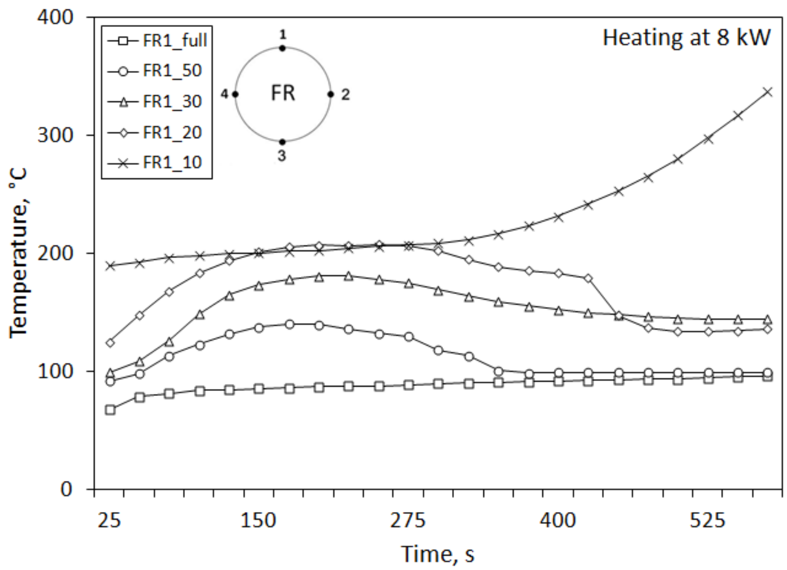

Fig. 3.9: Temperature transient for top section of the FR (exposed one) at different water level

3.1.3 Flow Pattern study :

It is evident from fully submerged experiments, a steam and water stratified counter current flow gets established. The generated steam leaves the upper section of the annulus flow path whereas the deficient water is replenished with incoming water from tank pool. A stratified flow condition exists during the boil-off period, exposing the upper section of FR to a high steam void condition. For partially submerged experimental cases similar counter current flow is evident within the test section. The generated steam travels through the upper exposed FR section of the annulus flow path where as water from tank pool enters through the lower submerged FR section of the test section.

3.1.4 Test Summary

Observed values of the temperature parameters are summarized in Table-3.2 as illustrated below.

Table 3.2 : Test summary on peak temperature for single channel experiment

Tests at 6 kW Power level	Initial Levels (mm)	Peak Temperature (FR1 position)	Time for peak temperature turn around	Pseudo Steady State Temperature (FR1 position)
	110^{+}	98°C	-	98°C
	50	103°C	-	98°C
	30	123°C	75 s	102°C
	20	185°C	675 s	140°C
	10	250°C at 575 s	-	Not attained
Tests at 8 kW Power level	110^{+}	99°C	-	99°C
	50	125°C	175 s	99°C
	30	178°C	225 s	150°C
	20	204°C	300 s	140°C
	10	350°C at 575 s	-	Not attained

3.1.5 Heat Transfer Analysis for characterization :

A heat transfer analysis has been carried out to characterize the defined heating system. Eqn. 3.1, 3.2 and 3.3 are being used to estimate steam generation rate, heat transfer coefficients for exposed/submerged section respectively.

$$\dot{m}_s = \frac{q_s}{h_{fg}} \tag{3.1}$$

$$h_{es} = \frac{q_e}{A_e(T_{es} - T_b)} \tag{3.2}$$

$$h_{ss} = \frac{q_s}{A_s(T_{ss} - T_b)} \tag{3.3}$$

Where, $\dot{m}_s$ is the generated steam flow from the submerged section of heater power (q_s), h_{fg} is the latent heat vaporization at atmospheric pressure and temperature condition, q_e and A_e are the power generated and surface area in the exposed section. T_{es}, T_{ss} and T_b are the measured exposed, submerged surface and steam bulk temperature respectively. h_{es} and h_{ss} are the evaluated heat transfer coefficients of the exposed and submerged section.

The estimated generated steam mass flow rate has been found to vary between 2.65 – 0.26 gm/s for 6 kW power and 3.55 – 0.355 gm/s for 8 kW power, depending on the submergence level as shown in Table 3.3. The convective heat transfer coefficients for the exposed section (h_{es}) and the submerged (h_{ss}) of the heater body are estimated with the help of pseudo steady state measured electrical power, apportioned to submerged and exposed section of the heat generating body, steam and water and surface temperature difference. An assumption is made that under pseudo steady state condition that a negligible amount of heat generated in the exposed section being conducted to the submerged section.

Table 3.3 : Estimated steam generation rates

Power level	Submergence levels (mm)	Submerged section heater power (%)	Estimated Steam generation (gm/s)
6 kW	110+	100	2.65
	50	69.3	1.84
	30	48.24	1.28
	20	37.93	1.01
	10	25.9	0.68
8 kW	110^{+}	100	3.55
	50	69.3	2.46
	30	48.24	1.71
	20	37.93	1.36
	10	25.9	0.92

For establishing the assumption, amount heat that flows is estimated to be 0.025 kW for the maximum difference of top to bottom temperature of 50°C of FR as observed in maximum exposed condition. The estimated h_{es} is found to vary from as low as 0.7 kW/m^2 °C to as high as 15.5 kW/m^2 °C depending on the level of submergence and power level. The estimated hs_s is found to vary between 15.5 -13.6 kW/m^2 °C depending on the level of submergence and power level. Table 3.4 and 3.5 illustrates the variation h_{es} and h_{ss} respectively with submergence level.

Table 3.4 : Estimation of convective heat transfer coefficient (h_{es}) for exposed section

Power	Submergence levels (mm)	Exposed heater power (%)	Exposed heater surface area (%)	T_{es} and T_b (°C)	h_{es} (kW/m^2 °C)
6 kW	50	30.7	30.7	98, 96	15.5
	30	51.76	51.76	102, 96	5.16
	20	62.61	62.61	140, 96	0.704
8 kW	50	30.7	30.7	99, 96	8.26
	30	51.76	51.76	150, 96	0.76
	20	62.61	62.61	140, 96	0.94

Table 3.5 : Estimation of convective heat transfer coefficient (h_{ss}) for submerged section

Power	Submergence levels (mm)	Submerged heater power (%)	Submerged heater surface area (%)	T_{ss} and T_b(°C)	h_{ss} (kW/m^2 °C)
6 kW	110^+	100	100%	98, 96	15.5
	50	69.3	69.3	98,96	15.5
	30	48.24	48.24	98, 96	15.5
	20	37.93	37.93	99, 96	15.5
8 kW	110^+	100	100%	99,96	13.66
	50	69.31	69.31	99, 96	13.66
	30	48.24	48.24	99, 96	13.66
	20	37.93	37.39	99, 96	13.66

The variation heat transfer coefficient for exposed section with respect to difference in surface and fluid temperature (ΔT) is shown in Fig. 3.10. The variation shows that with drop in level i.e. heater submergence level, the heat transfer coefficient for exposed section drops drastically for both the cases of heating. This is due to degradation of convective heat transfer environment as less steam is generated from less submerged sections.

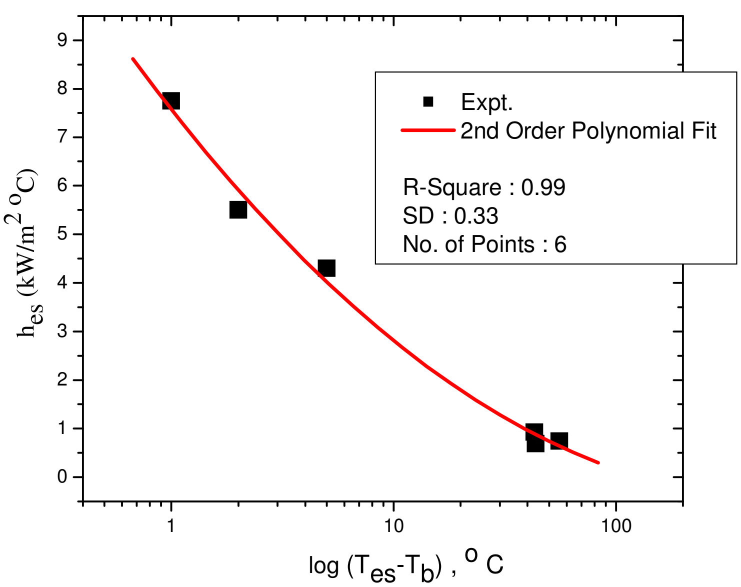

Fig. 3.10 : Variation of convective "htc" for exposed section of FR with temperature difference

The heat transfer coefficient for exposed section is found to vary with ΔT significantly where as for submerged section the heat transfer coefficient does not vary as it is under strong nucleate boiling condition.

Uncertainty in evaluating of heat transfer coefficient (h_{es}) has been carried out considering 0.2°C variation in temperature measurement of K-type thermocouples. Variation of 2.26% and 1% variation in power and exposed surface measurement are considered. The power variation is arrived at variation in current and voltage and surface area variation is on the water level measurement variation. Uncertainty (U_{hes}) in evaluating the h_{es} is as follows,

$$\frac{U_{hes}}{h_{es}} = \sqrt{\left(\frac{U_{qe}}{qe}\right)^2 + \left(\frac{U_{T_{es}}}{T_{es} - T_b}\right)^2 + \left(\frac{U_{T_b}}{T_{es} - T_b}\right)^2 + \left(\frac{U_{A_e}}{A_e}\right)^2}$$

A maximum uncertainty of 14.3% and minimum uncertainty of 2.56% are estimated. Maximum uncertainty is estimated at lower surface temperature whereas minimum uncertainty is estimated for higher surface temperature.

An attempt has been made to generate relation between Nusselt number with Reynolds and Prandtl number for the exposed heated sections. Reynolds and Nusselt number for this case are expressed as follows (Eqn. 3.4),

(3.4)

(hydraulic diameter) and (mass flux) are evaluated from Eqn. 3.5 and 3.6 respectively,

(3.5)

(3.6)

The exposed section is estimated from the various submergence levels geometry. The flow area is estimated from graphical method as the fuel bundle and PT are eccentric to each other leading a variable flow area with change in elevation. The heated equivalent diameter D_{he} for the Nusselt number is estimated from Eqn. 3.7 as given below,

$$D_{he} = 4\ \frac{expsoed\ section\ flow\ area}{expsoed\ section\ heated\ perimeter} \tag{3.7}$$

Where h_{es} is evaluated from experiment as given in table 3.4 and D_{hy} and D_{he} is evaluated the various submergence levels geometry. Table 3.6 illustrates the variation of Nu number with Re and Pr.

Table 3.6: Variation of Nu with Re for exposed section

Power level	level (mm)	h_{es} (kW/m^2 C°)	Nu	Re
6 kW	50	15.5	7.75	410.0
	30	5.16	2.58	285.0
	20	0.704	0.352	225.0
8 kW	50	8.26	4.13	548.0
	30	0.76	0.38	381.0
	20	0.94	0.47	303.0

The variation of Nu with Re for 6 kW is illustrated in Fig. 3.11. Following relation (Eqn. 3.8) is proposed to estimate the heat transfer coefficient for partially to nearly exposed sections for single maximum rated channel debris for 6 kW (≈ 1% decay power).

$$Nu = \ 0.024\ (Re) + 2.1e^{-5}\ (Re)^2 \tag{3.8}$$

Data obtained for 8 kW - power shows that below 50 mm level the Nu number falls drastically and no correlation could be established for this power level. At the accident transient time the decay power is likely to be 1% or lower as channel disassembly is a late phase phenomena for PHWR. Hence the developed correlation is applicable for a decay power 1% or lower for maximum rated or lower power channels.

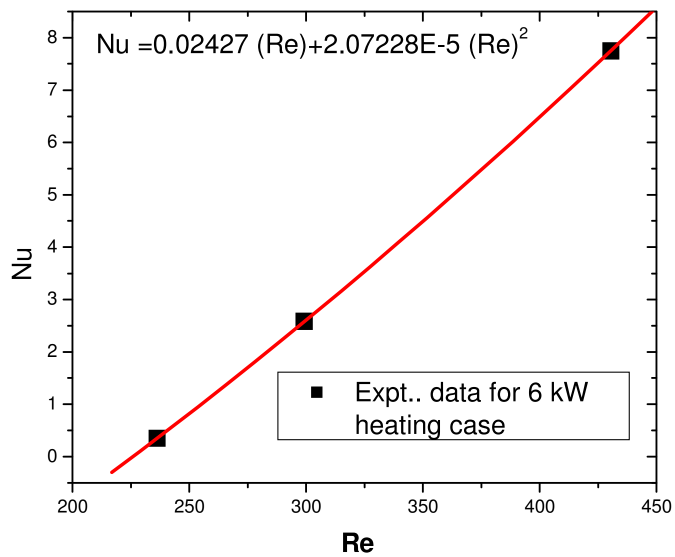

Fig. 3.11 : Variation Nu number with Re for exposed section of FR

3.1.6 Comparison of heat transfer coefficient with flat surface:

A comparison has been made between estimated heat transfer coefficients for fully submerged condition (h_{ss}) for the discussed system and heat transfer coefficients estimated by Jakob's [48] correlation for a horizontal surface atmospheric pool boiling. The Jakob's correlations are as follows (Eqn. 3.9 and Eqn. 3.10),

$$h\left(\frac{w}{m^2K}\right) = 1042\,(T_s - T_b)^{0.33} \text{ for } \frac{q}{A}\left(\frac{kW}{m^2}\right) < 16\,,\, 0 < (T_s - T_b) < 7.76\,°\text{C} \quad (3.9)$$

$$h\left(\frac{w}{m^2K}\right) = 5.56\,(T_s - T_b)^3 \text{ for } 16 < \frac{q}{A}\left(\frac{kW}{m^2}\right) < 240, 7.32 < (T_s - T_b) < 14.4°\text{C} \quad (3.10)$$

Though the range of heat fluxes (30-401 kW/m^2) for the present experiment is applicable to second correlation (Eqn. 3.10) , however the observed (T_s-T_b) is not applicable for the correlation as they are smaller (2-3°C) against the given temperature range (7.32°C-14.4°C) for the correlations (Eqn. 3.9 and 3.10). Hence estimation has been done using both the correlations. The comparison is given in Table 3.7 which shows a very high value of heat transfer coefficients (htc) of 15.5-13.66 kW/m^2 °C estimated from the present experiment as compared to the maximum value estimated from Jakob's correlation (1.3-1.49 kW/m^2 °C).

Table 3.7 : Estimated heat transfer coefficient comparison for fully submerged condition

Fully submerged cases	q/A (kW/m^2)	T_s-T_b (°C)	"htc" with Jakob's Correlation (kW/m^2 °C), using Eqn. 3.9	"htc" with Jakob's Correlation (kW/m^2 °C), using Eqn. 3.10	"htc" from the experiment (kW/m^2 °C)
6 kW	31.0	2	1.309	0.044	15.5
8 kW	41.1	3	1.4973	0.150	13.66

The many fold higher values of heat transfer coefficients derived for submerged section experimental observation strongly indicates that presence of the enclosure (PT) has introduced a strong convective current which has enhanced the heat transfer coefficient many folds as compared to open pool boiling condition.

3.1.7 Conclusion

From the experimental study following conclusions could be drawn:

(i) The steam outlet and inlet within a channel is found to be a counter current flow. The flow rate of steam is found to be much higher than water flow as steam being a lighter medium and the axial pressure gradient remained same. Hence it is considered that steam flow rate is independent and not influenced by presence of water phase.

(ii) The Fuel Rod (FR) does not undergo heat-up during a full submergence situation. Strong convective steam flow rate removes the generated heat and limits the heater surface temperature close to saturation temperature.

(iii) As the level of pool water drops below FR surface, the temperature of exposed part of FR rises above the boiling point of water.

(iv) When the water level is more than 10 mm height of the FR, the temperature of the exposed FR follows a specific trend: initially it rises to a peak value, which is above boiling point of water, and then drops down to stabilize at a certain value depending on water level and heating load applied. The FR undergoes heat-up when the water level is made close to channel bottom.

With the perspective to PHWR debris bed, it can be concluded that fully or partially submerged reactor channels will remained cooled by generated steam due to boil-off of moderator. Dryout condition at a heat flux of 30-40 kW/m^2 is not expected even though a large extent of steam void is present in the submerged channel.

3.2 Multiple Debris bed experimentation:

In this experimentation planning, the single segmented channel boil-off behavior has been extended to study the boil-off behavior of a debris bed constituted with multiple segmented channels of 8 heated and two unheated channels. As there is limitation of power supply for multiple debris bed experimentation hence the experiments are planned at a lower decay power levels 0.75%, 0.5% and 0.25% with respect to core average power as compared to single segmented channel experimentation carried out at 1% decay power level for a maximum rated channel. As uncertainty lies in decay power at which channels may undergo disassembly process, three decay power levels of 0.75%, 0.5% and 0.25% with respect to core average power are considered for experimentation which corresponds to ANS decay power levels after ½ hrs, 1 day and 6 days of reactor shutdown [56]. The decay power of 0.75%, 0.5% and 0.25% are represented by 30, 20 and 10 kW of power for the scaled down setup. The experiment simulates the situation of post core collapse where a debris bed gets formed with long segments of reactor channels. The debris bed is expected to get submerged in moderator at saturated condition corresponding to atmospheric pressure. Hence the experimental simulation of debris heat-up is carried at similar moderator condition.

The objective of multiple channel debris bed experiment is to characterize heat transfer and fluid flow of this bed. Identification of hot spot formations in the exposed debris bed and establishment of closure relation are also probed.

Scaling for this setup considers conservation of (i) debris bed decay power (220 MWe ≈ 756 MWth) per unit channel length (1:1) (ii) debris bed power/moderator volume (1:1), hydraulic and heated equivalent diameter of debris bed (1:1) (iii) debris bed power to structural heat sink area ratio (1:1) for exposed debris bed and (iv) moderator thermal hydraulic conditions like pressure and temperature (1:1). Following are the comparison of scaling ratios,

(i) Debris bed average decay power of 0.75% of 756 MWth per unit channel length (1:1)

(a) Reactor power (0.75%) : channel length = 5670 kW /1666.17 m = 3.4 kW/m

(b) Electrical power for experiment: channel Length in expt. = 30 kW/ 8 m (1.075 m x8 nos.) = 3. 5 kW/m

(ii) Debris bed average decay power of 0.75% of 756 MWth /moderator volume (1:1),

(a) Reactor power (0.75%) : moderator vol. (half filled) = 5670 kW /76.5 m^3 = 74 kW/ m^3

(b) Electrical power for experiment : moderator (water) volume in expt. = 30 kW/0.4 m^3 = 75 kW/m^3

(iii) Hydraulic and heated equivalent diameter of the debris bed (1:1)

The hydraulic and heated equivalent diameters of the debris bed of the test setup are made similar to reactor case by selecting same diameter PT and CT and stacking the channels in the most compact form by arranging the channels in a triangular pitch.

(iv) Power to structural heat sink area ratio (1:1) for exposed debris bed

(a) Reactor power (0.75%) : Calandria surface area = 5670 kW /113 m^2 = 50 kW/m^2

(b) Electrical power for experiment: Enclosure surface area = 30 kW/ 0.59 m^2 = 50 kW/m^2

(c) Moderator thermal hydraulic conditions like pressure and temperature (1:1).

During the accident conditions moderator is expected to be at atmosphere in pressure due to rupture of over pressure relief devices and in saturation conditions. Similar conditions in the experiment are conserved. The conservation of key parameters aims to achieve similar heat up and fluid flow pattern of the debris bed.

For lower power experiments the levels are adjusted to conserve power to moderator volume ratio. This is applicable for all the submerged and partially submerged debris bed.

3.2.1 Experimental setup :

The setup consists of a tank (scaled Calandria) of 1.1 m diameter and 1.2 m length which houses a debris bed kept in an enclosure, circulating pump and a plate type heat exchanger. The schematic diagram of experimental set-up is shown in Fig. 3.12.

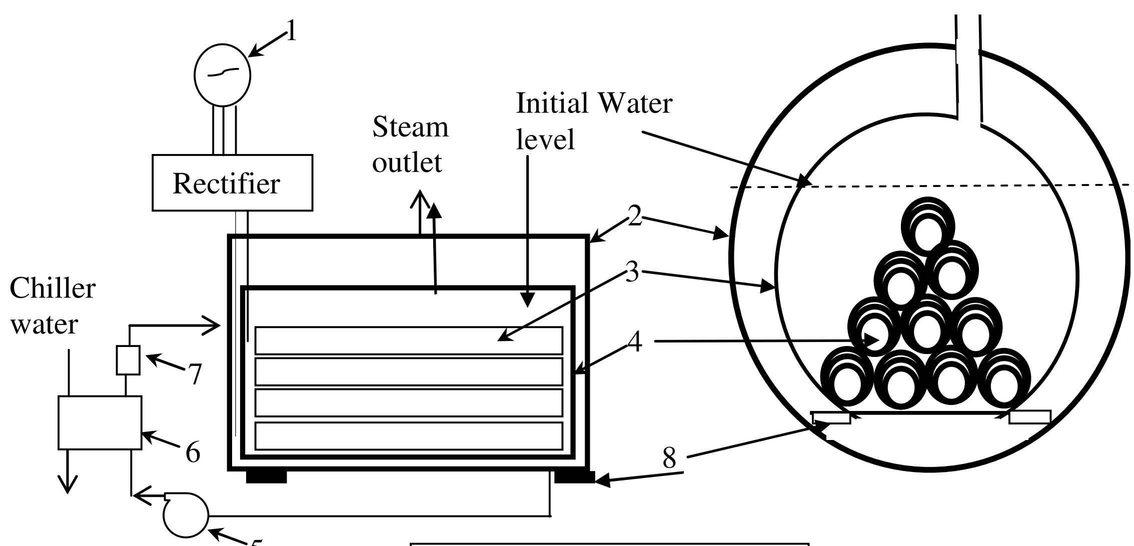

1. AC 3 Phase mains
2. Tank
3. Debris bed (10 channels)
4. Enclosure
5. Circulating pump
6. Plate type HX
7. Rotameter
8. Enclosure Supports

Fig 3.12: Schematic of multiple debris bed heat-up setup

The tank sizing is done to conserve the scaling requirement for debris bed power to water volume ratio. However with tank internal wall surface area which acts as a heat sink, it was difficult to maintain the scaling requirement for debris bed power to surface area ratio of 50 kW/m^2. Hence an enclosure over the debris bed has been introduced to maintain scaling requirement. This enables to conserve power to structural heat sink surface area ratio to 50, otherwise the power to the tank (scaled Calandria) surface area ratio would have been 38.5. The enclosure is cut open from bottom so that the tank water communicates with enclosure water conserving the power to water volume ratio. With this arrangement both the scaling i,e power to volume and power to heat sink area are conserved.

Fig. 3.13 shows the photographs of the setup along with simulated debris bed. A 42 kW DC rectifier is used to heat the debris bed. The debris bed is simulated with 10 segmented reactor channel simulators of approximately one meter length as shown in Fig. 3.13. However, only eight channels are heated in the experiment and the rest two unheated channels in the lower most row acts as support channels for the debris bed. 19 fuel pin bundle of 220 MWe equivalent fuel bundle is simulated with a Fuel Rod (FR) simulator. FR (1074 mm, O.D 64 mm and 2 mm thick) is placed inside the PT which is in contact with the CT. FRs are connected in series/parallel using copper end plates and power is supplied to the FR rods through bus-bar with copper clamp having thickness of 6 mm as shown in Fig. 3.13. The power supply scheme to eight FRs is shown in Fig. 3.14. To simulate the heat generation in the reactor channel, a DC rectifier of 42kW capacity (12V/3500A) is being used. The rectifier can operate from 10 to 100 percent load variation with the option of varying current or power continuously. The connection type has been decided after a design optimization study to maximize the power input in the setup.

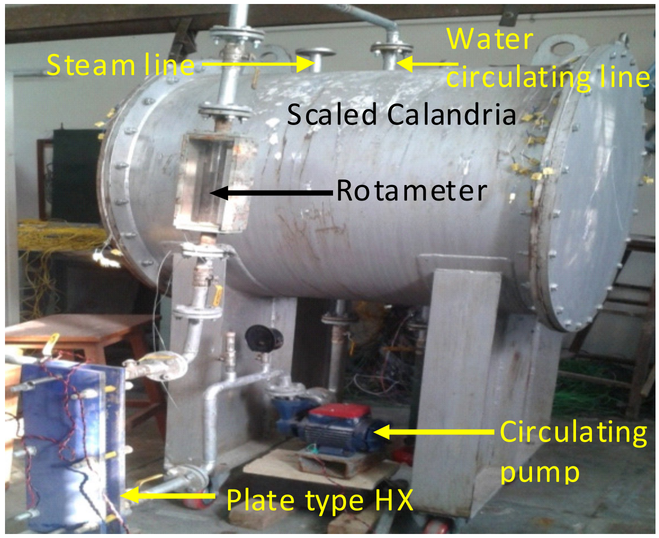

Photograph of the Test Setup

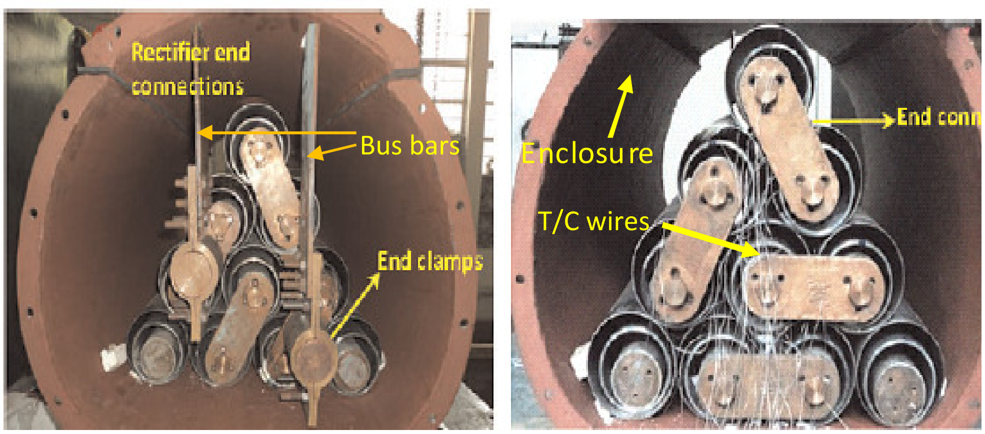

Debris bed with End Connectors and Enclosure

Fig. 3.13: Photograph of the test setup and PHWR specific debris bed

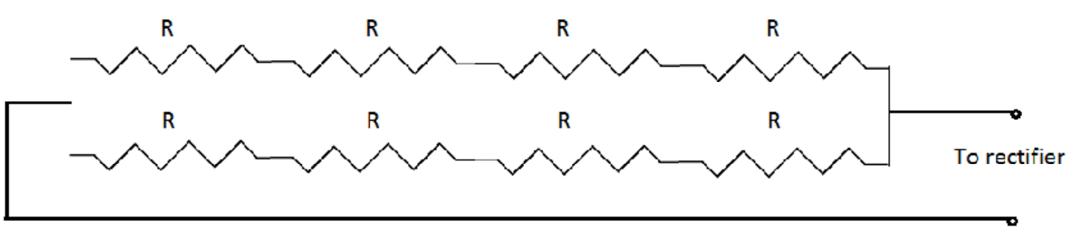

Fig. 3.14. Arrangement of series and parallel electrical connectivity of eight FRs

Following calculation shows the current requirement in the circuit. Neglecting the end resistance due to copper end plates, the resistance of the SS rod assembly (used for heating) is calculated with Eqn. (3.11):

$$R = \rho \frac{l}{A} = 7.2e^{-7}\,\frac{0.97}{3.86^{-4}} = 0.0018\;\Omega \tag{3.11}$$

Where,

A : FR cross section area ($3.86\ e^{-4}\ m^2$)

ρ : electrical resistivity ($7.2e^{-7}$ ohm.m)

l : length of the FR (1.050 m)

The evaluated net resistance of the fuel rod assembly as mentioned in electrical network (Fig. 3.14) at 20°C is found to be 0.0036 Ω. The current estimated for this resistance has been evaluated to be 3415 A. The estimated current in the bus bar will be below the limiting rating of the rectifier. As the experiment is planned up to 700°C, the resistivity is found to vary from $7.2e^{-7}$ ohm.m at 20°C to $11.6e^{-7}$ ohm.m at 700°C. The rectifier has been operated into a constant power mode to take care the change of electrical resistance with temperature rise. The heated reactor channel numberings are shown in Fig. 3.15 which identifies the heater rod locations.

For the purpose of measurement of temperature, K-type thermocouples are placed at the centre of each of the tube (FR, PT, and CT). The circumferential position of the thermocouples for each row is shown in Fig. 3.16. Five thermocouples are used for measurement of water temperature corresponding to the top of each row. One thermocouple was used for the measurement of steam temperature in the tank outlet. Sixty four thermocouples were used for the temperature measurement.

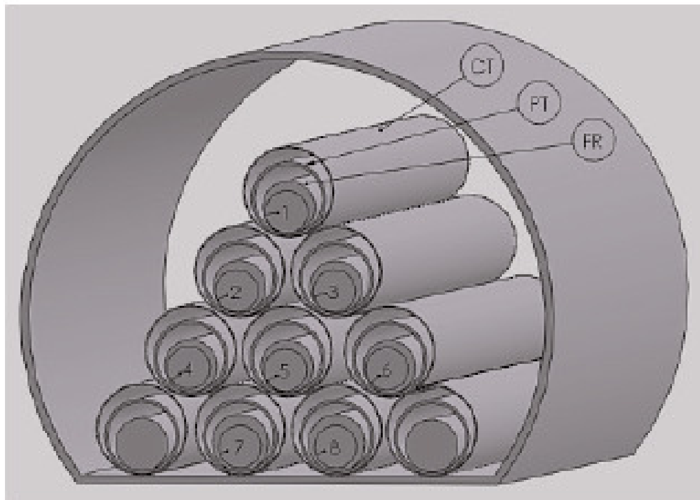

Fig. 3.15: Heated channel numbering in the debris bed

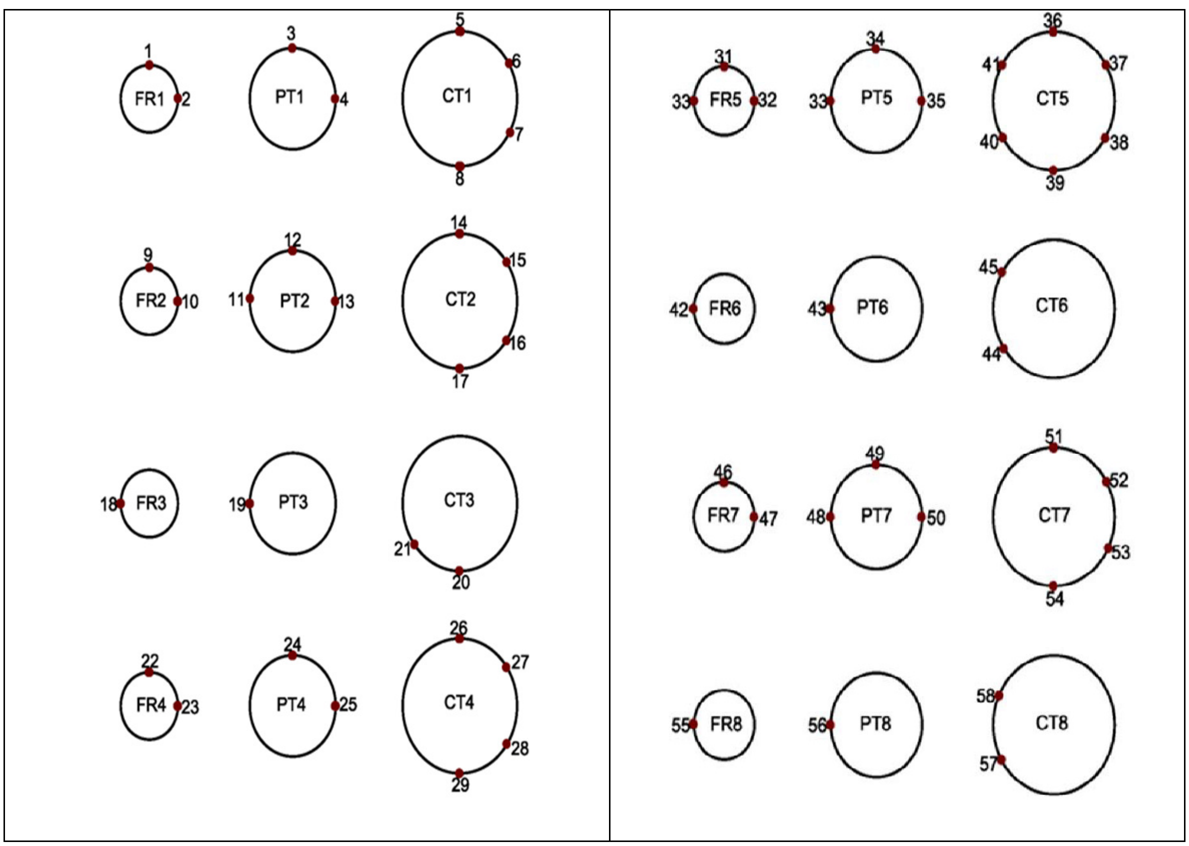

Fig. 3.16 : Circumferential position of thermocouple on FR, PT and CT for each of the rows of the debris bed

Under a reactor accident scenario boil-off moderator will lead to exposure of channel row by row, as it needs prolonged operation of the DC rectifier and huge electrical cost, the situation is studied in different steps. For a certain power level the study has been carried out first with all channels fully submerged, followed by experimentation with different row of channels exposed. Water has been successively drained to expose the row of channels. A test matrix as furnished in 3.8 has been followed to find out the debris bed heat-up behaviour.

Table 3.8: Test matrix for multiple channel debris bed experiment

Experiment type	Power	Submergence level
Short term (≈1000 s)	10 kW & 20 kW	All channels submerged in water
		First row (channel 1) half submerged
		First row (channel 1) fully exposed to air
		Second row (channel 2 and 3) half submerged in water
		Third row (channel 4, 5 and 6) half submerged in water
		Fourth row (channel 7 and 8) half submerged in water
	30 kW	All channels submerged in water
		First row (channel 1) half submerged
		First row (channel 1) fully exposed to air
		Second row (channel 2 and 3) half submerged in water
Long Term (≈3000 s)	10 kW & 20 kW	Fourth row (channel 7 and 8) half submerged in water

The test matrix is divided into two sections. The first section deals with experimentation to understand the effect of different submergence levels on the debris bed heat-up and the second sets of experimentations has been carried out to understand the behaviour of exposed debris bed. The first section of experimentations are for shorter duration (1000 s) as this section of experiments are similar to the single channel experiment at fully and partially submerged condition which has generated sufficient insight. The second sets of experimentation are for longer duration (≈3000 s) duration as this section of experiments aim to achieve a thermal equilibrium of all the heaters rods (FR) which is essential to characterize the heat-up pattern of the exposed debris bed.

This is to mention here that long term experiment with 30 kW experiment for exposed debris bed was unsuccessful as the connectors between fuel rods (FR) failed repeatedly due to local overheating.

The experiment begins with a calibration phase where the electrical power to thermal power and thermocouples are calibrated. Initially water in the tank is being heated up to a temperature of 80^0C followed by thermal calibration at 80% of experiment set power to avoid boiling. The electrical power to thermal power calibration is done by circulating the pool water through a plate type heat exchanger. The circulating flow rate and heat exchanger inlet and outlet temperatures are measured with a rotameter and thermocouples. Heat input to water is estimated by Eqn. (3.12)

$$q = \dot{m}C_p(T_o - T_i) \tag{3.12}$$

Where $\dot{m}$, C_p, T_o and T_i are circulating water mass flow rate, water specific heat at average of inlet and outlet water temperature, heat exchanger inlet and outlet temperatures respectively. The measured electrical power from current and voltage input across the FR is found to be in well agreement with thermal power calculated from heat-up input to water and system heat loss. The system heat loss is found to be 3% of the electrical power input power. After a successful calibration the FR power is increased to 100% of set desired power. The experiments for each case continued till a steady pseudo state of FR temperature has been achieved. For each case 2-3 experiments have been conducted and the average values are presented for discussion. However for most of the cases the measurement values were found to vary by 2-5 °C at lower temperature (100 °C – 250 °C) and 10-15°C for higher temperature range (250 °C – 650 °C).

3.2.2 Experimental results and discussion

As the temperature history of channels 2 and 3 (refer Fig. 3.16) are found to be similar, for purpose of clarity, the temperature of only one channel is presented. Similarly channel 4 and 6 also have similar characteristics; hence temperature of the rods of either 4th or 6th channel is presented. Channel 5th is the most critical channel as it is completely enclosed by other channel and may have maximum constrain for steam/water flow. Hence temperature history of channel 5 is presented. As channel 7th and 8th show similar characteristics, only one of the channels result is presented. Whenever a channel is partially submerged, the top of the FR is exposed to air/steam and the thermocouple on the side (90^{o}) is submerged in water. In such a case, the temperature of these two locations is significantly different, hence for such cases both the temperatures are presented. The fuel rod (FR) numbers of various channels are provided in Fig. 3.15 for ready reference.

A. Short term experiments

Experiment I: Heating with 10 kW

(i) Fully submerged condition

Fig. 3.17 (a) shows the variation of the maximum temperature of FR for each row. It can be observed that the maximum temperature is about 101^0C, which is slightly above the boiling point of water (98^0C at experiment site). The maximum temperature is observed in the FR5, which is completely enclosed by other channel. This could be attributed due to less flow circulation in around the channel housing FR5 as compared to other channels. It can further be observed that with time the temperature of each channel decreases slightly and reaches to a steady state. The channel at the top has maximum exposure to the surrounding fluid flow and is at minimum temperature with respect to other FRs. Fig. 3.17 (b) and 3.17 (c) show the temperature of PT and CT for all channels which follow the FR heat-up. It can be observed that for all channels these temperatures are at about the boiling point of water. Boling is observed in all channels as they are at same power. The generated steam leaves from both the ends of the channels.

(ii) Channel 1 (1st row) fully exposed to air

Fig. 3.18 (a) shows the variation of the maximum temperature of FR for each row. It is observed that the temperature of the FR1 increases with time and reaches a steady state of about 200^oC at the top and about 150^oC at it's side location. Hence an asymmetric temperature distribution is observed in the exposed channel. The stabilization of temperature could be attributed due to limited cooling by steam generated by submerged channels. Even though the channel was without water at the start of heating, some water enters into the channel PT due to the vigorous boiling that takes place from lower channels. Fig. 3.18 (b) and 3.18 (c) show the temperature of

PT and CT for all channels. Unlike the previous case, the temperature of both the PT and CT increases at the top for channel one. This could be due to the radiation heat transfer between the FR1 and PT. The maximum temperature attained by PT and CT are 108°C and 106°C respectively. The temperatures of all other channels are below 100^{o}C as they are submerged in water. Among these submerged channels temperatures of PT and CT for channel 5 show maximum temperature. It is to be noted that PT5 and CT5 of channel 5 temperature (Fig. 3.18 (b) and (C)) are highest among the all submerged channels. This again confirms cooling limitation to FR5 channel.

(iii) Channel 2 and 3 (2nd row) half submerged in water condition

Fig. 3.19 shows the variation of the maximum temperature of FR for each row. The top row is completely exposed to air. The temperature of FR1 increases at a faster rate at the beginning. The rate of temperature rise decreases with time and stabilizes around 200°C. The maximum temperature of FR2 is found to be 130^{o}C. Fig. 3.19 (b) and (c) show the temperature of PT and CT for all channels. It can be observed that for all channels these temperatures are at about the boiling point of water.

(iv) Channel 4, 5 and 6 (3rd row) half submerged in water condition

Fig. 3.20 (a) shows the variation of the maximum temperature of FR for each row. Half submergence of 3rd row leads to top two rows exposure to air. The temperature profile of these two FRs are similar to fully exposed FR in previous case. The maximum temperature of FR1 is 210^{o}C, FR2 is 200^{o}C, FR4 is 124^{o}C and FR5 is 127^{o}C respectively. Fig. 3.20 (b) and (c) show the temperature of PT and CT for all channels. One can observe that the temperatures of the PTs and CTs fully exposed to air also increases due to convective heat transfer from FRs. The temperatures of all submerged channels remain near the boiling point of water.

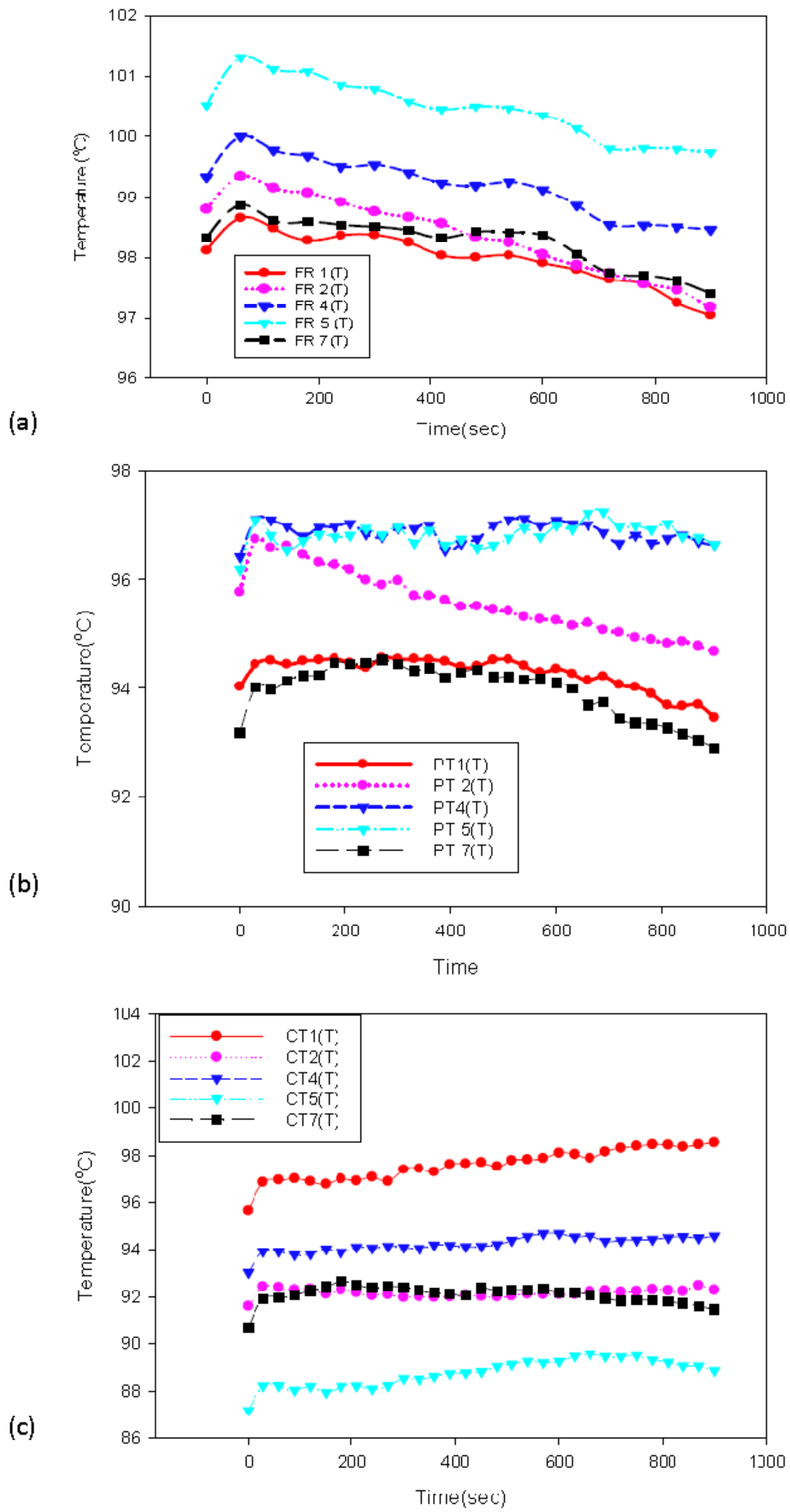

Fig. 3.17 : Temperature history of all channels submerged in water (10 kW)

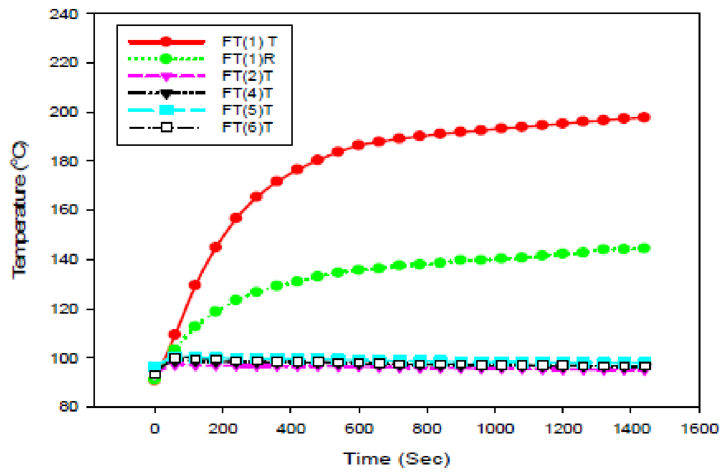

(a)

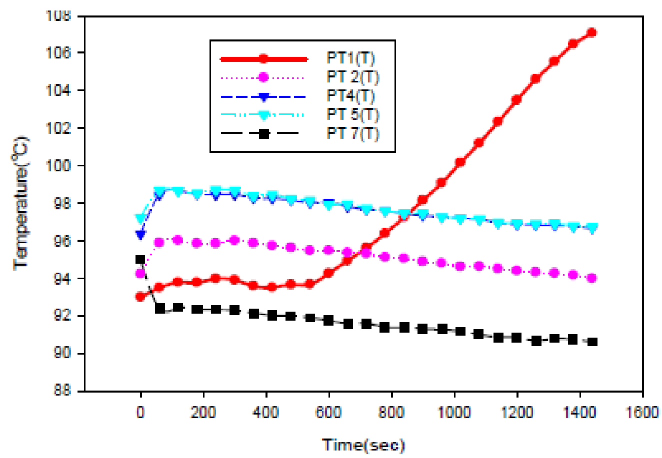

(b)

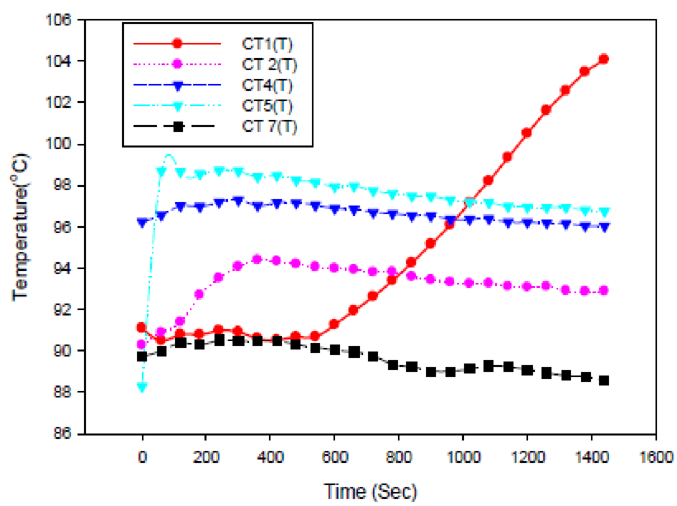

(c)

Fig. 3.18 : Temperature history of all channels for 1st row fully exposed (10 kW)

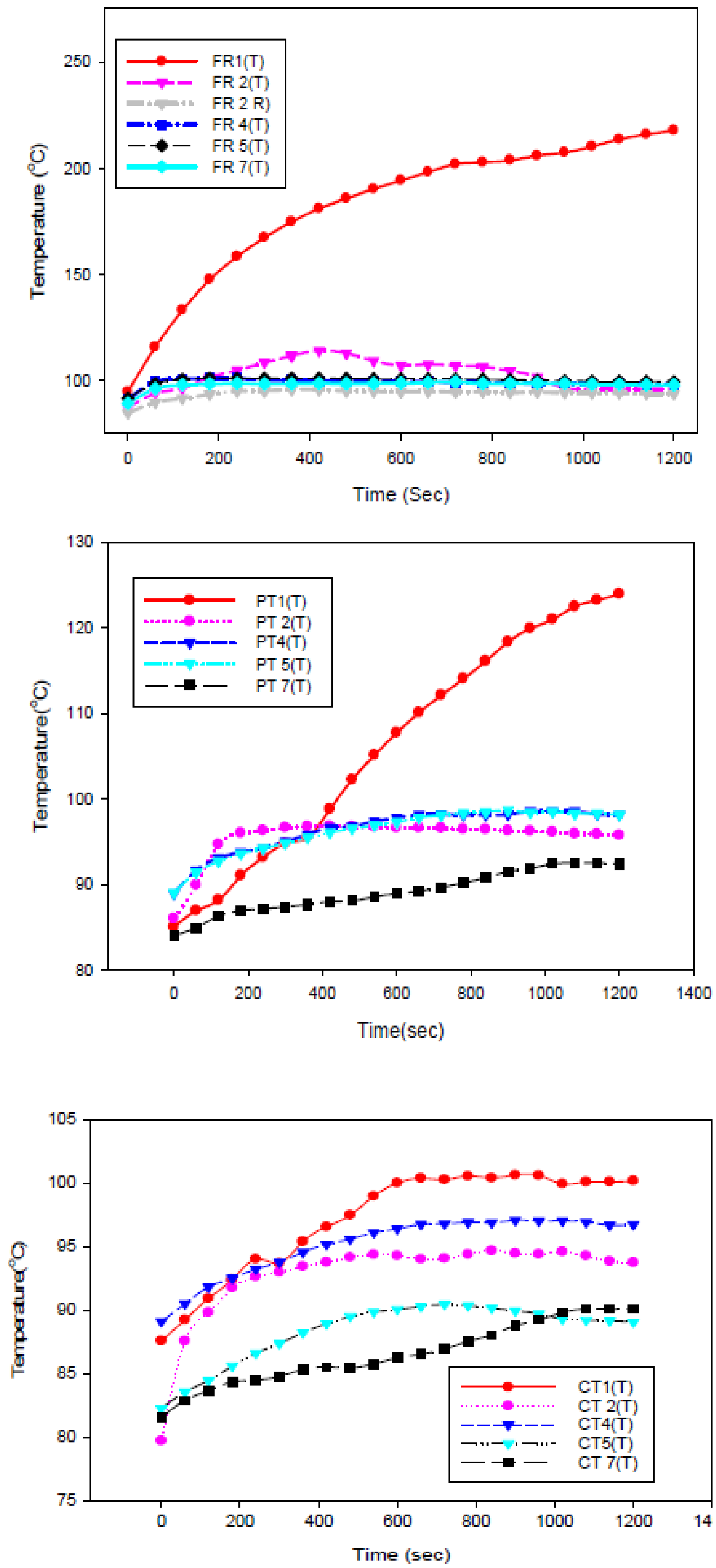

(a)

(b)

(c)

Fig. 3.19 : Temperature history of all channels for 2nd row half submerged (10 kW)

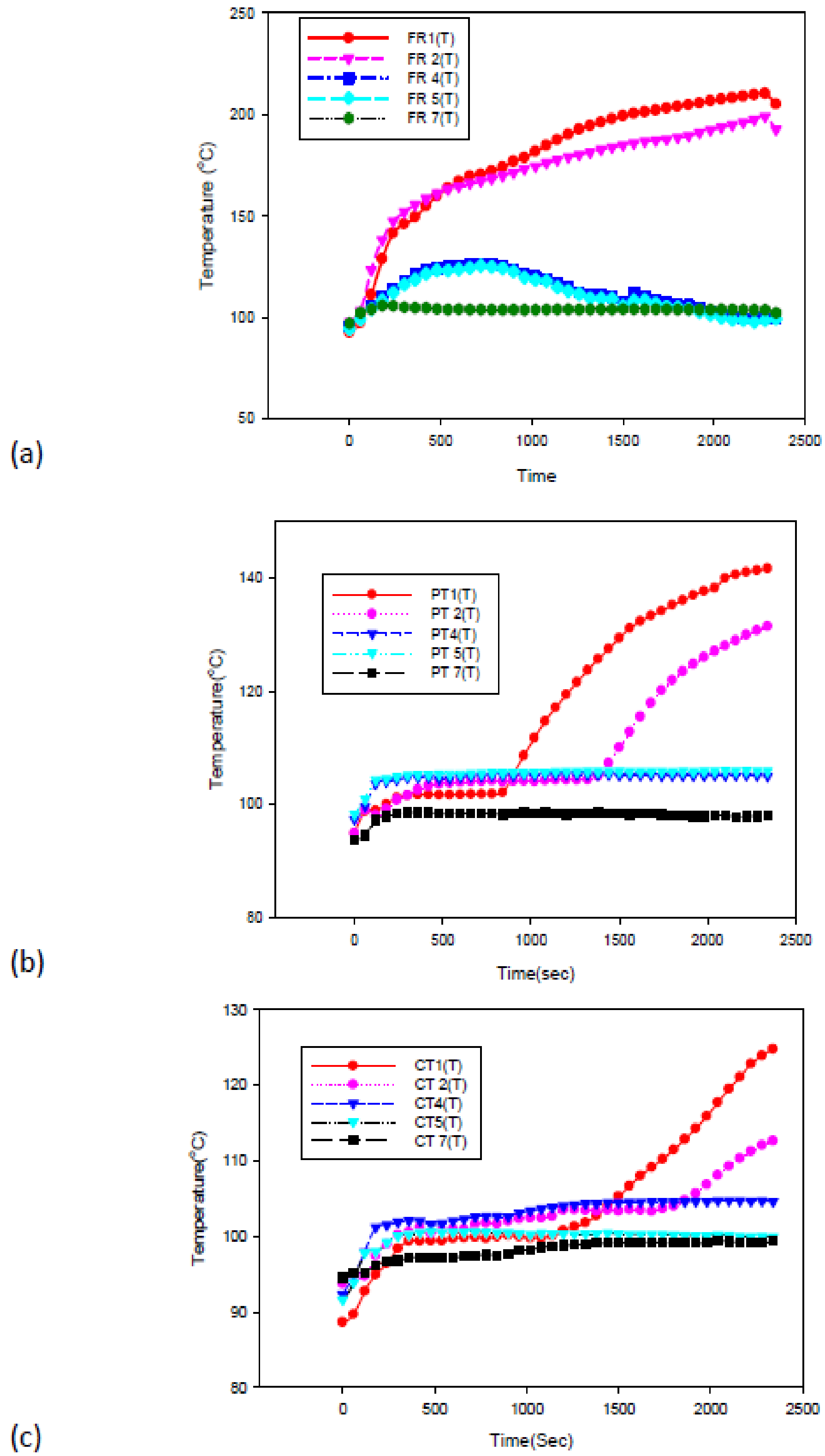

Fig. 3.20 : Temperature history of all channels for 3rd row half submerged (10 kW)

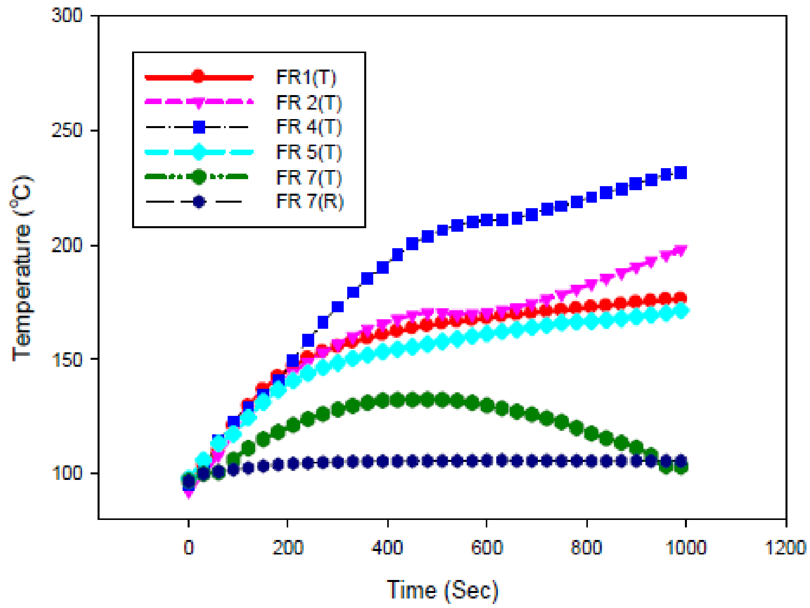

(a)

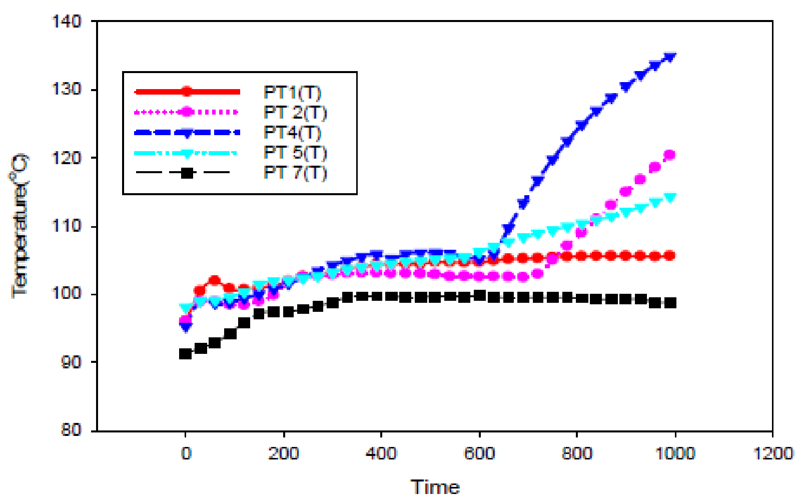

(b)

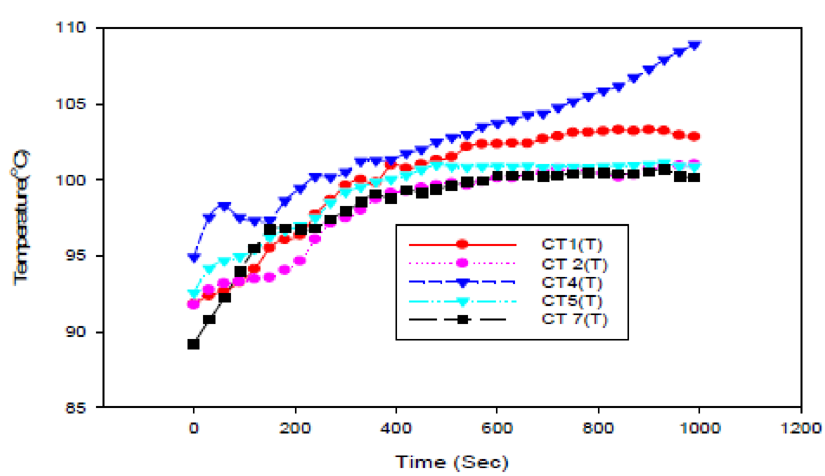

(c)

Fig. 3.21: Temperature history of all channels for 4th row half submerged (10 kW)

Channel 7 and 8 (4th row) half submerged in water condition

Fig. 3.21 shows the variation of the maximum temperature of FR, PT and CT for each row. In this case top three rows are completely exposed to air. The temperature profiles of these FRs are similar to fully exposed FRs as observed in previous case. However in this case due to very small amount of steam generation from half submerged heaters of channel 7 and 8 convective heat transfer of the exposed channel is poorer. This leads to temperature rise of the exposed channels higher than previous case. It is to be observed that top most channel (FR1) temperature is lower as compared to below row channels. This is due to sufficient radiation heat transfer from top channel to the enclosure wall where the 2nd (FR2) and 3rd row channels (FR4) radiation heat transfer gets limited by above and bottom channels. For this case FR4 temperature is found to be more than FR5 inspite of FR4 being a peripheral channel with a better heat sink of the bed. This trend is unexpected and probably the alteration of electrical resistance from arising from it's connectivity with the bas bur (refer Fig. 3.13) has caused this effect.

Experiment II: Heating with 20 kW:

Experiments carried out with 20 kW heating shows similar heat-up trend to 10 kW heating; however the maximum temperature is higher as compared to 10 kW heating. Fig. 3.22 shows the temperature history for fully submerged conditions. No local heat-up is evident at this elevated power for fully submerged condition. Different conditions like partial submergence to nearly exposed conditions are also shown in Fig. 3.22. For nearly exposed condition of the debris bed, FR5 shows maximum temperature as compared to its neighboring channels as well compared to top most channels. This confirms less cooling available for the channel surrounded by other channels which are having a better heat sink.

Experiment II: Heating with 20 kW

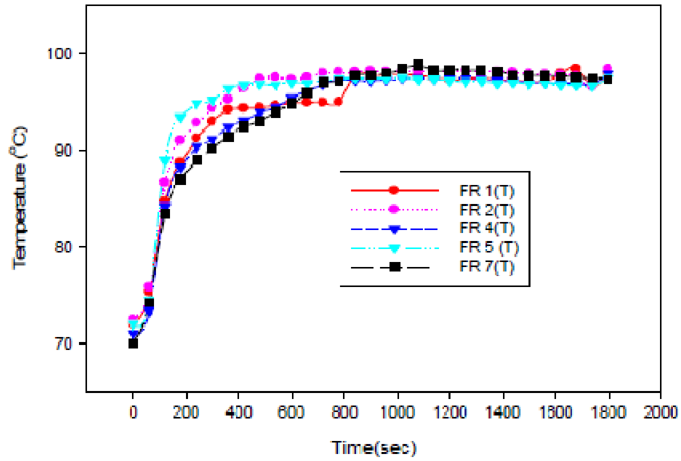

Fully submerged

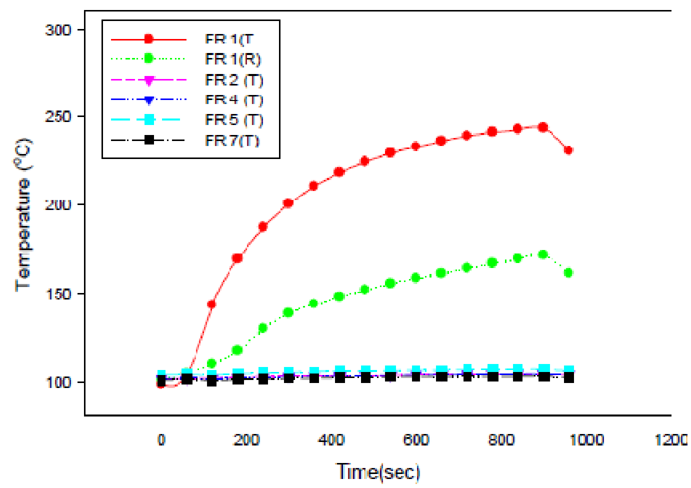

1^{st} row fully exposed

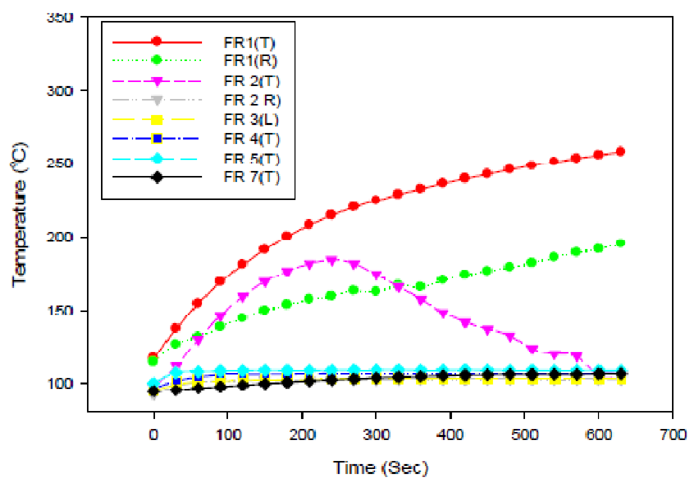

2^{nd} row half submerged

Experiment II: Heating with 20 kW (contd.)

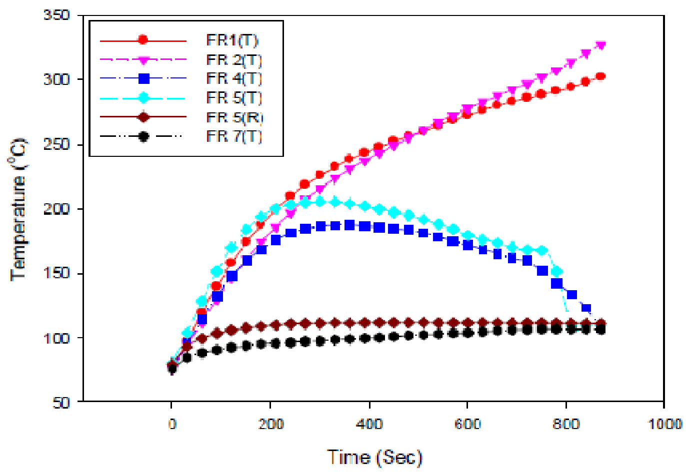

3rd row half submerged

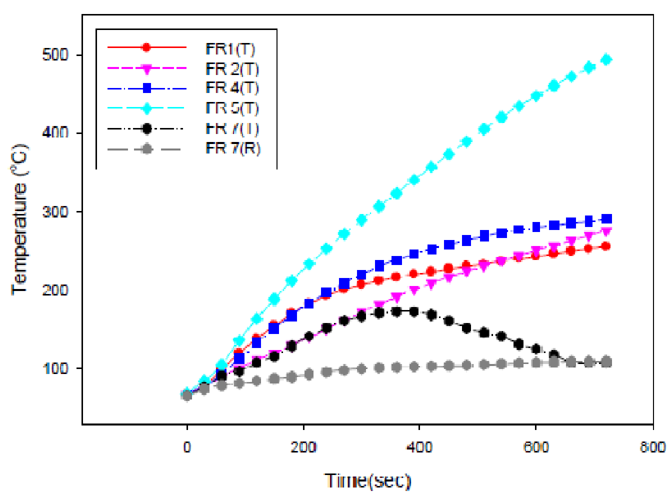

Fig. 3.22: Temperature history of debris bed from fully submerged to nearly exposed condition for 20 kW heating

Experiment III: Heating with 30 kW

Experiments for higher exposed debris bed could not be conducted due to repeated failures of the copper clamps which connects one heaters to the other heater. The experimental results 30 kW heating is illustrated in Fig. 3.23.

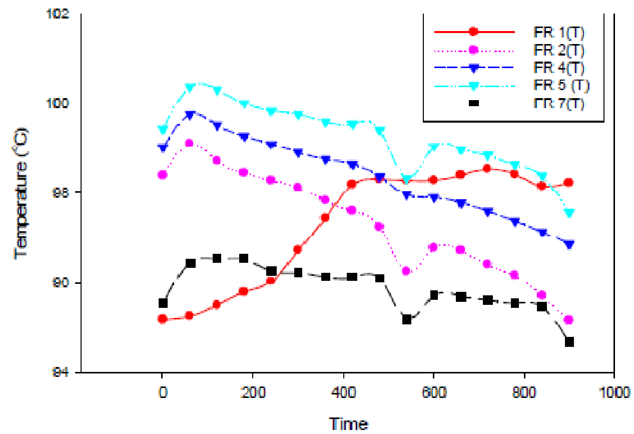

(a) Fully submerged

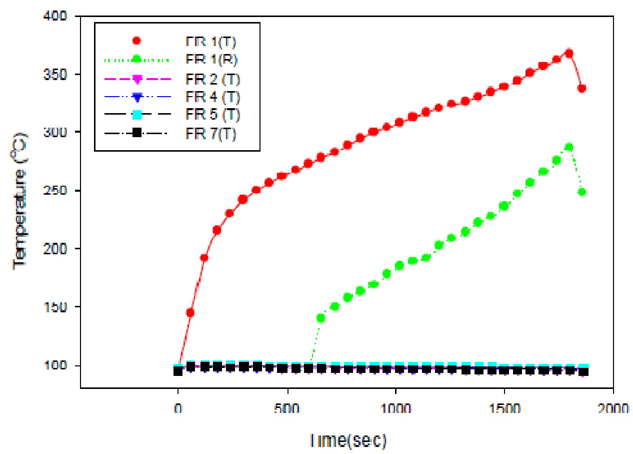

(b) 1st row fully exposed

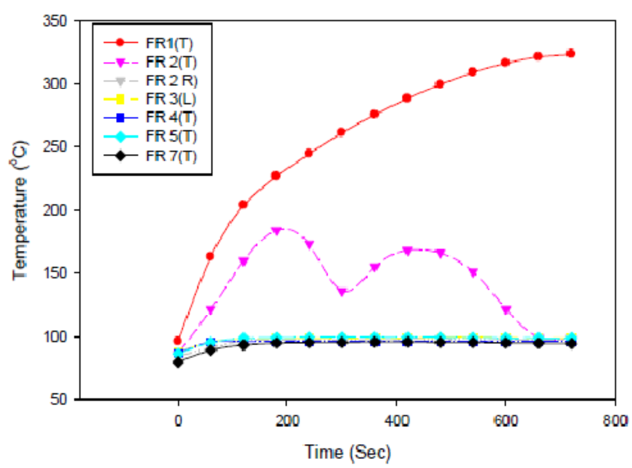

(c) 2nd row half submerged

Fig. 3.23: Temperature history of debris bed for 30 kW heatin

The figure shows similar temperature behaviour as observed for 10 and 20 kW heating, experiments however the exposed maximum temperature of top FR1 is found to be higher as compared to 10 and 20 kW. This is due to higher power of the channel only.

It observed from all the test that for a circumferential temperature gradient exists for FR during it's exposure. The circumferential temperature observations for top and right side for FR1 (FR1 (T) and FR1 (R)) is only provided here. The gradient is found to range between 40-90°C for 10-30 kW experiments. Similar observation was also made for single channel experiment

3.2.3 Effect of level on channel temperatures

A comparison of channel temperature FR measurements at the end of experiment is furnished in Table 3.9. It is confirmed that for full submergence state the debris remain cooled. It is very clear from the Table 3.9 that with decrease in level the channels get heated up, however the heat-up gets limited from steam convective heat transfer or radiative heat transfer to neighboring channels or enclosure wall. In case of nearly exposed condition of debris bed which is equivalent to dry debris bed, the channel (FR5) surrounded by neighboring channels (FR4 and FR6) tend to get heat-up more due to unavailability of convective and radiative heat sink as compared to it's neighboring channels.

Table 3.9: Debris bed behaviour under different submergence levels

Power (kW)	Submergence	FR1 (°C)	FR2/FR3 (°C)	FR4/FR6 (°C)	FR5 (°C)	FR7/FR8 (°C)
10	full	97.2	97.3	98.2	100	99.5
	1st row exposed	190	98.5	98.5	99.0	99.0
	2nd row half exposed	200	100	100	100	100
	3rd row half exposed	210	200	100	100	100
	4th row half exposed	160	190	225	160	100
20	full	98.5	98.5	98.5	98.5	98.5
	1st row exposed	245	100	100	100	100
	2nd row half exposed	255	100	100	100	100
	3rd row half exposed	300	330	110	110	110
	4th row half exposed	250	260	270	500	110
30	full	98.5	96	97.5	98.1	95
	1st row exposed	275	100	100	100	100
	2nd row half exposed	325	98	98	98	98

B. Long term experiments

As mentioned in the test matrix two long term experiments are carried out for 10 and 20 kW power with 4th row half submerged condition.

Experiment I : 10 kW heating :

In this experiment all the rows are exposed to steam environment, except the bottom row which is made half submerged. The experiment has been started at a water level in the tank of 100 mm. As most of the channels are exposed, steam generation is also very low in this case. As a result, the fluctuation in water level is also very small. Hence the temperature of the row 3 is unaffected by water level fluctuation of fourth row of channels and behaves like fully exposed channel. Fig. 3.24 shows the temperature variation of FRs, PTs, and CTs. The maximum temperature attained by FR1 is observed to be 478°C with corresponding PT temperature of 360°C and that of CT is 215°C. A pseudo steady state has been attained for this case after one hour of experimentation. It is observed that heat-up trend of FRs (FR5 and FR6) for similar row of channel FR5 and FR6 is similar. The experiment reveals that FR1 and FR2 heatup rates are considerably lower as compared to FR5 and FR6 before they attend a steady state. It is inferred that the convection current at the channel boundary was sufficient for FR1 and FR2 to limit the heat-up rates of top channels as compared to limited convection current available for bottom channels due to space constrain at bottom section of debris bed (refer Fig. 3.12).

Experiment II : 20 kW heating :

Fig. 3.25 shows the temperature variation of FRs, PTs, and CTs for 20 kW heating. As the thermocouple on FR2 didn’t function in this experiment the temperature for FR2 is not shown in the figure. Maximum temperature attained by FR1 is about 607°C with corresponding PT temperature of 485°C and that of CT is 312°C. A pseudo steady state has been attained for this case which has taken nearly one hour of experimentation.

It is to be noted that for both 10 and 20 kW experiment the FR5 temperatures has attained nearly similar to all the other FR temperature. The channel belonging to FR5 is surrounded by neighboring channels as compared rest channels which are having a better heat sink in terms of steam convection and radiation to the enclosure wall. This brings that fact that for longer period the cooling mechanism at the innermost part of debris bed i,e FR5 has established in an efficient way to limit the temperature rise. A comparison of short term experimentation (Fig. 3.22) for 4th row half submerged case with long term (Fig. 3.25) experimentation with similar conditions show that during initial period the FR5 temperature rises higher than neighboring channel temperatures however for long duration, setup of sufficient cooling limit it’s temperature rise and attains similar temperatures to channel FR1 and FR6 which gets a better heat sink due to their proximity to enclosure wall.

3.2.4: Heat transfer characterization study :

As the fully and partially submerged heat-up behaviour for multiple channel debris bed experiment is found to be similar to single segmented channel, in this section the heat transfer characterization is attempted only for exposed section in presence of very low steam flow emerging from bottom most section of the debris bed. The characterization has been carried out to understand how equivalent conductivity and convective heat transfer modes can influence heat transfer of the bed. Temperature information from FR5 for 20 kW case has been used for this evaluation as it resides amidst of all the channels representing the debris bed internal characteristic. The major flow paths are inter channel spacing, spacing between debris bed and enclosure and flow path between PT and CT. No flow path is envisaged between FR and PT as FR being heated the pressure inside PT will remain high as compared to outside.

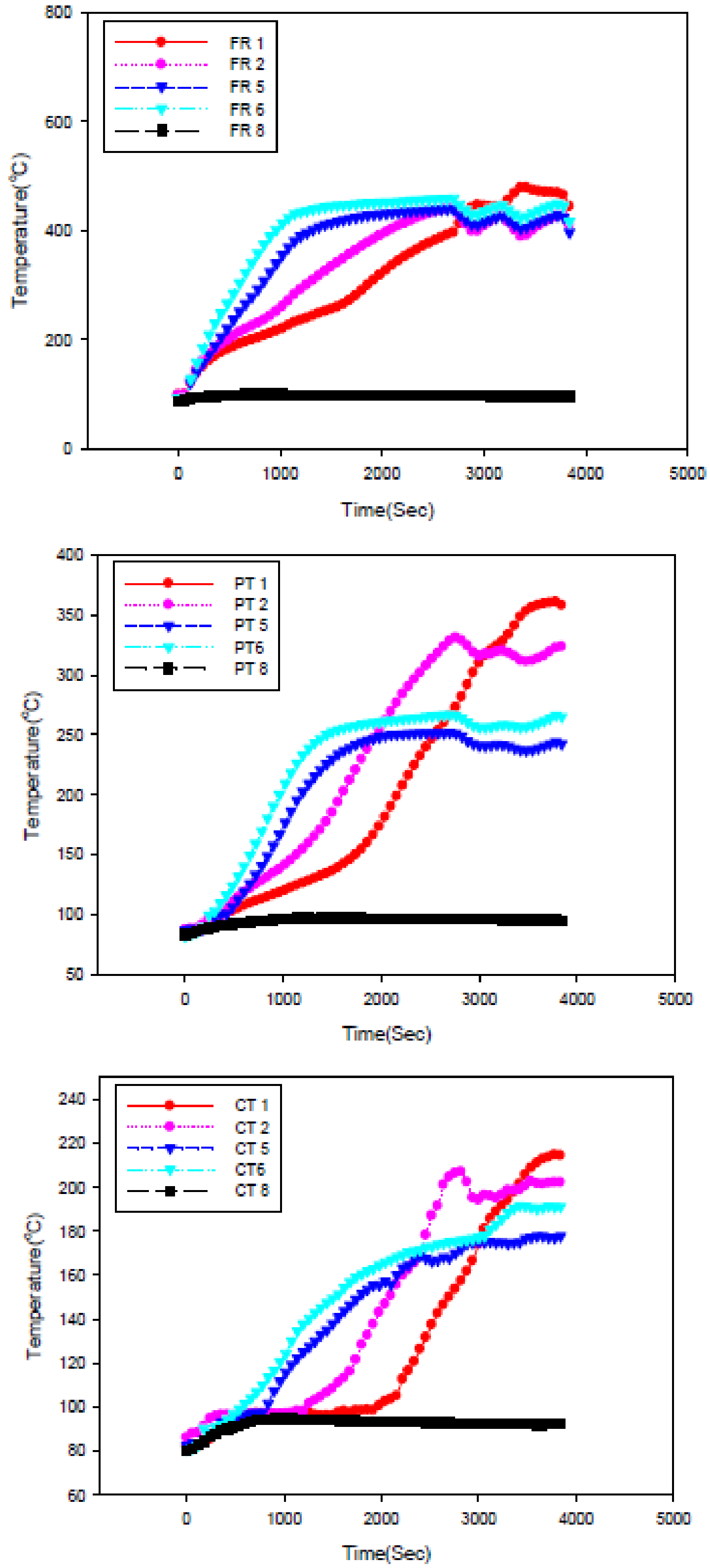

Fig. 3.24: Temperature Transient for long term multiple channel debris bed at 10 kW heating

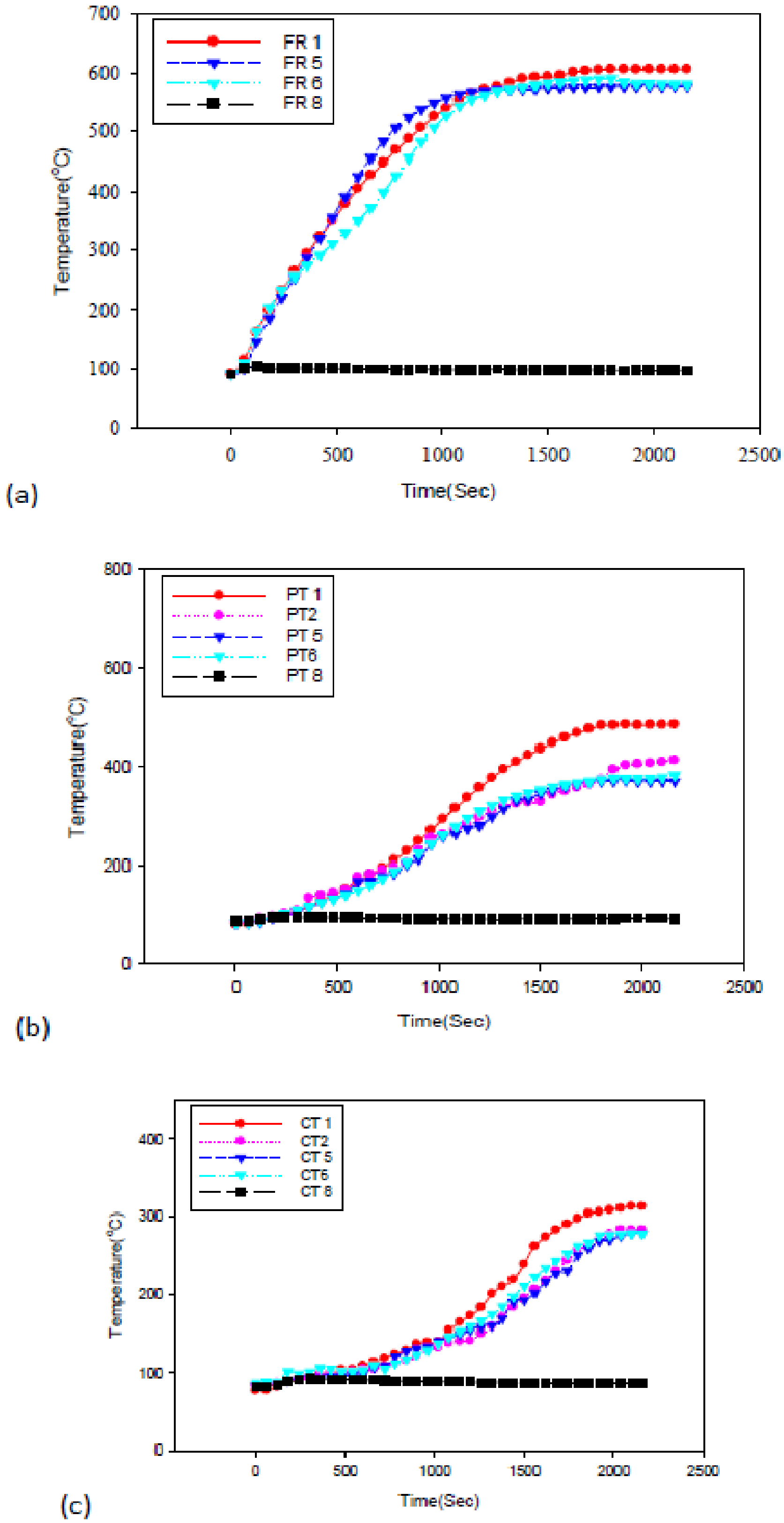

Fig. 3.25: Temperature Transient for long term multiple channel debris bed at 20 kW heating

Fig. 3.26 illustrates the intra debris bed flow paths responsible for equivalent conductivity and convective flow path.

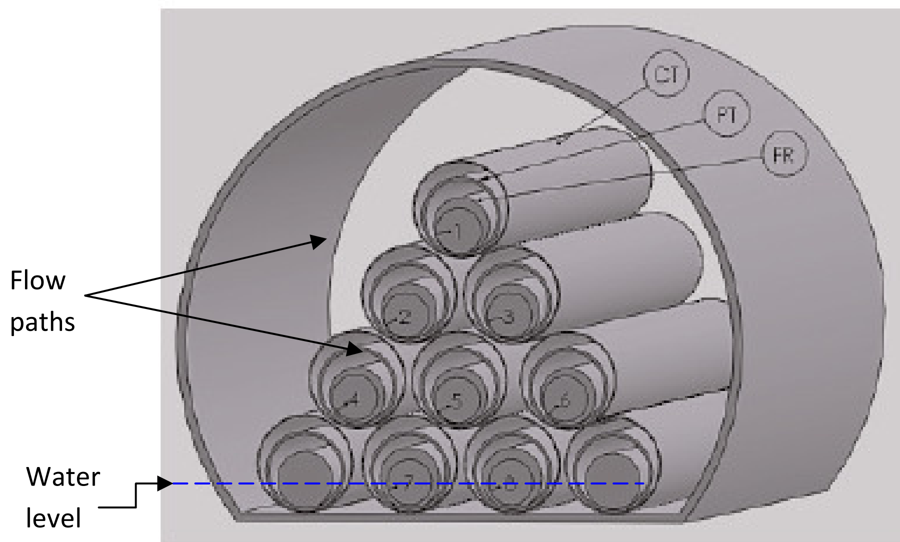

Fig. 3.26: Intra Debris bed flow paths

As mentioned in Chapter 2 the debris bed heat up pattern under single phase is dependent on the local equivalent conductivity as well as on the convective heat transfer coefficient. For this study the effective conductivity at local void levels is considered to be summation of conductivity contributed by conduction and radiative part as represented by Eqn. 2.1. The conductivity (conduction only) k_{ec} part of the effective conductivity is modeled with Imura-Takegoshi [34] relation and the radiative part k_r is model with Vortmeyer model. The convective heat transfer is modeled with Edward's model for natural convection [41] as described in Chapter 2.

It is to be noted that the above mentioned models are used for regular debris bed configuration. In this study it is proposed to use heated equivalent and hydraulic diameters as "characteristic lengths" instead of particle diameter as used in correlation. Major heat transfer to the interior part of exposed debris bed takes place through inter channel flow paths as illustrated in Fig. 3.27. The heated equivalent and hydraulic diameter is considered as characteristic length of this flow path. No convective flow is expected within the PT from outside to inside as there is no major driving head exist between the environment and inside the channel as mentioned in previous paragraph.

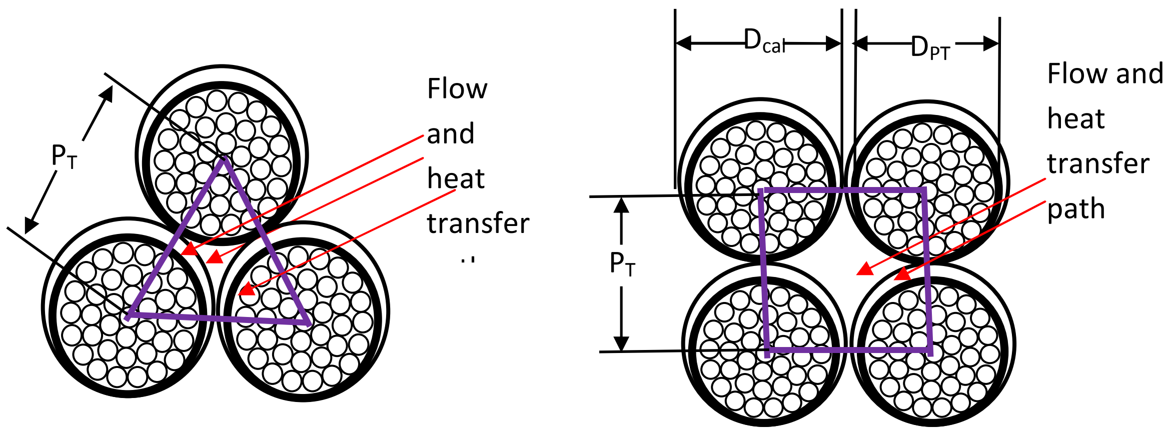

Triangular Pitch arrangement

Square pitch arrangement

Fig. 3.27: Flow and heat transfer paths among the channels

The heated equivalent diameter for triangular and square pitch are given in Eqn. 3.13 and Eqn. 3.14 respectively,

For Triangular pitch arrangement,

$$D_h = 4\frac{(0.5P_T \times 0.86\,P_T - 0.5\,\pi\,D_{PT}^2\,/4)}{0.5\pi\,D_{PT}} \tag{3.13}$$

For Square pitch arrangement,

$$D_h = 4\frac{(P_T^2 - \pi\,D_{PT}^2/4)}{\pi\,D_{PT}} \tag{3.14}$$

Where P_T is the pitch between the two Calandria Tubes and equal to D_{cal} , the diameter of the Calandria Tube. In the multiple debris bed experiment as the channels are arranged in triangular pitch, Eqn. 3.13 is being used for D_h for the charaterisation study.

For characterization study the influence of temperature on the change in effective conductivity is illustrated in Fig. 3.28. It is observed from Fig. 3.28 that as the temperature of FR5 increases the effective conductivity increases substantially during heat-up period. The increase in effective conductivity by 2.6 times is primarily from radiative conductivity as conductivity due to conduction only components increases marginally due to influence of porosity and steam conductivity [Refer Eqn.2.6 - 2.9]. As effective conductivity decides the transient heat-up rate of the debris bed [Refer. Eqn. 2.30], a higher effective conductivity at elevated temperature helps to improve the thermal diffusivity ($k/\rho c_p$) of the bed which in turn establishes the pseudo steady state earlier as compared to lower thermal diffusivity.

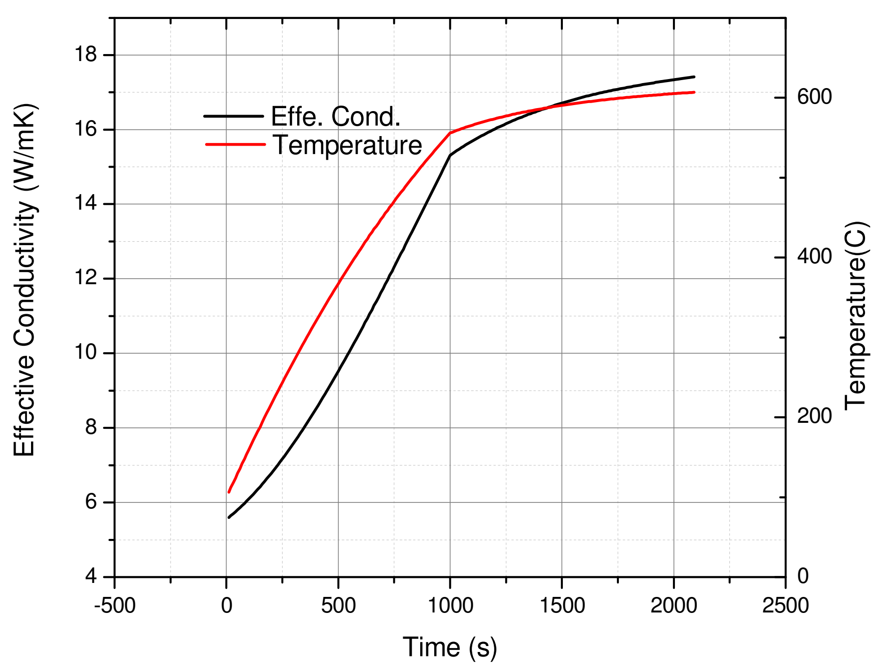

Fig. 3.28 : Variation of effective thermal conductivity with FR5 temperature

For characterization of convection mode of heat transfer as mentioned earlier that Edward's correlation with heated equivalent diameter as characteristic length has been used. For natural convection as Nusselt numbers is a function of Rayleigh number, the evolution of these two dimensionless numbers are evaluated with FR5 temperature. Fig. 3.29 illustrates the behaviour.

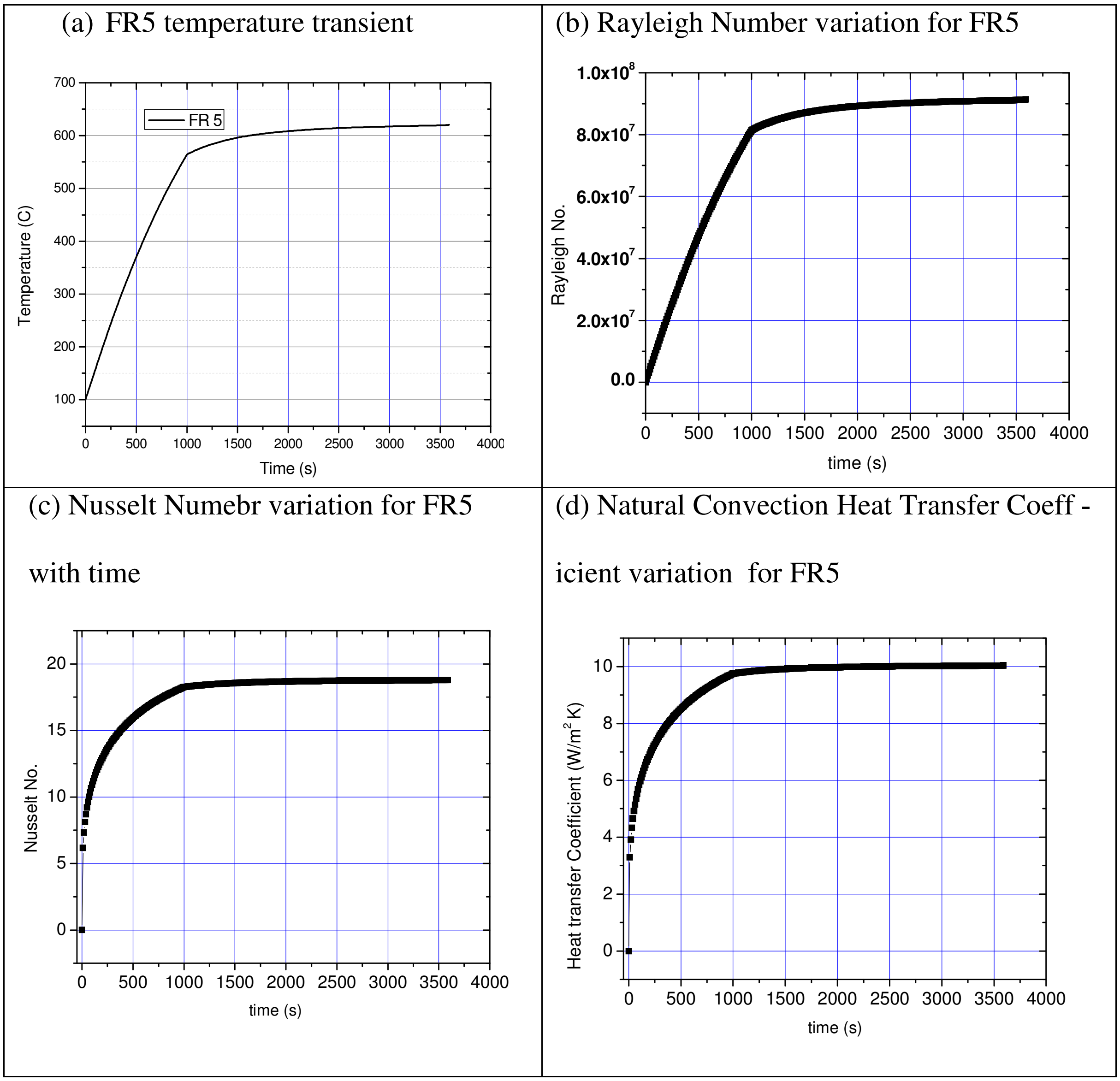

Fig. 3.29 : Characterization study for debris bed heat up by convection

The behaviour shows a linearity of Raleigh number and non linearity of Nusselt number during heat-up phase. (0-1000 s). Raleigh number being proportional to ΔT ($T_{surface} - T_{bulk}$) [Refer Eqn. 2.20], a linear behaviour of Raleigh number is expected as the FR5 temperature changes in a linear manner during heat up phase. As the relation between Nusselt number and Raleigh number is non linear [Refer Eqn. 2.19] hence Nusselt number is found to be change in a non-linear fashion with change in FR5 temperature. The change in convective heat transfer coefficient is found to change from low value to 10 w/m^2K for a change of temperature from 100-670°C.

As observed in Fig. 3.29 that the Raleigh number varies from 0 - $9x10^7$ during the heat-up which is found to be within the range (10^8) of Edward's correlation. Hence the applicability of the correlation for PHWR specific debris bed can be considered.

3.2.5 Conclusion

The following conclusion can be drawn from the multiple channel debris bed heat-up experiment:

(i) A PHWR debris bed will not undergo heat-up for a fully submerged conditions, however channels surrounded by other channels will he heated higher as compared to neighboring channels at the periphery of the debris bed.

(ii) In case of partially submerged channel, the temperature of FR at the top increases initially and reaches a peak temperature. With the formation of steam inside the channel, cooling of the FR takes place. This brings the temperature of the FR to a lower temperature.

(iii) The debris bed will undergo heat-up once they are exposed. However their heat-up is limited with convective and radiative cooling. Channel surrounded by other channels undergo higher heat-up as compared to channels at the periphery of the debris bed.

(iv) In all experiments, vigorous boiling was observed and steam leaves from both the end of the channels thus the central part of the debris does not get much steam flow unless driven towards steam outlet of the vessel.

(v) The Imura-Takegoshi model for k_{ec} and Vortmeyer model for k_r in conjunction with convective and radiative heat transfer to steam are used for charaterisation of the debris bed. However the heated equivalent diameter concept for certain arrangement (triangular/square) is being applied as a characteristic length for evaluating effective conductivity and Nusselt number for Edward's correlation.

As the decay power governs the steam generation and steam flow rate, the estimated Reynold's number are found to be very low. As this study is very specific to the conditions related to accident state for a certain reactor system, hence the developed correlation will have definitely limited use and situation specific.

Chapter 4

Development of Mathematical Model

This chapter includes discussion on the development of a PHWR specific debris bed heat-up model described in three sections. In the first section insights obtained from experiments are discussed and how they are included in formulation of debris bed model. The second section discusses the governing equation and closure relations. The third section discusses on the validation of the code against experimental results.

4.1 Insights from Debris bed Experimentation:

Debris bed flow behaviour

Post debris bed formation, the moderator will continue to boil-off causing further fall in moderator level. The fall in moderator level will cause the submerged channels (dry and pulled out) to get exposed layer-wise as expected from the debris bed configuration. For formulating the analytical model it is important to know the flow pattern during the boil-off period. Single segmented channel simulation experiments as described in chapter 3 described that till the channels are submerged the fuel bundles are cooled by generated steam. The generated steam leaves the reactor channel from both ends only, thus forming two columns of steam vapor at the end of simulated reactor channel. No mixing of steam bubbles laterally with bulk water has been observed as well above the water level the generated steam columns does not mix much laterally with the bulk air (see Fig. 4.1). Based on the experimental observation, a conceptual schematic is developed for debris bed flow pattern for reactor case as shown in Fig. 4.2. Hence for channels under submerged condition, steam bubbles will leave from all the channels at 5-6 m distance apart only. As observed in experiment, the major bulk steam flow for the exposed bed is from its side only as indicated in the Fig. 4.2, the steam flow through the inter channel spaces is only dependent on the vessel outlet locations. For Multiple debris bed heat-up experiment as described in Chapter 3, the outlet is kept at the centre of the vessel (Fig. 3.12), hence some steam travels through the channel interspaces. For PHWR, four Over pressure Relief Devices outlets are present in Calandria which are near to the vessel end (Fig. 1.2) rather than at centre. Hence the generated steam will be driven towards these outlets, traversing through the inter spaces of the collapsed channels. For both the cases i.e. experimental as well as for reactor cases though steam will emerge from the reactor channels end, some steam will pass through the channel interspaces, but the majority is expected to travel from two sides as shown in Fig. 4.2. It is expected no steam will enter inside the exposed channel due to lack of driving head between the exposed channel inside and outside. It is to be noted that channel inside being heated the local pressure will be higher than outside so that steam ingression inside the PT of exposed channel is highly unlikely. Some steam is found to be entering between PT and CT gap. Such phenomenon is also envisaged by Lee et al. [1].

Debris bed heat-up pattern

As the debris bed is constituted of reactor channels, a single segmented channel (1 m) simulation experiments as reported in chapter 3 conducted at two decay power levels of 6 kW and 8 kW reveals that fuel bundle does not get heated up till it is exposed to steam.

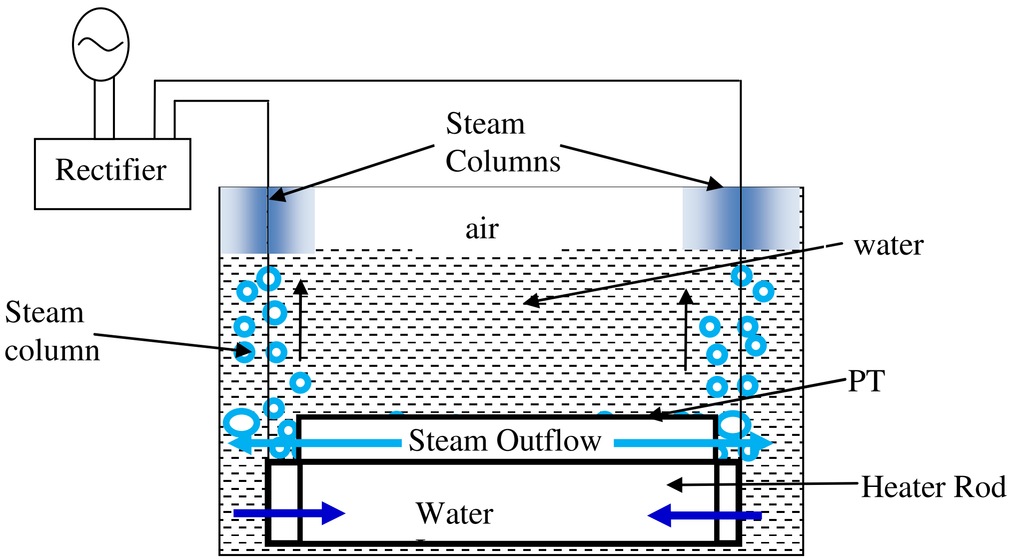

Fig. 4.1 : Schematic showing flow pattern as witnessed during the single channel tests

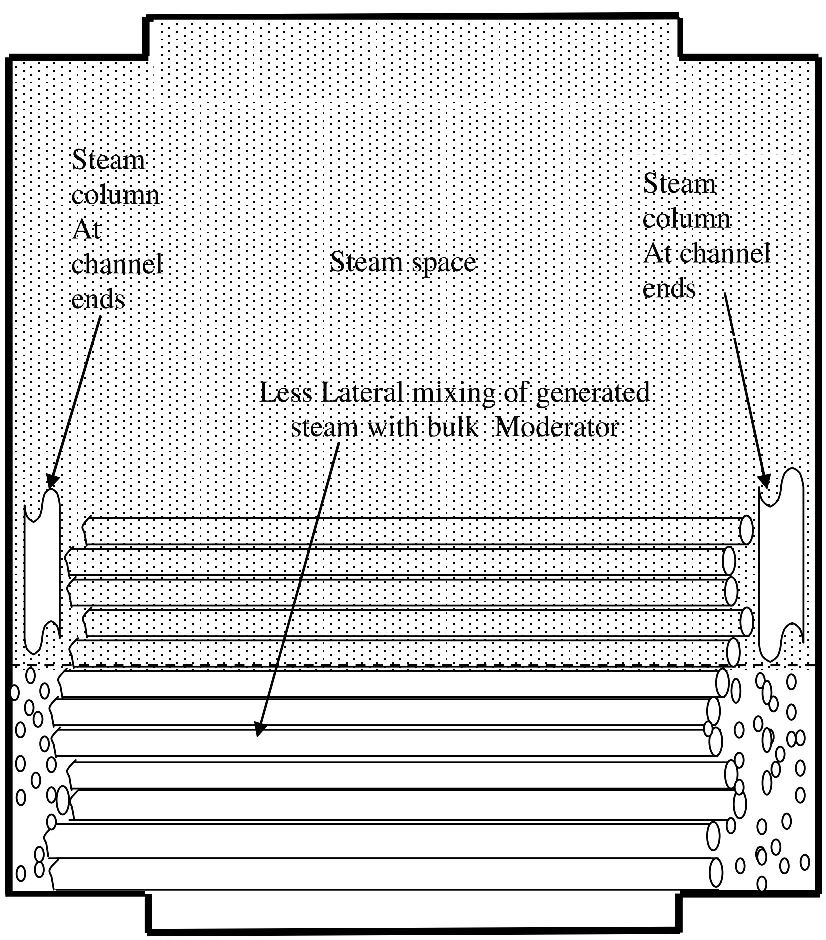

Fig. 4.2 : A conceptual schematic of flow pattern in the debris bed for the reactor based on experimental evidence

A very low submergence level also helps to keep the fuel bundle cooled with generated steam. Hence it is concluded from the single channel experimental study that the fuel bundles of submerged channels of the debris bed will remained cooled till the channel layer is exposed to steam. This observation is corroborated with multiple channel debris bed experimentation. Following is the list of heat transfer modes identified for the debris bed through experiments,

(i) For submerged or partially submerged channel internals

Fuel bundle to water: by boiling mode of convective heat transfer (submerged section)

Fuel bundle to steam : by forced convection (exposed section)

Fluid to PT : by forced convection (exposed section)

PT-CT : by natural convection (exposed section)

Remark:

(a) As there is a continuous generation of steam from the heated body hence the generated flow is a considered to be forced flow.

(b) As the component temperatures are limited to 100°C for submerged section only boiling heat transfer occurs..

(ii) For totally exposed channel internals

Fuel bundle-PT-CT : by radiation

Remark: As the component temperatures are going to 400-600°C and there is no steam ingression likely to occur inside the channel, hence radiation heat transfer is considered to be predominant mode of heat transfer.

(iii) For totally exposed channel external surface

a. Location : Inside the debris bed

Equivalent conductivity (material and steam conduction along with radiation) and natural convection heat transfer due to steam flow through the interspaces among the channels are the two heat transfer modes

b. Location : Periphery of the debris bed

Radiation heat transfer from top row of channels to enclosure wall, natural convection heat removal by steam from external surface of all peripheral channels and contact conductance between bottom row of channels with the vessel wall

Remark: The multiple channel debris bed heat-up experiment shows that heat transfer exist inside the debris bed as the channel temperature rise is limited which wouldn't have been a case if adiabatic condition prevails inside the debris bed. It is observed that the inside channel fuel rod temperatures get limited by peripheral channels which experience a better heat sink.

In general it is observed that the temperature variation in circumferential direction of any of particular channel components is not very significant. The maximum difference in temperature (top to bottom) of fuel rod is found to be 90°C for 30 kW case. For PT and CT the difference comes down to 5-10°C only. The effect of circumferential conduction on flow of heat from high to low temperature point is found to be insignificant (0.05 kW) as compared to the power (2.5 kW) generated in each FR for 30 kW case.

Physical Models as derived from the experiments

PHWR debris bed specific experiments conducted for a single channel and multiple channel debris bed have helped to understand the debris bed boil-off and heat up pattern. Heat transfer models are evolved out of these experiments so that it will be helpful/supportive for development of PHWR specific debris bed heat-up model. These models are being used as closure relations for the debris heat-up model. Following are the description of evolved heat transfer models,

(i) Heat transfer coefficient variation for exposed section of fuel bundle for partially submerged channel :

As described in chapter 3, the heat transfer coefficient is found to vary from 15.5 – 0.7 kW/m^2 K from fully submerged to nearly exposed channel and a suitable . heat transfer coefficient for exposed section has been proposed as described in chapter 3 (Eq. 3.4) Nusselt number with Reynold's number as illustrated in Eqn. 4.1

$$Nu = 0.024\,(Re) + 2.1e^{-5}\,(Re)^2 \tag{4.1}$$

(ii) Nusselt number for exposed debris bed :

As described in chapter 3, the Nusselt number variation with Raleigh number for PWR specific debris bed as proposed by Edward [42], is applied for assessment of variation of Raleigh number with experimental temperature. The correlation has been adopted as the applicability range for Raleigh number of the correlation is well within the experimental debris bed condition. It is proposed that for PHWR debris bed the characteristic length definition should be treated with "heated equivalent diameter" and "hydraulic diameter" for certain arrangement (triangular/square) instead of "particle diameter" as adopted for PWR specific debris bed [35].

4.2 Debris Bed Heat Up Analysis (DBHUA) Model

An analytical 2-D model (r, z) **D**ebris **B**ed **H**eat **U**p **A**nalysis (DBHUA) for PHWR debris bed heat-up study has been developed to calculate the heat-up of reactor channels that disassembled to the calandria bottom and is subsequently represented as debris. This model takes into account the decay heat and initial internal energy of collapsed channel and then calculates transport of heat radially and axially to the wall structures and water surrounding the debris. An important use of this model is the calculation of the heat-up of Calandria in response to contact with material from the core region slumping into it. The heat-up prediction of Calandria is useful to assess the integrity of the component. The capability of the DBHUA model include the modeling of the following: (i) spatially varying porosity (ii) thermal conductivity of porous debris (iii) radiation heat transfer in porous debris and (iv) oxidation in debris bed. The current limitation of the model is (i) molten material does not flow into adjacent porous region (ii) natural circulation flow of molten material is not modeled and (iii) fission product release does not occur in the debris bed.

The model consists of simulation of reactor channels arranged in layers as indicated in Fig. 4.3. This arrangement is a simplification of original arrangement with maximum channel compaction as shown in Fig. 3.1. This simplification led to an increase in bed height from 1.1 m to 1.3 m for an arrangement of several reactor channels for large PHWRs. This modification is done for simplification of formulation of numerical model.

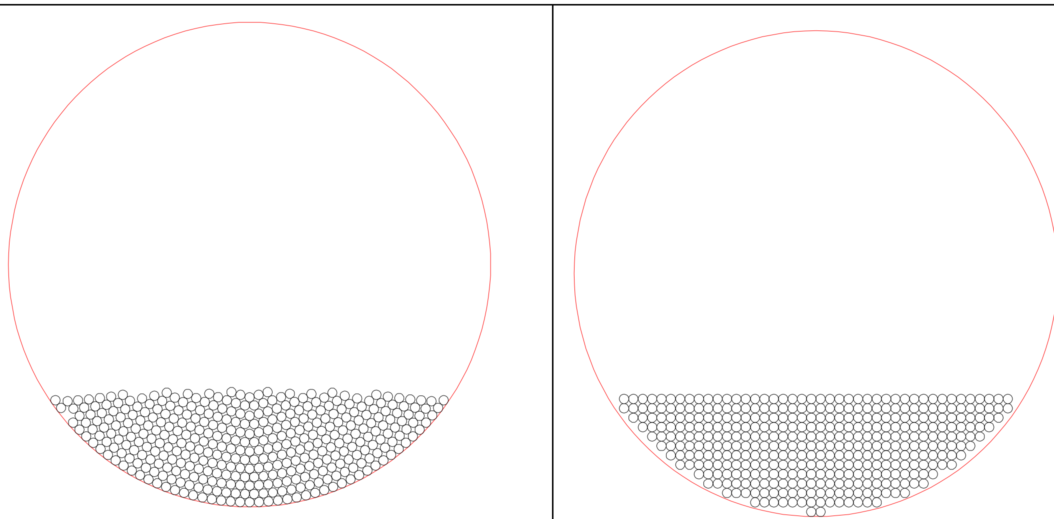

Maximum compacted debris bed configuration	Debris configuration with square pitch layout

Fig. 4.3 : Assumed Debris bed configuration for model development

The porosity calculated for square pitch arrangement of channels as shown in Fig. 3.27 is found to be 0.38. A value of 0.4 has been adopted for the model.

Following modes of heat transfer are considered for the model

(i) Heat transfer from submerged debris to water through boiling mode of heat transfer

(ii) Heat transfer from exposed debris to steam through convective and radiative mode of heat transfer

(iii) Heat transfer from exposed debris bed to Calandria structure by contact conductance (peripheral debris nodes to Calandria bottom and side nodes) and radiative mode of heat transfer (top layer of debris node to Calandria top)

(iv) Heat transfer from steam to Calandria structure

(v) Heat transfer from Calandria structure to Calandria Vault water by convection and boiling heat transfer

(vi) Calandria Vault concrete temperature is considered constant which acts as a heat sink

The DBHUA code is a two dimensional finite difference steady state and transient heat conduction code. Fig. 4.4 illustrates finite difference mesh for debris bed where each node represents a reactor channel.

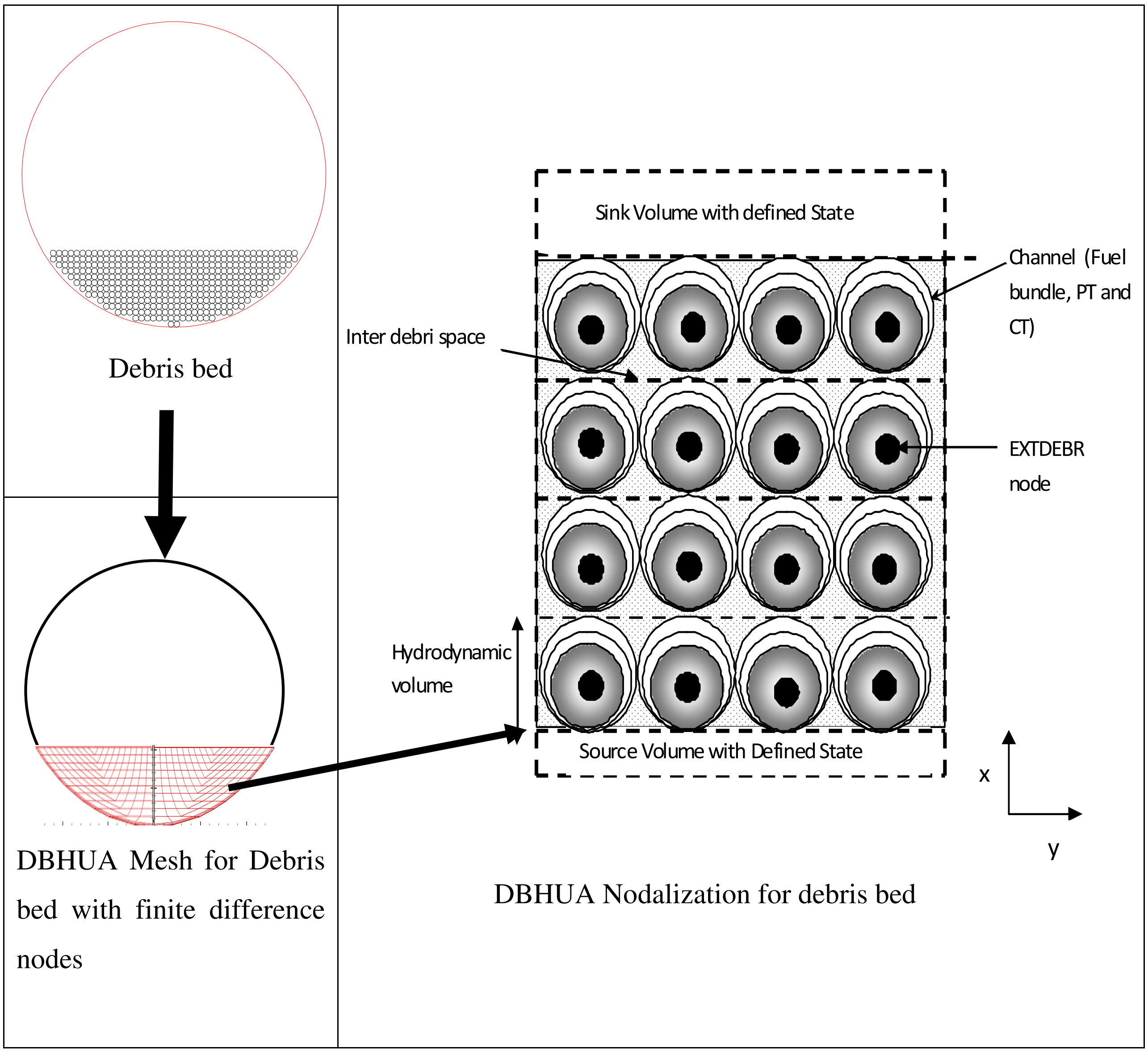

Fig. 4.4: Finite difference mesh for debris bed

The code has been developed to solve both plane and axi symmetry type heat transfer problem with anistropic thermal properties, subject to boundary conditions of the first kind (dirchlet), second kind (Neuman), and third kind (combination of both), and /or non linear boundary condition such as radiation. A boundary condition of first kind implies that the normal temperatures are prescribed along the boundary surface. A boundary condition of the second kind implies that the normal derivatives of the temperature are prescribed at the boundary surface. The code solves the following two-dimensional energy equation (Eqn. 4.2):

$$(1-\varepsilon)\rho_D c_D \frac{\partial}{\partial t}(T) = \frac{\partial}{\partial x}\left(k_e \frac{\partial T}{\partial x}\right) + \frac{\partial}{\partial y}\left(k_e \frac{\partial T}{\partial y}\right) + Q \tag{4.2}$$

Where,

ρ_D : density of debris particle

c_D : heat capacity of debris particle

k_e : effective thermal conductivity

Q : volumetric heat generation rate

T : temperature of mixture of debris bed and inter space fluid

ε : Porosity (pore volume/total volume)

The boundary conditions for Eqn. 4.2 are defined by user. The boundary conditions are defined for the bottom, top, left and right surfaces of the region being modeled by DBHUA code. The boundary conditions at these surfaces can be either adiabatic surface or convective/radiative heat transfer to fluid obtained from the different heat removal model discussed later on.

Model Assumptions:

The insights generated as described above from the experiments with single debris bed and multiple debris bed have been considered to build the model. Following assumptions are made for the model development which are derived from experimental observations,

(i) The single debris bed experiment clearly indicates that during boil-off, the heated rod never gets heated unless and until it is fairly well exposed and steam is released from both the ends of the channel till it is submerged/partially submerged condition. Steam generation is a simple boil-off process and it always flow from inside channel to outside due to positive pressure gradient, hence no momentum equation need to be solved for generated steam flow movement.

(ii) No momentum equation is also need to be solved for submerged and exposed section of the debris bed as the generated major amount of steam travels from both the ends of the debris bed as shown in Fig. 4.2. Due to large cross section of the flow domain the pressure gradient in r and z direction" is negligible.

(iii) As observed from the single and multiple debris experiments that temperature distribution (r, θ) in heater rod, PT and CT are contributing very less heat flow from heated to relatively less heated section of the components and PT and CT temperatures are found to follows the FR temperature with some time lag, hence, these three components are lumped as a single entity.

(iv) Uniform power distribution is considered in collapsed channels as compared to original cosine power distribution. This is justified as majority of fission products have come out from the fuel matrix prior to the time of collapse, thus it will be difficult to have a true cosine power profile.

(v) For reactor case all the fuel pins (19 or 37) of the fuel bundle are clubbed to represent an equivalent single fuel rod which is again clubbed with PT and CT.

(vi) The zrirconum oxidation kinetics model only the outer and inner surfaces of CT and outer surface of PT are considered as very less steam can ingress inside the PT.

The DBHUA code structures is represent in Fig. 4.5. This consists of major seven interacting modules to solve the thermal-hydraulic conditions in the debris bed, Calandria and Calandria Vault. Module “DEBR” solves the conduction equation for debris with effective conductivity, and average property of other thermo physical properties like density and specific heat. For hydrogen generation oxidation kinetics is modeled. The module “CALND” calculates for Calandria temperature with convective boundary conditions decided by CHF regimes. The “CALANDRIA VAULT” module calculates the Calandria Vault structure temperature after receiving heat from the Calandria Vault water. The Modules “MOD-HYD” and “CALANDRIA VAULT-HYD” calculates the moderator and Calandria Vault water levels from the heat-up process. Appropriate closure relations are used for conductive, convective and radiative heat transfer.

Closure models for DBHUA model:

Several closure models are used for the energy equations (2-D, 1-D and lumped parameter model) used to calculate temperature of various structures.

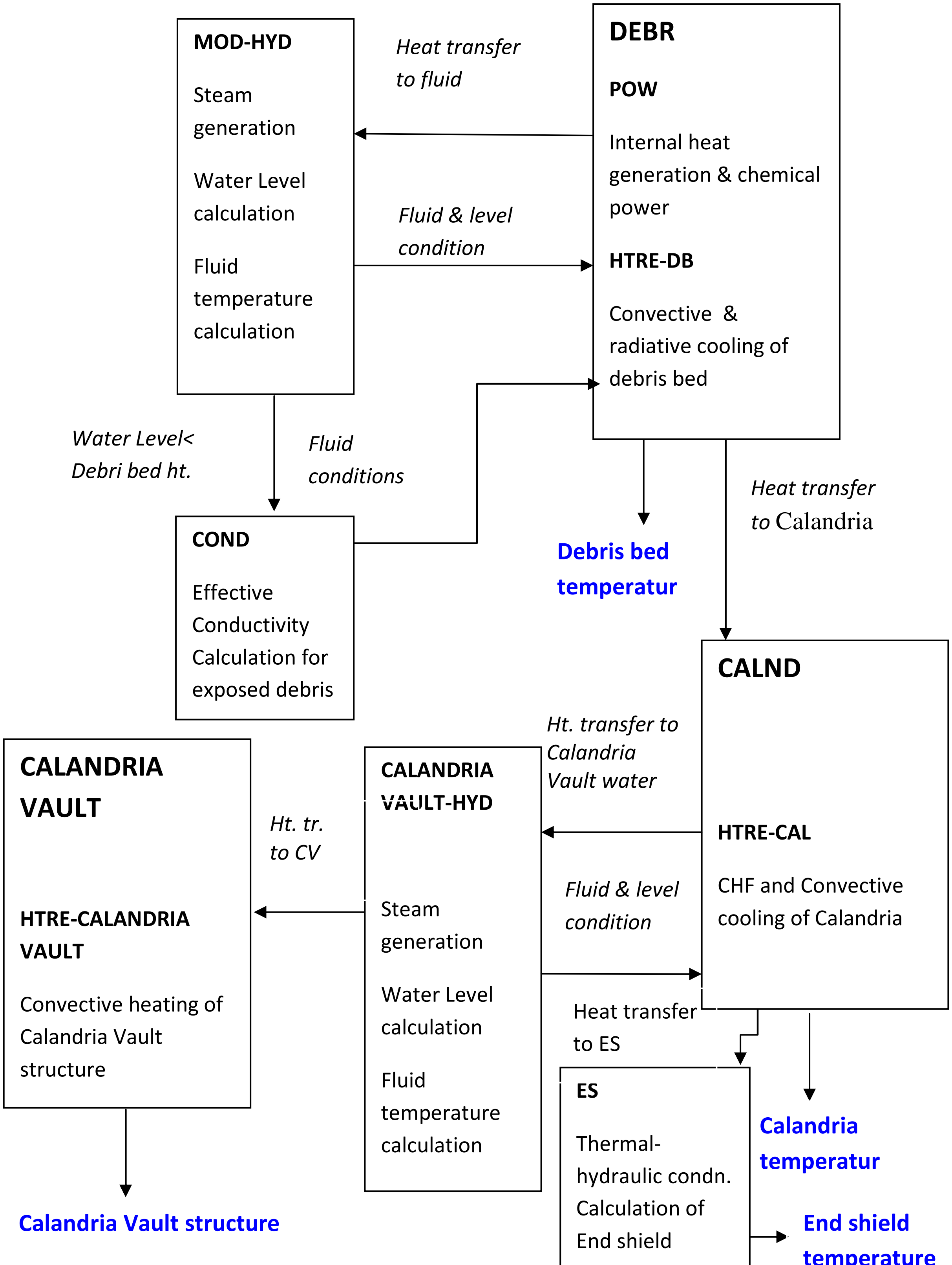

Fig. 4.5: The DBHUA Code Process Flow structure

The closure models include heat transfer coefficients for (a) submerged channels (b) partially submerged channels and (c) exposed debris bed (d) Calandria inside and outside. The other closure models are effective thermal conductivity for exposed debris bed, gap conductance between channel and Calandria and Critical Heat Flux for Calandria. Following is the description of such models in the following subsections,

(i) Closure model for submerged section of debris bed:

Fig. 4.6 illustrates the condition of the debris bed,

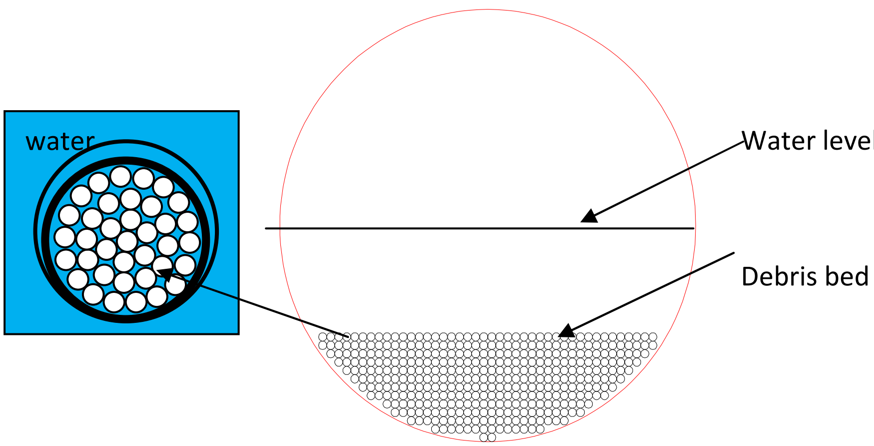

Fig. 4.6: Schematic for fully submerged debris bed condition

As evident from the experiments on PHWR debris bed, the submerged reactor channels which constitute the submerged debris bed, contributes to vapor generation in the moderator. Eqn. 4.3 accounts for the vapor generation,

$$\dot{m}_s = \frac{q_s}{h_{fg}} \tag{4.3}$$

q_s = total heat transfer from submerged debris to liquid phase by convection

$\dot{m}_s$ = vapor generation rate

The level (L_{hv}^t) at any instant of time of a hydraulic volume is computed with Eqn. 4.4,

$$L_{hv}^t = \frac{m_{hv}^t}{A_{cs}^t} \tag{4.4}$$

Where m_{hv}^t and A_{cs}^t are the mass and cross section of the hydraulic volume repsectivity at the time instant “t”

The fall in level (ΔL_{hv}) over time step “Δt” of the hydraulic volume is given by Eqn. 4.5

$$\Delta L_{hv} = \frac{m_{hv}^t - m_{hv}^{t+\Delta t}}{A_{cs}} \tag{4.5}$$

Where,

$$m_{hv}^{t+dt} = \dot{m}_s \, \Delta t \tag{4.6}$$

The surface temperatures of the lumped channel (Fuel Bundle, PT and CT) are calculated by Eqn. 4.7,

$$T_{ds} = \frac{q_s}{h_{ss} \, A_{ss}} + T_f \tag{4.7}$$

Where,

q_s : power going to submerged section liquid

A_{ss} : submerged section heat transfer area

T_{ds} : temperature of submerged section of a row of channels

T_f : liquid temperature

h_{ss} : nucleate boiling heat transfer coefficient (a fixed value 15.5 kW/m^2 K has been used) for submerged section

(ii) Closure model for partially submerged channels of debris bed:

Fig. 4.7 illustrates the condition of the debris bed,

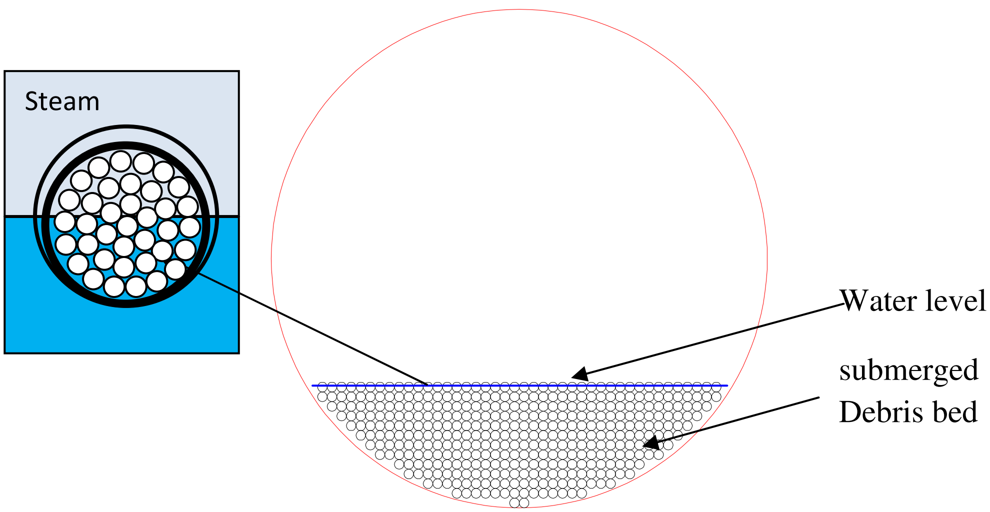

Fig. 4.7: Schematic for partially submerged channels of a row of the debris bed

The temperature of submerged section of the channel and exposed section is given by Eqn. 4.8 and 4.9 respectively.

$$T_{ds} = \frac{q_s}{h_{ss}\, A_{ss}} + T_f \tag{4.8}$$

$$T_d = \frac{q_e}{h_{es}\, A_{es}} + T_g \tag{4.9}$$

Where,

q_e : power going to exposed section gas

A_{es} : exposed section heat transfer area

T_{ds} : temperature of submerged section of a row of channels

T_d : exposed section of a row of channels which become a part of exposed debris bed

T_g : Vapor temperature

h_{es} : exposed section heat transfer coefficient (derived from Eqn. 4.1)

(iii)   Closure models for exposed section of debris bed:

Fig. 4.8 illustrates the condition of the debris bed,

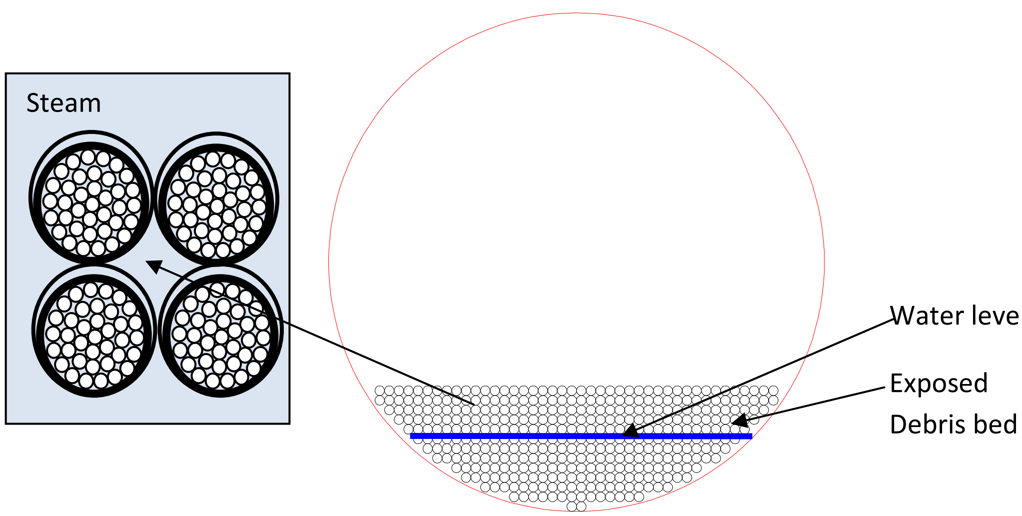

Fig. 4.8: Schematic for exposed section of debris bed

(a)   Thermal conductivity model used for exposed debris bed

The heat transfer in a dry porous bed involves both conduction and radiation. An effective thermal conductivity is considered. The effective conductivity is expressed by Eqn. 4.10.

$$k_e = k_{ec} + k_r \tag{4.10}$$

Where,

k_e = effective conductivity

k_{ec} = effective conductivity (conduction only)

k_r = radiative conductivity

A number of effective thermal conductivity models has been proposed for modeling a dry porous bed. Chapter 2 provides a review of such models. As examined, Imura-Takegoshi [34] model for thermal conductivity combined with the Vortmeyer radiation model [45] are found to be applicable and adopted for PHWR debris bed heat-up rates calculation as described in Chapter 3. The Imura-Takegoshi model is given by (Eqn. 4.11 to Eqn. 4.14),

$$k_{ec} = \left[\Psi + \frac{1 - \Psi}{\phi + \frac{1-\phi}{\nu}}\right] k_g \tag{4.11}$$

$$\Phi = 0.3P\varepsilon^{1.6}\upsilon^{-0.044} \tag{4.12}$$

$$\upsilon = \frac{k_s}{k_g} \tag{4.13}$$

$$\Psi = \frac{\varepsilon - \phi}{1 - \phi} \tag{4.14}$$

Where,

k_g thermal conductivity of fluid or vapour in pores

k_s thermal conductivity of solid material

ε porosity of debris

The conductivity contributed by radiative heat transfer as proposed by Vortmeyer in debris bed is expressed as a function of debris size (d_p), debris temperature and radiation exchange factor (F), as illustrated in Eqn. 2.24. For PHWR specific debris bed as discussed in Chapter 3, heated equivalent diameter as the characteristic length is used as characteristic length instead of particle diameter in the Vortmeyers relation. The proposed modified relation is given by Eqn. 4.15.

$$k_r \quad = \quad 4\, F\sigma\, D_h T_D^3 \tag{4.15}$$

Where,

F radiation exchange factor (0.9)

σ Stefan-boltzmann constant $W/m^2.K^4 (5.668 \text{ X } 10^{-8})$

D_h debris heated equivalent diameter

T_D Debris temperature

The radiation exchange factor of 0.9 is proposed by Vortmeyer for debris surfaces of 0.85 emissivity. The exchange factor 0.9 has been adopted as debris surface will have emissivity ranging from 0.8-0.85 from oxidized Zr surfaces.

(b) Heat transfer from debris bed to vapor

The heat transfer to the vapor is expressed as follows (Eqn. 4.16),

$$q = q_{conv} + q_{rad} \tag{4.16}$$

Where,

q : total heat transfer

q_{conv} : heat transfer by convection

q_{rad} : heat transfer by radiation

The convective heat transfer is expressed by Eqn. 4.17,

$$q_{conv} = A_s h(T_D - T_g) \tag{4.17}$$

Where,

q_{conv} : heat transferred through convection

h : convective heat transfer coefficient

As vapor velocity through the debris bed (channel inter spaces) is found to be low as majority of steam flow takes place by the two ends of the exposed debris bed (Fig. 4.1 and Fig. 4.2) hence heat removal from structure to the fluid is considered by natural convection and by radiation. Natural convection correlation proposed by Edwards et al (Eqn. 2.19) is adopted for PHWR debris bed as mentioned in Chapter 3. However the characteristic length "D_p" is changed with the heated equivalent diameter as given in Eq. 3.11/3.12. The Edwards correlation for PHWR specific debris bed is given by Eqn. 4.18,

$$\mathrm{Nu_{nat}} = \mathrm{KRa}^{0.25} \tag{4.18}$$

Where,

$\mathrm{Nu_{nat}}$: Nusselt number for natural convection,

K = 0.3 $0 \leq \mathrm{Ra} \leq 50$

0.4 $50 \leq Ra \leq 200$

0.5 $200 \leq Ra \leq 10^6$

0.6 $10^6 \leq Ra \leq 10^8$

Ra : Rayleigh number

The Rayleigh number is calculated by the Eqn. 4.19,

$$Ra = Gr\,.\,Pr = \frac{\rho_g^2\, g\, D_{hy}^3 \beta \Delta T}{\mu_g^2} Pr \tag{4.19}$$

Where,

g : acceleration of gravity

β : Volume coefficient of expansion of vapour

ΔT : Local temperature difference between debris and vapour $(T_D - T_g)$

D_{hy} : Hydraulic diameter

For PHWR debris bed the Nusselt number is defined as below (Eqn. 4.20),

$$Nu_{conv} = (hD_{he})/k_g \tag{4.20}$$

D_h is the heated equivalent diameter for triangular/square type of pitch arrangement of channels.

It is to be noted that for the PHWR debris bed both D_{he} and D_{hy} are the same.

The heat transfer to the vapor by radiation is calculated by the Eqn. 4.21 ,

$$q_{rad} = A_s F_g \sigma \left(T_D^4 - T_g^4 \right) \tag{4.21}$$

Where,

q_{rad} = heat transferred to vapor by radiation

F_g = gray body factor

σ = Stefan-Boltzmann Constant ($5.668 \times 10^{-8} W/m^2K^4$)

The gray body factor is calculated by the equation

$F_g = 1/\left[R_1\left(1 + R_3/R_1 + R_3/R_2\right)\right]$

where

$R_1 = \left(1 - \varepsilon_g\right)/\varepsilon_g$

$R_2 = 1/\varepsilon_g$

$R_3 = 1 + \left(1 - \varepsilon_D\right)/\varepsilon_D$

$\varepsilon_g = 1. - \exp(-a_g L_m)$

Where,

ε_D : emissivity of debris particle (0.4 considered for zircaloy material and 0.8 for ZrO_2 with 2µm layer [53])

a_g : absorption coefficient of vapor (0.2 considered)

L_m : Mean free length

L_m is calculated with the following Eqn. 4.22

$$L_m = \frac{4\varepsilon D_p}{6(1-\varepsilon)} \tag{4.22}$$

(c) Heat transfer at interface of debris region and structure

The rate of heat transfer from a debris region into a structure in contact with the debris is strong function of the conditions at the interface between the debris bed and structure. The modeling of this heat transfer is performed using a concept of null element which an element with zero volume and whose nodes overlay the interface between debris and structure. The heat transfer through the null element is calculated by Eqn. 4.23.

$$q''_{i} = h_{gap} \, (T_d - T_s) \tag{4.23}$$

Where,

q''_{i} : Heat flux across the interface

h_{gap} : Heat transfer coefficient for interface. (a value of 0.5 kW/m^2 K has considered for solid debris to structure contact and a value of 10 kW/m^2 K is considered for molten liquid to structure contact [35])

T_s : Temperature of structure at interface

(d) Phase change model

An enthalpy method has been adopted for calculating the phase change. The method consists of using the material enthalpy to determine an effective density times specific heat (ρC_p) value to use in Eqn. 4.24. The enthalpy change per unit volume is defined as,

$$dH = \rho C_p \, dT \tag{4.24}$$

thus,

$$\rho C_p = \frac{dH}{dT} \tag{4.25}$$

which can be written as,

$$\rho C_p = \frac{dH}{dX} \quad \frac{dX}{dT} \tag{4.26}$$

For computational purposes, it is easier to calculate $\frac{dH}{dX}$ and $\frac{dX}{dT}$ than $\frac{dH}{dT}$ directly.

(e) Ex-Calandria heat transfer :

The USNRC sponsored experimental program evaluates heat transfer from the outside of a hemispherical reactor vessel which has been flooded [48]. The experimental program produces a correlation as a function of contact angle. Following is the relation as given in Eqn. 4.27 [48].

$$q^{''}_{CHF}(\theta) = C_1 + C_2\,(\theta) + C_3\,(\theta)^2 + C_4\,(\theta)^3 + C_5\,(\theta)^4 \tag{4.27}$$

Where,

$q^{''}_{CHF}(\theta)$: critical heat flux as function of angle

C_1-C_5 : constants for different kind of vessel surfaces(plain, rough, surface with coatings etc.).

For ex-Calandria heat transfer Eqn. 4.22 has been adopted and for DBHUA code calculations, C1-C5 for plain vessel surface is considered.

The values for C1-C5 are given below,

C_1 : 7.161e+05,

C_2 : 9.952e+03,

C_3 : 1.120e+01,

C_4 : -1.416e-01,

C_5 : 0.0

For Pre-CHF and post CHF following heat transfer relations are used,

Table 4.1 : Heat transfer relations for ex-Calandria heat transfer at atm. condition

	Heat transfer mode	Condition	Correlation
Pre-CHF	Natural convection to liquid	T_f<100°C	Mcdam's (Horizontal plate) and Churchill & Chu's (vertical plate)
	Pool boiling	T_f =100°C and T_w >110°C	Forster-Zuber
Post-CHF	Film boiling	T_w > Leiden Frost temperature local steam void <1.0	Bromley's correlation for low flow
	Natural convection to steam	T_f > 100°C Steam void > 0.8	Churchill & Chu's correlation

The Leiden frost temperature is considered to be 260°C for the model

The McAdams [50] correlation (Eqn. 4.28) which is essentially developed for a flat plate with energy flowing in the direction of the gravity vector has been adopted for Calandria bottom (debris bed region) heat transfer.

$$Nu = \ 0.27\ Ra_L^{0.25} \tag{4.28}$$

Where,

L : characteristic length is considered to be ratio of surface area to perimeter as suggested by DeWitt [51].

The Churchill-Chu correlation (Eqn. 4.29) [52] developed for a vertical flat plate has been used for Calandria walls except the debris bed region, As the Calandria diameter is 6 m, the heat transfer surface area is very large, hence it is treated as vertical plate.

$$Nu = \left\{ 0.825 + \frac{0.387\ (Ra_L)^{1/6}}{\left[1 + (\frac{0.492}{Pr})^{\frac{9}{16}}\right]^{8/27}} \right\}^2 \tag{4.29}$$

For pool boiling Forster-Zuber correlation (Eqn. 4.30) [53] has been adopted as given below,

$$h = 0.00122 \left(\frac{K_f^{0.79} C_{pf}^{0.5} \rho_f^{0.49}\ g^{0.25}}{\sigma^{0.5} \mu_f^{0.29} h_{fg}^{0.24} \rho_g^{0.24}} \right) \Delta T_w^{0.24}\ \Delta P^{0.75} \tag{4.30}$$

where,

ΔT_w : T_w- T_f

ΔP : pressure based on wall temperature minus total pressure

For film boiling Bromley's correlation [54] has been adopted as given by Eqn. 4.31. As there is a weak flow hence the correlation is adopted made for very low flow condition,

$$h = 0.62\left(\frac{K_g^3 h_{fg}\rho_g g\ (\rho_f - \rho_g)}{L\ \mu_g \Delta T_{sat}}\right) \tag{4.31}$$

(f) Hydrodynamic boundary

The convective, radiative and interface boundary conditions for Eqn. 4.2 are given by 4.32 - 4.36. Theses boundary conditions are applied to boundary nodes to the debris bed.

$$-k_e(x,y)\frac{\partial}{\partial n}T(x,y) = q''_c(x,y) + q''_{rad}(x,y) + q''_{radw}(x,y) + q''_i\,(x,y) \tag{4.32}$$

Where q''_c, q''_{rad} are different heat fluxes as given below,

$$q''_c(\mathrm{x_b},\mathrm{y_b}) = h_c\left[T(\mathrm{x_b},\mathrm{y_b}) - T_g\right] \tag{4.33}$$

$$q''_{rad}(\mathrm{x_b},\mathrm{y_b}) = F_s\,\sigma\left(T_{xb,yb}^4 - T_g^4\right) \tag{4.34}$$

$$q''_{radw}(\mathrm{x_b},\mathrm{y_b}) = \sigma\,({T_{xb,yb}}^4 - {T_{wall}}^4) \tag{4.35}$$

$$q''_{gap}\,(\mathrm{x_b},\mathrm{y_b}) = h_{gap}\,(T(\mathrm{x_b},\mathrm{y_b}) - T_{wall}) \tag{4.36}$$

Where,

$\mathrm{T}(\mathrm{x_b},\mathrm{y_b})$: temperature of external surface of node on DBHUA mesh with coordinates $\mathrm{x_b},\mathrm{y_b}$

$\mathrm{k_e}(\mathrm{x_b},\mathrm{y_b})$: Effective thermal conductive at location with coordinates $(\mathrm{x_b},\mathrm{y_b})$

$\mathrm{h_c}(\mathrm{x_b},\mathrm{y_b})$: convective heat transfer coefficient for node on external surface with coordinates

$\mathrm{T}(\mathrm{x_b},\mathrm{y_b})$: calculated temperature of the fluid at surface coordinates $\mathrm{x_b},\mathrm{y_b}$

$\mathrm{q_{rad}}(\mathrm{x_b},\mathrm{y_b})$: Radiation heat flux at boundary nodes

$\mathrm{q''_{rad}}(\mathrm{x_b},\mathrm{y_b})$: Convective heat flux at boundary nodes

$q''_{rad}(x_b, y_b)$: Convective heat flux at boundary nodes with wall

$q''_{gap}(x_b, y_b)$ = convective heat flux for gap at boundary nodes

(g) Temperature estimation for reactor core structures

Temperatures are evaluated for several structures like Calandria, end shield structure, tube sheets and Calandria Vault concrete. 1-D Conduction equations are solved for different components. Eqn. 4.37 shows the generalized eqn. of heat conduction,

$$\frac{\delta^2 T}{\delta x^2} = \frac{1}{\alpha}\frac{\delta T}{\delta t} \tag{4.37}$$

For Calandria structure the conduction equation is solved for r-direction where as for End shield, Calandria Vault structure and tube sheet the conduction equation is solved in x-direction. Convective, conductive and radiative boundary conditions are applied to these structures as required. For convective boundary condition to the internal structure of Calandria, Calandria Vault concrete and end shield structure and tube sheets Eqn. 4.38 has been applied, as the developed flow is very low [55].

$$Nu = 4.0 \tag{4.38}$$

(h) Component summary:

Depending on the flow of heat in the domain of interest the models are developed either in 2-D or 1-D. As the porous debris bed is a large computational domain with variable boundary conditions (like top and bottom) which dictates differential heating, hence a 2-D approach is appropriate to treat heat transfer. In the Calandria vessel the major heat flow takes place in r-direction as compared to θ and Z-direction. Hence a 1-D approach is adopted for Calandria.

Table 4.2 summarizes different models used for DBHUA model.

Table 4.2: Models for component simulation

Component name	Component type	Type of model	illustration
Debris bed	Structure	2-D Porous debris bed model Total number of nodes = 99	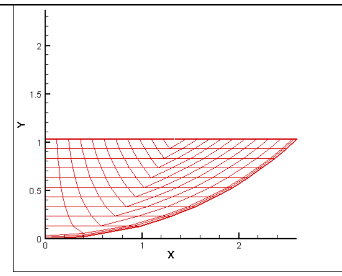
Calandria	Structure	1-D (r-direction) conduction model Total no. of nodes = 5	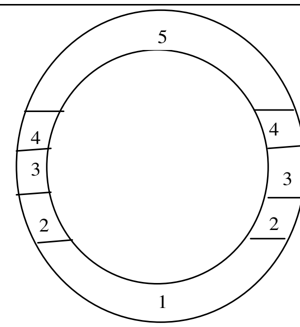
End shield balls and tube sheets (inside & outside)	Structure	1-D (r-direction) conduction model Total no. of nodes = 5 TS :Tube sheet ES : End shield balls Total no. of nodes = 5	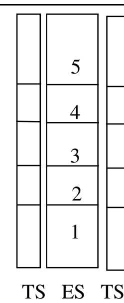
Calandria Vault concrete	Structure	1-D (r-direction) conduction model Total no. of nodes = 7	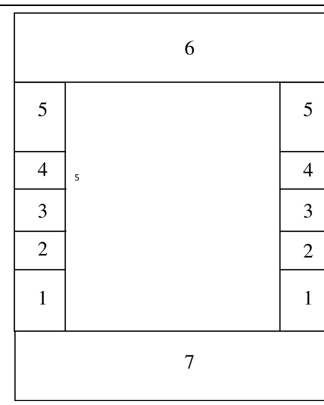

Table 4.2: Model for component simulation (contd.)

Component name	Component type	Type of model	illustration
Moderator	Fluid (water & steam)	Lumped model for each node Total no. of nodes = 15 Boil-off, steam void and predicted for each node	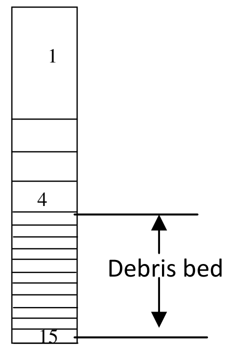
End shield water	Fluid (water & steam)	Lumped model for each node Total no. of nodes = 7 Boil-off, steam void and predicted for each node	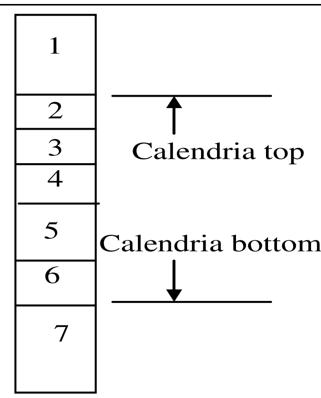
Calandria Vault Water	Fluid (water & steam)	Lumped model for each node Total no. of nodes = 7 Boil-off, steam void and predicted for each node	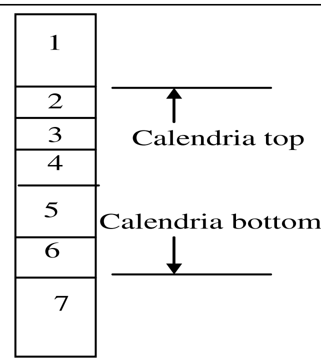

(i) Hydrogen generation model: The reaction of zirconium with steam above 980°C is of modeled with parabolic rate law [56] i.e. the mass per unit area "w" of Zr reacting with steam is related to the time by Eqn. 4.39,

$$w^2 = k_w t \tag{4.39}$$

Where,

k_w : $rate\ constant$

The rate constant proposed by Baker Just [57] is a good approximation (Eqn. 4.40),

$$k_w = 3300e^{(-\frac{22,900}{T})} \tag{4.40}$$

The rate of reaction at any time is obtained is obtained by differentiating Eqn. 4.41 with respect to time "t",

$$\frac{dw}{dt} = \frac{k_w}{2w} \tag{4.41}$$

Assuming that zirconium surface reacts uniformly with the steam, the depth of penetration δ m in time t sec is related to weight loss in w kg/m^2 by δ = w/ρ, where ρ kg/m^3 is the density of the zirconium; hence from Eqn. 4.39, Eqn. 4.42 and Eqn. 4.43 are derived as:

$$\delta^2 = \frac{k_w}{\rho^2} t = k_\delta t \tag{4.42}$$

and,

$$\frac{d\delta}{dt} = \frac{k_\delta}{2\delta} \tag{4.43}$$

Where,

$$k_\delta = \frac{k_w}{\rho^2},$$

The dependence of k_δ on temperature is derived from Eqn. 4.44,

$$k_\delta = 8X10^{-5}e^{\left(-\frac{22,900}{T}\right)} \tag{4.44}$$

For cylindrical body with r_o the outer radius, the reaction rate is given by Eqn. 4.45,

$$\frac{dm}{dt} = \pi\rho k_\delta\left(\frac{r_o}{\delta} - 1\right) \tag{4.45}$$

Where m is the mass of cladding that has reacted.

4.3 Validation of the Code with Experimental Data

The DBHUA code has been evaluated with 10 and 20 KW experimental results (Figs. 4.9- 4.11) As DBHUA code considers lumping of Fuel bundle, PT and CT as a single entity to evaluate temperature, the code predictions are compared with Fuel Simulator (FR) temperatures. The comparison is presented for short term and long term experiments. As there is no Calandria Vault and End Shield water simulated in the experiment, the related modules are not used. An atmospheric heat sink with a natural convection heat transfer coefficient of 5 watt/m^2 °C has been applied to outside surface of enclosure housing of multiple channel debris bed experiment

I Validating of DBHUA with Small Term Experiments:

The temperature of the fuel rod in the experiment and that of the combined channel predicted by the Code is shown in Fig. 4.9 for 2nd row, 3rd row and 4th row for the half submerged cases (ref. Table 3.8).

II Validating of DBHUA with Long Term Experiments:

The comparison results are shown in Fig. 4.10-4.11 for 4th row half submerged cases. In this case the behaviour of the exposed debris bed has been studied. As the experiment is conducted with 4th row half submerge condition, three rows of channels were exposed of the debris bed which gives maximum exposed debris bed height of the experimental debris bed.

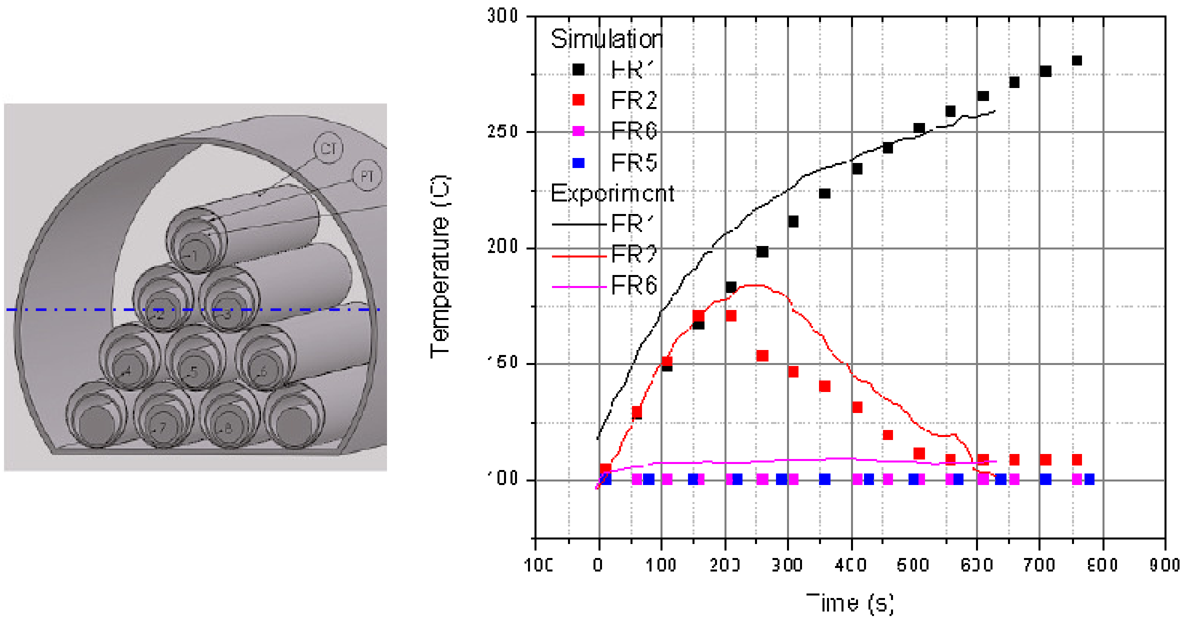

Case: 2nd Row half submerged (short term expt.)

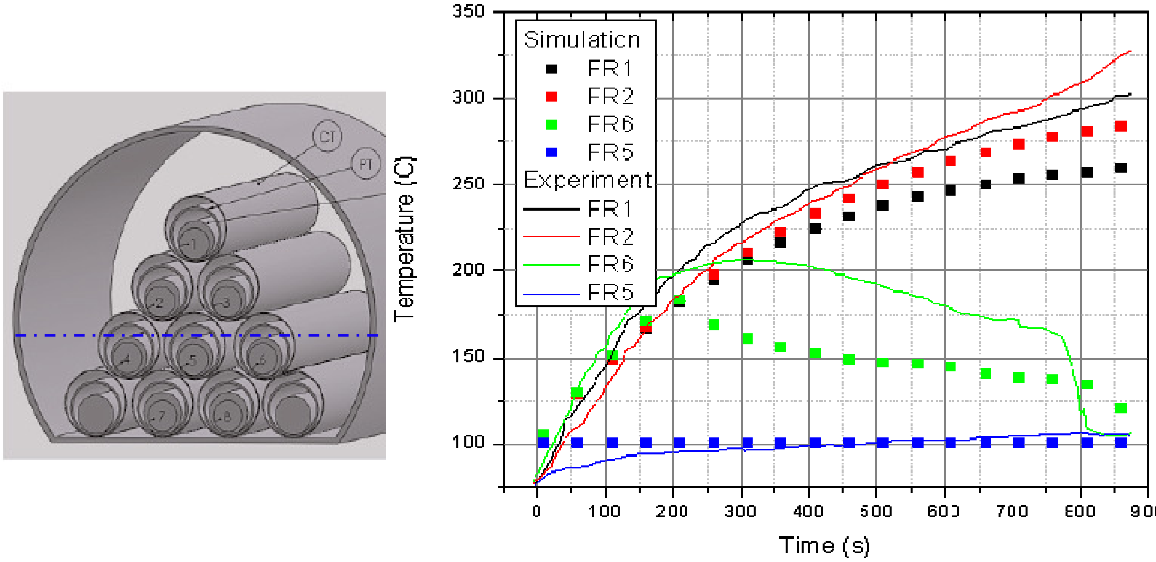

Case: 3rd Row half submerged (short term expt.)

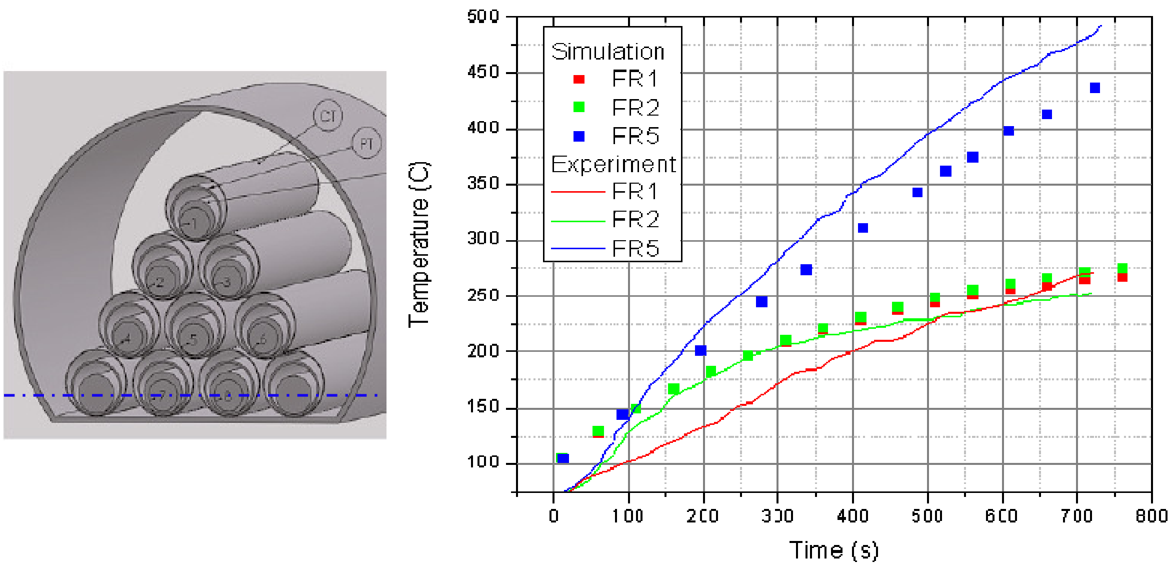

Case: 4th Row half submerged (short term expt.)

Fig. 4.9 : Comparison of predicted temperature with experimental data for 20 kW case for short term expt.

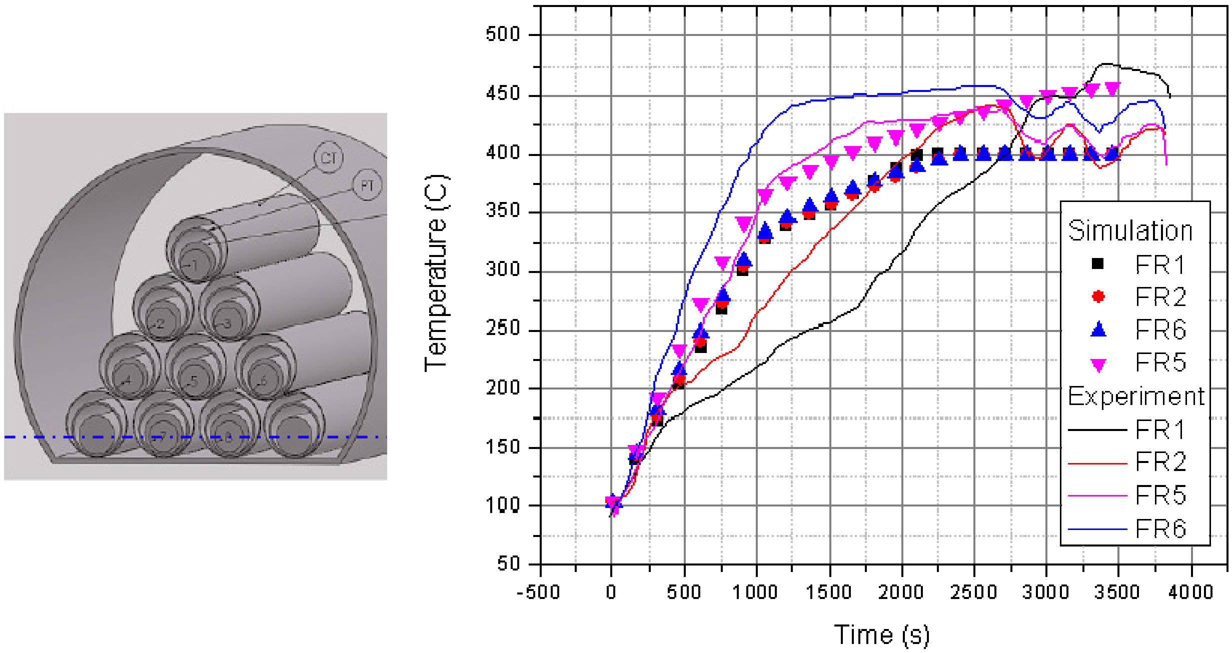

Fig. 4.10: Comparison of predicted temperature with experimental data for 10 kW case for long term expt.

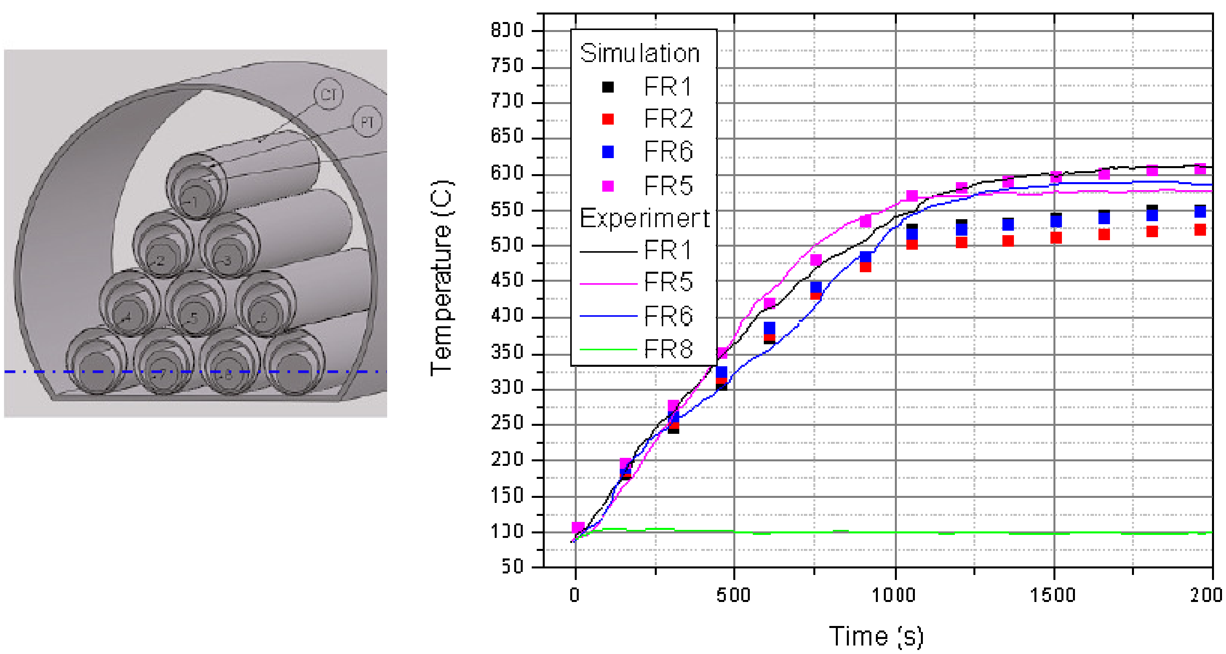

Fig. 4.11: Comparison of predicted temperature with experimental data for 20 kW case for long term expt.

Results and Discussion:

For all the experiments the water level is brought to a certain desired level prior to the heat-up. Hence during heat-up for half submerged channels, the temperatures for exposed section rises and then decreases due to steam cooling cases.

The temperature trends of code predictions for FR temperatures for short term experiments are found to be in agreement with experimental results however the code has under predicted around 8% at higher temperature region. The initial heat-up of the (hump) of the submerged channels are also well captured by the code. For long term experiment 20 kW case, the code predictions for debris internal (FR5) is found to be in good agreement however the peripheral nodes have under predicted by 8%. As these channel are closer to vessel wall, the radiative heat transfer calculated by the code has under predicted the temperature. This is due to inadequate modeling of view factors between peripheral channels and the wall. For 10 kW case the code prediction at the pseudo steady is found to be bounded by experimental results. The heat-up of debris bed interior FR5 is predicted well by the code. Over all the heat-up pattern and attainment of pseudo steady state are predicted well with code DBHUA.

Model Sensitivity Analysis:

The analysis for 20 kW is extended to understand the influence of heat removal modes like equivalent conductivity and natural convection along with radiation on the heat-up of FR5 which is located at the centre of debris bed (Fig. 3.26). Fig. 4.12 illustrates such study for 20 kW power experiments.

It is imperative from Fig. 4.12 that convection plays a majority role to decide the temperature behaviour of debris inside channel heat-up behaviour. The influence is dominant at higher temperature. The influence of effective conductivity is found to be not effective at higher temperature (T>500°C) for this kind of debris bed. This can be due to dominance of higher convective flow as substantial flow paths are available for such debris bed.

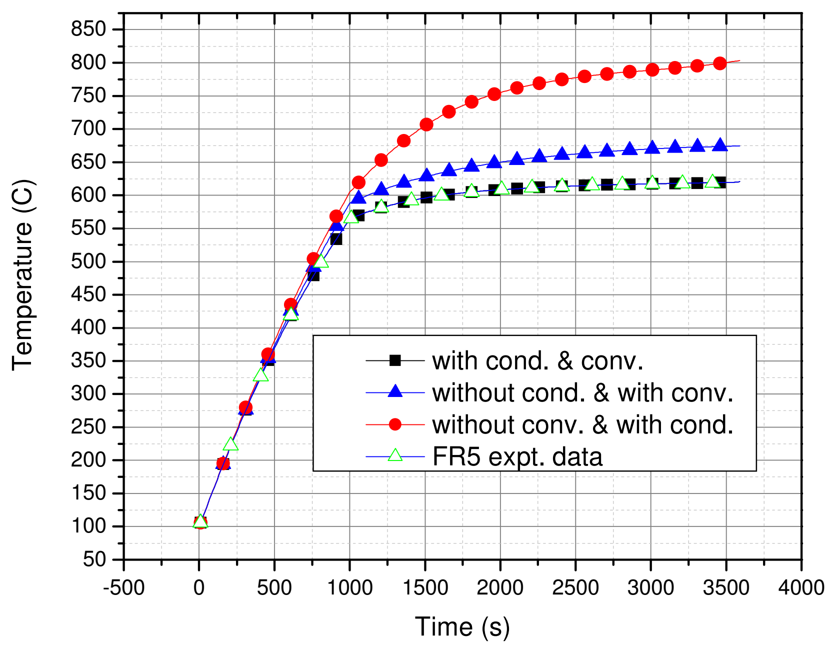

Fig. 4.12 : Influence of different modes of heat transfer on for debris bed central channel temperature for 20 kW case

4.4 Conclusion:

I. The insights generated from the experiments like flow behaviour and heat up pattern has helped to formulate energy based debris heat-up model. The model has not considered momentum continuity as the large cross section of Calandria leading to low pressure gradient in flow direction.

II. The DBHUA model is validated against short term and long term experiments. The model is validated upto 670°C of debris bed temperature.

Chapter 5

Severe Accident Simulation for PHWR Plant

This chapter describes the simulation of a large PHWR plant where the analytical model DBHUA has been used to predict the accident progression and the integrity of the Calandria. The chapter is divided into two parts. The first part describes the early phase of the accident analysis. In this analysis severe accident progression is calculated till the channels disassembled. The second part describes the late phase of the accident where remaining moderator boil-off followed by heat-up of the disassembled channels debris bed and Calandria. The analysis predictions from early phase of accident serves as initial and boundary conditions of the late phase of accident. The DBHUA model has been extended beyond the moderator boil-off to predict Calandria integrity.

5.1 Early Phase Accident Analysis

A full plant simulation has been carried out for a large IPHWR (540 MWe) under Station Black Out (SBO) scenario with no manual intervention and un-availability of crash cooling and Emergency Core Cooling System (ECCS). The objective of the analysis is to predict core degradation during early phase and estimate some parameters at the end of core collapse which acts as initial conditions for debris bed heat-up analysis with code DBHUA. The parameters are moderator and Calandria Vault water inventory at which the total core collapse takes place along with the exposed channel conditions (extent of oxidation of fuel bundle, PT and CT, surface temperatures) and temperatures of structures, moderator, Calandria Vault water and Calandria Vault concrete.

The large IPHWR is a two loop system as shown in Fig. 5.1. Each loop consists of several channels, steam generators and Primary Heat Transport System (PHTS) circulating pumps. Two loops are interconnected via a Pressurizer (Fig. 5.1) which maintains the pressure of the system.

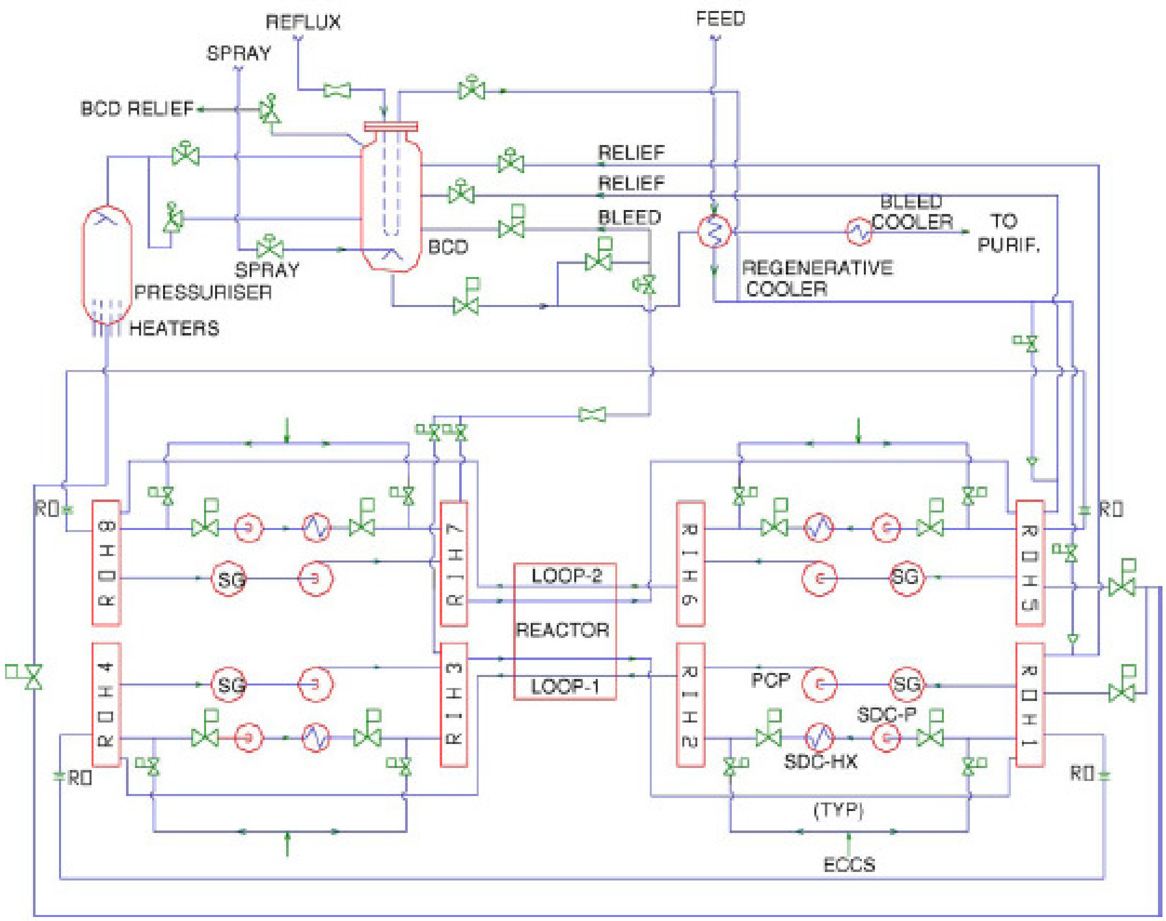

Fig. 5.1: Schematic of Large PHWR (540 MWe) System with Pressurizer

Plant Model Details:

The Large PHWR plant model for severe accident analysis has been built with code RELAP5/SCDAP [55] code to address initial stages of accident progression. The model simulates the following systems.

i. Primary Heat Transport system: Two loops including Fuel Channels, Inlet & Outlet Headers, inlet and outlet feeders, Primary Circulation Pumps (PCP), Steam Generators (tube side), Pressurizer, Instrumented Relief Valves (IRVs) etc.
ii. Secondary Heat Transport System: Steam Generator Secondary side which includes Steam Separator, down comer, riser and steam drum. Governors, Main Steam Safety Valves (MSSVs) are modelled. ASDVs are not modelled as they are considered to be unavailable.
iii. Moderator System: Calandria Vessel with moderator and Over Pressure Rupture Disks (OPRD), the connecting relief lines and bleed valves.
iv. Calandria Vault and End Shield: Calandria Vault and End shield with water and structural material along with common rupture disk.

Analysis has been carried out with a RELAP5/SCDAP mod3.2 [55] specific plant model.

Reactor Core Model

The large PHWR reactor core is symmetric by geometry about vertical axis. The core was divided into 8 zones for each loops depending upon the elevation of reactor channels. Division of 8 zones for one of the loops has been shown in Fig. 5.2. Numbers of channels are clubbed in zones. Elevation of the clubbed channels from Calandria vessel bottom and the average power for the representative zones are given in Table 5.1.

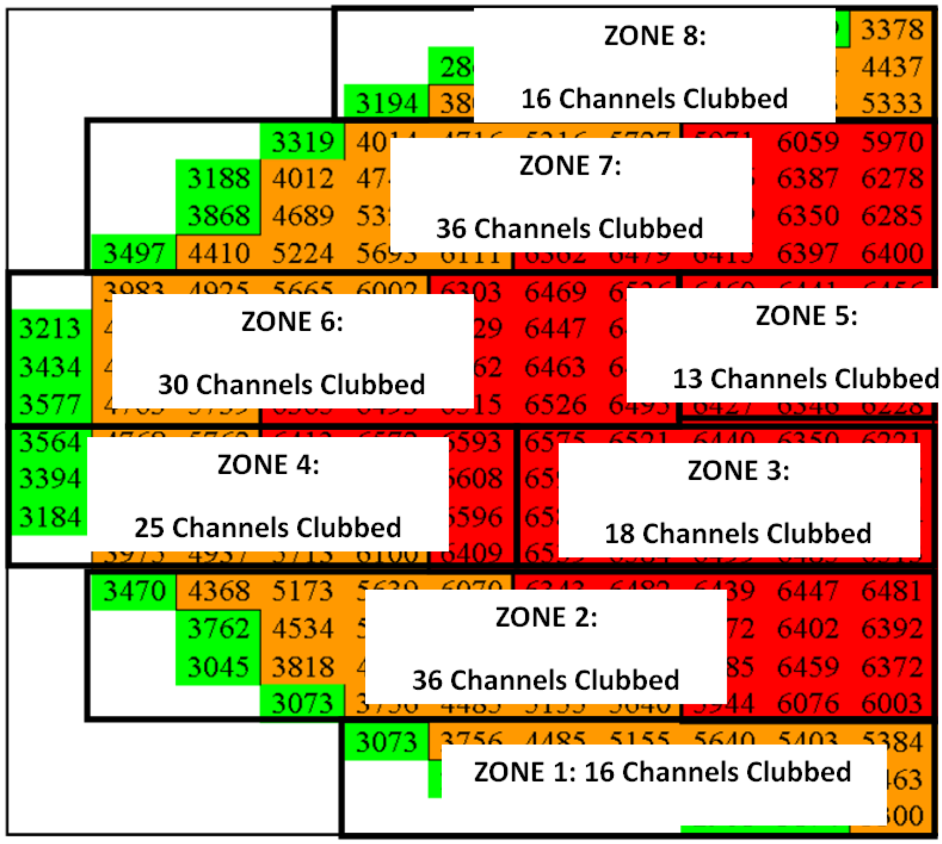

Fig. 5.2: Division of half core into eight zones

Table 5.1: Distribution of clubbed channels in each loop

Zone/Clubbed Channel No	No. of Channels Clubbed	Elevation from Calandria Bottom(m)	Average Power per channel (MW)
1	16	1.085	4.03
2	36	2.081	5.42
3	18	3.225	6.46
4	25	3.225	5.57
5	13	4.369	6.56
6	30	4.369	5.66
7	36	5.513	5.42
8	16	6.508	4.05

The convective heat transfer characteristic is conserved in the clubbed channel by providing equivalent fuel pins with internal heat generation, PT and CT with their corresponding surface areas. Equivalent flow rate has been provided in the clubbed channel to conserve the energy balance and dimensionless numbers like Nusselt number and Reynolds number.

The radiative heat transfer characteristics is conserved for a single channel and applied to the entire clubbed channel. SCDAP "fuel" and "shroud" components are used for simulating fuel elements, PT -CT respectively as illustrated in Fig. 5.3. Shield plugs at the end of each fuel channel are also modeled with "fuel" component of SCDAP structure with zero power generation.

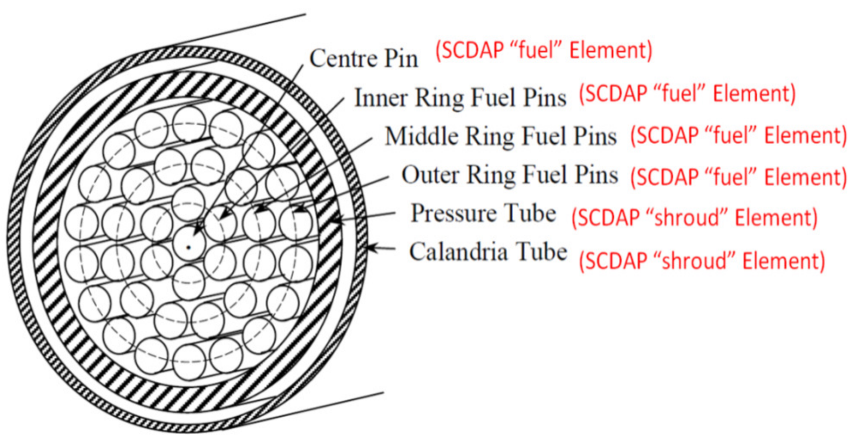

Fig. 5.3: SCDAP specific reactor channel model for 37 element bundle

Primary Heat Transport System Model

RELAP5 specific Primary Heat Transport System model has been developed which consists of two loops, each loop contains several reactor channels (Fig. 5.4). These channels are grouped with eight representative channels having different power as mentioned in the previous section.

Each channel is axially sub divided into 10 control volumes. The clubbed channel corresponding inlet feeders and outlet feeders of a single loop are clubbed into eight equivalent flow paths. Individual inlet and outlet headers are modeled. The flow path between the headers and the steam generators are modeled individually as well as the steam generators. Each steam generator consists of several number of tubes. All tubes are clubbed and represented by a single tube with

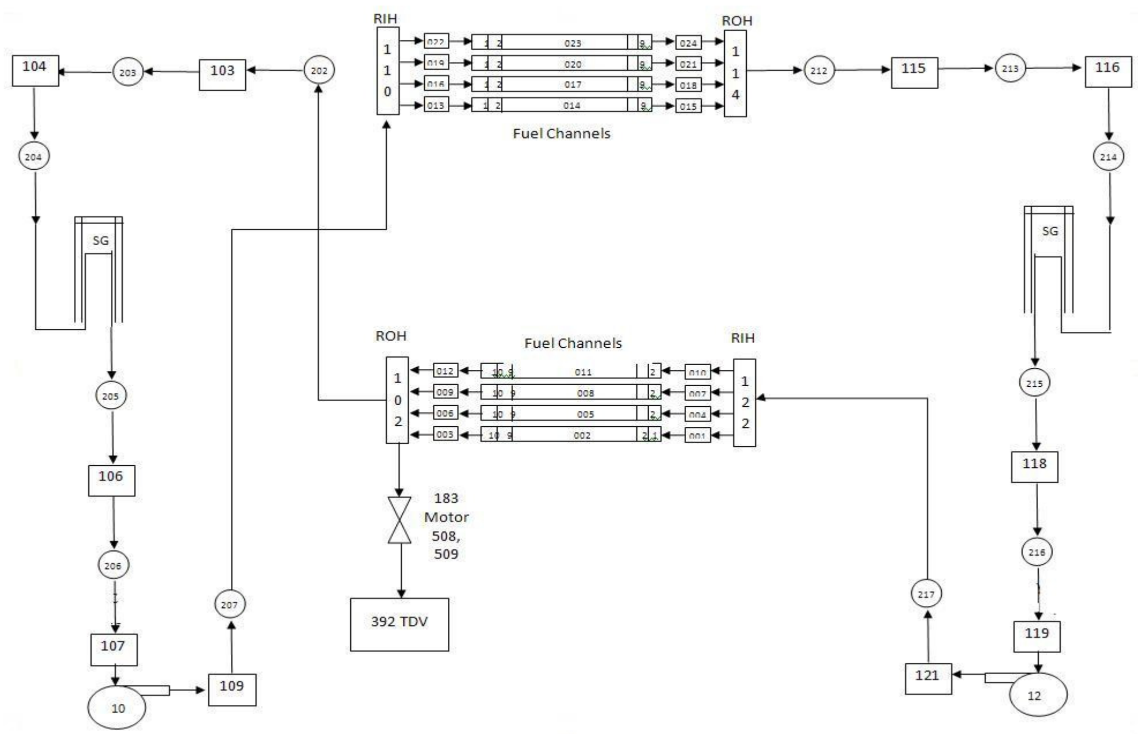

equivalent flow area.

Fig. 5.4: Nodalization of one loop of PHT system

The hydraulic diameter and heated equivalent diameter of this clubbed single tube is conserved for a proper thermal hydraulic calculation. PHTS circulation pumps are modeled individually with RELAP "pump" component model. The PHTS pump coast down is modeled with coast down data as obtained from the reactor designer. Two pump downstream flow paths are clubbed to represent a single flow path. Two IRVs mounted on outlet headers of both loops are modeled with "motorized valve" component. Flow areas of these valves are adjusted to get the desired flow at desired pressure. The Pressurizer is modeled with RELAP5 hydraulic and heat structure components. The stored heat of the pipe walls for all the systems are also modeled with RELAP heat structures with convective heat transfer as boundary condition.

Secondary Heat Transport System Model

The secondary heat transport system consists of steam generator secondary side, governor valves, main steam line stop valves and steam generator feed system. Fig. 5.5 shows the Nodalization of one of the four steam generators along with the corresponding steam drum, separator, feed line etc.

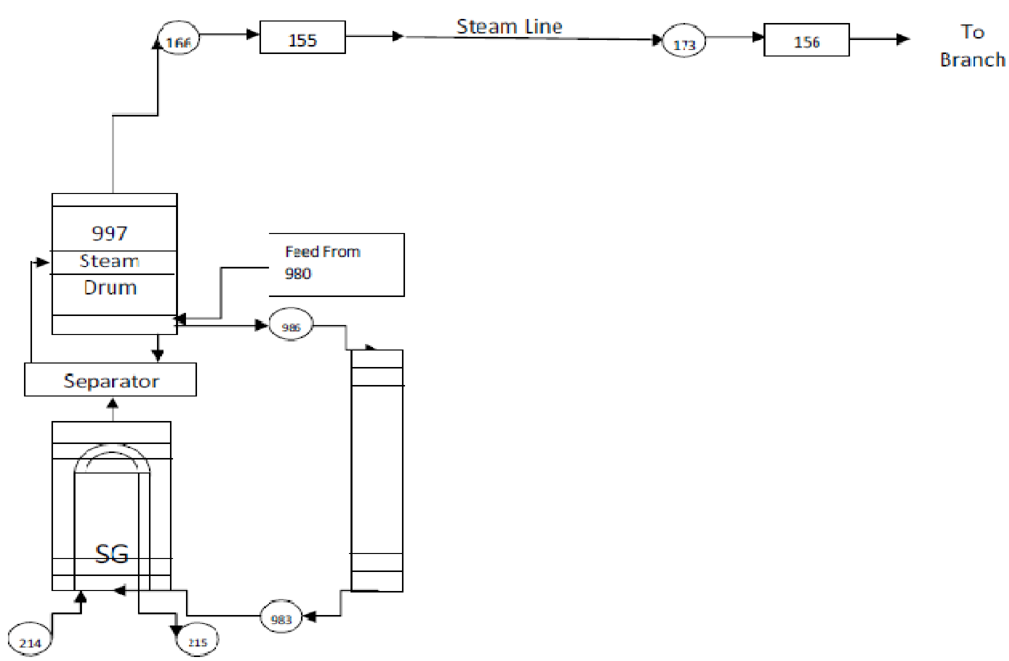

Fig. 5.5: Nodalization of steam generator secondary side

Heat structures have been used to model the structural part of steam generator that simulates heat transfer from the primary circuit to the secondary circuit. The steam obtained from all the steam generators is fed to a common header and the Main Steam Safety Valves (MSSV).

Moderator Calandria Vault (CV) & End Shield System Model

Moderator, Calandria Vault and End Shield model includes hydraulic volumes for the Moderator, End Shield Water, Calandria Vault Water, Calandria OPRDs, and Calandria Vault RDs. Fig. 5.6 shows the Nodalization for this system. RELAP5 heat structure component is used to simulate all the heat structures like Calandria vessel walls, Calandria Vault SS liner and concrete, Calandria tube sheet, end shield CS balls.

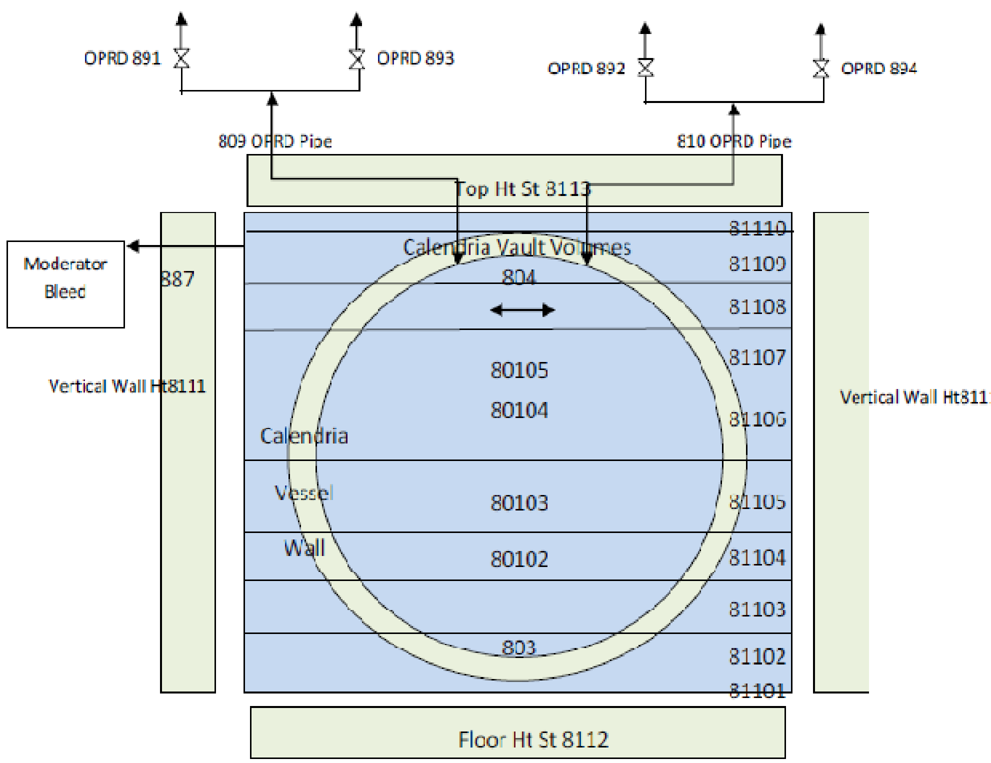

Fig. 5.6: Nodalization for moderator, CV & end shield

5.1.1 Postulated Scenario

The analysis has been carried out with a postulated scenario as given in Table 5.2.

Table 5.2 : Postulated scenario for SBO analysis

At t= 0 s, SBO is initiated with non-availability of Class III and IV power	
With Class III & IV Power un-availability	PHTS Pumps Trips
	Reactor Trips based on PHTS Pumps
	Turbine Trip
	Steam isolates due to closure of Main Steam Isolation Valve and Feed water to SG stops as the feed pump trips
	End shield circulation lost as the End shield pumps trips
	Calandria Vault circulation lost as the Vault cooling pumps trips
	Moderator Circulation and forced convective heat removal lost as the moderator pumps trip
Opening of Secondary side MSSVs	SG Pressure high (5.0 MPa)*
Opening of Primary Side IRVs	OH Pressure high (10.6 MPa)
Opening of Moderator Relief valves	Calandria Pressure high (0.11 MPa)
Opening of Rupture of OPRDs	Calandria Pressure high (0.12 MPa)
Opening of Bleed valve of End-shield and Calandria Vault	End shield and Calandria Vault pressure high pressure high (0.11 MPa)

*The ASDVS are designed for a fail safe “open” position for IPHWRs. However in this analysis ASDVs are assumed to be unavailable on loss of pneumatic pressure. This assumption is considered to extend for a slow boil-off condition of SG so that PHTS will remain pressurized leading to IRV actuation. Opening of IRVs mounted on PHTS will lead to loss of inventory from PHTS which in turn heat-up the reactor core earlier. Under realistic situation opening of ASDVs by loss of pneumatic pressure will lead to a crash cool down of PHTS resulting into cooling of fuel and depressurization. Under this situation further heat-up of core will take a longer duration as the sensible heat required to heat up the PHTS inventory will be large. The assumption considered for this analysis will lead to maximize clad heat-up before the moderator boil-off starts. It is to be noted that during SBO condition for IPHWRs, the Emergency Operating Procedures prescribes to carry out crash cool down operation manually (from control room) after 6 minutes of initiation of SBO followed by Fire Fighting Water injection into secondary side of SG. For this analysis manual actions are also not being considered.

5.1.2 Analysis Results and Discussion

The analysis is presented in two phases. The first phase spans from SBO initiation to uncovery of first row of channels and the second phase spans from first row uncovery to collapse of the core to Calandria bottom. As RELAP5 results are available in SI units hence they are presented in the same units. Following sub sections describes the analysis results,

Phase 1

Phase 1 of the analysis begins with initiation of Station Black Out at time t = 0.0 s, and ends at uncovery of first fuel channel (10,900 s). In the present analysis the uncovery of first fuel channel occurs at 10,900 s. Following figures show the transients for various parameters with respect to time. The outlet header temperature (liquid and vapor) and pressure are shown in Fig. 5.7.

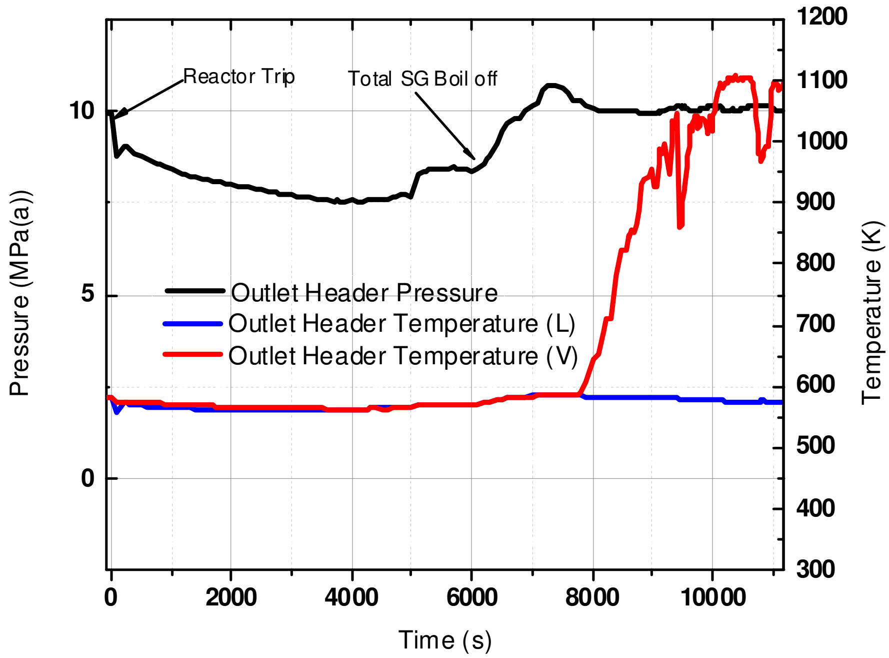

Fig. 5.7: Outlet header pressure and temperature transient

Fig. 5.7 illustrates that after the SG inventory boils off, the PHTS gets heated up leading pressurization and opening of IRVs. Around 7800 s the channels of PHTS full void condition. As RELAP5 code captures the thermal-non equilibrium hence two temperatures of fluid i.e. liquid and vapor at thermal non-equilibrium is computed. The vapor temperature shows that under two phase condition the vapor gets super heated from fuel heat-up which in turn deteriorates heat transfer from fuel.

As the SBO is initiated at t = 0 s, the PHTS pressure drops immediately (Fig. 5.7) owing to coasting down of PHTS circulation pumps followed by reactor trip. The PHTS pumps trip results in decrease in the PHTS mass flow rate as shown in Fig. 5.8. Steam Generator Secondary side pressure (Fig. 5.9) rises to the relief valve set point as Steam Generator inventory starts acting as heat sink for the natural circulation through the primary loops and removes heat by boil-off through Steam Relief Valves (Main Steam Safety Valves) till Steam Generator dryout occurs at 6000 s. The consequence of SG dryout (Fig. 5.10) and high SG secondary side sink temperature (as SG pressure remain at 5 MPa, Fig. 5.9) leads to drop in primary side natural circulation flow from 7000 s onwards as the secondary SG heat sink becomes unavailable. Degradation of heat transfer from primary to secondary leads to heat up of primary with large extent of steam formation from 7800 s onwards as discussed earlier (Fig. 5.7 and 5.13). This condition causes fuel temperature to rise from 7900 s onwards as illustrated in Fig. 5.11 End of the first phase, the fuel sheath attains a temperature of 1200 K.

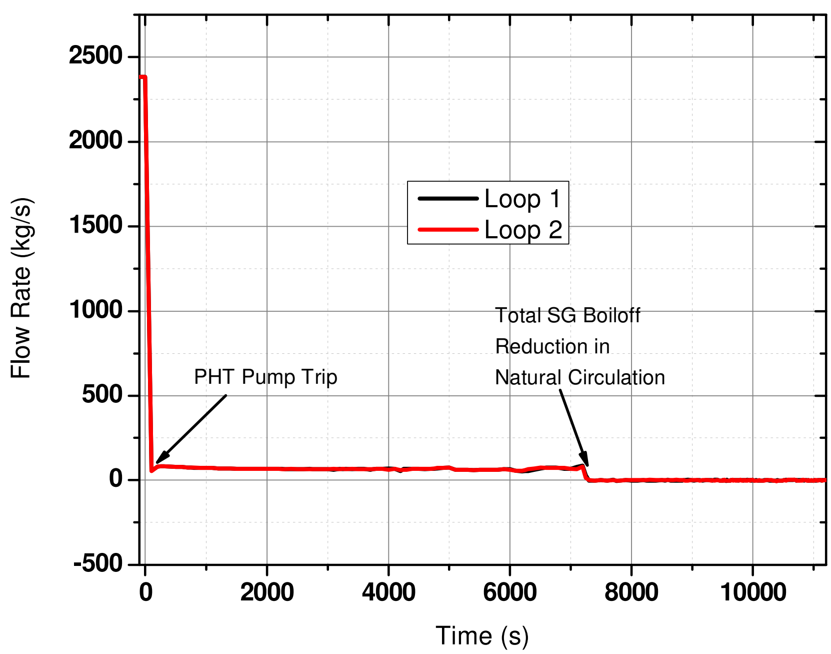

Fig. 5.8: PHTS flow rate transient

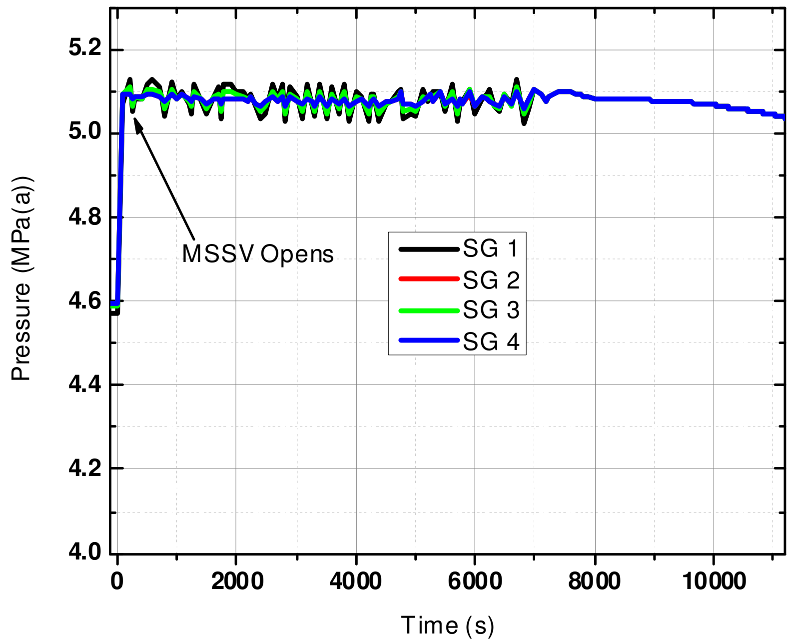

Fig. 5.9: Steam Generator pressure transient

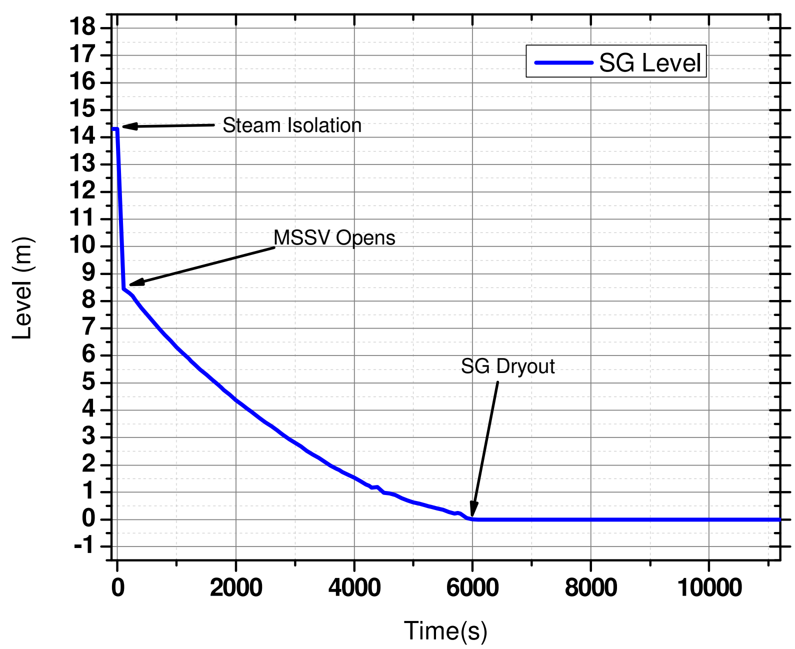

Fig. 5.10: Steam Generator level transient

The maximum fuel sheath temperature starts rising post SG dryout as shown in Fig. 5.11

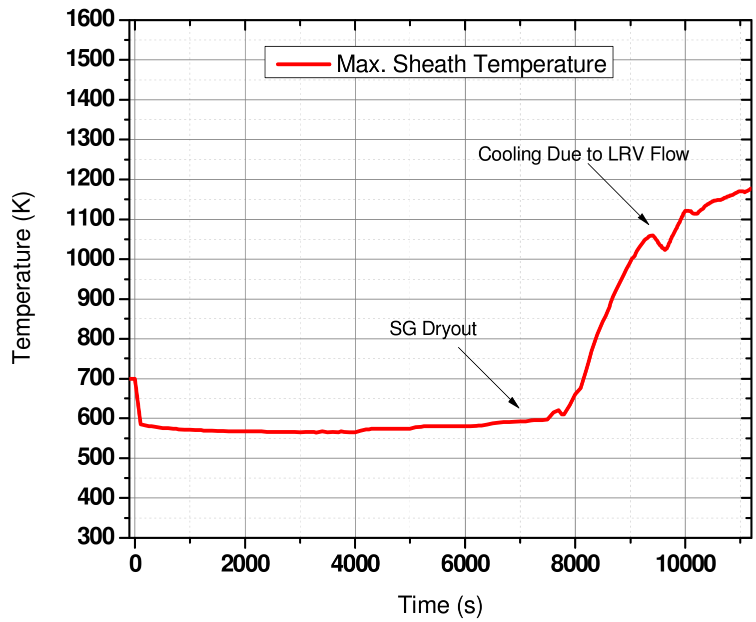

Fig. 5.11: Maximum fuel sheath temperature transient

The primary side IRVs get opened from nearly 7000 s onwards following PHT heat-up as a consequence to SG dryout (6000 s), This leads to loss of inventory on the primary side. The flow rates through the IRVs have been shown in Fig. 5.12. Loss of primary inventory and pressure also leads to voiding of the primary channels as shown in Fig. 5.13.

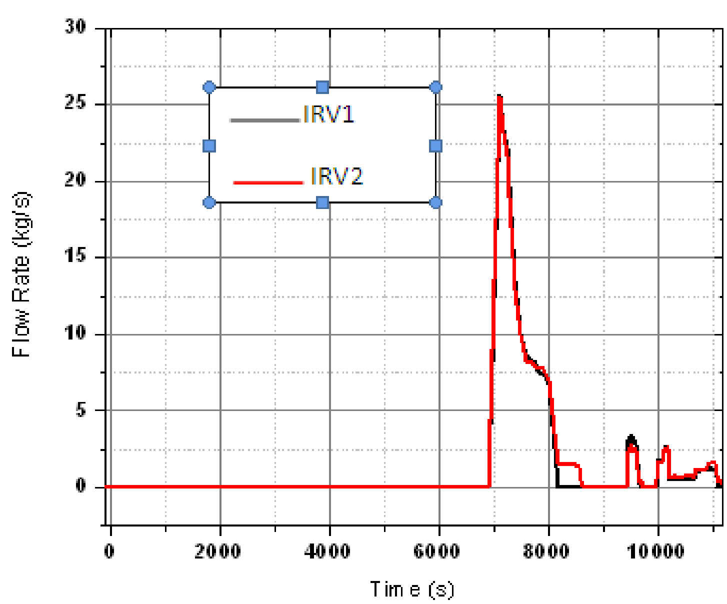

Fig. 5.12: IRV flow rate transients

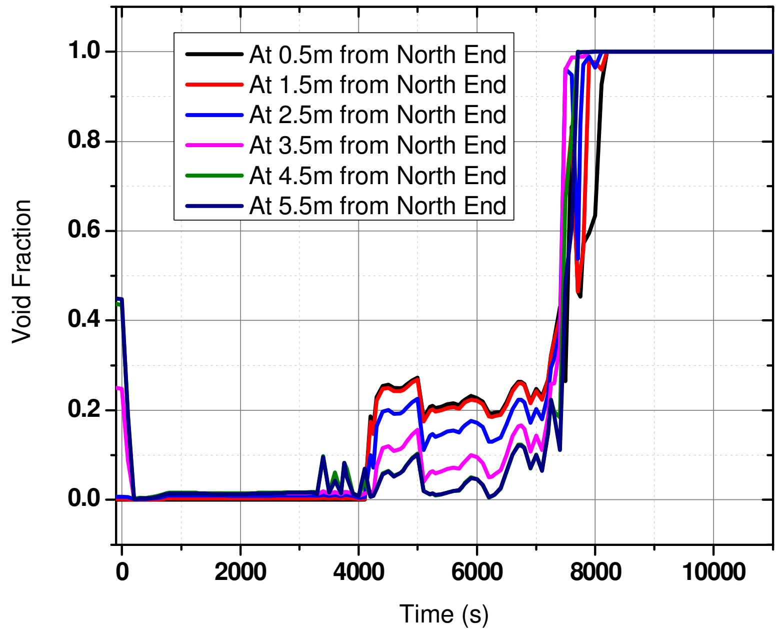

Fig. 5.13: Void fraction transient for top most channels

Figure 5.14 shows the average temperature for the topmost channel (PT-CT average). This temperature is the highest among all the modeled channels.

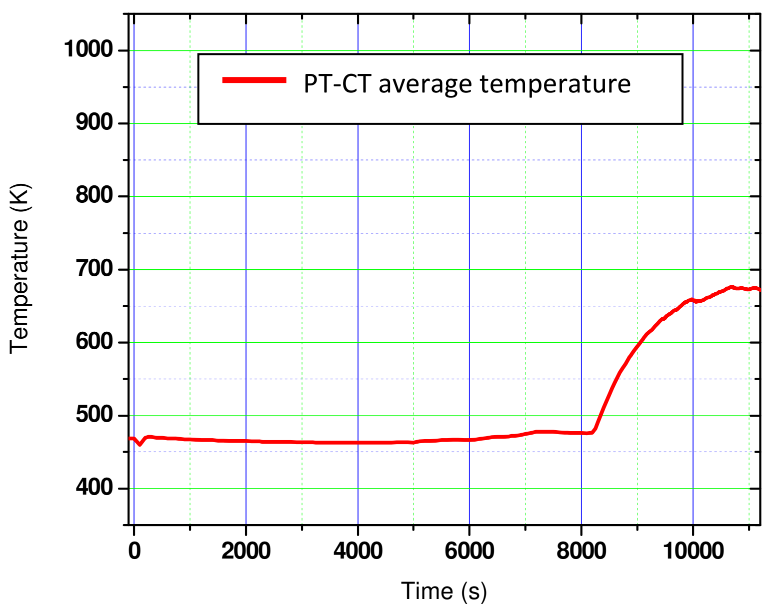

Fig. 5.14: PT-CT average temperature transient for topmost channel

Continuous addition of heat to the moderator causes pressurization in the Calandria as shown in Fig. 5.15. The initial pressure rise is accommodated by Calandria cover gas and later on by moderator relief valves from 9000 s onwards. It is observed that the relief valves are not sufficient enough to maintain the pressure rise due to heat addition as illustrated in Fig. 5.16. The continued heat addition causes rupture of Over Pressure Rupture Discs (OPRD) causing depressurization. The fall in level of moderator indicates moderator relief valve operation and OPRD failure.

The moderator temperature behavior is described in Fig. 5.16. There is an initial drop in moderator temperature due to reduction in heat load from channels as the reactor trips. Subsequently the temperature rises due to continuous addition of heat to the moderator as discussed earlier

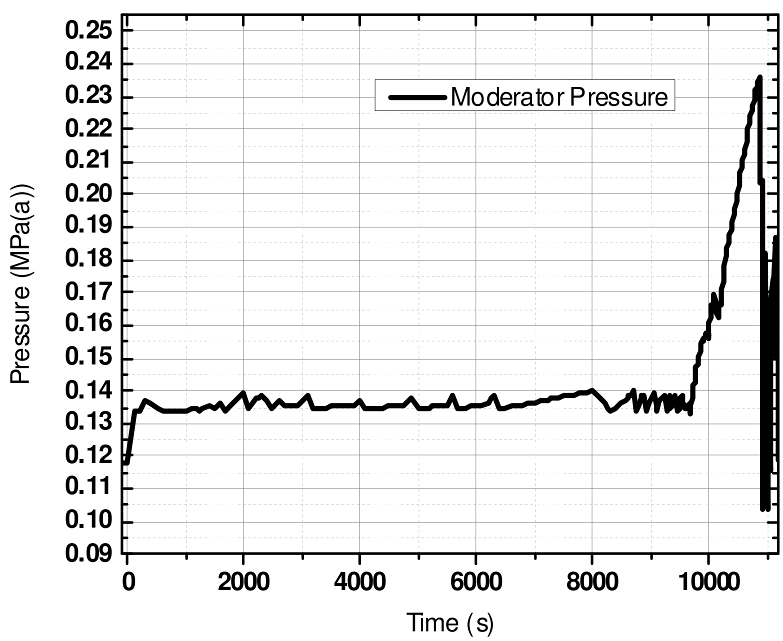

Fig. 5.15: Moderator pressure transient

.

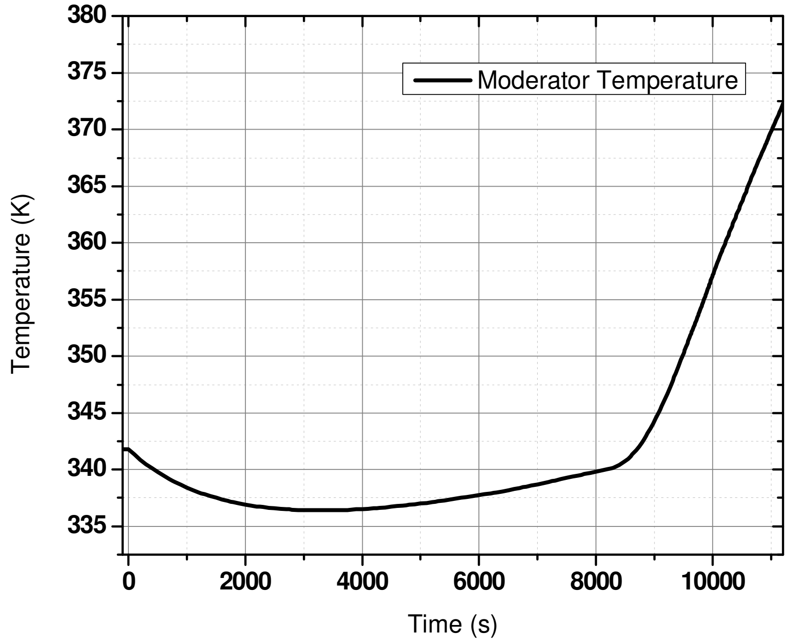

Fig. 5.16: Moderator temperature transient

The moderator level is illustrated in Fig, 5.17. Loss of moderator inventory through the OPRD also causes decrease in the moderator level exposing top most of the channels. This leads to heat-up of the top most channel. The CT temperature of that channel is shown in Fig. 5.18.

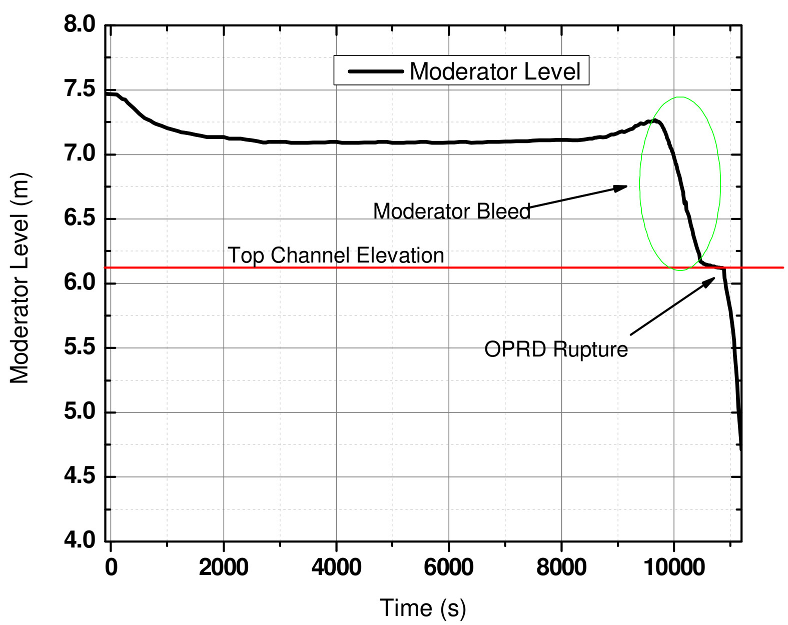

Fig. 5.17: Moderator level transient

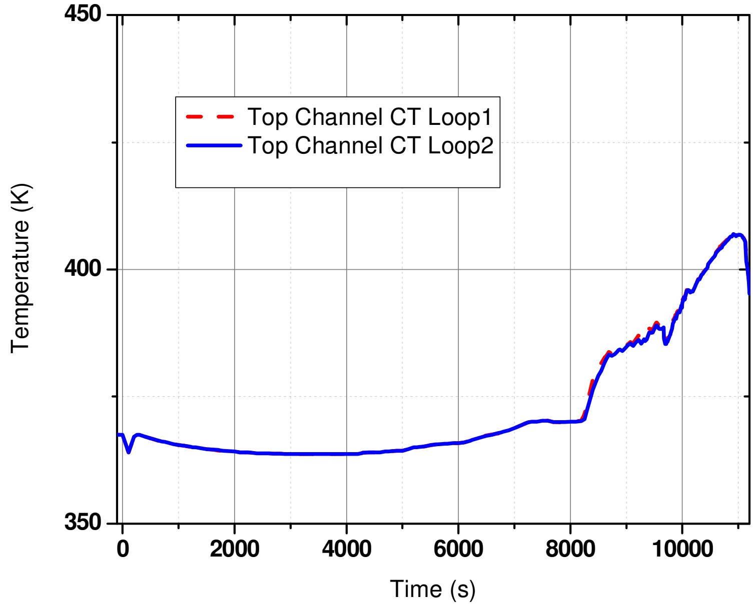

Fig. 5.18: CT temperature transient for top most channels

Since the fuel temperature does not rise beyond 1253 K (980° C) during this phase of the accident the hydrogen generation due to Zr oxidation [57] is rather small as shown in Fig. 5.19.

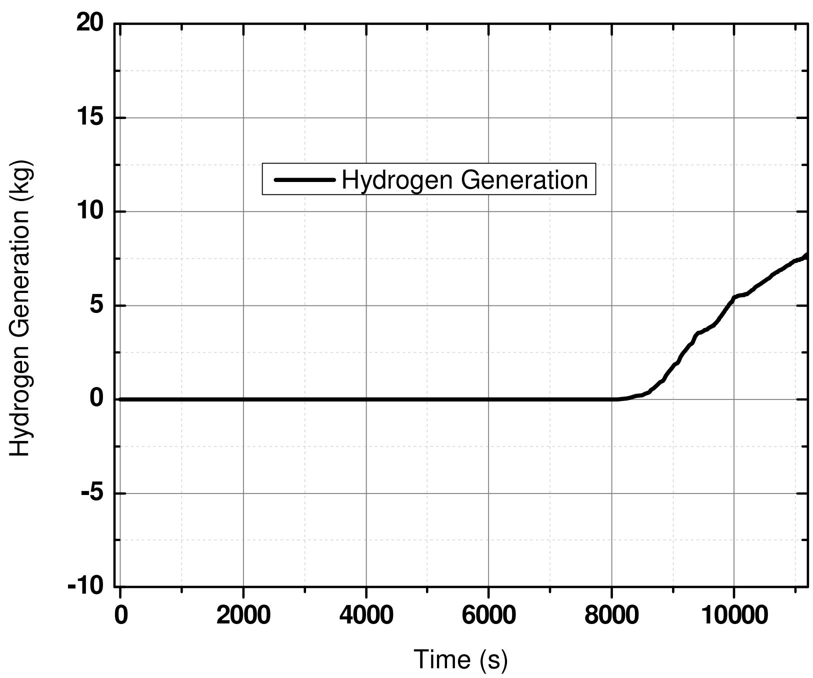

Fig. 5.19: Total cumulative hydrogen generation

Phase 2:

This phase begins from the uncovery of first reactor channel (t = 10,900 s) to the disassembly (collapse) of the entire reactor core (t = 17,936 s). As moderator attains boiling condition heat removal from the channels to moderator get deteriorated. The maximum powered channels at the central location get heated to a higher extent than the lower powered channels. Burst of high powered channels (10 nos. from each loop) take place on a combination of PT temperature high (1173 K) and PT internal pressure high (10 MPa) [1], causing PHTS high energy inventory to flow into moderator. A double ended failure of PT is assumed and the CT is considered to fail immediately from PT burst as CT is not a pressure retaining component. This channel burst leads further moderator expulsion as moderator get pressurized from added energy from broken PHTS. This event leads to more number of top row of channel exposure as the moderator level falls further from it's expulsion. As the temperature in the top most channels increases due to decrease in the moderator level, the channels reach disassembly temperature of 1473 K (average PT and CT temperature) [1]. Disassembly of 70 channels per loop, amounts to a weight of 25,000 kg on the intact channels below. These channels thus collapse under core collapse criteria leading to total core collapse [1].

Continuous addition of heat to the moderator causes increase in the moderator temperature to boiling point. This also results in increase in Calandria vessel temperature as shown in Fig. 5.20. Post channel burst as the pressure falls to atmospheric pressure the moderator temperature attain 373 K, thus the vessel temperature follows the fluid temperature with some time lag. At all point of time the vessel temperature follows the moderator fluid temperature.

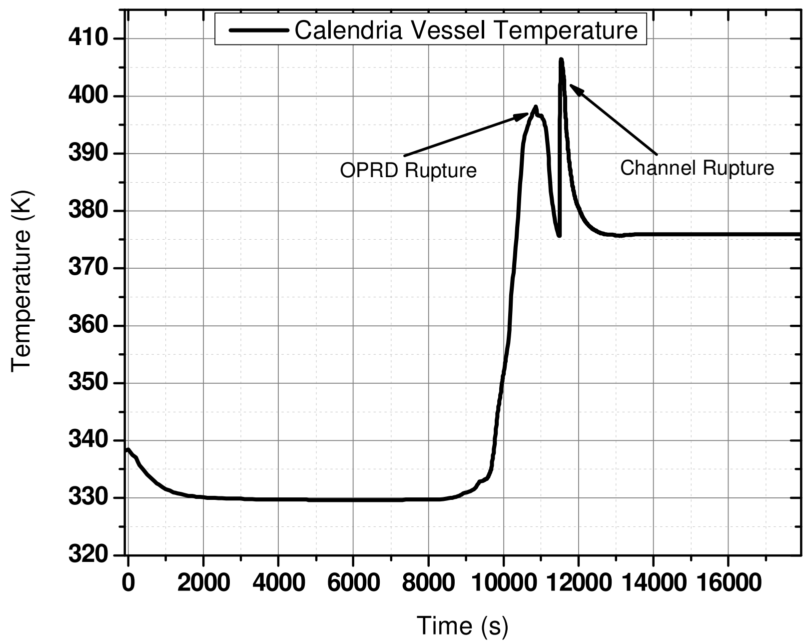

Fig. 5.20: Calandria temperature transient

.

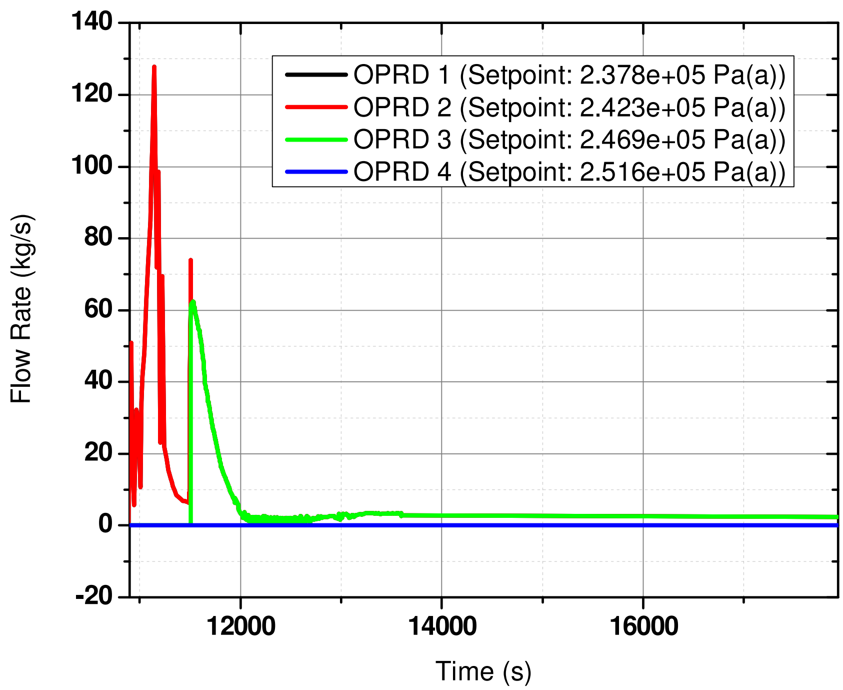

Fig. 5.21.OPRD flow rate transients

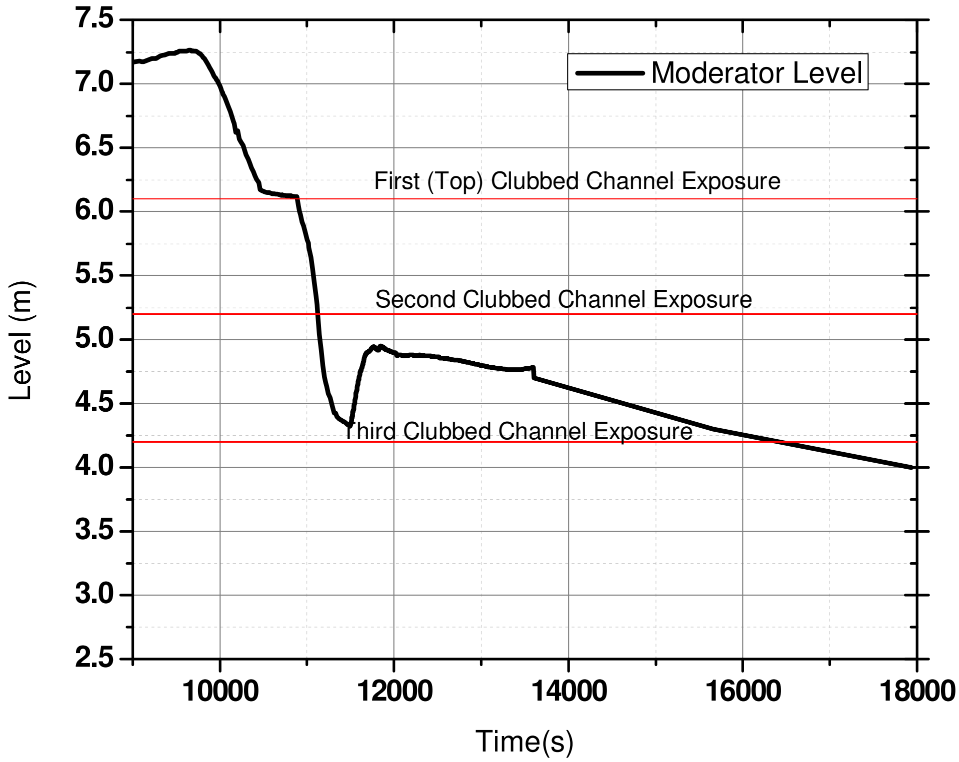

Fig. 5.22: Moderator Level Transients for phase 2

Further addition of heat to the moderator causes boil off of the moderator. Fig. 5.21 shows the flow rate through the OPRD and the drop in level in the moderator is shown in Fig. 5.22. Due to a drop in the moderator level the channels start getting exposed one by one. Lack of external cooling for the exposed channel results in an increase in the Calandria Tube and Pressure tube average temperature and subsequently reaches the disassembly criteria of 1473 K for channel disassembly as shown in Fig. 5.23.

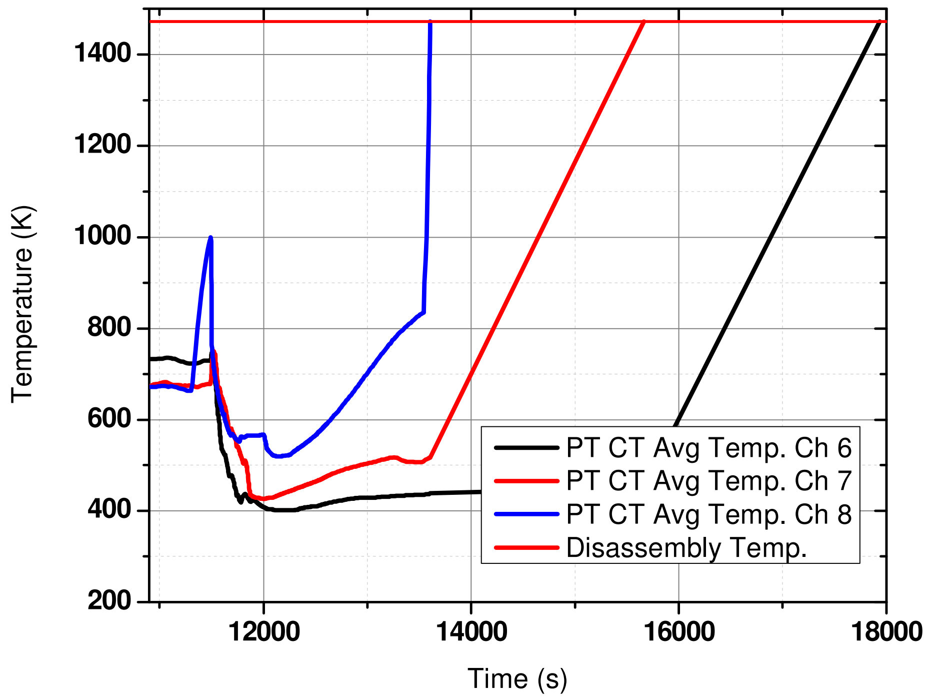

Fig. 5.23: PT-CT average temperature transients for phase 2

Since the core collapse criterion is addition of 25 tons of weight from exposed sagged channels on one row of submerged channel per loop [1], hence disassembly of minimum top three clubbed channels (Ch. 8, 7, 6 of Table 5.1) is required to meet this criteria. The time required for the top three clubbed channels to reach the channel disassembly temperature is around 17, 936 s where the PT-CT average temperature for these three channels reach 1473 K. As instantaneous core collapse has been assumed to occur at 17, 936 s. Post core collapse all the reactor channels are considered to be transferred to bottom of Calandria. Phase 2 calculation end with prediction of core collapse. A summary of events for Phase 1 and Phase 2 has been prepared and presented in Table 3 which are arranged in a chronological order.

Table 5.3: Summary of important events

	Scenario	Time (s)	Time (hr)
Phase 1	Class III and Class IV Power Loss	0.0	0.0
	Turbine Stop Valves Closes	0.0	0.0
	PHT Pump Trip and Feed pump Trip	0.0	0.0
	Reactor Trip	0.001	0.0
	Steam Isolation	20.0	0.0
	MSSV Opens for the first time	100.0	0.027
	Calandria Vessel Relief (Bleed) Opens	200.0	0.054
	SG Dryout in Loop 1	6000.0	1.81
	SG Dryout in Loop 2	6000.0	1.81
	IRV Opening in Loop 1	6900.0	1.91
	IRV Opening in Loop 2	6900.0	1.91
	Fuel Failure (clad rupture burst)	7000.0	1.94
	Pressurizer PORV Opens	7400.0	2.05
	At least 1 channel dry in Loop 1 (100% void)	8000.0	2.222
	At least 1 channel dry in Loop 2 (100% void)	8050.0	2.236
	OPRD Rupture	10 885.0	3.023
	First Channel Uncovery	10 900.0	3.027
Phase 2	PT-CT Rupture in Loop 1	11 500.0	3.194
	PT-CT Rupture in Loop 2	11 550.0	3.208
	Moderator Reaches Saturation Temperature	11 500.0	3.194
	First Clubbed Channel Disassembly in both loops	13 607.0	3.77
	Second Clubbed Channel Disassembly in both loops	15 666.3	4.35
	Third Clubbed Channel Disassembly in both loops	17 936.0	4.98
	Core collapse to Calandria vessel bottom for both loops	17 936.0	4.98

Parameters at the end of each phase have been tabulated in Table 5.4., At the end of phase 2 the reactor core lies at the bottom of the Calandria.

Table 5.4: Parameters at the end of each phase

Parameter	Units	Phase 1	Phase 2
Maximum Fuel Sheath Temperature	K	1442.4	1688.0
Exposed Channel (PT-CT) Average Temperature	K	1037.3	1611.0
Submerged Channel (PT-CT) Average Temperature	K	1037.3	1037.3
Maximum Calandria Tube Temperature	K	407.3	1490.0
Number of channel collapsed to Calandria bottom	-	-	380
H_2Produced per phase	Kg	20.23	198.97
Zr material oxidized per phase	%	1.14	11.23
Moderator level	m	7.0	4.0
Moderator temperature	K	473 K	473 K
Calandria Vault water Level	m	Full	Full
Calandria Vault water temperature	K	313 K	323 K
Calandria Vault Concrete temperature	K	305 K	318 K
End shield water temperature	K	333 K	473 K
End Shield structure temperature	K	333 K	473 K
Reactor Power	%	-	1%

5.2 Late Phase Accident Analysis

The late phase of accident has been carried out with the reactor core conditions obtained from the early phase accident analysis. Table 5.4 illustrates the conditions used for DBHUA analysis as initial conditions. ANS Power decay curve [56] has been used as boundary condition for decay power for calculating debris bed heat-up. The DBHUA model as used for the analysis is illustrated in Fig. 5.24.

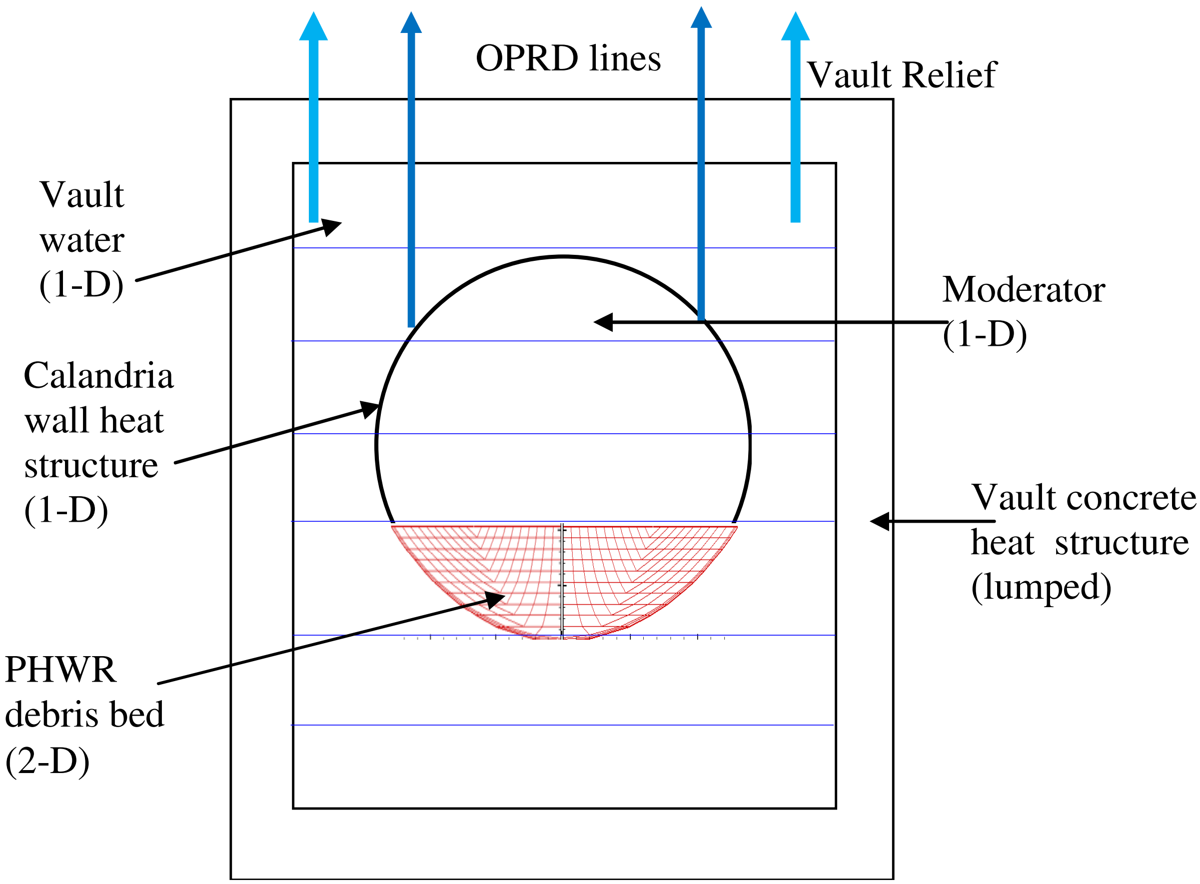

Fig. 5.24 : DBHUA model for reactor core simulation

5.2.1 Analysis Results and Discussion

The analysis is initiated at t= 0 s. The time t=0 s is the end of phase 2 period (4.98 hrs.) of early phase of accident analysis as illustrated in table 5.4. Fig. 5.25 shows the temperature transient for top, middle and bottom layer of debris bed along with bottom section temperature of Calandria. Fig 5.25 also shows the trend of boil-off of moderator and Calandria Vault water level as predicted by model.

Debris bed temperature:

It is evident from Fig. 5.25 that moderator boil-off take around 22,000 s causing the debris temperature (top and middle) to start rising earlier as compared with the bottom debris temperature. The bottom debris temperature rises at the last of these three sections. The central portion of the debris attains the highest temperature as against the top and bottom and stabilizes at 2000 °C. The top section of the debris bed remains at low temperature of 1000°C as the top layers radiates heat to the very large Calandria top. The bottom section of debris bed starts heating up after the moderator inventory is totally exhausted. The temperature remains at 1050 K up to 1,50,000 s (≈41 hrs) with the effective convective cooling from ex-Calandria heat transfer. The bottom debris temperature start heating up once Calandria bottom gets exposed at 25% Calandria Vault water level. The bottom section temperature increases as high as the debris bed mid section temperature of 2000 K. The rise in bottom debris bed temperature has caused marginal rise of middle section debris temperature as the ΔT between these two layers of debris bed temperature reduces thus causing less heat transfer. At this juncture i.e. 1,500,000 s , the top layer debris bed temperature shows marginal rise in temperature due to higher heat flow from central debris location. As the structural mass of the top layers of debris bed is higher as more number of channels is located, the temperature rise is not that significant. It is observed from the study that debris bed temperatures attain maximum temperature of 2000 °C which is far below the melting point of UO_2 of 2800°C. The majority of the bed remains solid, however at this temperature some U-Zr-O eutectic formation is expected.

Moderator and Calandria Vault level:

The fall in level of moderator and Calandria Vault from boil-off is found to be non-linear with time. This is attributed to non-uniform cross section of fluid volumes from top to bottom elevation as well as non-uniform heat rejection to these fluid volumes as the heat removal rates are different at different hydraulic nodes. The boil-off period for moderator is estimated to be 22,000 s from it's level of 4 m (end of phase 2 of early phase degradation)

Calandria bottom temperature:

The Calandria bottom section temperature as illustrated in Fig. 5.25 shows a stable temperature till 1,75,000 s (≈48.6 hrs) and after that rises after the exposure of this section starts from Calandria Vault water receding level. The wall undergoes nucleate boiling from almost beginning of the transient calculation as the wall temperatures remains higher than 110°C due to flow of heat bottom most layer of the debris bed. Tw> 110°C is a pre condition set for nucleate boiling in the DBHUA model, enabling a large amount of heat to transfer from debris lower bed to Calandria wall and from Calandria wall to Calandria Vault water. The temperature shoots up to 1800°C post exposure thus failing it by mode of ablation. It is interesting to note here that Calandria wall fails by ablation though the debris bed remains primarily solid. The debris bed temperature contour plots are shown in Fig. 5.26 (a)-(d) for the bottom section of the Calandria containing the debris bed at different time instants. All the time instants plots are for the situation before the Calandria exposure.

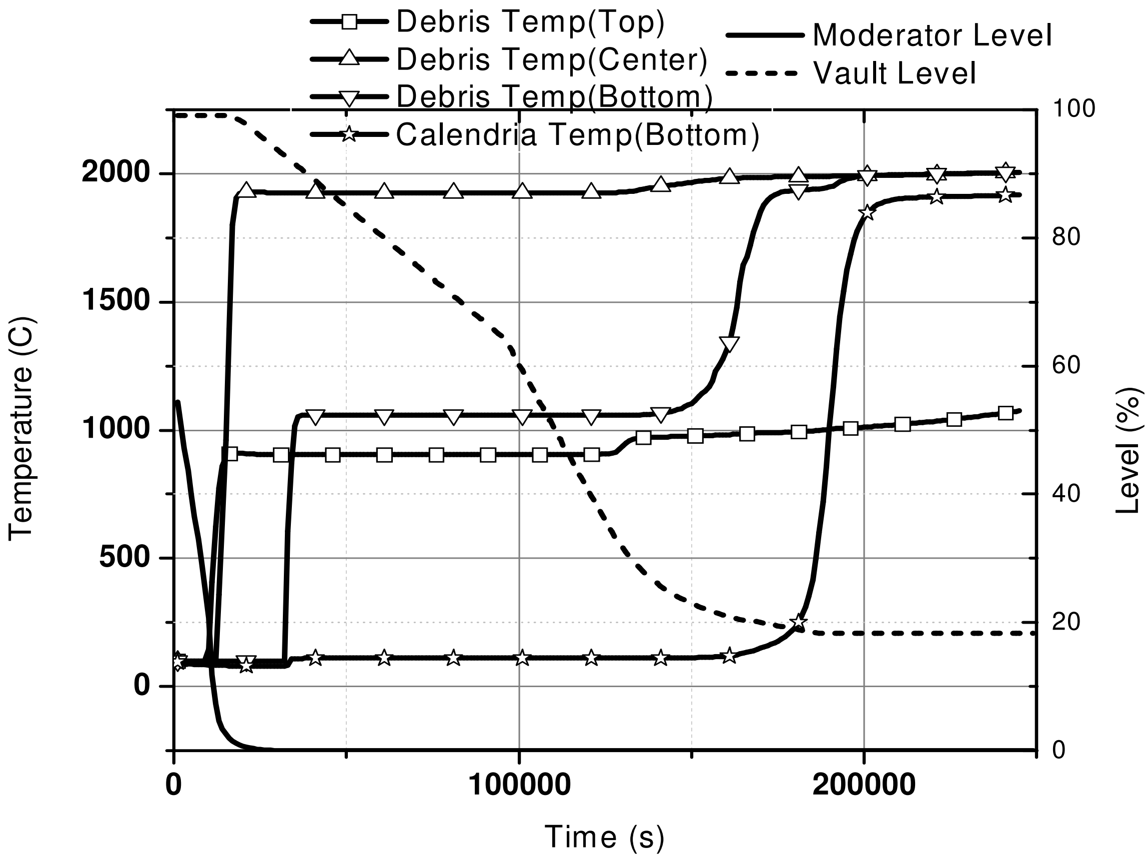

Fig. 5.25 : Temperature and level transient for different components as predicted by DBHUA

The plots illustrates that slowly the debris bed get heated up as the Calandria water gets boiled off and the heated section slowly moves towards the bottom as the large upper section of Calandria provides a better heat sink through radiation heat transfer rather than the lower section where the heat is being removed by nucleate boiling. Fig. 5.26 affirms the Calandria bottom condition which remains at a lower temperature prior to it's exposure. Thus the Calandria integrity from ablation point of view is demonstrated. The early phase and late phase analysis are being reported by Gokhale [58] and Mukhopadhyay [59] respectively.

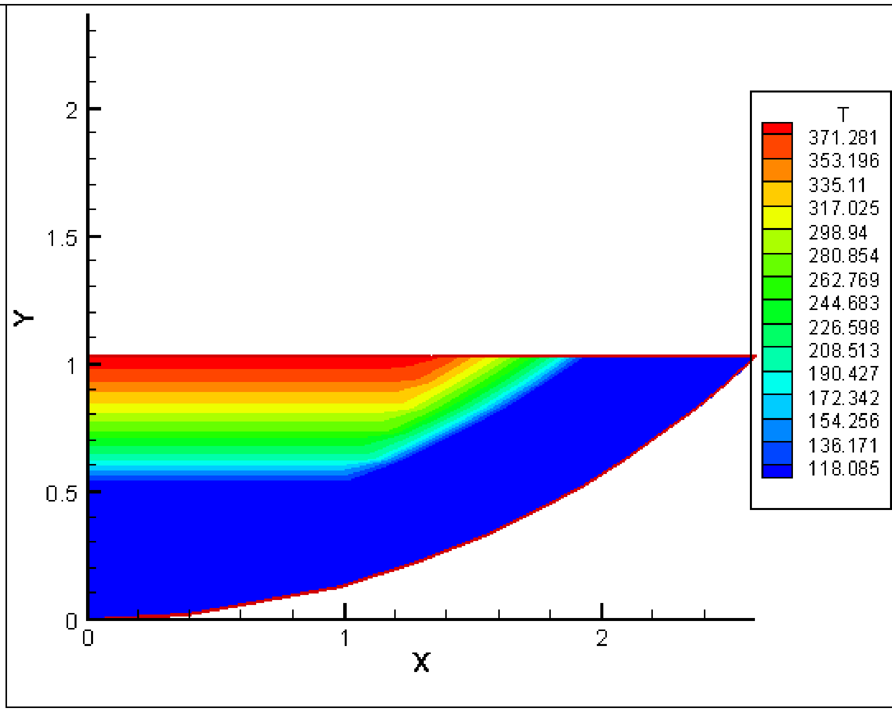

(a) : Debris bed temperature (°C) contour at 11000 s

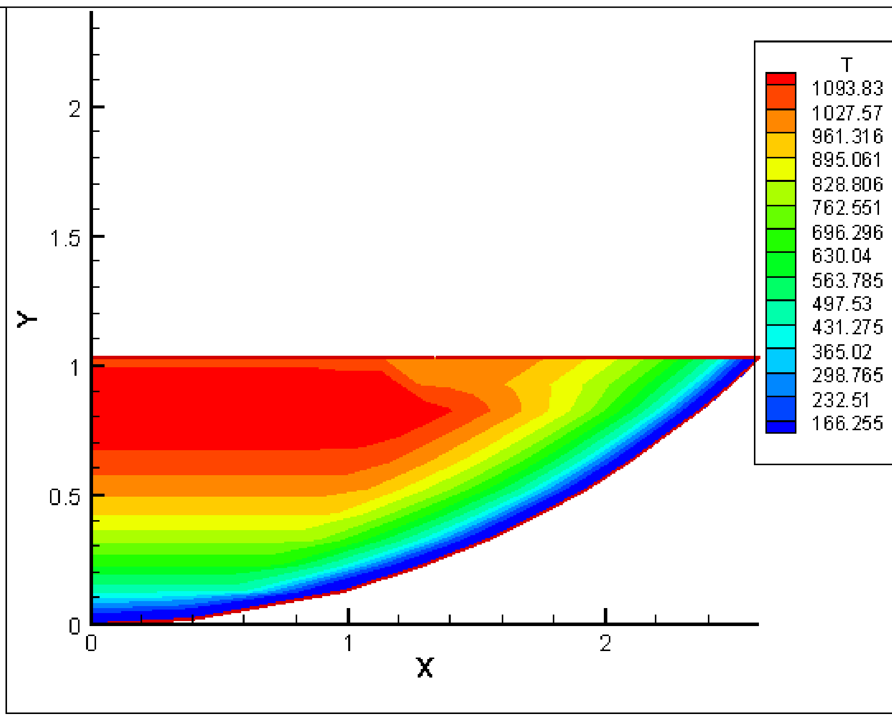

(b) : Debris bed temperature (°C) contour at 15000 s

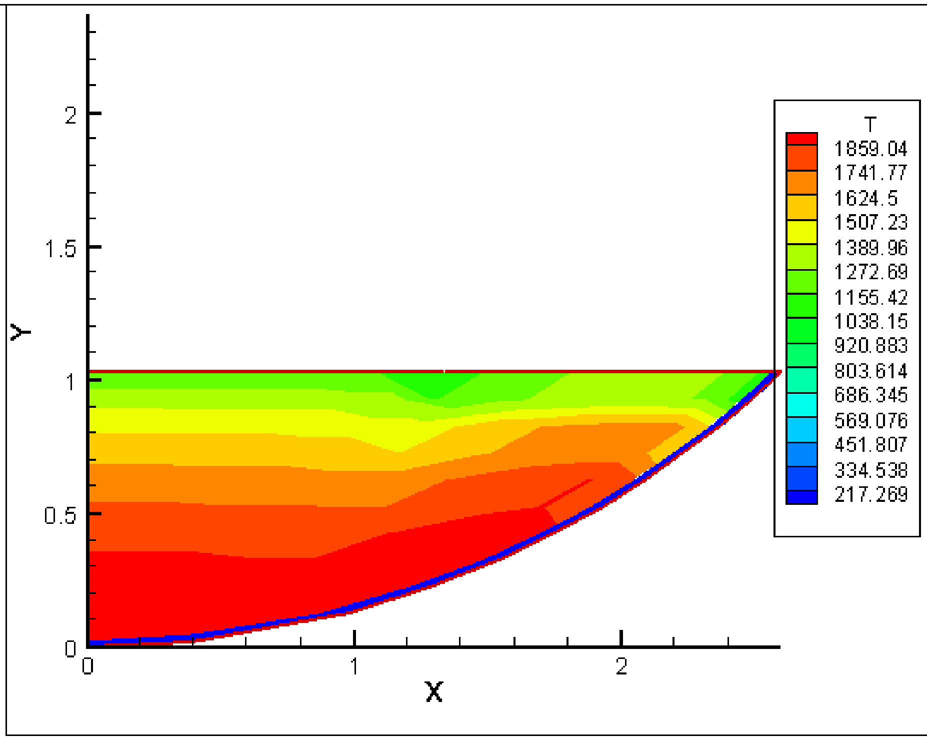

(c) : Debris bed temperature (°C) contour at 75000 s

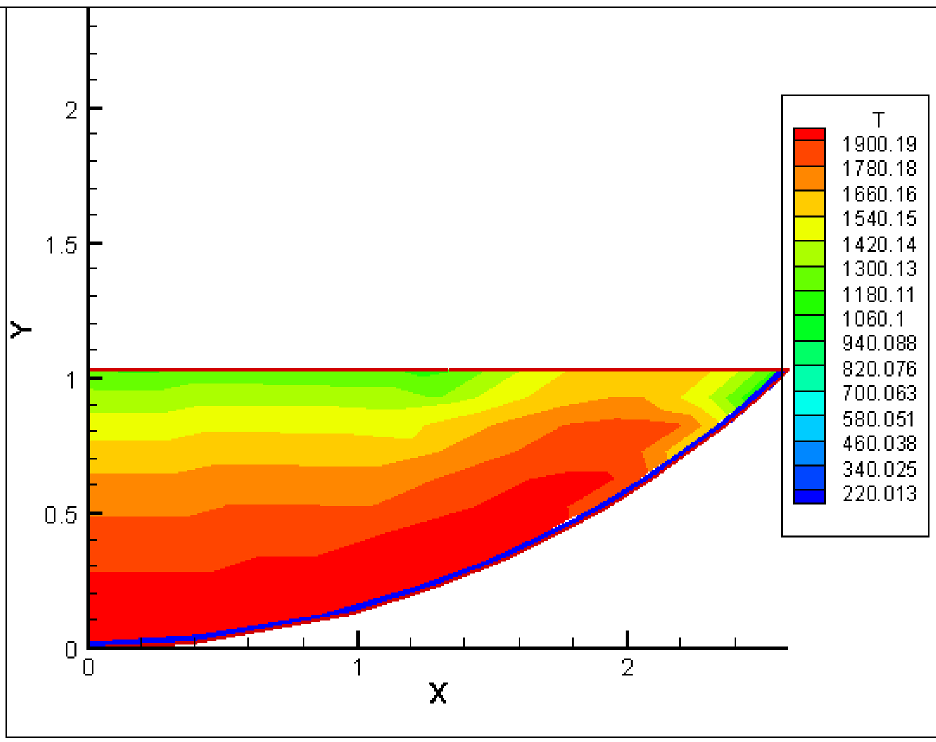

(d) Debris bed temperature (°C) contour at 150000 s

Fig. 5.26: Debris bed temperature contour at different time instants

A sensitivity analysis has been carried out to asses the influence of debris particle size on the debris bed heatup. The bed porosity has been varied from 0.2 to 0.6. Fig. 5.27 illustrates the influence of porosity on the heat up pattern.

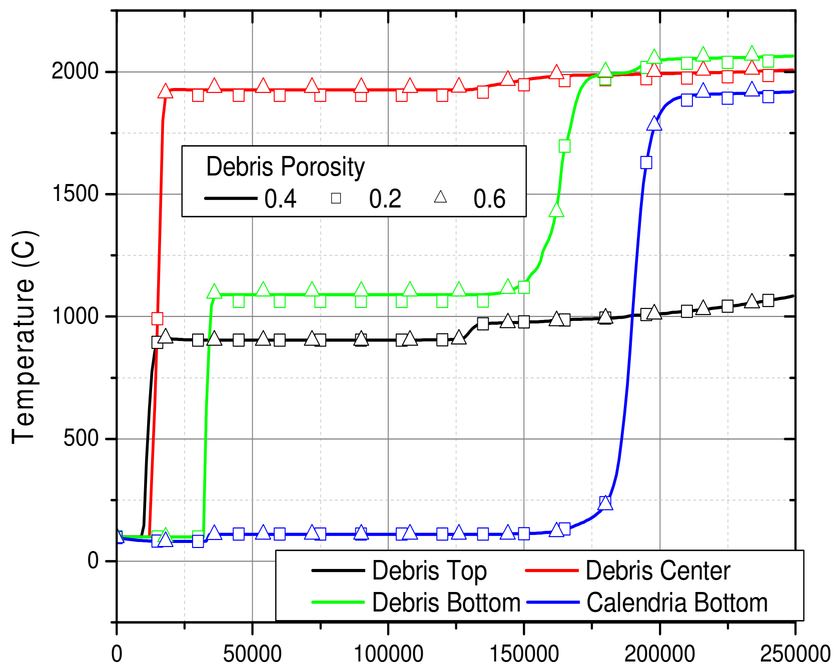

Fig. 5.26: Influence of porosity on debris bed heatup behaviour

As observed from Fig. 5.26, the heatup pattern is not sensitive to the debris bed porosity as the heat transfer largely depended on the convection mode rather than conductive mode where bed porosity plays an important role.

5.3 Conclusions

Early Phase of Accident

I. The early phase of accident initiated with unmitigated SBO lead to channel heat-up and burst as the pressure remains high

II. The channel burst leads to flow of energy from Primary Heat Transports system to moderator thus pressurizing the fluid leading to burst of Over Pressure Relief Device (OPRD).

III. The moderator expulsion from OPRD burst leads to several rows of channel exposure thus leading to channel disassembly of dry channels

IV. The disassembled channels thrust load on the still submerged channel thus failing the still submerged channels and form a debris bed at the bottom of Calandria. This takes a time of around 5 hrs

Late Phase of Accident

I. The debris bed does not show any heat up till the bed is submerged into water after the total exposure the bed heat up begins at around 22,000 s.

II. The heat up of the top and bottom most section of the debris bed is much lower as compared to the central location.

III. Debris bottom and Calandria bottom temperature starts rising once the Calandria Vault water falls below the Calandria.

IV. Till the end of calculation the debris bed did not attain melting temperature of UO_2 and ZrO_2 though the Calandria bottom gets exposed.

V. The Calandria bottom temperature attains it’s melting point once the bottom section of Calandria gets exposed from Calandria Vault water. The integrity of Calandria is found to be challenged post it’s exposure only.

VI. The sensitivity study shows that the debris bed heatup behaviour is not much sensitive to porosity variation. This is due to the dominance of convective heat transfer as compared to the conductive heat transfer where porosity plays a major role in decoding the heat transfer.

5.4 Model Criticism

The debris bed heat-up model for the exposed section has been validated for a temperature range of 100-670^{0}C. However, it has been applied for a higher temperature range of 100-2000^{0}C. The applicability of these models for PHWR specific debris bed needs to be validated at higher temperature (100-1500°C).

Chapter 6

Conclusion

A PHWR specific model has been proposed with governing energy equation and closure relations. The proposed model is validated against short and long term experiments debris bed carried out for different power levels simulating decay power levels. The comparison shows a good agreement predicting the trend and the magnitude of the parameters. The model is used for analyzing a severe accident scenario in a large IPHWR application which calls for additional models to simulate for all the reactor core components.

The major contribution of this work is the characterization of thermal-hydraulic behaviour of PHWR-specific debris bed which may arise from a severe accident condition. The study included experiments with a single segmented channel and multiple channel debris bed. It is concluded that only with full exposure the debris bed get heated up. The convective cooling through inter-channels space by generated steam is found to limit the heat up of the debris bed. The steam generated in the core is largely found to emerge from the open ends of the channels, bypassing the debris bed. New correlation has been proposed for heat transfer coefficients for heat transfer inside channel and for exposed debris bed the existing correlations are modified with respect to characteristic lengths for effective conductivity and convective heat transfer coefficient. The proposed relations are found to be adequate for predicting the PHWR specific debris bed heat-up.

The other important prediction of this study is the prediction of Calandria integrity till it remains submerged in the Calandria Vault water. As PHWR design does not feature a core catcher, it is imperative to examine the structure which can retain the core during a severe accident situation thus limiting the further progression of accident. It is also seen from the study that the post structural failure of the Calandria the debris bed does not undergo widespread melting, thus limiting the risk of ex-Calandria molten fuel-Calandria Vault water interaction.

The model developed and validated through experiments has a potential application for nuclear industry. They are (i) forming a Technical Basis tool for supporting Severe Accident Management Guideline (SAMG) evolution for PHWR where all the actions need to assessed against state-of-are analytical models (ii) realistic “Source Term” estimation for calculating risk to public domain for site evaluation and emergency preparedness (iii) assessment of hydrogen source term for quantification of Passive Autocatalytic Recombiners.

Future Work:

It is proposed to carry out experiment of the exposed debris bed at higher temperature (1000°C-1500°C) and with a larger debris bed configuration so that the model applicability could be validated for this temperature range. In the current study the electrical power and mode of heating of FRs are found to be the major constraints. Improvements for the model are proposed to simulate flow of molten material formed from eutectic formation within the debris bed, natural circulation of molten material and inclusion of fission product release mode in debris bed.

Nomenclature

a	:	absorption factor
A	:	cross sectional area
c	:	heat capacity
C	:	Constant
d	:	Debris bed particle diameter
D	:	diameter
F	:	radiative exchange factor, factor
g	:	acceleration of gravity
G	:	mass flux
h	:	convective heat transfer coefficient
k	:	Conductivity, rate constant
K	:	Permeability, constant
l	:	elementary volume dimensions
L	:	system dimension, level, mean free path
$\dot{m}$	:	mass flow rate
m	:	mass
Nu	:	Nusselt number
Pr	:	Prandtl number
q	:	Heat Flow
q''	:	heat flux

Q	:	volumetric heat generation rate
R	:	electrical resistance
Re	:	Reynold's number
T	:	temperature
u	:	velocity
w	:	mass per unit area

Subscript:

b	:	bulk
CHF	:	Critical heat flux
conv	:	convection
d	:	Diameter, porous bed, debris
D	:	debris
ds	:	Submerged section of row of channels
e	:	effective, exposed
ec	:	effective conductivity
es	:	exposed section
g	:	gas/vapour , grey body
gap	:	gap
hy	:	hydraulic
he	:	heated equivalent
i	:	Incident, inlet, interface
m	:	mean

o	:	angle between the incident and scattered beam, outlet
p	:	particle
r	:	radiative
rad	:	radiation
s	:	Steam, submerged, solid
ss	:	submerged section
w	:	Weight, wall

Greek alphabets

μ	:	viscosity
ε	:	Porosity, emissivity
β	:	volume coefficient of expansion of vapour
θ	:	scattered angle
Δ	:	difference
ρ	:	density, resistivity, reflectivity
δ	:	Depth of penetration

References

[1] Lee et al. Analysis of severe accidents in Pressurized Heavy Water Reactors, IAEA TECDOC 1594 (2008)

[2] Sehgal, Bal Raj, Stabilization and termination of severe accidents in LWRs, Nuclear Engineering and Design 236 (2006) 1941–1952

[3] Jean-Pierre Van Dorsselaere et al., Sustainable integration of EU research in severe accident phenomenology and management, Nuclear Engineering and Design 241 (2011) 3451– 3460

[4] Bajaj, S. S.; Gore, A. R.: The Indian PHWR, Nuclear Engineering and Design 236 (2006) 701–722,

[5] Hadaller, G.I., Sawala, R., Kohn, E., Archnoff, G.H., Wadswaorth, S.L., Experiments investigating the thermal-mechanical behaviour of CANDU fuel under severely degraded cooling, Proc. 5th Int. Mtg. on Thermal Nuclear Reactor Safety, Karlsruhe, Germany (1984).

[6] Wadswaorth, S.L., Hadaller, G.I., Sawala, R., Kohn, E., Experimental investigation of CANDU fuel deformation during severely degraded cooling, Proc. Int. ANS/ENS Topical Mtg on Thermal Reactor Safety, San Diego, CA (1986).

[7] Mills, P.J., Sanderson, D.B., Haugen, K.A., Hackee, G.G., Twenty-eight element fuel-channel thermal-chemical experiments, Proc. 17th Annual CNS Conf., Fredericton, NB (1996).

[8] Gillespie, G.E., Moyer, R.G., Hadaller, G.,Hildebrandt, J.G., An experimental investigation into the development of pressure tube/Calandria tube contact and associated heat transfer under LOCA conditions, Proc. 6th Annual CNS Conf., Ottawa, ON (1985).

[9] Sanderson, D.B., Moyer, R.G., Dutton, R., Effectiveness of the moderator as a heat sink during a loss-of-coolant accident in a CANDU-PHW reactor, Proc. Int. Centre for Heat and Mass Transfer Conf., Cesme, Turkey (1995).

[10] Loesel, P.M., et al., The Large-Scale vented combustion test facility at AECL-WL: Description and Preliminary Test Results, AECL-11762, NEA/CSNI/R(96)8, 219 (1997).

[11] Koroll, G.W., Muzumdar, A.P., Corima, M.A. Hunt, N.G., "Hydrogen management in CANDU reactors", OECD/CSNI Specialist Mtg. on Selected Containment Severe Accident Strategies, Stockholm (1984).

[12] Iglesias, F.C., Lewis, B.J., Reid, P.J., Elder, P., Fission product release mechanisms during reactor accident conditions, J. Nucl. Materials. 270 (1999) 21–38.

[13] Wright, A.L., et al., Primary system fission product release and transport — A state-of the-art report to the Committee on the Safety of Nuclear Installations, U.S. Nuclear Regulatory Commission Report NUREG/CR 6193, also released as Organization for Economic Cooperation and Development Report NEA/CSNI/R(94)2 and Oak Ridge National Laboratory Report ORNL/TM 12681 (1994).

[14] Mathew, P. M., Severe core damage accident progression within a CANDU Calandria vessel, https://www.oecd-ea.org/nsd/workshops/masca2004/oc/papers/CAN_mathew.pdf.

[15] Rogers, J.T., Thermal and Hydraulic Behaviour of CANDU Cores under severe accident conditions — Final Report, Vol. 1 & 2, Atomic Energy Control Board, INFO-0136 (1984).

[16] Rogers, J.T., A study of the failure of the moderator cooling system in a severe accident sequence in a CANDU reactor, Proc. Fifth Int. Mtg on Thermal Nuclear Reactor Safety, KfK 3880/1 (1984).

[17] Schaefer, D. W., Engineered Porous Materials, MRS Bull, (XIX): 14-17, 1994.

[18] Banavar, J.,, Koplik, J.,, and Winkler, K. W.,, Physics and chemistry of porous Media, AlP Conference Proceeding 154, AlP, 1987.

[19] Porter, H. E, Schurr G. A., Wells, D. E, and Seurau, K. T., Solid drying and gas-solid systems, in Perry's Chemical Engineer's Handbook, McGraw-Hill, New York, 20-79, 1984.

[20] Kaviany, M.,, Principles of Heat Transfer in Porous Media, 2d ed., Springer-Verlag, New York, 1995.

[21] Akers D. W., TMI-2 examination results from the OECD/CSNI Program, Volume 1", EGG-OECD-9168, 1992.

[22] TMI-2 Vessel Investigation Project Report, NUREG-CR 6197-part 02

[23] Broughton, J.M., Kuan, P., Petti, D.A., Tolman, E.L., A scenario of the TMI-2 accident. Nucl. Technol. 87, 34–53,1989

[24] Petti, D.A., Adams, J.P., Anderson, J.L.,. Analysis of fission product release behavior from the Three Mile Island Unit-2 Core. Nucl. Technol. 87, 243–263, 1989.

[25] Olsen, C.S., Jensen, S.M., Carlson, E.R., Cook, B.A.,. Materials interactions and temperatures in the TMI-2 core. Nucl. Technol. 87, 57–94, 1989.

[26] Eidam, G.R.,. The TMI-2 scenario. In: Proceedings of the Seminar on Fission transport Processes in Reactor Accidents, Dubrovnik, Yugoslavia, pp. 819–832, 1990.

[27] Akers, D.W., McCardell, R.K., Core materials inventory and behaviour. Nucl. technol. 87, 214–223. 1989

[28] Wolf, J.R., Rempe, J.L., Stickler, L.A., Korth, G.E., Diercks, D.R., Neimark, L.A., Akers, D.W., Schuetz, B.K., Shearer, T.L., Chavez, S.A. Thinnes, G.L., Witt, R.J., Corradini, M.L., Kos, J.A.,. TMI-2 Vessel investigation project integration report. Report NUREG/CR-6197; EGG-2734. EG&G Idaho, Inc., Idaho Falls, 1994.

[29] Magallon, D., Characteristics of corium debris bed generated in large-scale fuel-coolant interaction experiments, Nuclear Engineering and Design 236, 20061998–2009

[30] Mathew, P.M., Kuferschmidt , W.C.H., Snell, V.G., Bonechi, M., CANDU-specific severe core damage accident experiments in support of Level 2 PSA, Proceedings of 16th Int. Conference on Structural Mechanics in Reactor Technology, SMiRT 16, Washington, DC, 2001.

[31] Prasad, V., Kladas, N., Bandyopadhaya, A., and Tian, Q., Evaluation of correlations for stagnant thermal conductivity of liquid-saturated porous beds of spheres, Int. J. Heat Mass Transfer, (32): 1793-1796, 1989.

[32] Nozad, I., An experimental and theoretical study of heat conduction in two- and three-phase systems, Ph.D. thesis, University of California, Davis, 1983.

[33] Hadley, G. R., Thermal conductivity of packed metal powders, Int. J. Heat Mass Transfer, (29): 909-920, 1986.

[34] Imura S., and Takegoshi, E., Effect of gas pressure on the effective thermal conductivity of pack beds, Heat transfer Japanese Research, vol. 3, no. 4, 1974, p-13

[35] Siefken, L. J., Coryell, E. W., Paik S., and Kuo, H., SCDAP/RELAP5 Modeling of Heat Transfer and Flow Losses in Lower Head Porous Debris, INEEL/EXT-98-00820, Rev. 2, 1999.

[36] Scheidegger, A. E. ,Statistical hydrodynamics in porous media, J. Appl. Phys., (25): 994-1001, 1974.

[37] Brinkman, H. C., A calculation of the viscous force exerted by a flowing fluid on a dense swarm of particles, Appl. Sci. Res., (A1): 27-34, 1947.

[38] Lundgren, T. S., Slow flow through stationary random beds and suspensions of spheres, J. Fluid Mech. (51): 273-299, 1972.

[39] Dybbs A., and Edwards, R. V., A new look at porous media fluid mechanics--Darcy to Turbulent," in Fundamentals of Transport Phenomena in Porous Media, Bear and Corapcioglu, eds., Martinus Nijhoff Publishers, 199-254, 1984.

[40] Tung,V. X. ,Dhir,V. K., A hydrodynamic model for two-phase flow through porous media, Int. J. Multiphase Flow, Vol. 14, No. 1, pp 47-65,1988.

[41] Edwards, D. K., Denny, V. E., and Mills jr., A., Transfer Process, McGraw-Hill Book Comp., New York, 1979.

[42] Chandrasekhar, S., Radiation Transfer, Dover, New York, 1960.

[43] M.N. Ozisik, Radiative Transfer and Interaction with Conduction and Convection, Werbel and Peck, New York, 1985.

[44] R. Siegel, and J. R. Howell, Thermal radiation heat transfer, 3d ed., Hemisphere, Washington, DC, 1992.

[45] D. Vortmeyer, Radiation in packed solids, in Proceedings of 6th International Heat Transfer Conference, Toronto, (6): 525-539, 1978.

[46] C. L. Tien, and B. L. Drolen, Thermal radiation in particulate media with dependent and independent scattering, Annual Review of Numerical Fluid Mechanics and Heat Transfer, (1): 1-32, 1987.

[47] B. P. Singh, and M. Kaviany, "Independent theory versus direct simulation of radiative heat transfer in packed beds, Int. J. Heat Mass Transfer, (34): 2869-2881, 1991.

[48] Jakob, M., Hawhin, G. Elements of heat transfer, 3rd Edition, John Wiley Sons., 1957.

[49] Rempe, J.L., Knudson, D.L., Margin for In-Vessel Retention in the APR1400 –VESTA and SCDAP/RELAP5-3D Analyses, INEEL/EXT-04-02549. Idaho National Engineering and Environmental Laboratory. 2004.

[50] W. H. McAdams, Heat Transmission, 3rd edition, New York: McGraw-Hill, 1954.

[51] L. C. Burmeister, Convective Heat Transfer, New York: John Wiley & Sons, 1983.

[52] S. W. Churchill and H. H. S. Chu, Correlating equations for laminar and turbulent free convection from a vertical plate, International Journal of Heat and Mass Transfer, 18. pp.1323-1329, 1975.

[53] H. K. Forster and N. Zuber, Dynamics of vapor bubbles and boiling heat transfer, AIChE Journal, 1, No. 4, , pp. 531-535. 1955.

[54] L. A. Bromley, Heat transfer in stable film boiling, Chemical Engineering Progress, 46, pp. 221-227, 1950.

[55] RELAP5/Mod3.2 Code Manual, , NUREG/CR-5535, INEL-95/0174, 1995.

[56] Samuel Glasstone and Alexander Sesonske, Nuclear reactor engineering, 1st Edition, Delhi, CBS Publishers & Distributors, 1986.

[57] L. Baker . Jr. and L. C. Just, Studies of metal-water reaction at high temperature, part III, U. S, AEC Report ANL-6548, 1962.

[58] Gokhale, O., Mukhopadhyay, Deb, Ghosh, A. K. , Severe accident analysis to evolve insight for severe accident management guide lines for large pressurized heavy water reactor", Proceedings, 2nd International Conference on Reliability, Safety & Hazard (ICRESH 2010), December 2010, Mumbai, IEEE catalog No.: CFP1082L-ART, ISBN: 978-1-4244-8342-6/10 ©IEEE

[59] Mukhopadhyay, Deb, Vijayan, P. K., Ghosh, A. K., Investigation of Calandria vessel as an ultimate barrier to Corium relocation for PHWRs, paper no. HMTC1300581, Proceedings of the 22th National and 11th International ISHMT-ASME Heat and Mass Transfer Conference Dec. 28-31, 2013, IIT Kharagpur, India